Some pages of this thesis may have been removed for copyright restrictions.

HEIKO GERHAUSER

Doctor of Philosophy

Aston University

June 2003

1

THESIS CONTAINS

VIDEO   CD✓   DVD   TAPE CASSETTE

Aston University

CFD APPLIED TO THE FAST PYROLYSIS OF BIOMASS IN FLUIDISED BEDS

HEIKO GERHAUSER

Doctor of Philosophy

June 2003

SUMMARY

Fast pyrolysis in bubbling fluidised beds is a novel biomass conversion technology that gives a liquid, bio-oil, as its main product. Bio-oil has a much greater energy density than most biomass feedstocks, and as a liquid is easily transportable and storable. Potential applications include chemicals, such as fertilisers or resins, and fuels that can be burnt in boilers, engines or turbines.

To take advantage of these opportunities, the process needs to be scaled up from the laboratory scale to the pilot plant and industrial scale.

This thesis employs computational fluid dynamics (CFD) to that end. As a first step, the CFD predictions for the hydro-dynamics are validated against cold flow experiments, for 3-D up to a scale of 7.5 cm in diameter, and for 2-D up to a scale of 50 cm. Variables investigated in this validation effort include the effect of reactor and freeboard geometry, particle diameter and density, fluidising velocity, temperature, initial bed height, pressure fluctuations and scale.

The CFD modelling is then extended to take account of heat transfer, particle entrainment and fast pyrolysis reaction kinetics. The interaction of the pyrolysis reaction and hydro-dynamics is found to be significant. While the location of pyrolysis vapour release may lead to maldistribution, the hydro-dynamics have an effect on vapour residence time and therefore bio-oil yield.

There are no adequate correlations for the special case of selective entrainment of char out of a bed of sand. This situation has been successfully addressed through the development of a CFD based estimating procedure.

Heat transfer, selective char entrainment and vapour residence time are shown to be such important limitations to scale-up for plants with a capacity of more than 100 t/day that new design concepts will likely be required, the most promising of which are identified.

Keywords: Entrainment, reaction kinetics, scale-up

2

DEDICATION

To Annette, my wife

ACKNOWLEDGEMENTS

The author would like to thank the following:

- o his supervisor Dr. Sotos Generalis for continuous support and advice over the last three years

- o his co-supervisor Professor A. V. Bridgwater, Convener of the Subject Group of Chemical Engineering & Applied Chemistry at Aston, who provided support and guidance throughout, and without whom the opportunity to undertake this work would not have arisen

- o the European Commission for financial support under Contract JOR3-CT97-0197

- o his wife Annette, for encouragement, support and forbearance

- o his co-workers in the Bio Energy Research Group

- o Gero Ferges for experimental work on the 2-D fluidised bed performed together with the author

LIST OF CONTENTS

7

8

Audio-visual and electronic material:

1 CD with pictures, movies and text files containing pressure data

LIST OF FIGURES

LIST OF TABLES

1. Introduction

The work described in this thesis has largely been undertaken as part of the contribution of Aston University to the EU project "Development of advanced fast pyrolysis processes for power and heat". The specific subtask assigned to the author, and therefore the overall objective of the work here reported, was the development of *pyrolysis reactor models for performance prediction, optimisation, design and scale-up[1]*.

The EU project was aimed at assisting with the commercialisation of fast pyrolysis of biomass in dense fluidised beds. This technology is considered in detail in this thesis, therefore a brief, introductory summary is appropriate at this point.

Slow pyrolysis, mostly for the production of char coal, but also sometimes for the production of tars employed for such purposes as ship building, is an ancient process. Fast pyrolysis is of recent origin and achieves high liquid yields of up to 80% through careful optimisation of the pyrolysis process. Very short vapour residence times of generally less than two seconds, high biomass heating rates and reactor temperatures of around 500 degrees Celsius are particularly prominent requirements that need to be met by the reactor[2].

A bed of sand fluidised by an inert gas is suitable for providing the necessary reaction conditions. It affords excellent temperature control and fast heat transfer between the sand and biomass particles. Furthermore, the vapour phase products can be rapidly removed with the surrounding fluidising gases to achieve low vapour residence times. An illustration of a generic bubbling fluidised bed biomass pyrolyser is shown in Figure 1 to give a basic overview of the technology.

Heat is transferred to the bed via its walls and by pre-heating the fluidising gases to 600 to 800 degrees Celsius. Biomass is fed via a screw feeder and pyrolysed by contact with the hot fluidised sand, which also acts as a large reservoir of heat providing thermal inertia. The char produced is entrained and together with the pyrolysis vapours and fluidising gas leaves the reactor via the freeboard above the bed.

16
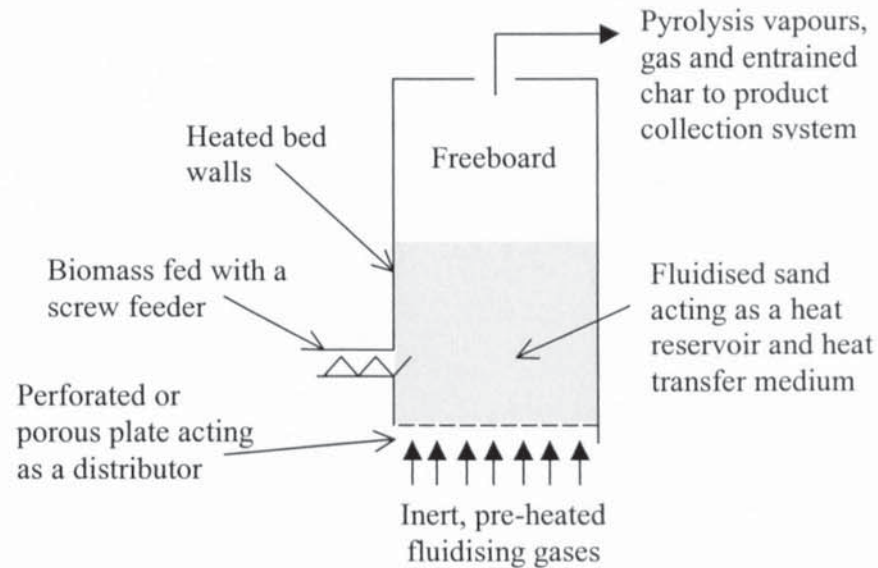
Figure 1 Illustration of a generic bubbling fluidised bed pyrolyser

Apart from Aston five other companies and research institutions from several EU nations were involved in the project. Particularly noteworthy is the close co-operation between Aston and Wellman Process Engineering Ltd., which was responsible for the design and construction of a scaled-up pilot plant. It has been noted in the literature that examples of collaboration between industry and academia in the field of fluidisation engineering are rare[3]. In this case the co-operation has proven so successful that a follow-up project has been launched, in which Aston is a subcontractor to Wellman, which in turn has attracted 50% financial support from the DTI[4,5].

The work was also of an interdisciplinary nature, which is reflected by the fact that two supervisors were appointed. While Dr. Generalis supplied CFD (computational fluid dynamics) expertise, Prof. Bridgwater, together with the rest of the Bio Energy Research Group of which he is the leader, provided long years of experience in the field of biomass pyrolysis.

The nature of the research, that is both the fact that it is interdisciplinary and that it is based on a collaborative effort between academia and industry, has several important consequences that bear mentioning.

Firstly, there is the issue of confidentiality. Wellman Process Engineering, and also the other partners in the EU project, though this is less of a concern, have a commercial

interest in the technology they are developing. It is therefore not possible to reveal any details of Wellman's technology without their written consent. Consequently, in some instances specific information had to be withheld that the reader might feel would be of interest.

As Werther[3] notes industry and academia often have different objectives, while *researchers prefer fundamental, well-defined problems and systems,* which then, hopefully, give results that are applicable to a wide range of situations, industry is primarily interested in finding solutions to its specific design and operational challenges that work.

The research presented in this thesis does take account of industrial requirements. It therefore primarily stresses applied science specific to the design challenges of biomass fast pyrolysis.

Both CFD and fast pyrolysis are very specialised fields. Consequently, it cannot be expected that a CFD expert would be likely to know much about fast pyrolysis and respectively an expert on fast pyrolysis would probably at first be baffled by the particular terminology employed in CFD.

This presents the danger that the reader may be confronted with material that is just beyond their comprehension and frustrates them needlessly. The author has tried to attack this problem by making the bulk of the presentation understandable to the non-expert, while issues that may be of special interest to an expert in a particular area, notably CFD, are often treated separately in a fashion that makes it clear that they are optional.

It should also be stressed that the research here presented is often novel mainly in the way it combines concepts and models from different research areas. CFD specialists in particular should appreciate and gain knowledge from this thesis primarily by seeing it as an example of how CFD can be applied to a particular problem, in this case fast pyrolysis of biomass, and usefully combined with other modelling approaches to assist with performance prediction, optimisation, design and scale-up of industrial plant. This thesis is not, on the whole, aimed at being an attempt to improve fundamental CFD techniques.

Validation of the basic CFD models is performed mainly with a view of satisfying industry that they work.

Specialists in the area of biomass pyrolysis should be able to take away from reading this thesis that CFD has been shown to be a useful tool that may help them solve the special challenges they face in scaling and operating fast pyrolysis plant.

PREVIOUS WORK AND RESEARCH NEEDS

The specific research area dealt with in this thesis, that is the design of scaled-up bubbling fluidised bed biomass fast pyrolysis plant, has received very little attention in the literature. There are no industrial scale operations using this technology, nor are there any design studies published in the literature for such plant. Apart from Wellman Process Engineering only two other groupings, Dynamotive and possibly Fortum/Vapo/VTT, are believed to be actively involved in commercialising bubbling fluidised bed fast pyrolysis[6,7]. The basis for their designs, presently at the pilot plant stage, is proprietary and not publicly available. In the case of Fortum/Vapo/VTT it is not even entirely clear, whether their technology involves a bubbling or a circulating fluidised bed.

No systematic study identifying key design challenges for scale-up of this technology is available. Initial work at Aston on the modelling subtask of the EU contract, performed before the author's contribution had started, was carried out in response to a particular operating problem experienced with a laboratory scale (1 kg/h) fluidised bed. After a run it was found that a very large char layer had formed in the reactor. Low liquid yields and poor liquid quality were also observed. Two MEng projects[8,9] and an MPhil thesis[10] were consequently devoted to investigating selective entrainment of char out of the reactor.

When the author joined the research group, the first task performed was to examine the results of these three reports. They indicated that char removal was an important issue. Not removing the char efficiently would significantly degrade pyrolysis plant performance. However, they also showed that the particular task at hand, selective entrainment of less dense but similarly sized particles out of a fluidised bed with a short freeboard, had never been investigated before. Furthermore existing correlations were found to be grossly inadequate for this situation, as is explained very briefly in chapter 3.

Wunder, who wrote the MPhil thesis just mentioned, therefore chose to rely on cold flow modelling work using glass/Perspex replicas of the hot reactor, and on a simple analysis of the physics underlying the separation problem.

Biomass size reduction is expensive and it is therefore desirable to be able to process relatively large biomass particles. Those, however, result in large char particles that are more difficult to entrain. While the detailed design of the Dynamotive process is proprietary and unpublished, it is clear that the company has attacked the problem by reducing the biomass particle size to 1-2 mm or less[11,12], that is sufficiently small for the resulting char particles to easily be entrained.

Wunder examined the terminal velocities of char and sand particles, and found a small overlap between 1.5 and 2 m/s, that is most of the char particles examined had terminal velocities less than 1.5 m/s, while most of the sand particles were above 2 m/s. The biomass particle size his experiments were based on was 2-3 mm, while the sand used had an average diameter of 0.503 mm.

Wunder noted that the allowable superficial velocity in the bed was much lower than 1.5 m/s and that the gas forcing its way through the fluidised bed in the form of bubbles (voids of gas in the sand bed that appear similar in shape and behaviour to bubbles in a boiling liquid) would throw a small amount of sand and char into the freeboard, when the bubbles/voids reached the surface of the bed. With a low superficial velocity in the freeboard, those particles would then fall back into the bed. Wunder reasoned that efficient separation could be achieved by narrowing the freeboard sufficiently for the superficial velocity in it to be between 1.5 and 2 m/s. Almost all the ejected sand particles would then fall back into the bed, while nearly all the char particles that could reach the narrowed freeboard would be carried out.

Based on this reasoning a narrowing of the freeboards of the experimental reactors at Aston and of the pilot plant Wellman was building at the time was implemented. The exact kind of narrowing chosen by Wellman cannot be revealed in this thesis. The geometry of the reactors at Aston is described in chapter 5.

After considering the results of the prior work performed in the research group on selective char entrainment, and after also consulting the literature for work that had been done on entrainment that might be suited to the problem at hand, it was concluded by the author that indeed no existing correlations were adequate for design and scale-up purposes and that another approach would have to be used to scale the design advanced by Wunder with sufficient confidence. It was furthermore concluded that such scale-up would be desirable to allow the use of larger biomass particles, which would reduce the costs for biomass particle size reduction and make it easier for the product collection system to separate out the entrained char.

The identification of entrainment as a major design challenge arose as the result of an operational problem, as just described. Based on consultation with Wellman and within the research group, and also based on a review of the relevant fast pyrolysis and fluidised bed literature, several other design considerations were identified by the author to be of major importance, in particular, the ability to transfer sufficient heat into the reactor, the potential for excessive abrasion of the char, the hydro-dynamic behaviour of the fluidised bed, the need to keep the residence time of the pyrolysis vapours very short and the influence of pyrolysis reaction kinetics on the reactor design and achievable product yields.

The hydro-dynamic behaviour of the bed was concluded to be the most significant issue that needed to be addressed satisfactorily, both as it is a pre-requisite for estimating entrainment, heat transfer, abrasion and pyrolysis vapour residence time and also as it is known to be particularly scale and reactor geometry sensitive[13].

The hydro-dynamic design of commercial fluidised bed reactors tends to be based on a combination of empirical or sometimes semi-empirical correlations, cold models and pilot plant work[13]. Pilot plant and cold model work is expensive and time consuming, while correlations cannot easily or confidently be extrapolated to new reactor geometries and scales.

An alternative approach, the direct application of the fundamental laws of mass, momentum and energy conservation to the modelling of fluidised bed hydro-dynamics, has only become viable fairly recently due to advances in computing power. While holding the promise of reduced pilot plant expense and greater ability to cope with new reactor

configurations, this approach suffers from being burdened with a very complex and difficult to implement mathematical solution procedure, and little validation to date that is satisfactory from a practical engineering perspective. Van Wachem notes that *the research efforts of most groups are aimed at development of still more detailed models for two phase flow* modelling of fluidised beds, *while little attention is paid to the evaluation of the results from an engineering point of view*[14].

Considering its promising nature, a decision was made to pursue modelling of fluid bed hydro-dynamics based on first principles and raw computing power, in other words CFD.

As detailed in chapter 4, a commercial CFD code, CFX, was chosen, which already contains a model for the hydro-dynamics of fluidised beds. The main research focus therefore was on satisfactory validation, work that is detailed in chapter 6, and on applying the CFD to the aforementioned design challenges posed in particular by heat transfer, entrainment and pyrolysis reaction kinetics. Prior validation work of CFD predictions for fluidised bed hydro-dynamics, which can be found in the literature, is also further discussed in chapter 6.

While there is no prior work applying CFD to the estimation of entrainment, an attempt has been made by Kuipers[15] to model bed-to-wall heat transfer via CFD analysis and Bellan[16] has developed a model integrating pyrolysis reaction kinetics and CFD. These two authors are the only ones in the respective areas to have published such analyses and their work is discussed in the respective chapters, that is chapter 7 for reaction kinetics and chapter 9 for heat transfer.

In summary the main research needs were felt to be in the satisfactory validation of existing CFD models for fluidised bed hydro-dynamics, in the application of CFD or other design procedures to the identified design challenges of biomass fast pyrolysis in bubbling fluidised beds and in laying the foundation for scale-up design methodologies capable of meeting the needs of industry.

OBJECTIVES AND WORK PROGRAMME

The general objective of the work was to provide models, procedures and methodologies of practical use in the design of scaled-up bubbling fluidised bed biomass fast pyrolysis plant.

The specific objectives to be met during the time of the project, formulated during the course of the first year of the PhD, were:

1. Identification of key design challenges
2. Choice of CFD code (proprietary or self-developed) and platform
3. Obtaining predictions of hydro-dynamic fluid bed behaviour from the code
4. Satisfactory validation of the predictions with the help of cold model work, and in so far as practicable, also on laboratory or pilot plant scale hot reactors
5. Development and validation of a CFD based procedure or model to predict selective char entrainment
6. Inclusion of pyrolysis reaction kinetics into the CFD code, and in so far as practicable, validation of the resulting predictions
7. Inclusion of heat transfer, particle break-up, agglomeration and attrition into the CFD code, in so far as practicable; validation of the resulting predictions with cold flow work, and in so far as practicable, also on laboratory or pilot plant scale hot reactors
8. Assessment of ways to overcome the identified design challenges and of the available tools for designing scaled-up bubbling fluidised bed biomass fast pyrolysis plant

The programme of work was flexible. None of the above objectives was assigned a hard time frame, within which all the work had to be completed and after which point in time no further work would be added. Rather, the programme of work established during the course of the first year of the PhD called for minimum requirements to be met by loosely specified target dates, as shown in Table 1. In addition it called for continuous reassessment and reconsideration of objectives 1, 2 and 8.

Target date (from start of project)	Minimum requirement
1-3 months	Initial identification of key design challenges
3-6 months	Initial choice of CFD code and platform
6-9 months	First hydro-dynamic predictions
6-12 months	Development of entrainment estimating model or procedure and initial validation
6-12 months	Initial validation of hydro-dynamic predictions on small-scale cold flow rigs
12-24 months	Design and construction of larger scale cold flow rig(s), and validation on that scale (preferably comparable to Wellman pilot plant)
12-30 months	Inclusion of reaction kinetics, attrition, heat transfer, particle agglomeration and break-up and validation, all in so far as practicable

Table 1 Target dates in the programme of work

STRUCTURE OF THE THESIS

This thesis is arranged into the following chapters:

Chapter 1, Introduction

In addition to the introductory comments and this overview of the structure of the thesis, this chapter contains a detailed discussion of the opportunities and competitive challenges for bio-energy with particular emphasis on the fast pyrolysis of biomass.

Chapter 2, Biomass and Fast Pyrolysis Fundamentals

This chapter gives an overview of biomass that ranges from its definition to the chemical composition of available biomass feedstocks. Furthermore, the history and present state of development of fast pyrolysis technology and modelling are discussed.

Chapter 3, Fluidised Bed Technology

This chapter provides a brief explanation of some particularly relevant aspects of fluidised bed technology, such as the calculation of the minimum fluidising velocity or the Geldart classification

Chapter 4, CFD Theory and Practice

A general introduction to the field of CFD is given. This is followed by an explanation of the specific theory employed for the work reported in this thesis. Finally, practical CFD issues, ranging from gridding to the operational details of the CFD package employed are discussed.

Chapter 5, Experimental Set-up

The experimental equipment used is explained in this chapter.

Chapter 6, Hydro-dynamics

CFD results for fluidised beds are presented in this chapter and where it proved feasible validated against experimental work.

Chapter 7, Reaction Kinetics

A combination of reaction kinetics modelling with CFD is given in this chapter and used to predict the impact of their interaction on reactor design. A comparison with the work of other authors is performed also.

Chapter 8, Entrainment and Attrition

A CFD based estimating procedure for entrainment is presented and compared with experimental data in this chapter. Possible improvements to reactor design are discussed.

<u>Chapter 9, Heat transfer</u>

Results from the Eulerian modelling of the heat transfer with surfaces in fluidised beds are presented, discussed and compared with previous work.

<u>Chapter 10, Discussion of Design Options</u>

A number of possible design choices for scale-up are discussed in the light of the results obtained during the work reported in this thesis.

<u>Chapter 11, Conclusions</u>

This section sums up the findings of the work performed.

<u>Chapter 12, Recommendations</u>

Recommendations for the direction of future work are given in this chapter.

RESEARCH BACKGROUND – OPPORTUNITIES AND COMPETITIVE CHALLENGES FOR BIO-ENERGY AND FAST PYROLYSIS

There are three main areas the interdisciplinary research presented in this thesis builds upon, CFD, fluidised bed technology and fast pyrolysis of biomass. The first two areas have a very wide scope for application and are already well established. CFD is being applied in fields that range from the design of drug delivery systems[17] to climate modelling[18]. Fluidised beds have uses ranging from catalytic cracking of oil[19] to the manufacture of silicon for photovoltaic cells[20]. For CFD and fluidised bed technology, one can say that this thesis presents research of an incremental nature, it is an example of the use of an already established technology in a new application. By comparison, fast pyrolysis of biomass is a novel and unestablished technology[21].

The rest of this chapter will therefore concentrate on the opportunities and competitive challenges for bio-energy and fast pyrolysis. The technology itself will be discussed in chapter 2.

The treatment of the background for policy and economic choices is by issue, starting with climate change, which is followed by a discussion of the depletion of fossil fuels. Environmental concerns, notably about pollution, erosion, desertification and bio-diversity are addressed next, finally followed by other concerns, such as the preservation of rural culture. Conclusions are then drawn.

Climate change

Growing biomass sustainably absorbs the same amount of carbon dioxide that is released when it is burnt as a fuel. While some carbon dioxide emissions may result, when fossil fuels are used in the transportation, planting and processing of the biomass, its use is still close to carbon neutral and will result in a reduction of carbon dioxide emissions, particularly when compared to burning coal[22].

Anthropogenic emissions of carbon dioxide have been linked to climate change[23]. In summary, it has been found that the global average surface temperature has increased by 0.6 ± 0.2 degrees Celsius over the last 140 years, while the average global sea level has risen by 10 to 20 cm over the last 100 years. About half of the warming, namely the portion that has occurred over the last fifty years, may, with some confidence, be attributed to greenhouse gases[24], of which the most important is carbon dioxide.

While there is still some uncertainty in the modelling of climate as a whole, the climate forcing of greenhouse gases is understood with a very high level of confidence[25]. Consequently, the impact of a given emissions scenario on the global average surface temperature, which is in addition to natural variability due to other climate forcings, is not the most important source of uncertainty for the overall climate outcome. In fact, it is the emissions scenarios that are the most uncertain. They are responsible for the fact that the temperature range predicted by the IPCC, which is an increase of 1.4 to 5.6 degrees Celsius by the year 2100, is so wide. Excluding the two scenarios featuring large emissions from coal leads to a clustering of most of the predictions between 2 and 3 degrees Celsius. Predicted sea level changes by the year 2100 range from 9 to 88 cm.

Climate change will have a great variety of consequences, such as a lengthening of the growing seasons, the need to abandon some land close to the sea or employ dikes, greater agricultural yields due to the fertilising effect of carbon dioxide and many more. Some of these may have positive economic consequences, while others are potentially damaging. The studies that have been done disagree on the level of economic damage or benefit that may result from climate change. Most studies see economic damage of around 2-3% of world GDP in the year 2100, while some more recent ones come to the conclusion that there may be a small net benefit[26]. There is also widespread agreement that damage will be concentrated in the developing world, while most developed countries are very likely to receive net benefits from climate change.

The future costs of climate change can be used to calculate an appropriate price for carbon emissions today based on economic models. Nordhaus[27], reviewing a number of policy options, gives one such estimate as $6 per ton today rising to $13 by 2015. $10 per ton is roughly equivalent to 0.5 cents per litre of petrol according to Nordhaus.

These estimates leave out non economic impacts of climate change, such as the potential for extinctions of economically unimportant species, and they do not consider the possibility of apocalyptic climate change, that is the risk that there may be much more serious consequences than a loss of a few percent of global GDP in the year 2100. There is, however, little scientific evidence that such extremely unlikely apocalyptic scenarios, as for example run away global warming of 20 degrees Celsius or sea level changes of 50 metres within decades, are made any less likely by reductions in carbon dioxide emissions.

As pointed out above, biomass is carbon neutral and climate change is therefore one issue it might benefit from. Compared to the present costs of biomass and fossil fuels, the value of reducing carbon dioxide emissions, is, however, negligible using standard economic analysis. Taking into account political and other considerations, has, nevertheless led to the formulation of policies that explicitly or implicitly attribute a much higher value to carbon dioxide emissions reductions. Those are in particular the Kyoto protocol and various renewables obligations.

The Energy Information Administration for example calculates that the full implementation of Kyoto without international emissions trading would result in a national

price for carbon emission certificates of $310 to $349 per metric tonne in the year 2010 for the United States[28].

EIA also provides an analysis of the likely impacts of a 10% renewables obligation for electricity production[29]. It estimates that emissions in the electricity generating sector would be reduced from 790 to 737 million metric tonnes per year, while electricity costs would rise by $3.1 billion, which amounts to a cost per tonne of carbon equivalent of approximately $58. The marginal costs would be considerably higher, as EIA project that renewables will not be able to meet all of the 10% target at less than the 3 cent per kWh cost ceiling imposed on the renewables certificates (which are effectively a subsidy).

Fast pyrolysis of biomass will likely benefit from the issue of climate change. Risks are manifold, firstly policy support may not be forthcoming or may only provide a small monetary remuneration for low carbon dioxide emissions. Another potential pitfall is the competition posed by other technologies, such as carbon sequestration, nuclear power generation, and other renewables. Finally, fast pyrolysis also has to be proven to be a better solution, at least for some niche applications, than alternative biomass conversion technologies. It is worthwhile to point out that EIA project co-firing of biomass with coal to be the main biomass technology likely to benefit from a renewables standard, as this would involve the lowest capital costs.

Fossil fuel depletion

The oil crises of the 1970's raised the spectre of fuel scarcity and rapidly rising energy costs. A particularly influential publication was the book the Limits to Growth[30], which was widely perceived as predicting imminent resource depletion. One of the pieces of evidence for concern about resource scarcity provided by the book is a table listing the reserves lives of various minerals at the time. Petroleum reserves, for example, were given as 455 billion barrels. They now stand at over 1000 billion barrels, in spite of roughly 30 years of annual petroleum consumption ranging around 25 billion barrels. This does not imply that the estimate of reserves made in 1972 was wrong. Rather, reserves are not a suitable indicator of how much petroleum will be pumped in the future. Laherrere[31] points out that for the last fifty years the reserves to production ratio in the United States has fluctuated around ten, simply because reserves in that country tend to be estimated as being

29

roughly ten times current production. Campbell[32] explains that OPEC reserves are purely political estimates. They are not provided by petroleum geologists, but are, to a large degree, what OPEC governments wish them to be.

Those two petroleum geologists just quoted, that is Campbell and Laherrere, are responsible for a widely cited paper published in Scientific American[33] that again raises concerns about imminent petroleum scarcity, this time using a method successfully employed by Hubbert to estimate the peaking of US lower 48 petroleum supply. Lynch has criticised the Hubbert method for giving consistently overpessimistic results in virtually all other cases where it has been applied[34].

Campbell and Laherrere do not consider the potential of non-conventional oil to be substantial. They also largely leave out coal liquefaction processes. These assumptions are in contradiction with those made by the IPCC for obtaining their emission scenarios[35].

While depletion is counteracted by technological and economic change, the price differential with renewables, such as biomass, should in principle decline over time. The potentially available resources of fossil fuels are, however, so large that they do not represent a limitation as such, even when a time scale of a hundred years is considered. US coal resources alone for example amount to 4 trillion short tons[36], which may be compared with current world energy consumption of about 9 billion tonnes of oil equivalent[37] or the emissions scenarios of the IPCC[38] ranging from roughly 5 to 30 billion tonnes of carbon equivalent per year by the year 2100.

Resource depletion is a very gradual process and is unlikely, taking the predictions by the EIA, IPCC or IEA, to lead to substantial cost increases for fossil fuels in real terms. The costs of bio-energy will, therefore, have to fall in real terms to achieve general competitiveness with fossil fuels. Furthermore, because the process is gradual, the case for market intervention by government policy measures is very weak, as gradual price increases should also lead to gradual adoption of alternative technologies along a close to economically optimal path without the need for policy incentives.

A concern related to fossil fuel depletion, is security of supply. The oil crises in the seventies illustrate the potential for damage to the economy when supply is suddenly

disrupted. It can therefore be argued that energy sources such as domestically produced oil, coal, nuclear energy and renewables should be favoured over uncertain foreign suppliers. The potential benefit for solid biomass is low, as it primarily competes with coal and natural gas. Fast pyrolysis produces a liquid product, which is, however, unsuitable as a transportation fuel that could replace diesel, kerosene or petrol without upgrading that would be more expensive than liquefaction of coal. In the space heating and electricity markets, the competition is again primarily coal, gas, nuclear power and other renewables, and not OPEC oil. Other competing alternatives for ensuring security of supply are stock building, as has been done in the United States in the form of the Strategic Petroleum Reserve, and diversification of supplies away from the Middle East, for example by favouring producers in the former Soviet Union or in the Atlantic basin.

Environmental concerns

Traditional biomass burned inefficiently in developing countries is responsible for a greater fraction of energy related deaths than all other sources of energy together. WHO[39] estimate that of the order of 2 million deaths per year may be due to indoor air pollution, which is largely caused by the burning of dung, wood and crop residues in open fires or inefficient stoves. They also give the contribution of traditional biomass to the global burden of disease as 4%, which puts it into the top ten causes of disease.

The IEA also points out that the burning of traditional biomass fuels is a sign of poverty. In *rural sub-Saharan Africa many women carry an average of 20 kg of fuel wood an average of five kilometres every day*, an activity that uses up a large fraction of their daily calorie intake. Furthermore, excessive use of biomass can lead to deforestation, erosion, desertification and loss of bio-diversity[40].

Biomass is often perceived to be a dirty fuel. Used in modern pellet burners or efficient plant, biomass may, on the other hand, contribute to significantly lower emissions of some air pollutants, sulphur dioxide in particular, as the sulphur content of biomass is much lower than is the case for most fossil fuels. Nox emissions, however, are similar for both fuel oil and willow[41].

Other environmental concerns often raised include the use of artificial fertilisers and pesticides in the growing of the biomass, and the energy balance of biomass production[42]. While ethanol only has a modestly positive energy balance, its use can be justified by the fact that it is a premium octane enhancer displacing alternatives such as lead or MTBE.

For woody biomass life cycle analyses show large net energy ratios, which indicate that little fossil fuel is used in the production of the woody biomass compared with its energy value. Based on the case of domestic heating, Forsberg[43] gives typical values of 2-3% for this fraction.

The overall effect of the above environmental concerns and benefits on the use of biomass is uncertain, but is unlikely to be a major driver, as tough anti-pollution laws and regulations may provide as great a hurdle to the use of biomass as they do for fossil fuels.

The preservation of rural culture and other issues

All industrialised nations have large budgets for supporting farmers. President Bush, for example, recently signed a $182 billion farm bill. Developed countries spend more than $311 billion a year on agricultural subsidies[44]. These expenditures represent an opportunity for subsidised biomass production that replaces the growing of surplus food.

Kaltschmitt and Dinkelbach estimate that energy crops grown on EU set-aside land (about 15% of the overall agricultural land) could provide as much as 5.6% of current EU primary energy supply[45].

Supporting the growing of such energy crops, and other biomass dedicated to energy production, may be beneficial in providing rural employment opportunities, in preserving rural cultures and societal structures and in alleviating regional poverty.

Biomass is also a decentralised source of energy, a concept, which appeals to many energy consumers who do not like dependence on large, centralised energy suppliers.

Other opportunities for biomass energy include the management of waste, be it municipal waste, sewage sludge or industrial waste generated in saw mills and similar facilities.

Biomass plantations may also be used as a means of erosion control and for the remediation of contaminated soils[46].

Conclusions

Forecasts[47,48] by international or governmental agencies and bodies, such as the IEA, EIA and IPCC, indicate that biomass will likely struggle to keep its present share of world energy consumption over the next two to three decades. IEA suggest, in particular, that traditional biomass in the developing world, which is responsible for the bulk of present world biomass consumption, will grow much more slowly than energy consumption overall.

The Shell scenarios for the future are widely quoted[49,50]. The scenarios presented in 1995 included one where renewables would supply 50% of world energy demand by 2050. To some degree that scenario should be seen as aspirational, rather than a forecast. The latest scenarios give new biofuels shares of 1% by 2025 and 6-10% by 2050. In other words, including the probable decline in the share of traditional biomass, the overall contribution is not likely to change substantially.

While the EU has a number of targets for renewable energy, for example a doubling from 6% to 12% by 2010, it believes that those are very unlikely to be met. The European Union Energy Outlook[51] to 2020 states that all of the scenarios, including the most optimistic one, exhibit a renewables share of less than 8.4% of primary energy supply by 2020.

Targets should be seen as motivational, rather than as firm goals that one expects to reach. This also puts the failure of previous EU targets into perspective. One particular and noteworthy example are two targets for fast pyrolysis put forward by the European Commission[52] in 1992, namely commercialisation of bio-oil in power stations by 1997 and of hydro-carbon synthesis from bio-oil by 2002.

While it is unlikely at this stage that biomass will gain overall competitiveness against fossil fuels, or a much increased market share, over the next two to three decades, there are nevertheless good opportunities through likely policy actions, such as renewables

standards or subsidies. Furthermore, there are a number of promising niches where biomass is already competitive, in particular for home heating in rural areas and for the generation of heat and electricity from wastes. One such example of co-generation is the utilisation of bagasse[53].

It is in those niches that biomass fast pyrolysis is likely to be employed first. Here the competition is not fossil fuels or other energy sources, such as nuclear power or wind energy, but rather other conversion technologies, namely combustion and gasification.

Combustion is by far the most developed of those technologies and technical uncertainty is therefore very low. It suffers from low efficiencies in small scale electricity generation and from the high transportation costs of unprocessed biomass. The former issue is adequately addressed when the biomass is utilised to produce heat, rather than electricity. The latter issue may be partially dealt with by densifying and pelletising the biomass, an option particularly suitable for home heating.

Gasification is more advanced than pyrolysis, but still high risk from a technological viewpoint. A recent example of a major technical failure for gasification is the 8 MW ARBRE project in the UK[54]. The advantage of gasification compared to combustion is that higher efficiencies might be achieved for electricity production.

A similar case can be made for fast pyrolysis, particularly for small scales and if the bio-oil can be used to generate electricity in diesel generators[55]. Bridgwater et al also point out that systems de-coupling may be a major advantage of pyrolysis systems, as the production of the bio-oil can be separated, in terms of both time and location, from the generation of electricity. This represents a number of opportunities, such as generating electricity for peak demand periods at a central location, while producing the bio-oil in small decentralised plants during the harvesting season. The bio-oil could also be produced centrally and then distributed to several small co-generation schemes.

2. Biomass and Fast Pyrolysis Fundamentals

In this chapter an overview of biomass, from its definition to the chemical composition of available biomass feedstocks, is given. Furthermore, the history, and the present state of development, of biomass fast pyrolysis are presented. Descriptions of the available technology options, such as for example ablative and fluidised bed pyrolysis, and of the most widely used models for describing biomass pyrolysis are provided.

DEFINITION OF BIOMASS

The American Department of Energy defines biomass as *organic nonfossil material of biological origin constituting a renewable energy source*[56].

Usually biomass is considered to be organic matter that is renewable in the short term. With peat and old growth forests there is a grey area, as to whether their use should be classified as renewable. The IEA, for example, considers peat to be a subcategory of coal in its statistics[57], while the European Union considers peat part of bio-energy in its managEnergy initiative[58].

Another area of confusion is the classification of waste. A considerable fraction of waste is of biological origin and renewable and could therefore be classed as biomass. While the IEA has attempted to gather separate statistics for renewable and non-renewable waste since 1999, the process of standardising the definitions in different countries has not been completed yet[59].

BIOMASS FEEDSTOCKS

The available biomass resource base may be subdivided into the following main groupings[60,45]:

Wood

Wood is used both for energy purposes and as a raw material in the timber and paper industries. A relatively recent development is short rotation coppicing, in which fast growing species like poplar or willow are harvested every few years[61]. Wood species may be subdivided into hard and softwoods. The latter are also referred to as gymnosperms or evergreen trees, while the former are deciduous and angiosperms[62].

Forestry and other woody residues

Only about half the biomass contained in a tree is harvested in conventional forestry. Leaves, small branches and other residues are generally left behind. Collecting this biomass is expensive and therefore rarely done. There are also some concerns that such operations may disrupt forest ecosystems and remove nutrients that would then have to be returned to the forest in the form of fertiliser.

Some woody residues are available from other sources, such as public parks or horticulture.

Grasses grown as energy crops

The most widely investigated species is miscanthus[63]. Other grasses that have been considered as energy plants are Sudan grass, Alfalfa and reed canary. Currently work in this area of biomass energy is mostly at the early trial stage.

Agricultural residues and wastes

Straw and dung are widely used for cooking and other small scale heating applications in the developing world[40]. Their use for energy in industrialised nations is very limited by comparison.

Bagasse, the residue available from sugar cane plantations, is commonly burnt in low efficiency Rankine cycle boilers to provide process heat and a small amount of electricity[64].

Other waste biomass available from agricultural operations includes manure, and recently for a short period, culled cattle.

<u>Organic wastes</u>

This category includes municipal solid waste, landfill gas and sewage sludge. Their use as an energy source is a useful additional benefit of an overall waste management strategy, but rarely the main objective.

BIOMASS COMPOSITION

There are three main ways to describe the composition of biomass, namely the proximate analysis, the ultimate / elemental analysis and the biochemical composition.

The proximate analysis is the easiest of the three methods of characterising biomass. It only requires an oven, a few crucibles and a balance for weighing. The four components it can identify are moisture, volatile matter, residual carbon and ash. They are obtained by first driving off the moisture by drying at 105 degrees Celsius, then the volatile matter by exposing the biomass to 950 degrees Celsius, and finally by burning off the residual carbon, which just leaves char[65].

While the elemental composition is more difficult to determine analytically, it is easy to understand. It gives the mass percentages of the elements making up the biomass, the most important of which are oxygen, carbon, hydrogen and nitrogen.

The biochemical composition of biomass gives the major classes of biochemical compounds the biomass consists of. The most important ones are cellulose, hemi-cellulose and lignin.

Typical values for the proximate and elemental analysis of wood are presented in Table 2. The values were gathered by ECN and represent an average of values collected from a variety of published sources[66]. Fixed carbon is not given by ECN, presumably as it can be calculated by difference.

Table 2 Proximate and elemental analysis of wood, typical values as gathered by ECN

Component	Average	Minimum	Maximum	Number of References
Moisture wt% wet	19.6	0.0	71.2	228
Volatiles wt% daf	82.0	54.9	94.9	267
Ash wt% dry	2.2	0.0	39.4	466
C wt% daf	50.7	42.4	59.7	408
H wt% daf	6.1	4.6	8.9	408
O wt% daf	42.7	33.1	52.5	408
N wt% daf	0.4	0.0	3.4	377

Bridge provides a table for the typical biochemical composition of a few biomass feedstocks, which was originally compiled by Shafizadeh[67] (see Table 3). As can be seen from Table 3, the most important component of most biomass feedstocks is cellulose, followed by hemi-cellulose and then lignin.

Table 3 Typical biochemical composition of some biomass types, wt%

Types	Total ash	Solvent soluble	Water soluble	Lignin	Hemi-cellulose	Cellulose
Softwood	0.4	2.0	--	27.8	24.0	41.0
Hardwood	0.3	3.1	--	19.5	35.0	39.0
Wheat straw	6.6	3.7	7.4	16.7	28.2	39.9
Rice straw	16.1	4.6	13.3	11.9	24.5	30.2
Bagasse	1.6	0.3	--	20.2	38.5	38.1

PHYSICAL PROPERTIES OF BIOMASS

There is a great amount of variation between different biomass feedstocks, as can be seen in Table 4, which gives an overview of the physical properties of biomass gathered from several sources. It might be noted at this point that biomass typically has a much lower energy density than petroleum. The value for light fuel oil is included in Table 4 for purposes of comparison.

38

Table 4 Physical properties of typical biomass feedstocks

Property	Type of feedstock	Value	Unit	Source
Bulk density	Straw	150-200	kg/m^3	[68]
	Solid wood	600-900	kg/m^3	[68]
Lower heating value	Wood	8.4-17.0	MJ/kg	[68]
	Straw	12.0	MJ/kg	[68]
Energy density	Solid wood	5-15	MJ/l	by calc. from [68]
	Straw	1.8-2.4	MJ/l	by calc. from [68]
	Light fuel oil	34	MJ/l	by calc. from [69]
Thermal conductivity	Pelletised wood	0.23	W/mK	[70]
Heat capacity	Pelletised wood	1.8k	kJ/kgK	[70]
Elastic modulus	Wood fibres			[71]
transverse		0.6	GPa	.
longitudinal		18	GPa	

One important property of most biomass is its anisotropic grain structure. The elastic modulus of wood fibres listed in Table 4 for example indicates that it is much harder to pull wood apart along the grain than across it. A microscopic picture of small wood particles taken by the author is illustrated in Figure 27 in chapter 5. For the purpose of showing the structure of wood a picture with a greater resolution is more helpful. A scanning electron micrograph of an eastern spruce[72] is therefore shown in Figure 2.
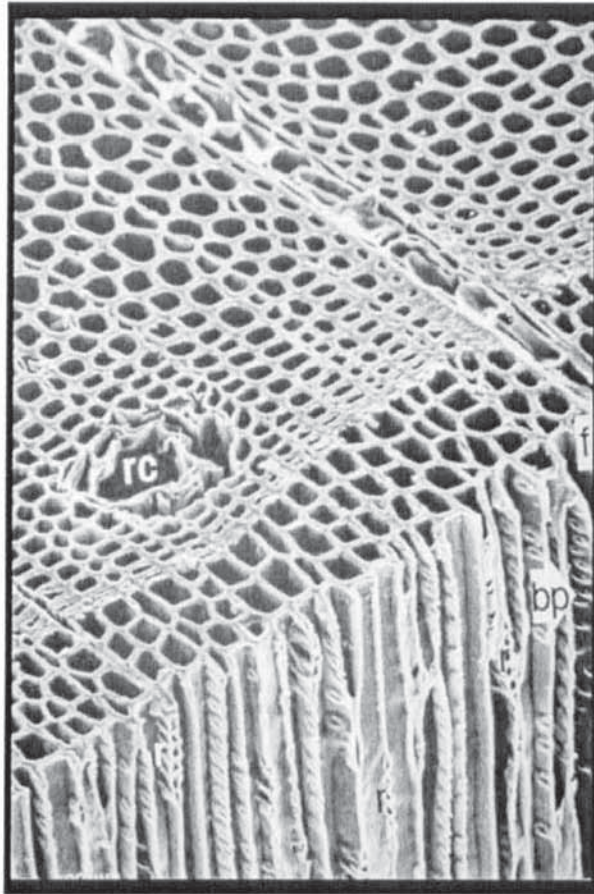
Figure 2 Scanning electron micrograph of eastern spruce

FAST PYROLYSIS OF BIOMASS

Pyrolysis may be defined as the thermal decomposition of a material in the absence of air. Slow pyrolysis has been used for millennia for the production of char coal. The liquid by-product tar has been used for ship building since Roman times. From the seventeenth century up to around the First World War, the largest exporter of wood tar was Finland, and tar represented one of its most important exports with production running as high as 25 million litres per annum in some years[73].

Fast pyrolysis is a much more recent process with its beginnings in the late 1970's spurred by the oil crises. The primary product of fast pyrolysis is a liquid, rather than char or gases. The main features required to achieve high yields of liquid products are[74]:

1. Very rapid heating of the biomass
2. Good temperature control to maintain reaction temperatures around 500 degrees Celsius
3. Fast quenching of the vapours to achieve vapour residence times of typically less than two seconds

The three products obtained in fast pyrolysis are a reactive char, non-condensible gases and bio-oil, which is a liquid mixture of water and organics. The respective yields are 60-80% for bio-oil and 10-20% for both the gases and the char. Typical properties of wood derived pyrolysis oils[75] are given in Table 5. As was done for biomass, the energy density is calculated by the author from the density and the heating value for purposes of comparison with light fuel oil. While the values obtained are higher than for biomass, they are still only around half to two thirds of those achieved by petroleum derived fuels.

Table 5 Typical physical properties for wood derived pyrolysis liquids

Property (wet basis)	Range
Density (15C), kg/m^3	1.11-1.30
Lower heating value, MJ/kg	13-18
Energy density, MJ/l	14.4-23.4
Viscosity at 50C, cSt	13-80
Thermal conductivity, W/mK	0.35-0.43
Specific heat capacity, J/kgK	2.6-3.8 at 25-60C
Pour point, C	-9 - -36
Coke residue, wt%	14-23
Flash point, C	50-110
Water, wt%	15-30
pH	2.0-3.7
Char, wt%	0.01-1
C, wt% (dry basis in parentheses)	32-49 (48-60)
H, wt%	6.9-8.6 (5.9-7.2)
N, wt%	0-0.1
O, wt%	44-60 (34-45)

AVAILABLE TECHNOLOGIES FOR FAST PYROLYSIS

There are a number of technologies and reactor configurations that have been investigated for fast pyrolysis of biomass, which satisfy the general requirements of rapid heating and cooling combined with short residence times and good temperature control listed earlier. An excellent review of the status and development of fast pyrolysis processes is provided by Bridgwater[76]. It is recommended for readers interested in more than the necessarily very brief overview that can be provided in this thesis. While an introduction to the available fast pyrolysis technologies can be found in this chapter, a further discussion reflecting the author's research results can be found in chapter 10.

Fluidised beds for fast pyrolysis

Fluidised bed reactor systems represent the most widely used technology for fast pyrolysis of biomass. They can be subdivided into dense, bubbling fluidised beds and fast, circulating fluidised beds. The main distinguishing factor is the superficial velocity of the fluidising gases. In bubbling fluidised beds it is only sufficient to carry out the char, while in fast fluidised beds the sand is entrained as well and then returned to the bed.

The type of fluidised bed considered in this thesis is the bubbling fluidised bed.

Ablative reactors

In ablative pyrolysis high heat transfer rates to the biomass are achieved by pressing it against a surface in differential motion at high contact pressures. There are two principal types of ablative reactors. In spinning disk reactors the relative motion of the biomass perpendicular to the direction of the applied force is achieved through the rotation of the disk[77]. In vortex reactors centrifugal forces are employed to press the biomass against the reactor walls in a sliding motion[78]. In the vortex reactor unreacted biomass may have to be recirculated and reinjected into the reactor. One of its advantages is that no moving parts are required, which at high temperatures and in a potentially corrosive environment may require significant maintenance.

All the ablative reactor types produce significant amounts of very fine char that is difficult to remove via cyclones. Bridgwater points out that in the ablative process pioneered by BCC 30% of the char was too fine to be collected in the installed cyclones, as it had a particle size of less than 10 microns[76].

The rotating cone reactor

The rotating cone is a novel transported bed reactor system[79,80]. The biomass and hot sand are fed to the bottom of the cone, where they mix and are transported upwards by the motion of the rotating cone[81]. An illustration of the concept is shown in Figure 3. One advantage of the system is that it does not require large amounts of inert carrier gases that detract from the efficiency of alternative reactor types.

Aston University

Illustration removed for copyright restrictions

Figure 3 Illustration of the rotating cone reactor concept, adapted from a figure by BTG[81]

Vacuum pyrolysis

In vacuum pyrolysis short vapour residence times are achieved by quickly withdrawing the vapours with the assistance of a vacuum pump[82]. In the multiple hearth vacuum pyrolysis process investigated by the University of Sherbrook the major limitation of vacuum pyrolysis was found to be heat transfer[83].

It has been shown that elevated pressures enhance char yields in slow, low temperature pyrolysis[84]. It is therefore possible that operating at reduced pressure may allow the maximisation of liquid yields at the expense of char at lower temperatures than is the case for operation at atmospheric pressure. As pressure impacts the efficiency of heat transfer

and therefore heating rates, it is difficult to design experiments that show the impact of pressure alone, however.

Experiments performed by Roy[82] give maximum bio-oil yields of around 65% at 425 degrees Celsius for vacuum pyrolysis at a pressure of 1.9 kPa. The residence time of 40 seconds was much longer than in other fast pyrolysis processes that usually aim to keep it below 2 seconds.

Like the rotating cone technology vacuum pyrolysis does not require large amounts of inert fluidising gases.

KINETIC MODELS OF BIOMASS PYROLYSIS

This section provides an overview of models available for the pyrolysis kinetics of biomass and some of its main constituents, that is cellulose, hemi-cellulose and lignin. Two primary general reaction routes are commonly identified, namely dehydration and depolymerisation[85]. The former is preferred at low reaction temperatures and leads to char, carbon dioxide, carbon monoxide and water. The latter is kinetically favoured at higher temperatures and yields unstable tars, which are mostly composed of anhydrosugars and oligosaccharides. The primary tars will decompose into gases, secondary tars and under some conditions char, if they are exposed to high temperatures for more than a few seconds.

All models pointed to in this section utilise the Arrhenius equation:

$$k = A \exp(-E/RT)$$

The most straightforward model, which for applications other than fast pyrolysis is also the most widely used, is a one step global model[86], which is illustrated in Figure 4.

$$\text{Biomass} \xrightarrow{\text{K}} \text{Char and Gaseous Products}$$

Figure 4 Illustration of one step global reaction kinetics model

44

Table 6 Reaction rate constants for the global one step model[86]

Species	A	E
	1/s	kJ/mol
Deal wood	$5.3 * 10^8$	138.8
Beech	$2.0 * 10^3$	63.4
Oak	$2.5 * 10^4$	74.4
Maple	$2.5 * 10^8$	125.0

Parameters for a number of feedstocks are provided in Table 6. The most serious drawback of one step global models is that they do not give any information about how the product distribution changes as a function of temperature. They also require a new set of reaction kinetics data for each new type of biomass considered.

The second concern just mentioned may be addressed to some degree by considering the pyrolysis of the major biomass components separately and then adding up the contributions made by the individual constituents[87].

In order to allow predictions of relative yields of char, tar and gas to be made, semi-global models with competing reactions are generally employed. The most widely used of these is the Broido-Shafizadeh model[88], which is illustrated in Figure 5.
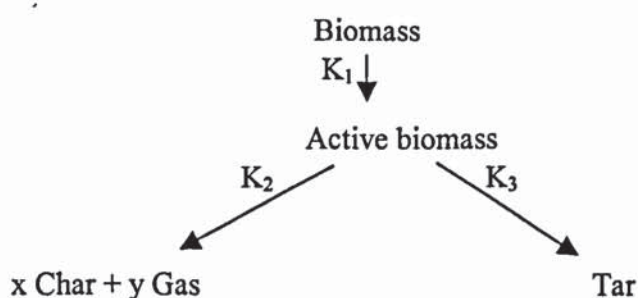
Figure 5 The Broido-Shafizadeh scheme

The Broido-Shafizadeh scheme can be applied to the individual biomass components. The overall pyrolysis kinetics are then again determined from the sum of the individual contributions. Values for the Arrhenius parameters listed by Miller and Bellan are given in Table 7.

Table 7 Reaction parameters of the Broido-Shafizadeh scheme applied to the major biomass components

Reaction	Component	A 1/s	E kJ/mol
1	Cellulose	$2.8 * 10^{19}$	242.2
2	Cellulose	$3.3 * 10^{14}$	196.5
3	Cellulose	$1.3 * 10^{10}$	105.5
1	Hemi-cellulose	$2.1 * 10^{16}$	186.7
2	Hemi-cellulose	$8.8 * 10^{15}$	202.4
3	Hemi-cellulose	$2.6 * 10^{11}$	145.7
1	Lignin	$9.6 * 10^{8}$	107.6
2	Lignin	$1.5 * 10^{9}$	143.8
3	Lignin	$7.7 * 10^{6}$	111.4

The treatment of secondary reactions is not considered in many studies, as they are only concerned with the evolution of the primary vapours. For the modelling of fast pyrolysis, however, those secondary reactions are vital. There are two main approaches. In the first, the tars are considered to degrade to secondary organic vapours and gases. In the second, the production of secondary char is also allowed for[89]. The latter approach suffers from the fact that secondary char production is a complex process that is believed to be auto-catalytic. Furthermore, the location of char deposition in a reactor cannot easily be included in a model.

The extended Broido-Shafizadeh scheme and primary and secondary reaction kinetics parameters used in this thesis are shown in Figure 83 and in Table 13 in chapter 7. The approach chosen only allowed for secondary decomposition of the organic vapours into gases. An illustration of a more complex mechanism that also allows for secondary char formation is shown in Figure 6 and based on work by Yu and Zhang[90]. The assumed fractions of the secondary decomposition products were 0.35 for char, 0.3 for gas and 0.35 for secondary tars.

Cellulose
$K_1\downarrow$

Active cellulose

K_2 K_3

x Char + y Gas   Primary volatiles
$K_4\downarrow$

Gas + Char + Secondary tar
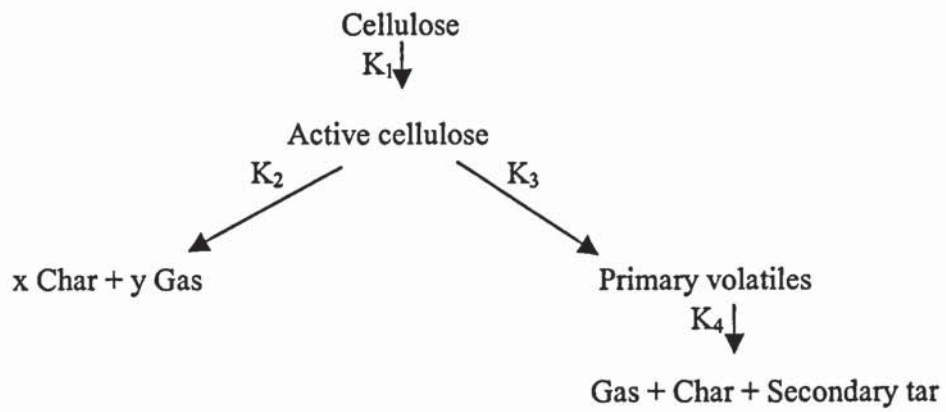
Figure 6 Modified Broido-Shafizadeh scheme used by Yu and Zhang

3. Fluidised Bed Technology

This chapter discusses some aspects of fluidised bed technology that are of particular interest for the work reported in this thesis.

INTRODUCTION

Initial development of fluidised bed technology on an industrial scale occurred in the 1920's in Germany and was directed at coal gasification to provide feedstocks for the chemical industry. The most important application of fluidised beds to date, fluid bed catalytic cracking of crude oil, was developed during the Second World War in the United States[13].

The discussion of fluidised bed technology presented in this chapter is rather selective in that it only describes a few aspects that help understand the material discussed in the rest of this thesis. For a more detailed introduction to fluidised beds, the excellent textbook by Kunii and Levenspiel is recommended[13].

MINIMUM FLUIDISING VELOCITY

When a fluid is passed upwards through a bed of loose particles, it experiences a pressure drop. The point at which this pressure drop becomes large enough to counterbalance the weight of the particles is known as the minimum fluidising velocity. Figure 73 provides an
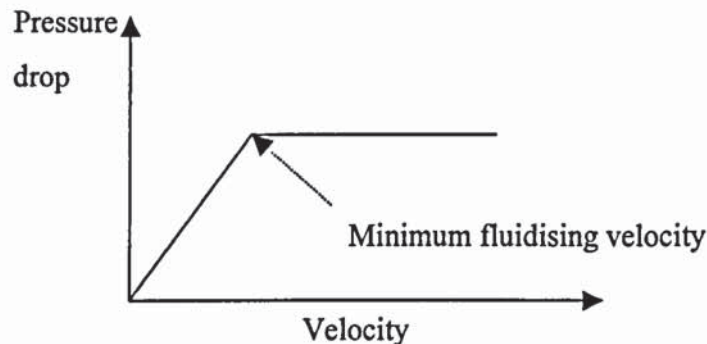
Figure 7 Dependence of the average pressure drop on the fluidising velocity

48

illustration from the author's work. Idealised textbook behaviour for the dependence of average pressure drop on fluidising velocity is shown in Figure 7. A common correlation for determining the minimum fluidising velocity has been proposed by Wen and Yu[13]:

$$Re_{mf} = [(33.7)^2 + 0.0408 \, Ar]^{0.5} - 33.7$$

THE GELDART CLASSIFICATION SYSTEM

A widely accepted system for classifying fluidised bed behaviour according to particle density and diameter has been advanced by Geldart (see Figure 8). There are four classes:

A) These are small particles that fluidise easily. The catalyst particles used in fluid catalytic cracking of petroleum fall into this category, which makes it one of the most frequently studied.
B) Most sand particles belong to this category, which also gives good fluidisation.
C) Flour and starch are representatives of this class, which shows very unsatisfactory fluidisation behaviour due to the fact that the interparticle forces are stronger than those exerted by the fluidising gases.
D) These are beds of very large particles, such as grains, beans or more relevant to the work reported in this thesis, large sand particles. Class D exhibits very erratic bed behaviour. There may be channelling or spouting, particularly so in deep beds.
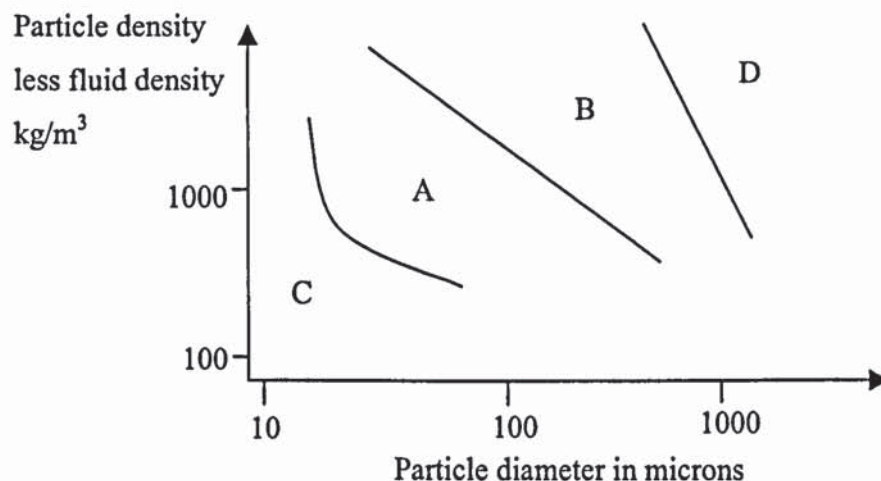
Figure 8 Geldart classification, note the logarithmic scale

49

ENTRAINMENT

An important variable in discussions of entrainment is the transport disengaging height, or TDH, first proposed by Zenz and Weil[91]. The eruption of bubbles in fluidised beds results in the ejection of material into the freeboard, some of which then falls back into the bed. The TDH describes the point at which no further material returns to the bed and at which the maximum solid loading of the fluidising gases is determined only by their capacity to transport those solids pneumatically.

A great deal of experimental work has been done that considers the entrainment of fines out of a bed that mostly consists of coarse particles that are too large to be entrained, and where the freeboard has a greater height than the TDH. Leva's pioneering work is still valid for this situation. He gives the following two relationships[92]:

$$c = c0 \exp (-2.303tk)$$

$$k \propto u^4$$

where c is the fines concentration at time t, c0 the original fines concentration at time t=0 and k a constant proportional to the fourth power of the velocity u

Much less work has been done for entrainment with the freeboard shorter than the TDH. No studies could be identified for the special subcategory of this case investigated in this thesis, namely the selective entrainment of a material that is less dense than the main bed material, but has a diameter that is comparable in size.

A very complex correlation by Kunii and Levenspiel[93], selected after detailed consideration of other correlations available from the literature, has been tested in an MEng project undertaken at Aston University and found to give non-sensical results for this special case, that is the net rate of entrainment given was negative[8].

THE IMPACT OF PARTICLE SIZE AND FLUIDISING VELOCITY ON BED-TO-WALL HEAT TRANSFER

These relationships have been studied experimentally during the course of this work as a by-product of CFD validation efforts. The results are reported in chapter nine and are in qualitative agreement with experimental results from the literature[94] shown in Figure 9 and Figure 10.
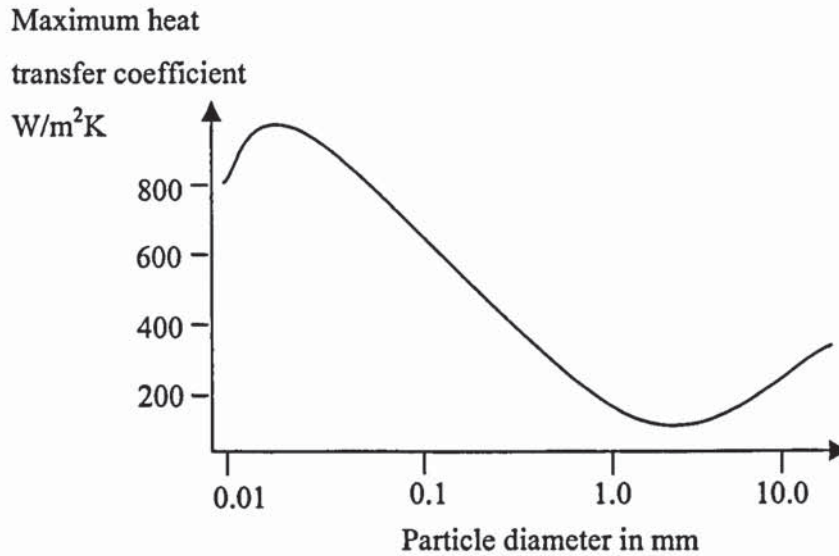
Figure 9 Dependence of heat transfer coefficient on particle diameter
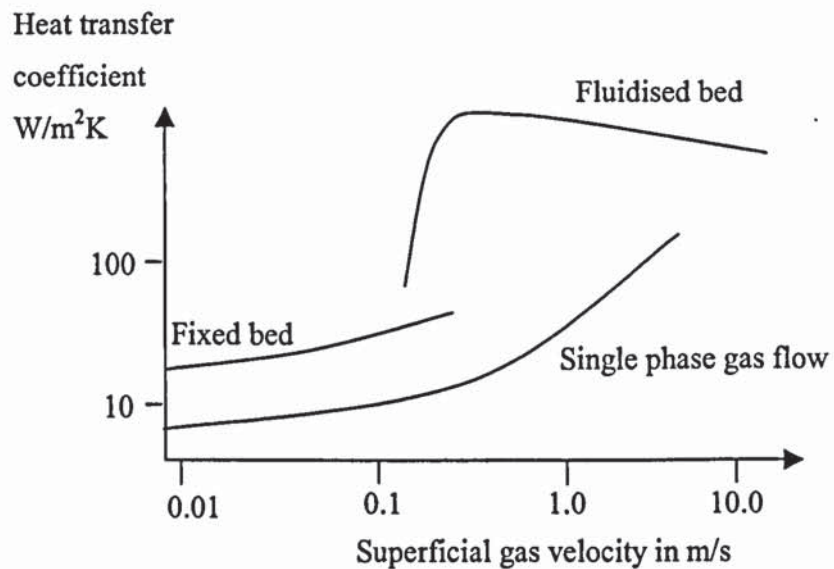
Figure 10 Dependence of heat transfer on superficial velocity

4. CFD

This chapter presents a short introduction to CFD in general. Then the choice of CFD code and computer platform is explained. This is followed by a more specific discussion of the theory relevant to fluidised beds, which was employed in this work. Finally, issues related to the practical operation of the chosen CFD code, CFX, are discussed.

INTRODUCTION

As mentioned in chapter 1, there are numerous applications for computational fluid dynamics. It is a well established technology now, and yet it is also a very young discipline that is evolving at a rapid pace.

While the early beginnings of CFD are as recent as the 1960's and first significant successes only occurred in the 1970's, the decade of the 1990's was marked by an enormous expansion[95].

By far the most important driver that has pushed and still is pushing CFD forward is the precipitous fall of the cost of computing power[96], which is illustrated in Figure 11. Over the last sixty years, the cost of doing calculations has decreased by over a factor 10^{12}.

Some of the most compute intensive tasks, such as the modelling of two-phase flows by CFD used in this thesis, have therefore only become of practical significance very recently.

The equations for fluid flow, which will be explained in the next section, are considerably older than their numerical solution by CFD. The derivation of the Navier-Stokes equations notably, which are the fundamental differential equations governing the flow of single phase fluids, was finished in 1845 by George Stokes, who continued earlier work by Leonhard Euler and Claude Navier[97].

The general introduction to CFD provided in the next section, which explains the Navier-Stokes equations and their numerical solution, is intended primarily to help those with little prior knowledge of CFD.

Aston University

Illustration removed for copyright restrictions

Figure 11 Decline of cost of computing power, adapted from Moravec[98], cost estimate for today (5000 MIPS per $1000) based on Lycoris PC from Walmart.com[99] and MIPS benchmark for Via C3 800 MHz[100]

THE NAVIER-STOKES EQUATIONS

The equations governing the flow of fluids are based on the following three fundamental physical principles:

1. Conservation of mass

2. Conservation of momentum, Newton's second law of motion, F=ma

3. Conservation of energy

Each of those can be used to perform a balance (of mass, momentum or energy) across a control volume in a fluid. For a non-compressible fluid the equations first derived by Navier are obtained (illustrated below). In a compressible fluid, density may change as a function of time. In the continuity equation, this means that the partial differential of the density with time has to be added to the left hand side of the equation giving the full Navier-Stokes equation. As the partial differential of the density with time is zero, when the fluid is non-compressible, the full Navier-Stokes equations reduce to the Navier equations for non-compressible fluids. The Navier-Stokes equations look daunting. However, the methods for solving them are the same as those illustrated for the much simpler partial differential equations used as examples in the rest of this section introducing CFD. The Navier-Stokes equations just have more terms making for lengthier arithmetic.

The continuity equation:

$$\frac{\partial(\rho u)}{\partial x} + \frac{\partial(\rho v)}{\partial y} + \frac{\partial(\rho w)}{\partial z} = 0$$

The momentum equations:

$$\rho\left(\frac{\partial u}{\partial t} + u\frac{\partial u}{\partial x} + v\frac{\partial u}{\partial y} + w\frac{\partial u}{\partial z}\right) = \rho g_x - \frac{\partial p}{\partial x} + \mu\left(\frac{\partial^2 u}{\partial x^2} + \frac{\partial^2 u}{\partial y^2} + \frac{\partial^2 u}{\partial z^2}\right)$$

54

$$\rho\left(\frac{\partial v}{\partial t}+u\frac{\partial v}{\partial x}+v\frac{\partial v}{\partial y}+w\frac{\partial v}{\partial z}\right)=\rho g_y-\frac{\partial p}{\partial y}+\mu\left(\frac{\partial^2 v}{\partial x^2}+\frac{\partial^2 v}{\partial y^2}+\frac{\partial^2 v}{\partial z^2}\right)$$

$$\rho\left(\frac{\partial w}{\partial t}+u\frac{\partial w}{\partial x}+v\frac{\partial w}{\partial y}+w\frac{\partial w}{\partial z}\right)=\rho g_z-\frac{\partial p}{\partial z}+\mu\left(\frac{\partial^2 w}{\partial x^2}+\frac{\partial^2 w}{\partial y^2}+\frac{\partial^2 w}{\partial z^2}\right)$$

The energy equation:

$$\frac{\partial}{\partial t}\left[\rho\left(e+\frac{1}{2}v^2\right)\right]+\frac{\partial}{\partial x}\left[\rho u\left(e+\frac{1}{2}v^2\right)\right]+\frac{\partial}{\partial y}\left[\rho v\left(e+\frac{1}{2}v^2\right)\right]+\frac{\partial}{\partial z}\left[\rho w\left(e+\frac{1}{2}v^2\right)\right]=$$

$$k\left(\frac{\partial^2 T}{\partial x^2}+\frac{\partial^2 T}{\partial y^2}+\frac{\partial^2 T}{\partial z^2}\right)-\left(u\frac{\partial p}{\partial x}+v\frac{\partial p}{\partial y}+w\frac{\partial p}{\partial z}\right)$$

$$+\mu\left[u\frac{\partial^2 u}{\partial x^2}+\frac{\partial}{\partial x}\left(v\frac{\partial v}{\partial x}+w\frac{\partial w}{\partial x}\right)+v\frac{\partial^2 u}{\partial y^2}+\frac{\partial}{\partial y}\left(u\frac{\partial u}{\partial y}+w\frac{\partial w}{\partial y}\right)+w\frac{\partial^2 u}{\partial z^2}+\frac{\partial}{\partial z}\left(u\frac{\partial u}{\partial z}+v\frac{\partial v}{\partial z}\right)\right]$$

$$+2\mu\left[\left(\frac{\partial u}{\partial x}\right)^2+\frac{\partial u}{\partial y}\frac{\partial v}{\partial x}+\left(\frac{\partial v}{\partial y}\right)^2+\frac{\partial v}{\partial z}\frac{\partial w}{\partial y}+\left(\frac{\partial w}{\partial z}\right)^2+\frac{\partial w}{\partial x}\frac{\partial u}{\partial z}\right]+\rho u g_x+\rho v g_y+\rho w g_z$$

GRIDDING AND DISCRETISATION

The Navier-Stokes equations cannot readily be solved analytically for most problems, barring some of the most simple flow situations, of practical significance. It is therefore necessary to resort to numerical methods for their solution.

For these the flow domain has to be subdivided into a number of cells, a grid is generated to use CFD terminology. Furthermore, the partial differential equations have to be transformed into difference equations. The procedure is best explained with the help of an illustration (see Figure 12).

A simple forward difference with respect to x for example would transform the partial of the u velocity with respect to x as follows:

$$\frac{\partial u}{\partial x}\approx\frac{u_{i+1,j}-u_{i,j}}{\Delta x}$$

55
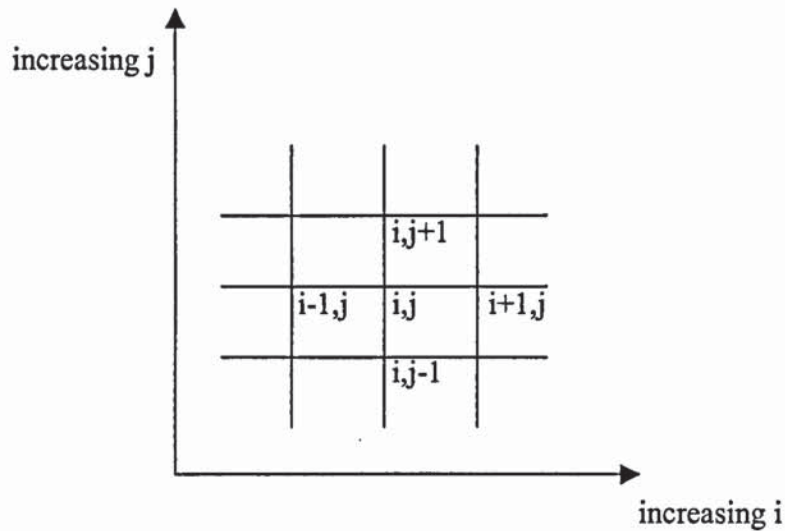
Figure 12 Illustration of gridding and discretisation

Another scheme that has been used for discretisation in the work here reported is central differencing, which would, to give another example, approximate the partial of the pressure with x as follows:

$$\frac{\partial P}{\partial x} \approx \frac{P_{i+1,j} - P_{i-1,j}}{2\Delta x}$$

NUMERICAL SOLUTION OF THE DIFFERENCE EQUATIONS

After discretisation of the governing equations and grid generation to subdivide the flow domain of interest, initial and boundary conditions need to be defined. Then a suitable numerical procedure needs to be employed to solve the equations. This is best illustrated with a simplified example. Suppose the following partial differential equation described a particular flow adequately:

$$\frac{\partial u}{\partial t} = t^2$$

56

This partial differential equation could be used to generate a difference equation:

$$\frac{u_{t+\Delta t} - u_t}{\Delta t} = t^2$$

The initial condition could be t and u being equal to zero. u at time t is five seconds could then be obtained by using the technique of time marching after rearranging the equation:

$$u_{t+\Delta t} = \Delta t \bullet t^2 + u_t$$

Using a time step delta t of 1 second, the velocity after a second could be estimated and from that, the velocity after 2 seconds and so forth until arriving at the velocity at t is five seconds.

As the sample equation can be solved analytically, the results of the numerical method can be compared with the correct value of 41.667. Employing a time step of 1 second gives u as 30, which is clearly rather unsatisfactory. 0.1 seconds give 40.425 and 0.001 seconds give 41.65, which is just 0.03% away from the correct analytical solution.

The numerical solution of partial differential equations can be continued until an estimate of the error (known as the residual in CFD terminology) is deemed to be sufficiently small.

It should be stressed again that the numerical solution of the Navier-Stokes equations differs from the above simplified example mainly in the number of terms that are involved, which means that the difference equations will be much longer and require more effort to rearrange.

For a more detailed introduction to CFD in general the reader is referred to the very good literature that deals with this subject, e.g. [96,101,102,103,104,105].

To summarise this section introducing CFD, balances for mass, momentun and energy are used to derive the fundamental equations for fluid flow, known as the Navier-Stokes equations. Those are too difficult to solve analytically for most problems of significance,

requiring a numerical solution. For this the partial differential equations are turned into difference equations and the flow domain of interest is subdivided into many cells. After defining the initial and boundary conditions a numerical method can then be chosen in an attempt to solve the difference equations to the desired level of accuracy.

CHOICE OF CFD CODE

At the beginning of the work here reported a choice had to be made, whether a new computer code should be developed from scratch as part of the modelling effort or whether a commercial offering should be used as a basis.

The difference between the two options is not as great as one might think at first glance. Developing a new CFD code for a specialised area such as biomass fast pyrolysis would have involved writing a main programme of moderate length that would delegate nearly all complex tasks to subroutines, which could be gathered from the internet as freely available code or paid for from a software company specialising in the provision of subroutines for common mathematical tasks, such as for example Compaq's CXML which provides thousands of functions and routines[106].

Commercial CFD software can usually be, and for new tasks often has to be, supplemented by user written subroutines. In comparison to writing a new CFD code, employing commercial software may nevertheless be less flexible and the workings of the code may also be less transparent. These benefits, however, come at a price, as developing a new CFD code from scratch may require considerable programming effort to merely duplicate work done by others, which is already well tried and tested.

The transparency of a CFD code depends on the amount and quality of documentation provided. Sometimes, it is also possible to pay extra for the right to inspect the source code of the product offered by a commercial CFD company. The sheer volume of code may mean that good documentation may be more helpful in guaranteeing transparency for practical purposes than access to the source code. A similar consideration applies to both the commercial, and the freely available open source, subroutines one would want to rely on for complex, but standard mathematical operations in a code developed from scratch.

58

Having access to 4000 lines of source code will do little good, if the time to go through them and understand them is unreasonable.

The work undertaken in this thesis focuses on combining CFD with other modelling approaches, such as the modelling of the reaction kinetics during fast pyrolysis. It was therefore decided that choosing a commercial CFD product would be beneficial to allow more time to be spent on the new aspects to be integrated, as long as the chosen code would be both flexible and transparent enough to allow that integration easily.

A number of codes were investigated in detail. Apart from CFX, which was finally chosen, quotations were obtained for Estet-Astrid, Star-CD and Fluent. CFX was found to be flexible, transparent because of largely sufficient documentation, capable of running on many computer platforms and strong in multi-phase modelling.

Estet-Astrid was rejected, as it only ran on four computing platforms, all UNIX workstations[107], which made it impossible to check the performance claims for Estet-Astrid[108,109]. The choice of computing platform will be discussed shortly.

Star-CD[110], which can be run on all major platforms, was tested for a week and found to have severe weaknesses in multi-phase flow modelling that would have required extensive user Fortran programming merely to replicate the functionality available with CFX.

Fluent[111], which is likewise available for all major platforms, was the closest contender to CFX. It was rejected, as it was felt to be slightly less flexible and weaker in two-phase flow applications and also, as it was twice as expensive.

The choice of commercial CFD code dictated the Fortran compiler, as CFX will currently only work with subroutines compiled with Visual Fortran[112] on Windows or with the Portland Group Fortran Compiler[113] on Linux. The open source g77 compiler may also work with CFX[114]. However, so far no attempt has been made to try out this option.

59

CHOICE OF COMPUTING PLATFORM

The term computing platform refers to both the hardware and the operating system that are used for running the CFD software.

The main hardware choices available, in order of increasing cost, are a single processor PC, a dual processor PC with shared memory, a cluster of single processor PC's linked via a network, a high end Xeon PC server with four processors sharing memory, a Unix workstation, a cluster of Unix workstations and finally a massively parallel system such as the machines available from Cray.

There are three main operating system choices, Windows, Linux or a proprietary Unix. The latter option is usually limited to Unix workstations. Linux will run on nearly any hardware with only a few exceptions, such as Cray's vector computers[115], while Windows will run on any PC processor based platform, on the new Itanium processor[116] and unsupported on the Alpha processor[117].

All the main hardware options were investigated at some stage. For initial work, because it was the cheapest and most easily procured and set up platform, a 450 MHz single processor PC running Windows NT was chosen. This system was found to be capable of simulating about one second of fluidised bed hydro-dynamics with a simple two dimensional geometry and no complications, such as including reaction kinetics.

To allow more complex simulations in the future, it therefore became clear that one of the other hardware platforms would be required. Unix workstations were found to be inordinately expensive, more than ten times as costly as PC's, for a comparatively small improvement in computational speed, a few percent when comparing the latest Pentium processor with the most powerful Alpha processor. It was also apparent that within a period of about four months the speed advantage would disappear when compared to the latest PC's then available. Considering the price difference, this level of outperformance was felt to be inadequate. Furthermore, there is a learning curve when adopting a new system, both for the user and for physical computer maintenance. Relatively limited experience of Unix in the subject group and no experience in maintaining workstations were therefore considered to be significant disadvantages for this choice of platform.

Requiring outside assistance, either for training or for repair of equipment, would also have been considerably more expensive for Unix workstations than for PC's, which were already well supported in-house.

The use of Xeon processors, which are commonly employed in high end Windows servers, was investigated by performing a benchmark on a system set up by Dell for that purpose. It was found that the Xeon processors scaled according to clock speed. Considering their relatively low clock speeds compared to ordinary Pentium processors, even employing four Xeon processors would have yielded little advantage, but would again have come at a price differential of more than a factor ten. It may be surmised that Xeon based Windows servers are optimized for such tasks as acting as a web server, and not for computationally intensive tasks, such as CFD.

Xeon based Windows servers, dual CPU PC's and multiple CPU workstations share memory among the CPU's. Clusters of PC's or workstations communicate via a network and each CPU has its own memory, a system referred to as distributed memory. Programming of Fortran is easiest for single processor systems. It becomes more complex for shared memory systems, and further modifications are required for distributed memory platforms.

Clusters, do, however, enjoy a significant price performance advantage, which can be explained by the large economies of scale available in the manufacture of processors and components for standard PC's. Clusters are widely employed in UK research institutions[118] and worldwide for computationally intensive tasks. When physical limitations to further clock speed improvements occur, which may happen as early as 2010, parallel computing will also be the only way to achieve maximum computational speeds[119]. Making the additional effort required for parallelising the CFD work may therefore be considered to be an act of future proofing.

The scaling behaviour of clusters, that is the speed-up achieved by adding further computer nodes, depends on the individual application and the amount of effort put into parallelising the code. A further consideration is the quality of the communication equipment used to transfer information between the processors and to memory. The fact that the speed of communication equipment has increased much more rapidly over the last decade than the

clock speed of computers is one reason, why clusters have gained such widespread acceptance in the recent past[119]. Communication speed refers to the available transfer rate, the frequency at which data can be exchanged and delays in switching. Generally, the more communication is required the less efficient the scaling will be. CFD can scale well, that is benefit significantly from adding more nodes, when the number of grid points is large. Each node can then take care of computations related to its allocated share of grid points, and communication is only necessary to exchange information at boundaries between domains of grid points handled by the individual nodes. When there are few grid points, however, the communications load often becomes quite significant, which means that little benefit may be achieved from running in parallel.

The subject group in the end decided to invest in two clusters, an eight node 1.2 GHz Athlon cluster and a sixteen node 2.2 GHz Pentium 4 cluster. Both clusters employ fast Ethernet for communication between the nodes. Only the Athlon cluster has been used for work reported in this thesis. Both Windows NT and Linux have been employed.

Massively parallel vector computers are so expensive that few research institutions can afford to buy them. The CSAR (Computer Services for Academic Research) service provided on behalf of the Research Councils[120] was therefore investigated as an option. It was found that only a very limited amount of hours (100 for the most likely grant) would be available after submitting a detailed application and justification. In addition, CFX would have charged over a £1000. It was felt that the benefit of potentially getting 100 hours of computing time on a Cray T3E was not worth the expense, particularly as part of the available computing time would have been required for testing the Fortran on the new platform or might have been wasted when a run would fail to converge.

EULERIAN VERSUS LAGRANGIAN MODELLING

Fluidised beds contain an exceedingly large number of sand particles, which represents a challenging modelling problem. There are two main approaches to handle this task using computational fluid dynamics. One option is to track the particles individually using Newton's second law of motion, while accounting for, or neglecting, particle collisions and fluid drag. This approach is known as Lagrangian modelling. Another option is to apply a similar model to the sand particles as is done for fluids in general. Instead of averaging the

62

motion of molecules to obtain average local pressures and velocities, sand particles are considered. The equations so obtained are similar to the Navier-Stokes equations. This approach is known as Eulerian modelling.

The computational effort required for Lagrangian modelling depends on the number of particles that need to be considered. Currently, this only allows the simulation of very small fluidised beds, which are of little industrial significance. To adequately account for collisions within fluidised beds using the Lagrangian approach, the discrete element method has been developed. Examples of the application of this method to small fluidised beds containing relatively large particles are provided by Tsuji et al[121] and Hoomans et al[122]. Considering the industrial orientation of the work reported in this thesis, the discrete element method for Lagrangian modelling of fluidised beds was not pursued any further.

TWO-PHASE FLUID BED MODEL

The Eulerian approach treats sand particles in a very similar fashion as standard fluid mechanics treats molecules. The main differences are firstly that collisions between the sand particles are not perfectly elastic, and secondly that sand particles are much larger than molecules. The Eulerian approach will fail when the particle concentration is too low and the dimensions considered are too small. This is quite comparable to the limitations of standard fluid mechanics, which will have to be modified for very low pressures and very small dimensions, as individual particles can no longer be averaged to give for example an average pressure.

The equations for the solid phase are very similar to the standard Navier Stokes equations. They were first derived by Gidaspow[123]. Each phase has its own set of equations that are solved individually, but linked through inter-phase transfer terms. The equations for continuity, momentum and energy are as follows.

Continuity:

$$\frac{\partial}{\partial t}(r_\alpha \rho_\alpha) + \nabla \bullet (r_\alpha \rho_\alpha \mathbf{U}_\alpha) = \sum_{\beta=1}^{N_P}(\dot{m}_{\alpha\beta} - \dot{m}_{\beta\alpha})$$

63

Momentum:

$$\frac{\partial}{\partial t}(r_\alpha \rho_\alpha \mathbf{U}_\alpha) + \nabla \bullet (r_\alpha (\rho_\alpha \mathbf{U}_\alpha \otimes \mathbf{U}_\alpha - \mu_\alpha (\nabla \mathbf{U}_\alpha + (\nabla \mathbf{U}_\alpha)^T)))$$

$$= r_\alpha (\mathbf{B} - \nabla p_\alpha) + \sum_{\beta=1}^{N_P} c_{\alpha\beta}{}^{(d)}(\mathbf{U}_\beta - \mathbf{U}_\alpha) + \mathbf{F}_\alpha + \sum_{\beta=1}^{N_P}(\dot{m}_{\alpha\beta}\mathbf{U}_\beta - \dot{m}_{\beta\alpha}\mathbf{U}_\alpha)$$

Energy:

$$\frac{\partial}{\partial t}(r_\alpha \rho_\alpha H_\alpha) + \nabla \bullet (r_\alpha (\rho_\alpha \mathbf{U}_\alpha H_\alpha - \lambda_\alpha \nabla T_\alpha))$$

$$= \sum_{\beta=1}^{N_P} c_{\alpha\beta}{}^{(h)}(T_\beta - T_\alpha) + \sum_{\beta=1}^{N_P}(\dot{m}_{\alpha\beta}H_\beta - \dot{m}_{\beta\alpha}H_\alpha)$$

where r refers to the volume fraction, the subscripts α and β to the respective phases and **B** to body forces

In order to obtain the interphase momentum transfer term in regions with a gas volume fraction less than 0.8 the Ergun equation[124] is adapted:

$$c_{\alpha\beta}{}^{(d)} = 150 \frac{(1-r_\alpha)^2 \mu_\alpha}{r_\alpha d^2} + 1.75 \frac{(1-r_\alpha)\rho_\alpha |\mathbf{U}_\beta - \mathbf{U}_\alpha|}{d}$$

In regions with lower particle volume fractions a modified form of the single particle drag correlation is used instead:

$$c_{\alpha\beta}{}^{(d)} = \frac{3}{4} \frac{C_D}{d} r_\beta \rho_\alpha |\mathbf{U}_\beta - \mathbf{U}_\alpha| (1 - r_\beta)^{-1.65}$$

The drag coefficient C_d is obtained from the particle Reynolds number:

$$Re = \frac{\rho_\alpha U d}{\mu_\alpha}$$

$C_d \quad = 24\,Re^{-1}(1+0.15Re^{0.687}) \qquad \text{for Re}<1000$

or $\quad = 0.44 \qquad\qquad\qquad\qquad \text{for Re}>1000$

Theory and equations relevant for entrainment, heat transfer and reaction kinetics are explained in the respective chapters.

NUMERICAL SOLUTION OF THE EQUATIONS, MODEL DEFINITION AND BOUNDARY/INITIAL CONDITIONS

The equations are solved numerically using a pressure correction technique, commonly known as SIMPLE[125], and a semi-implicit method to handle the strong coupling between the two phases similar to the IPSA algorithm by Spalding[126].

The pressure correction technique roughly works as follows. First, a pressure field is guessed, for example the pressure may be assumed to be the same across the whole flow domain. Then based on that guessed pressure field the momentum equations are solved for the velocity components. Those velocity components are then substituted into the continuity equation, which may not be satisfied as the pressure field was guessed. The error in the continuity equation is then used to correct the pressure field, which in turn can be used to obtain a better estimate of the velocity components. The pressure correction technique is an iterative procedure that can be continued until the mass source residual, that is the error in the continuity equation, approaches zero.

The inlet boundaries are specified using the standard Dirichlet boundary condition with a constant velocity. The outlets are pressure boundaries.

The velocity and volume fraction of each phase is specified separately for the inlet boundaries, but is the same for all the cells allocated to a particular inlet boundary. It should be noted that any biomass feedpoint in the calculations performed for the work reported on reaction kinetics in chapter 7 represents an inlet boundary in the modelling. While any inlet boundary at the distributor is modelled with a gas phase volume fraction of 1 and a solids volume fraction of 0, any inlet boundary representing a feedpoint will have a gas phase volume fraction less than 1 with the remainder being occupied by biomass. The mass flow rate of each phase then depends on its density, the specified volume fraction and the specified velocity, which as said need not be the same for the two phases.

A symmetry plane was employed in some of the early simulations, so that only half the reactor was modelled. This procedure was later abandoned, as the behaviour of the two sides of the reactor is not symmetrical and the use of a symmetry plane is therefore not appropriate.

In some cases a jet, that is a small inlet region with a higher gas velocity, was used to artificially induce bubble formation. Initially it was believed that this might be necessary to break the symmetry of the bed, an issue that is discussed further in chapter 6. As explained there, it was found that numerical error would cause breaking of the symmetry without any need to induce bubbles.

The initial condition is no flow, or flow at the minimum fluidising velocity, and particles filling the bed up to a specified height (that is the volume fraction of particles is specified).

Other important solver settings and model choices in CFX that apply to all, or at least to a large majority of runs, are shown in tables 8 to 11. Important exceptions made for runs, from which data are presented in the text of this thesis, are given in a list, presented as an appendix, which also includes detailed information about each of those runs. The solver settings and model choices given in the following tables are stated in particular for the benefit of readers who wish to perform similar calculations. For an explanation of technical terms such as adaptive time stepping, Rhie-Chow interpolation or under-relaxation factors, which go beyond the introductory treatment of CFD provided in this thesis, such readers are referred to the CFD literature and the manuals accompanying commercial CFD codes. For users of CFX itself the sample 'command file' (CFX terminology that is explained

towards the end of this chapter) provided as an appendix may prove a more convenient source of information than the tables given below.

Solver setting	Selected value or option
Time step for fixed time stepping	0.00025 s
Initial time step for adaptive time stepping	0.00025 s
Minimum time step for adaptive time stepping	0.000000000025 s
Maximum time step for adaptive time stepping	0.00025 s
Time step multiplier for adaptive time stepping	5
Interval between increments	10
Time step divisor for adaptive time stepping	5
Maximum number of contiguous decrements	5
Minimum number of iterations per time step	2
Maximum number of iterations per time step	40
Differencing scheme in time	Backward difference Linear time differencing

Table 8 List of important transient solver settings

Solver setting	Selected value or option
Divergence ratio	10000
Convergence on	Mass source residual
Under relaxation for u velocity	0.65
Under relaxation for v velocity	0.65
Under relaxation for w velocity	0.65
Under relaxation for pressure	1.0
Under relaxation for enthalpy and temperature	1.0
Under relaxation for scalars	1.0
Under relaxation for volume fraction	0.65
Differencing scheme	First order, either central or forward differencing
Standard Rhie-Chow interpolation	Selected

Table 9 Important settings controlling the numerical solution of the equations

Solver setting/choice	Selected/pre-set value/option
Buoyancy	Selected for both phases
Buoyancy reference density	Gas/vapour phase density
Compressible flow options	Incompressible flow
Diffusion	Selected for scalars in both phases
Wall treatment	Zero shear stress boundary
Gas/vapour phase continuous or disperse	Continuous
Solid phase continuous or disperse	Disperse
Granular flow modelling	Kinetic theory
Coefficient of restitution	0.6111
Solid compaction modulus	-600
Compaction volume fraction	0.376
Modify solids velocity to 0 in cells with	A volume fraction less than 0.0001

Table 10 Important model constants and options

Solver setting/choice	Selected value or option
Grid spacing	0.01 m
Solid phase density	2440 kg/m^3
Solid phase viscosity	10^{-12} kg/ms
Gas phase density	1.2 kg/m^3
Gas phase viscosity	0.000018 kg/ms

Table 11 Other important settings or choices

Finally, it should be pointed out that all two-phase simulations were transient, as there is no steady state for fluidised beds; in other words the flow field keeps on changing.

PRACTICAL ISSUES IN RUNNING CFX

Tackling a CFD problem can be subdivided into three stages:

1. Pre-processing
2. Numerical solution
3. Post-processing
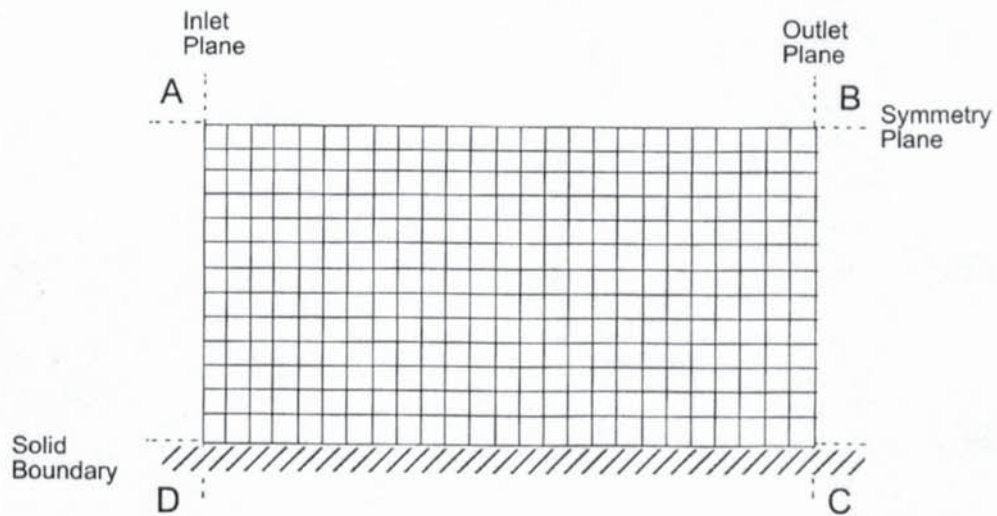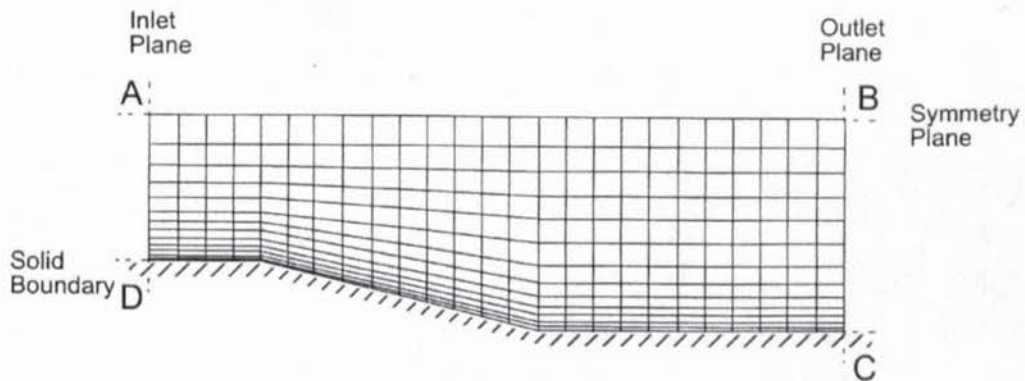
The points A, B, C, D in computational space map onto A, B, C, D respectively in physical space.

Figure 13 Body-fitted gridding by mapping physical space onto a stretched computational grid, figure adapted from the CFX user manual[127]

Pre-processing involves creation of a grid that adequately represents the flow situation being investigated. After the numerical solution, post-processing may be performed to obtain a graphical representation of the results. Both the specification of the numerical solution and pre-processing deserve some further explanation. Post-processing does not throw up any issues worth discussing within the scope of this thesis and will not be dealt with further.

Pre-processing

For pre-processing CFX offers three options. The first is a stand alone programme called CFX-Build, which allows geometry and grid creation through a graphical interface. CFX-Build is the preferred option for complex geometries.

The other two options involve editing text files also used to specify the numerical solution of the difference equations. CFX refers to a text file that contains instructions for how to solve the CFD problem, as the command file. Another text file may be used to provide CFX with extra Fortran code in subroutines.

The geometry and grid can either be specified with the help of the command file alone, if they are very simple, or, if they are slightly more complex, using both the command file and user Fortran. The latter option is illustrated in the appendices.
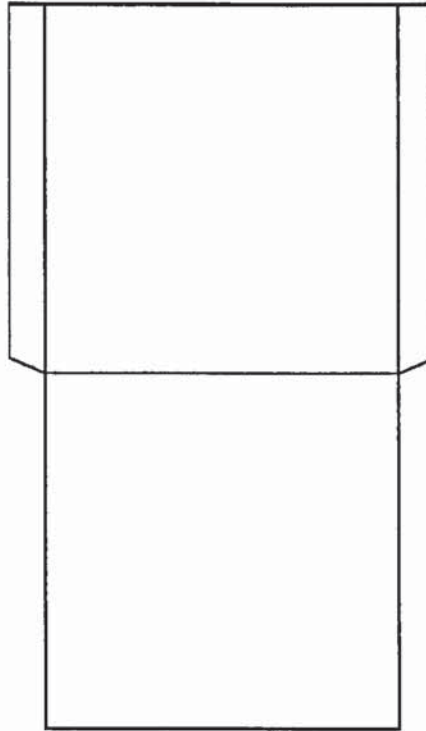
Figure 14 Example of multi-block structure with four blocks

The grid used in CFX is body-fitted and allows a multi block structure. These terms are best explained with the help of illustrations. Figure 13 shows how the orthogonal computational grid can be stretched, both to allow denser gridding in one region of the flow domain, and to model geometries that are not rectangular.

Figure 14 illustrates the use of several blocks. When the geometry cannot easily be stretched into a single rectangle in computational space, the flow domain can be constructed out of several blocks that either are rectangular, or can be stretched to be rectangular in computational space. In the example illustrated in Figure 14, two of the blocks are rectangular already, while the other two can be easily stretched in the fashion illustrated in Figure 13. Excessive stretching of the computational grid can lead to numerical difficulties and should therefore be avoided.

In parallel operation CFX restructures and rearranges the blocks before proceeding with a numerical solution. Each node is then allocated full blocks, and information only needs to be exchanged between nodes for cells bordering the block boundaries. The main impact

71

this aspect of parallelisation has on writing Fortran subroutines is that one can no longer refer to specific blocks.

This is best illustrated with an example, where a specific block is referred to in the user Fortran:

```
     CALL IPREC('BLOCK-NUMBER-1','BLOCK','CENTRES',IPT,ILEN,JLEN,KLEN,
   +         CWORK,IWORK)
     DO 203 K=1,KLEN
       DO 202 J=1,JLEN
         DO 201 I=1,ILEN
           ...
201        CONTINUE
202      CONTINUE
203    CONTINUE
```

Because 'BLOCK-NUMBER-1' will disappear in the block restructuring undertaken for parallelisation, one has to implement a different loop structure:

```
     CALL IPALL('USER3D1','USER3D','PATCH','CENTRES',IPT,NPT,
   +         CWORK,IWORK)
     DO 111 I=1,NPT
       ...
111  CONTINUE
```

Instead of referring to a block, a "user patch" is now employed, which circumvents the block restructuring by being directly based on physical rather than computational coordinates.

The command file

Instructions to the solver are mainly given with the assistance of the "command file". It is helpful to briefly go through its structure. A sample command file is also given in the

appendices. The major headings of the command file are the following (a brief explanation of the section coming under each heading is given in italics):

```
>>CFX4
  general options
>>MODEL TOPOLOGY
  creation of the geometry
>>MODEL DATA
  properties and more detailed options
>>SOLVER DATA
  similar to MODEL DATA, but emphasis on numerical procedures
>>CREATE GRID
  grid generation
>>MODEL BOUNDARY CONDITIONS
  boundary conditions
>>OUTPUT OPTIONS
  options for presenting the output
>>STOP
```

A few examples of commands illustrate the procedure. To change the differencing scheme for pressure from central differencing (the default) to upwind, a forward difference, the following command is put into the section MODEL DATA:

```
>>DIFFERENCING SCHEME
  PRESSURE 'UPWIND'
  END
```

To specify the velocity through the inlet of phase1, that is of the fluidising gases, the following boundary condition may be specified in the command file:

```
>>INLET BOUNDARIES
  PATCH NAME 'GAS INLET'
  PHASE NAME 'PHASE1'
  VOLUME FRACTION 1.0
  V VELOCITY 0.35
  U VELOCITY 0.0
  END
```

73

This example is two dimensional, so both the u and v components of velocity needed to be specified. The "patch" referred to is a grouping of cells that must be specified beforehand, for example as follows:

```
>>CREATE PATCH
  PATCH TYPE 'INLET'
  PATCH NAME 'GAS INLET'
  BLOCK NAME 'BLOCK-NUMBER-1'
  PATCH LOCATION 1 1 1 20 1 1
  LOW .J
  END
```

While this short introduction to the structure of the command file is less than exhaustive, it is hoped that, together with the example given in the appendices, it will help the reader to appreciate the general procedure that needs to be employed to fully specify a CFD run. It may be remarked that flexibility in CFD currently comes at the price of a steep learning curve and some user unfriendliness.

5. Experimental Set-up

The experimental set-up employed is explained in this chapter. Furthermore, some experimental work of an ancillary nature, such as sieving or microscopic examination, is described. The experimental work can be divided into hot work, where the contribution of the author was of a contributory rather than a leading nature, 3-D modelling done exclusively by the author and 2-D modelling where the majority of the work was performed in collaboration.

3-D MODELLING

Initial work was performed on an existing glass and Perspex replica of Aston's 1 kg/h pyrolysis reactor (Figure 15). This cold flow rig was subsequently modified (see Figure 16) in line with the modifications performed on the actual 1 kg/h pyrolysis reactor. The motivation for the modifications is explained in chapters 6 and 8.
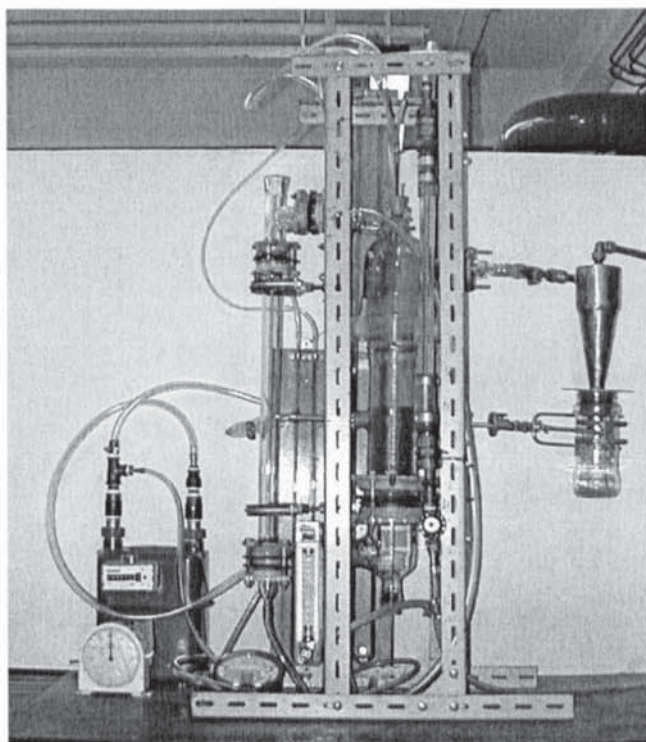
Figure 15 1 kg/h fluidised bed cold flow model
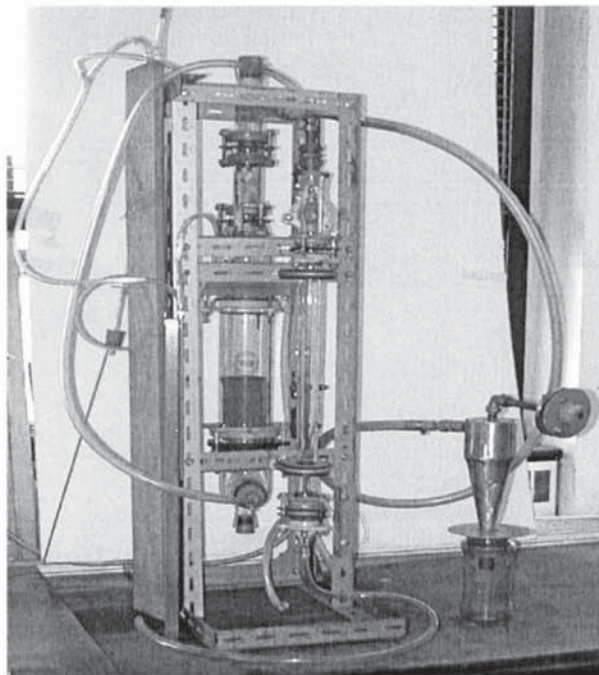
Figure 16 Modified 3-D model

The dimensions of the hot reactor and the original cold model are illustrated in Figure 17. There are some minor differences, for example the cross-sectional area of the cold rig is about 5.5% larger than for the hot reactor. These can be explained by the need to use
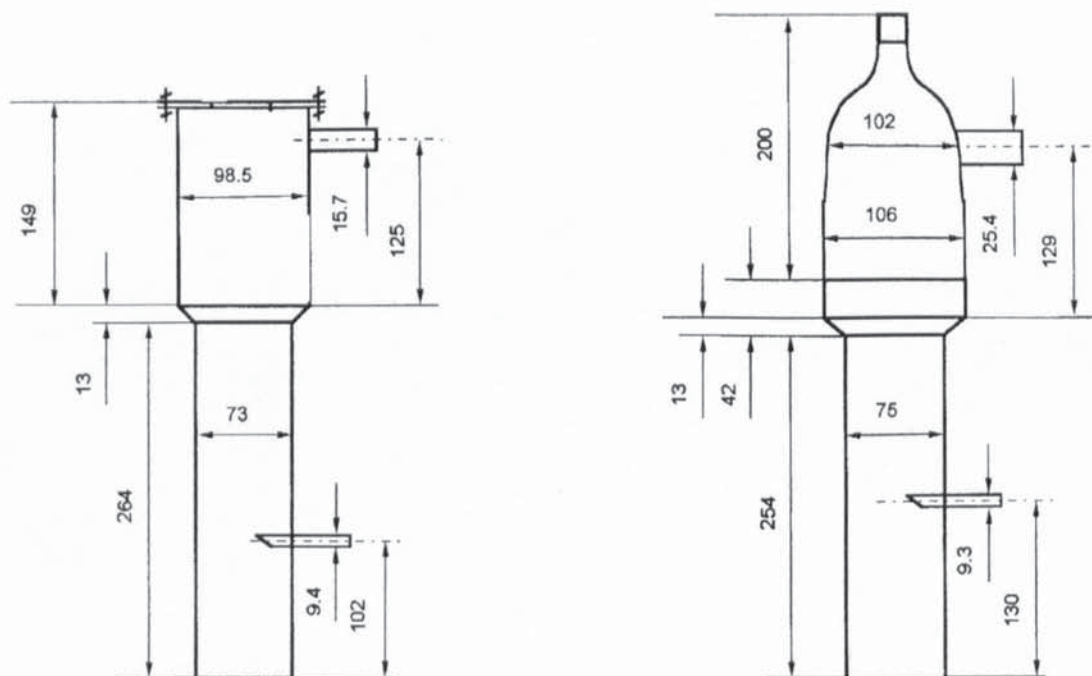
Figure 17 Left, hot reactor, right, cold model, all dimensions in mm, figure based on Wunder[10]

available components rather than specially fabricated ones. The main construction material used was glass. The distributor consisted of a perforated plate. There were 96 holes with a diameter of 0.5 mm.

The dimensions of the modified cold flow model are illustrated in Figure 18 and also in Figure 51 in chapter 6 where a picture based on CFD simulation is shown. The annulus was manufactured out of Perspex rather than glass. In order to implement the modification, all the glassware on top of the distributor had to be changed. The diameter of the lower section, however, stayed the same.
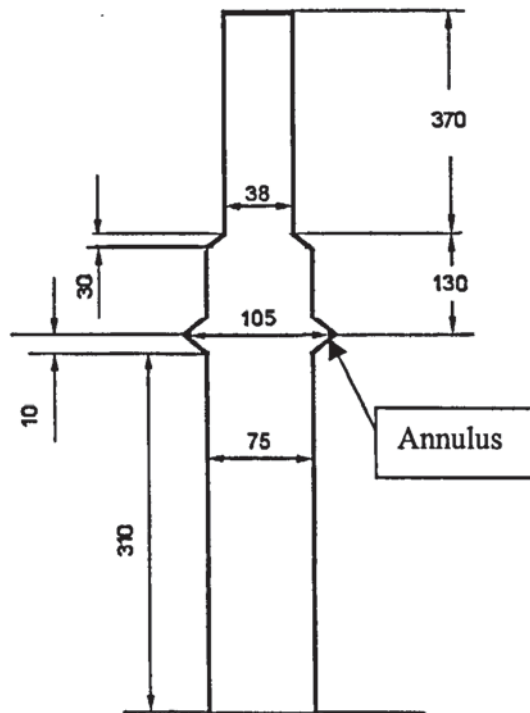
Figure 18 Modified cold model, all dimensions in mm

The 1 kg/h and 5 kg/h hot pyrolysis reactors were modified in a similar fashion as the cold flow model, namely a narrowing in the freeboard was introduced. This was done by introducing a dummy cyclone rather than a thinner freeboard. This modification is illustrated in Figure 19.
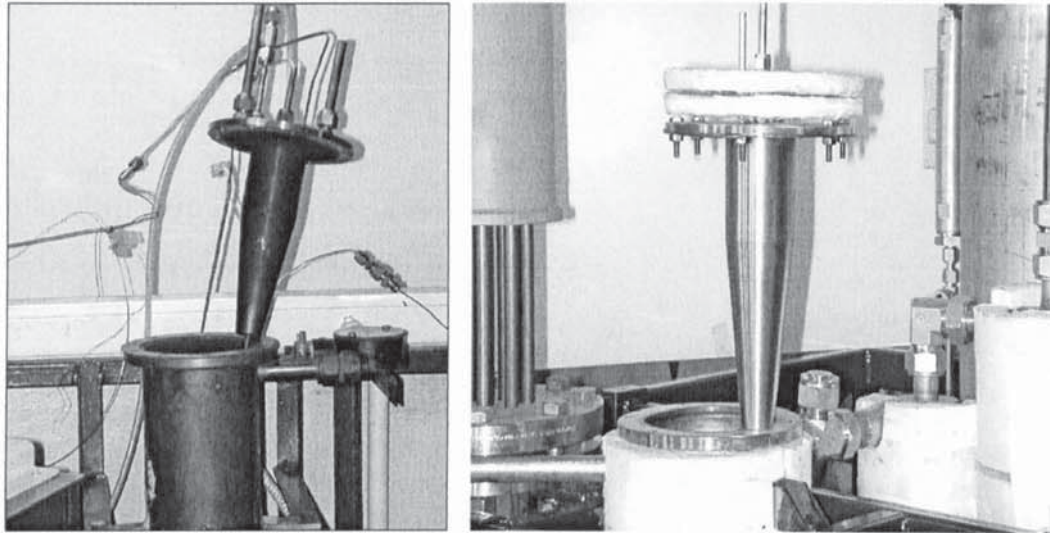
Figure 19 Dummy cyclone, left, 1kg/h, right 5 kg/h hot pyrolysis reactors

While a reactor that includes a widening with a similar purpose as the annulus used on the cold flow rig has been constructed, it has not yet been used for experiments. A CFD simulation of that modified 5 kg/h reactor is illustrated in Figure 54 in chapter 6, while a picture of this further modification to the 5 kg/h reactor is shown in Figure 20. A discussion of advantages gained by employing a freeboard widening can be found in chapter 8.
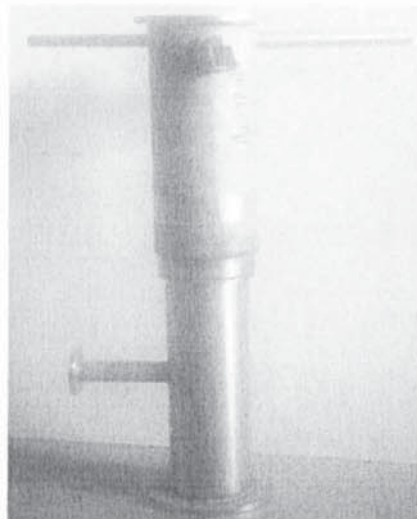
Figure 20 Further modification of the 5 kg/h reactor

A simplified process flow diagram is shown in Figure 21. A similar configuration was used to determine the terminal velocities of sand and char particles. Instead of the fluidised bed,

a 1 inch (2.54 cm) tube was employed for that task, and the cyclone was not required. The technique used for determining terminal velocity is explained in chapter 8, where its importance for entrainment is discussed in detail.
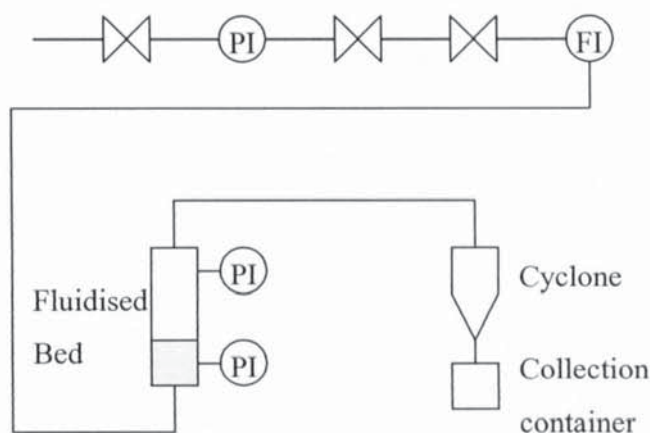
Figure 21 Simplified process flow diagram for the cold flow rig

5 KG/H PYROLYSIS REACTOR

While the author's involvement with the actual running of experiments on the 5 kg/h pyrolysis reactor was of a more contributory rather than leading nature, this rig was the subject of a considerable fraction of the CFD modelling work and deserves detailed description. A process flow diagram is shown in Figure 22.

Biomass is stored in a hopper and metered out via a screw feeder. A small amount of entraining gas is then employed to feed the biomass via a fast screw to the pyrolysis reactor. An illustration of a CFD simulation of that reactor is given in Figure 54 in chapter 6. The total height of the reactor is 73 cm, the diameter is 12 cm and the initial height of the sand is 30 cm. The pressure in the reactor is close to atmospheric and the temperature around 500° Celsius. Residence times are generally under 2 seconds. Char is removed from the reactor via entrainment together with the fluidising gases and organic vapours released by the pyrolysis reaction. The char is then separated in two cyclones and collected in two char pots. The vapours are then rapidly cooled and condensed in a quench column that uses isopar and some recycled bio-oil as the quench liquid. To keep the quench column close to room temperature, heat is exchanged with cooling water. The isopar and bio-oil are then stored in a tank, and recirculated to the top of the quench column by a pump. The

79

remaining vapours and incondensable gases are then passed through an electrostatic precipitator.
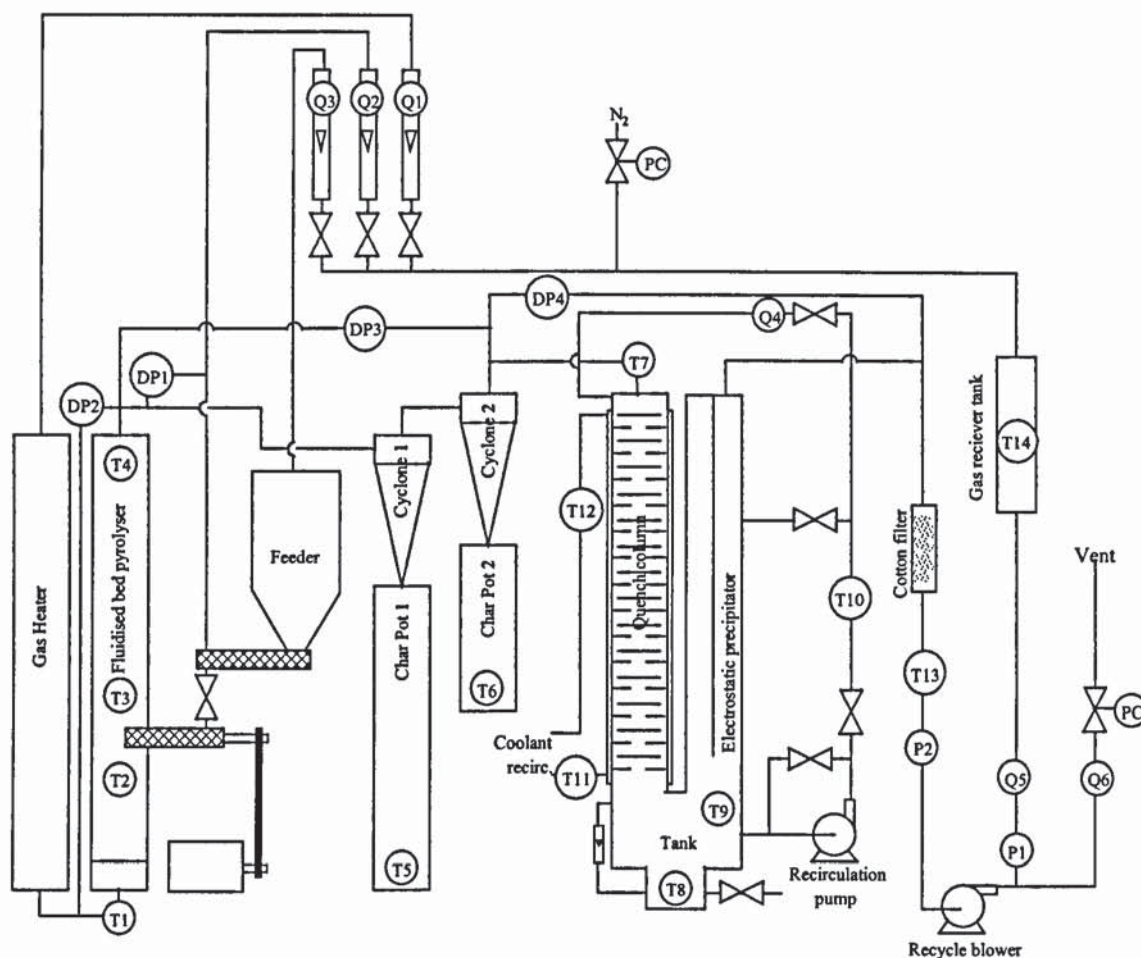
Figure 22 Process flow diagram of the 5 kg/h reactor, adapted from Hague[128]

This is necessary to remove aerosols carried along by the gases. A fraction of the bio-oil and isopar is also recirculated to the electrostatic precipitator in a similar manner as for the quench column. The remaining incondensable gases are then passed through a cotton filter, which is employed to protect downstream equipment in case of failure of the electrostatic precipitator. A small fraction of the gases is analysed via an on-line GC. The bulk of the gas is recycled with the help of a powerful blower. A fraction of the gas may then be vented while the remainder passes through a tank used to buffer surges in the gas flow rate. Then the flow is divided into two or three streams. The bulk of the gas is sent to the reactor via a heater. A small amount is used to help with the transport of the biomass to the reactor. Some gas can also be diverted to the top of the feeder, though this was not usually

done. After finishing with a run, the bio-oil and isopar in the collection tank will separate and the bio-oil can then be withdrawn. Likewise, the char pots are then emptied and the char is weighed and analysed. For an accurate mass balance all the equipment, where this is practicable, is weighed before and after the run. For equipment, where this is not practicable, the organic residues remaining inside can be dissolved in an organic solvent such as methanol or ethanol and then weighed after evaporation of that solvent. Before a new run can be started, the rig needs to be flushed with nitrogen and heated to the operating temperature, which generally requires a few hours.

2-D MODEL

A 2-D (that is with one of the three dimensions significantly smaller than the other two) cold flow model was built later on and used to investigate the scope for extrapolation from 2-D to 3-D work, and also for easier variation of geometry and scale. A conceptual illustration of the 2-D rig may be found in Figure 23 and a photographic illustration in Figure 24. A number of detailed engineering drawings can be found in the appendices. The flow could be varied between 0 and 160 l/min. The thickness of the model (10 mm) was chosen to be sufficiently large to avoid substantial wall effects and is comparable to other 2-D work found in the literature which employed thicknesses ranging from 8 to 15 mm[129,15,130]. Furthermore, several holes were drilled at the side of the rig to allow the performance of pressure readings with transducers. Those holes were at heights of 1.5 cm, 5.5 cm, 15 cm, 30 cm, 45 cm and 63 cm.

Plate glass

Air outlet

Movable plastic strips

Distributor

Air inlet

Plenum
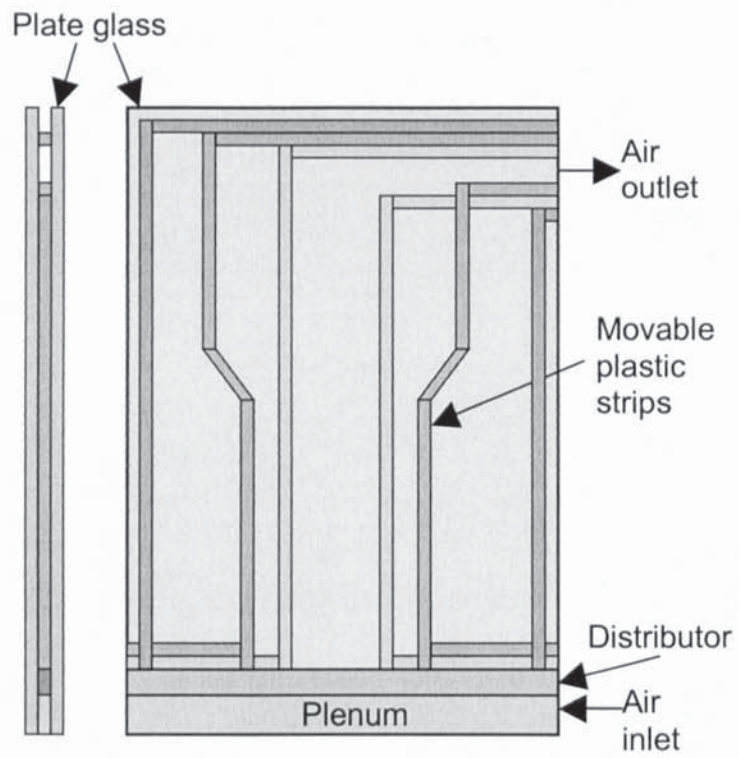
3 configurations are shown, but only one is used at a time

Figure 23 Conceptual illustration of 2-D rig
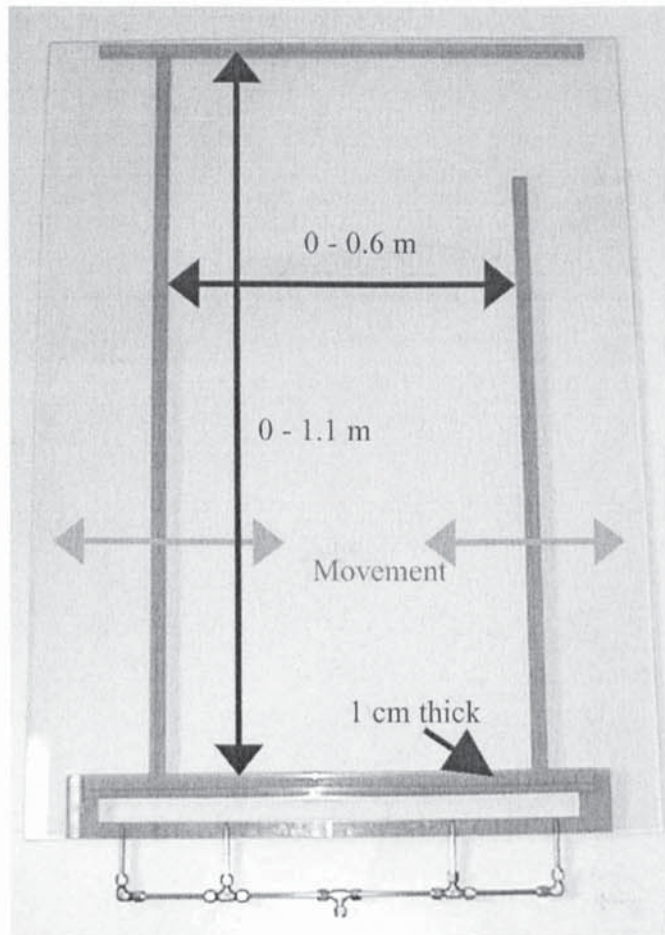
Figure 24 Photographic illustration of 2-D rig

Main construction details

To prevent scratching of the glass by the fluidised sand particles toughened glass panes with a thickness of 6 mm were used. This gave satisfactory performance, though thicker glass panes could have reduced the effect of bending. The material of the walls and the distributor consisted of Perspex, which was chosen, as it is easy to machine allowing straightforward construction of new geometries. Perspex is not entirely translucent. However, the glass panes afforded an ample view, so that there was no need for this.

The distribution of the fluidising gas was realised in two steps. First the incoming gas is divided across four smaller pipes. These pipes lead to the bottom of the distributor chamber, which consists of a gap of 3 cm employed to minimise the effect of the air jets emanating from the four pipes on the main distributor.
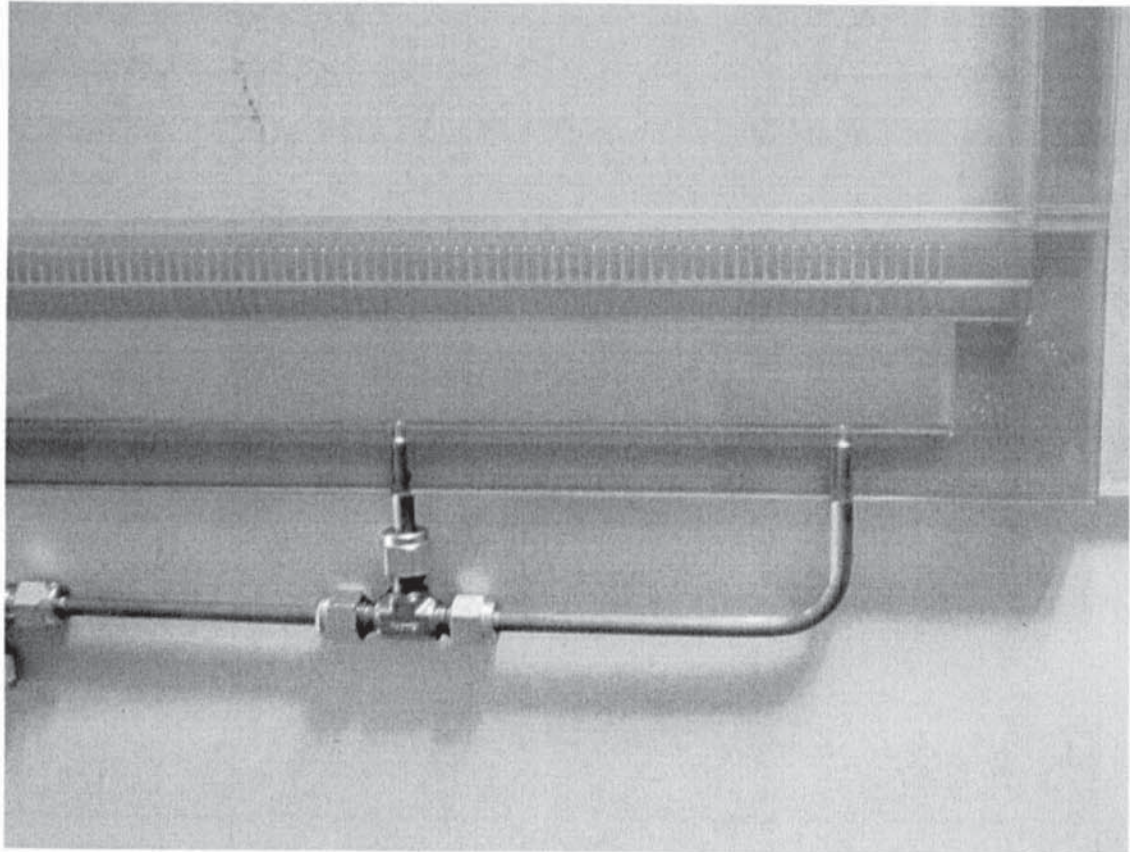
Figure 25 Photographic illustration of the distributor used on the 2-D rig

The main distributor was a strip of Perspex with a length of 60 cm, a width of 2 cm and a height of 1 cm. Holes with a diameter of 0.5 mm were drilled every 4 mm. To reduce the pressure drop and for easier machining (drill bits as small as 0.5 mm in diameter are prone to breaking) the first section of these holes was drilled with a 1 mm drill bit and only for the final section a 0.5 mm drill bit was used. A photographic illustration of the distributor is shown in Figure 25.

For good gas distribution, it is essential that the gas distributor has a sufficient pressure drop[131]. The maximum fraction of the area of the distributor that should be taken up by the distributor holes is given by the following equation:

$$f_{or} = \frac{u_W}{C_d} \sqrt{\frac{\rho_{gw}}{2\Delta P}}$$

For a velocity of 0.25 m/s, which is close to the minimum fluidising velocity, and a bed pressure drop of 0.05 bar, the above equation gives f_{or} as 0.0049, which indeed works out as roughly 125 holes with a diameter of 0.5 mm spaced every 4 mm.

Clamping was employed to press the two glass panes onto the Perspex strips. The material used was aluminium, which was chosen as it is light, strong, easy to machine and still reasonably priced. The clamping consisted of U-sections, which contained threaded holes every 10 cm on both sides of the U-sections. To put pressure onto the glass plates, screws were inserted into the U-sections and tightened. In addition, the U-sections constituted a sturdy frame for the rig.

The 2-D cold flow model was designed for easy modification, in order to allow the investigation of a number of geometries. Therefore a method had to be found that would seal the rig effectively, while permitting straightforward and quick dis- and reassembly. At first, it was attempted to achieve this by using rubber strips with a thickness of 3 mm that were inserted between the Perspex and the plate glass panes. This method only worked at small velocities, but was ineffective at greater velocities, as the pressure in the distributor chamber would become so high as to force open leaks between the glass and the Perspex strips. It was attempted to remedy this problem by putting vacuum grease onto the surface of the rubber strips to achieve better sealing. However, this still proved to be insufficient in securing an acceptable seal.

The main factor that made this approach impractical was that the pressure put onto the glass via the clamping would make it bend excessively.

After these unsuccessful efforts another method had to be found to seal the rig. Several types of glue were tried to replace the rubber strips with the aim of finding one that would bond sufficiently well, but at the same time would still allow ready disassembly. Standard silicone was found to be the best solution. After some further trial and error it was found that the silicone had to be allowed at least 48 hours to achieve satisfactory drying. Furthermore all surfaces had to be cleaned with ethanol when changing from one configuration to another in order to ensure that the bonding of silicone to the glass and the Perspex would not be disturbed by dust or grease on the surface. While the seal so achieved was flexible and strong, it would deteriorate with time. Also some difficulties were experienced with ensuring that the silicone would be distributed evenly.

For the heat transfer experiments a carbon steel plate and a second set of Perspex strips were added in between the two glass panes. This is illustrated conceptually in Figure 26. The reader is reminded that more detailed engineering drawings of all the features of the 2-D rig can be found in the appendices.
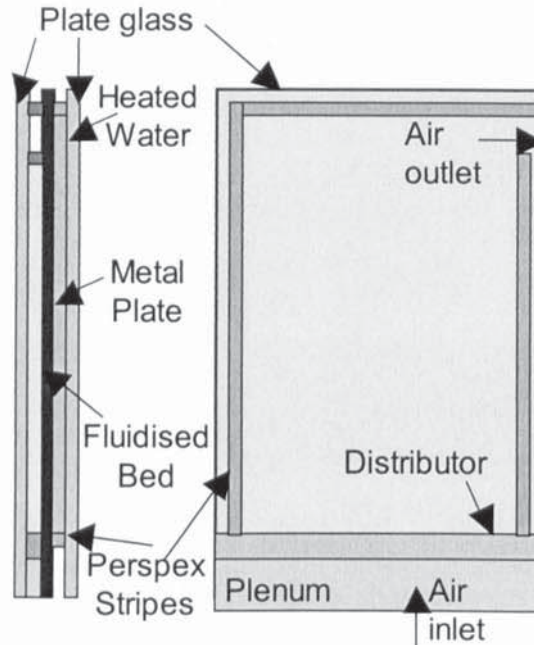
Figure 26 Conceptual illustration of the 2-D rig as used for heat transfer

The dimensions of the metal plate were the same as for the plate glass, with the exception of the thickness, which was only 1.7 mm. The metal plate divided the rig into two main chambers, one filled with water and the other containing the fluidised bed. To ensure better stability of the assembly three baffles were added to the water chamber. Nevertheless, for very high flow rates problems were experienced due to excessive vibrations and movement of the thin metal plate. It was therefore decided to replace the plate with a stronger one with a thickness of 3 mm, which still represents negligible resistance to heat transfer via conduction in comparison to the film coefficients.

Temperature readings were taken at three points at the wall on the water containing site of the rig and at four points on the fluidised bed site. Two of those four points were immersed

in the fluidised bed and the other two were located above it. Furthermore, the temperature of the pressurised air entering the system was recorded giving a total of eight measurements.

Additional details applicable to mixing and entrainment

For work on mixing and entrainment it was necessary to feed char to the 2-D model. This was achieved by using the twin-screw feeder and feed rate controller also employed on the 5 kg/h rig. Some of the fluidising gas had to be diverted to act as entraining gas, which was required to assist in the transport of the char from the screw feeder to the fluidised bed. The fraction of the overall gas flow diverted could be adjusted. By choosing connecting flexible tubing with a small diameter entraining gas speeds of roughly 1.5 m/s were achieved.

This feeder had to be calibrated for each material used. This was done by noting the mass of char metered out by the screw feeder for a number of controller settings.

For collecting the entrained sand and char particles the cyclone already used in the 3-D work was employed.

Data acquisition

For data acquisition a datalogger from Microlink, the 751 USB-unit, with 10 channels was employed. In the standard set-up, 8 channels were used for temperature readings with K-type thermocouples, while 2 channels were used for pressure indicators. The accuracy of the thermocouples was +/- 1.5 degrees Celsius and the range of measurement they were capable of –50 to 200 degrees Celsius. The pressure transducers were capable of measuring pressures in the range 0 to 1 bar and were accurate to approximately 100 Pa. The accuracy of the thermocouples was checked against several mercury thermometers, while the pressure transducers were calibrated using a column of water. The calibration of the pressure transducers was necessary, as the default output signal was a voltage and as no information was available from the instruction manuals as to the conversion factor between the voltage output and the measured pressure. To protect the pressure transducers from the sand in the fluidised bed, a metal wire mesh was employed. The frequency of the readings varied depending on the exact set-up, but could at most reach 20 readings per second. A short piece of piping was necessary to connect the pressure transducers to the fluidised

bed. It was checked by calculation that the short length of piping employed was unlikely to have a significant dampening effect on the measured fast pressure fluctuations. The datalogging software employed was the Windmill package and the computer used a 133 MHz Pentium S PC running Windows 98. The output of the datalogger was an ASCII file containing text and numeric data in columns, which were then imported into an MS Excel spreadsheet.

Description of the geometries used

A number of combinations of geometry and scale were investigated. The two scales chosen were widths at the base of 0.075 m and 0.5 m. The smaller scale was chosen for comparison with the 3-D cold flow rig (both before and after modification).

On the larger scale three geometries were investigated, a widening by 20%, a narrowing by 20% and a straight geometry. The total height was always 1 m, while the widening/narrowing occurred from a height of 0.5 m to a height of 0.52 m.

For the smaller scale, only two configurations were considered:

1. a total height of 40 cm, widening from 7.5 to 11 cm between heights of 25 and 27 cm
2. a total height of 80 cm, narrowing from 7.5 to 5 cm between heights of 40 and 42 cm

PARTICLE SIZE ANALYSIS

The bed material is sand, which is mixed with char produced by the pyrolysis of biomass. Three methods were used for size analysis: sieving, microscopic examination and laser diffraction. All the methods gave similar values for the particle diameters of sand and char from wood, though microscopic examination showed that many smaller char particles from wood were needle shaped and therefore had one significantly longer dimension that could not be captured by the other two methods. It was also found that care had to be taken not to overload the sieves with too much material, as proper separation would then no longer occur.

The different particles are illustrated in Figure 27 and the initial size distributions for sand and char in Figure 28 and Figure 29. Quantitative results of the microscopic examination

and of laser diffraction can be found in the appendices. A sample specification sheet for the sand provided by the manufacturer is also included.

Sieved char less than 351 microns
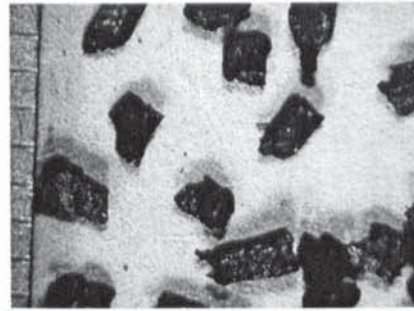
Sieved char greater than 1003 microns

Unsieved wood nominal size 3 mm.
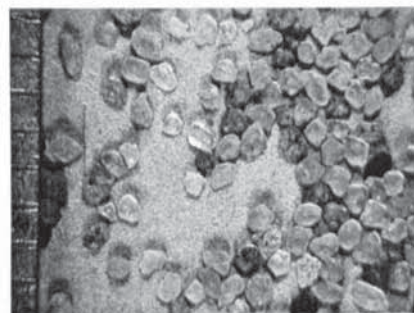
Sieved sand between 500 and 600 microns

Figure 27 Illustration of wood, char and sand particles
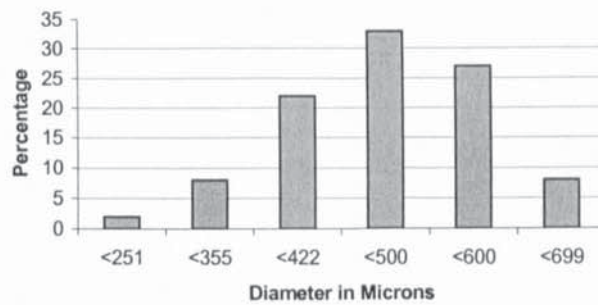
Figure 28 Size distribution of sand (average diameter 0.503 mm, u_{mf} 0.189 m/s)
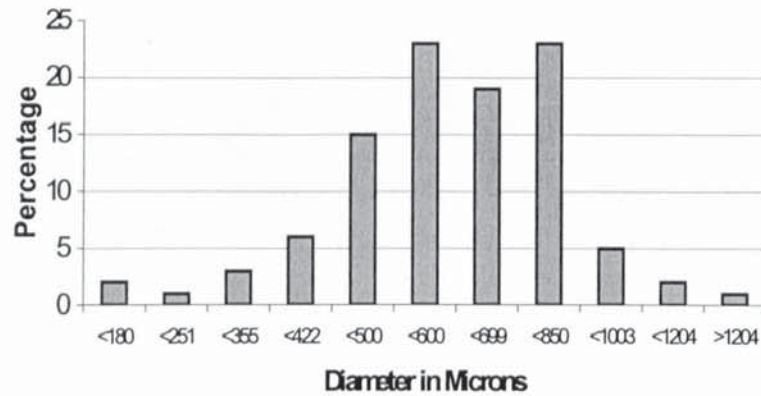
Figure 29 Size distribution of char from wood (mean particle diameter 0.550 mm, u_{mf} around[a] 0.21 m/s)

While sieving is the easiest and most frequently applied method of size analysis, it does suffer from drawbacks when particles of certain shapes are looked at. In particular needle shaped particles, such as those frequently found in small char particles from wood, will have much greater volumes than flat plates, a shape not uncommon in large barley straw particles, for the same range of diameters as given by sieving (see Figure 30 for an illustration). For example, a needle shaped particle of dimensions 190X190X3000 microns, would still pass through a 200 micron sieve, while a particle 210X210X100 microns would not pass through and nevertheless have a volume nearly 25 times smaller than the needle shaped particle. A description of the shape is therefore vital to adequately incorporate particle size data into the modelling effort. The matter is further discussed in chapter 8.
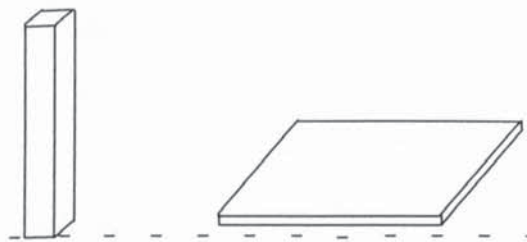
Figure 30 Illustration of the effect of particle shape on the determination of diameter by sieving

---

[a] The shape of the char particles is very irregular, which prevents an accurate calculation of the minimum fluidising velocity. An attempted experimental determination yielded channelling close to the expected minimum fluidising velocity.

6. Hydrodynamics

This chapter deals with the results obtained, both from computation and experiment, pertinent primarily to the hydrodynamics of a fluidised bed system. The effects of scale, particle size, fluidising velocity, temperature and geometry are looked at. A comparison between 2-D and 3-D work is performed also. The utility of rapid pressure fluctuations as a measuring tool for determining the quality of fluidisation and for validation of the CFD results in a larger working reactor is investigated. A few issues relating to the efficiency and reliability of the computational effort are also dealt with, notably the impact of the density of gridding.

INTRODUCTION

Fluidised bed hydrodynamics represent the most fundamental aspect that needs to be put on a firm basis before one can consider extensions that also include reaction kinetics, heat transfer, entrainment, mixing and abrasion. Furthermore, it is comparatively easy to validate modelling results by performing cold model experiments, a strategy that cannot be employed for validating the contribution to bed behaviour made by reaction kinetics.

A description of the equipment used for the experiments described in this chapter can be found in chapter 5. The theoretical background of the calculations presented here is explained in chapter 4.

In this chapter on hydrodynamics, validation of CFD calculations is discussed first, followed by a consideration of the usefulness of short duration pressure fluctuations as a tool for validation and monitoring in fluidised bed pilot plants. Finally, CFD predictions not yet validated are discussed, followed by a consideration of the degree of simplification that is the best compromise between the needs for accuracy and for preventing computing times from becoming excessive.

A list of all the modelling and experimental runs from which results are presented in the text may be found as an appendix. The runs have been given roman numerals for easy

cross-reference to this list, which provides a summary of the most relevant data for each run, such as, in the case of experiments, the geometry, flow conditions and measurements made, and in the case of CFD runs, the geometry, mesh size, boundary conditions and relevant solver settings

QUALITATIVE COMPARISON BETWEEN CFD AND EXPERIMENT

The qualitative fit of the experimental 2-D and 3-D arrangements and the CFD prediction is illustrated in Figure 31. The 2-D picture is taken from a video recording that was transformed into avi format using a video card. It is noteworthy that the structure depicted, a large bubble at the side, and a smaller bubble in the lower, opposite corner, occurred a large number of times during a few minutes of recording. This is an example of a typical flow structure for a given scale and geometry, i.e. commonly though not always one feature would occur in conjunction with another one (such as the large and small bubbles that can be seen in Figure 31). In other words, it was sufficient to go through just a few pictures to find one that compared well. In the particular and relatively short (about 5 seconds) video analysed to obtain the 2-D picture illustrated in Figure 31, a very similar bubble flow structure occurred three times. The other two instances are shown in Figure 32.

Volume fraction of gas phase

	1.0
	0.9
	0.8
	0.7
	0.6
	0.5
	0.37

2-D Experiment (I)   3-D Experiment (II)   CFD prediction (III)
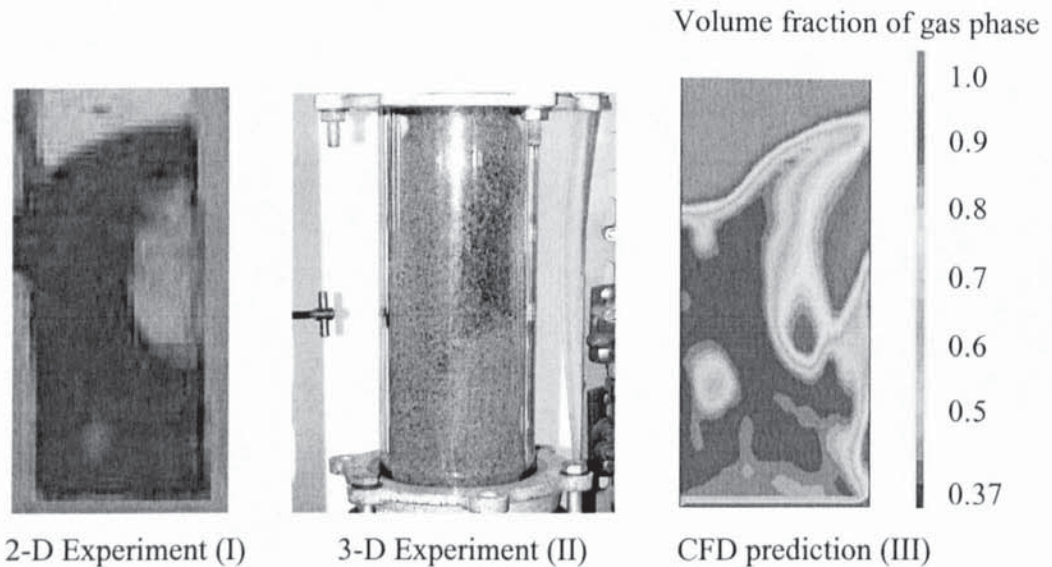
Figure 31 Comparison of 2-D experiment, 3-D experiment and CFD prediction
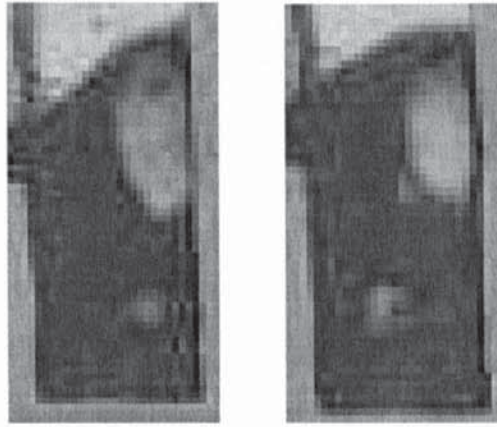
Figure 32 Similar bubble structures noted (I)

Movies or a series of pictures are even better at illustrating the good qualitative comparison between results generated by CFD and experiment than a comparison of single snapshots. As the software employed for turning a series of pictures into a movie required an unreasonable amount of operator time, only a small number of movies was produced from the CFD results, and comparison with videos taken from experimental runs was generally with a series of pictures from CFD. A selection of pictures and movies from CFD and of video recordings of experimental runs is included on a CD with this thesis.

The eruption of a bubble is shown as a series of consecutive snapshots separated by 0.04 seconds in Figure 33 and in Figure 34. The corresponding video recording is included on the CD in the directory videos as a file called runI. While features recur regularly and bed behaviour does exhibit distinguishing marker patterns, no bubble erupts in exactly the same fashion. To take account of this variability requires looking at more than one instance.

Judging the quality of agreement also needs to take account of small experimental errors and the resolution of the CFD calculations. It should be noted that it is difficult to achieve a constant superficial velocity of 0.3 m/s in the experiment with great accuracy. A 5% error in the thickness of the bed for example only translates into half a mm, which could come about through bent glass or differently compressed silicone sealant. Another source for error is represented by air line pressure, which will fluctuate slightly. It is estimated that the actual velocity may differ by up to around 10% from the target value.
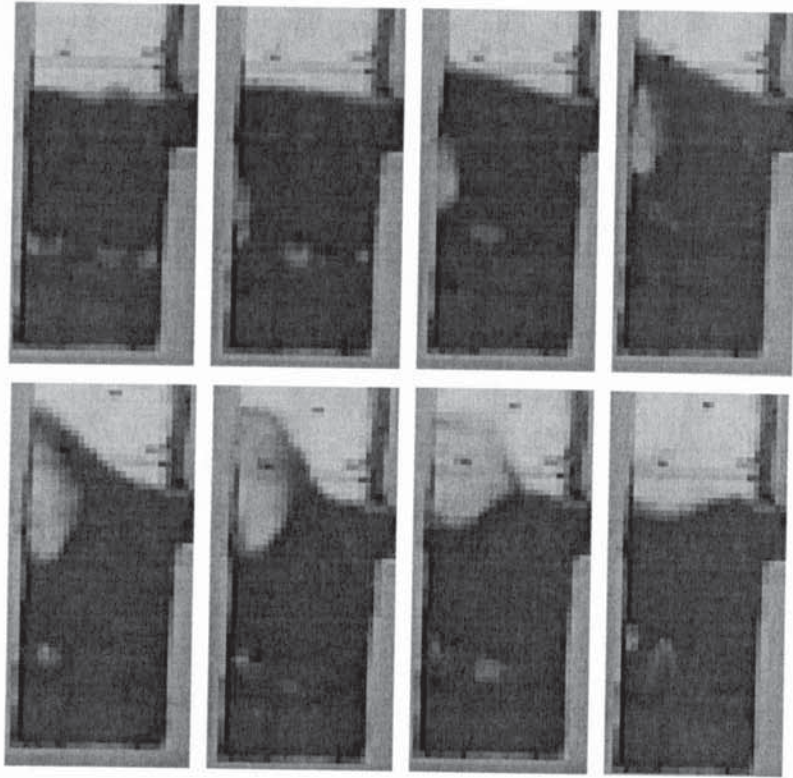
Figure 33 Bubble eruption 2-D experiment (I)
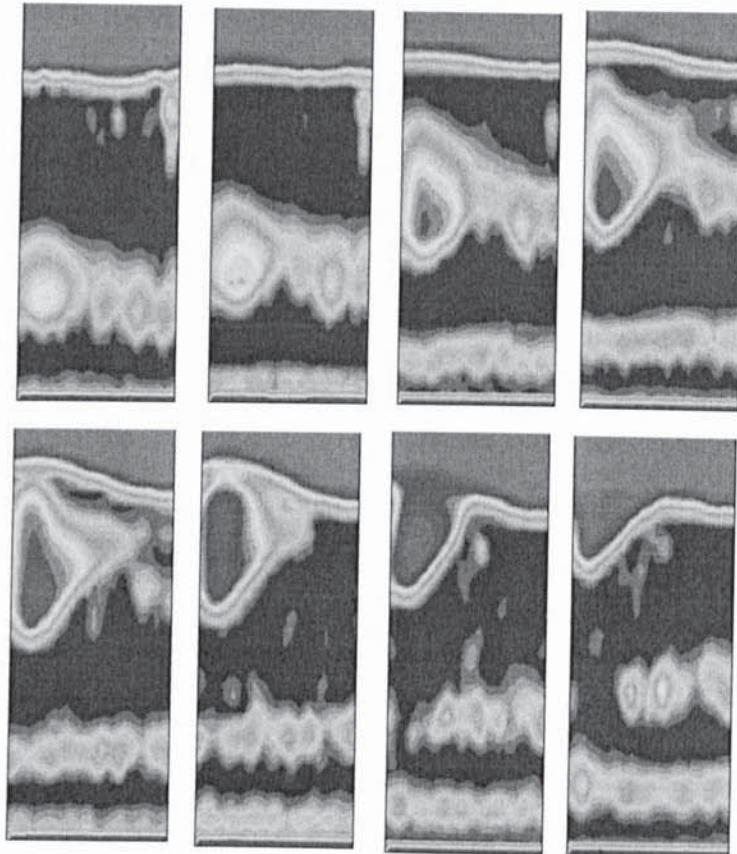
Figure 34 Bubble eruption, CFD (III)

The resolution is important when considering very small features, such as spray formation from erupting bubbles or the evolution of very small bubbles. CFD for example shows many areas of slightly smaller volume fraction in Figure 34, while experiment, in Figure 33, shows a few tiny bubbles in similar locations as indicated by CFD. As pointed out in chapter 4, Eulerian modelling will fail, when the dimensions of interest approach those of single particles. This is similar to standard hydro-dynamics, which likewise can no longer apply such concepts as gas pressure or viscosity once the dimensions of interest approach those of single molecules. Consequently, there is a limit to how much the mesh can be refined sensibly to resolve such small features as the tiny bubbles visible in Figure 33.

The post-processing software interpolates to indicate colours between grid points. It is important to keep this fact in mind when looking at the CFD generated pictures. Interpolation means that there are no sharp boundaries visible in the pictures, even when there is an abrupt change between two points. It also means that a single point with a slightly lower volume fraction appears as a small area of slightly depressed volume fraction.

3-D cold flow experimentation was rather limited in scale, one reason why 2-D experiments were undertaken. Figure 35 shows that the qualitative fit for larger scales is very good also.
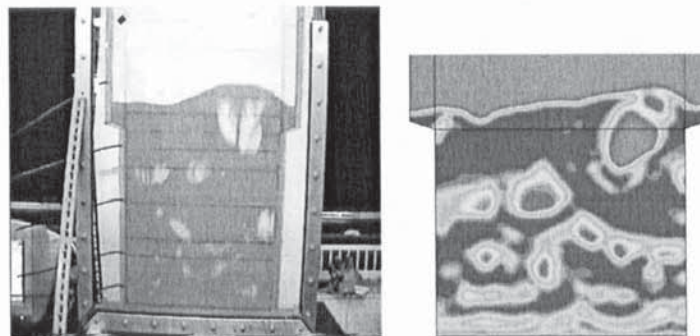
Figure 35 Comparison between 2-D experiment (IV) and CFD (V) on a larger scale (50 cm width, comparable to Wellman's pilot plant)

A video of the experimental run the picture in Figure 35 is taken from and a movie generated from CFD are included on the CD in the directory videos as runIV and runV

respectively. Two series of snapshots, again separated by 0.04 seconds, are shown as Figure 36.
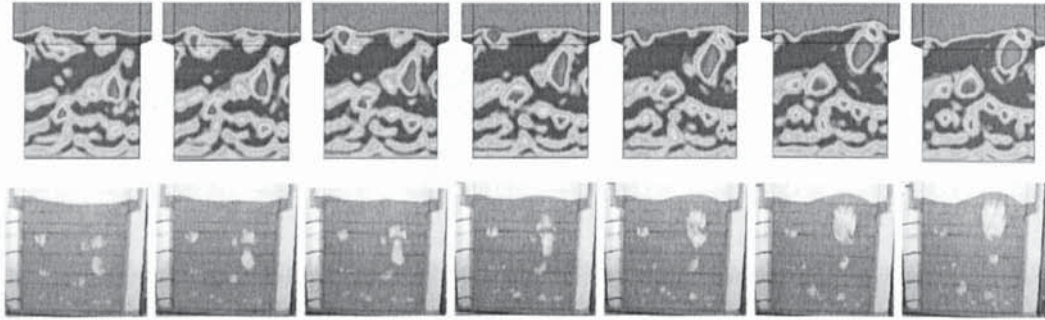
Figure 36 CFD (V) and experiment (IV) compared

It is noticeable that sand falls through larger bubbles in Figure 35 in a streak like fashion for the experimentally obtained picture, while this cannot be observed in the CFD simulation. As those streaks have a smaller dimension than the mesh spacing of 1 cm, a likely reason for this difference is the resolution of the CFD calculations. Further support is lent to this supposition by the fact that a sufficiently large bubble does exhibit comparable behaviour in CFD, as is illustrated in Figure 37. A movie made from the CFD calculations illustrated in Figure 37 is also included on the CD in the directory videos as runVI. The difference in behaviour shown by that movie compared to runIV and runV is striking.
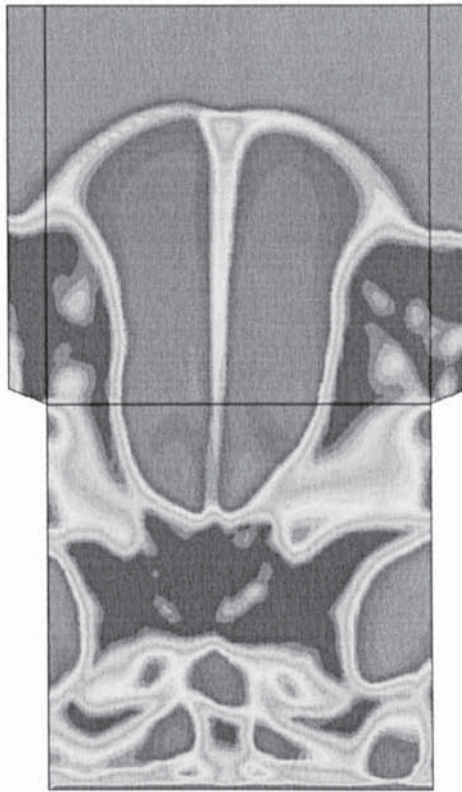
Figure 37 Possible effect of resolution on bubble appearance (VI)

A visual comparison between CFD and experiment has also been used by a few other authors for purposes of validation. One example is illustrated in Figure 38 and taken from a recent paper by Goldschmidt et al[132]. No visual comparison of CFD with experiment for scales of around 50 cm in diameter (comparable to that illustrated in Figure 35) has been found in the literature. The experimental set-up was either for a diameter of 15 cm or less, or other methods were used for purposes of comparison, such as measuring velocity fluctuations of the solids at a given point[133], measuring velocity/mass flux profiles[133,134] or determining the root mean square of the solids velocity by Laser Doppler anemometry[135]. It can be presumed that there are two main reasons for this state of affairs. Firstly, it is difficult to obtain graphical information from large scale reactors, particularly so of course in three dimensional ones. Secondly, computing requirements for performing simulations are large and have put such calculations out of the reach of the feasible until fairly recently.
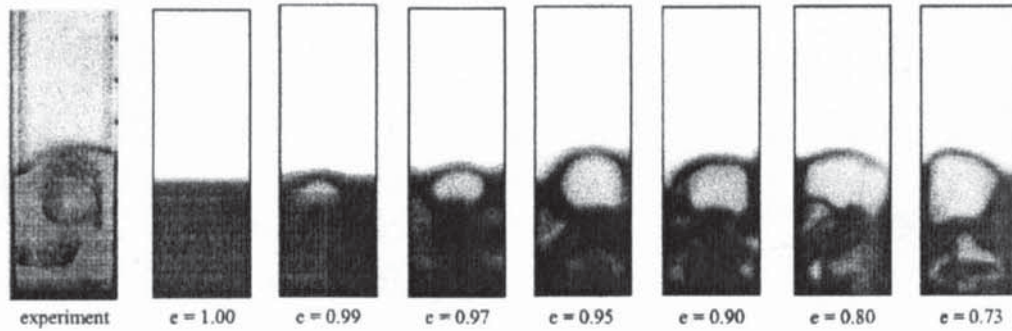
Figure 38 Example of the use of visual comparison between CFD and experiment for validation and model development taken from the literature (in this modelling approach e is an adjustable parameter, namely the coefficient of restitution for the particles)

BUBBLE VELOCITY

This variable was measured experimentally using a video camera. Several bubbles were analysed for each velocity and an average taken. Likewise a number of bubbles generated by the CFD software for the same conditions were examined. These values are also compared (see Figure 39) to a correlation for bubble velocity by Davidson and Harrison[136], which is widely employed in industry for design purposes[13]:

$$u_B = (u-u_{mf}) + 0.711 \ (g \ d_B)^{0.5}$$
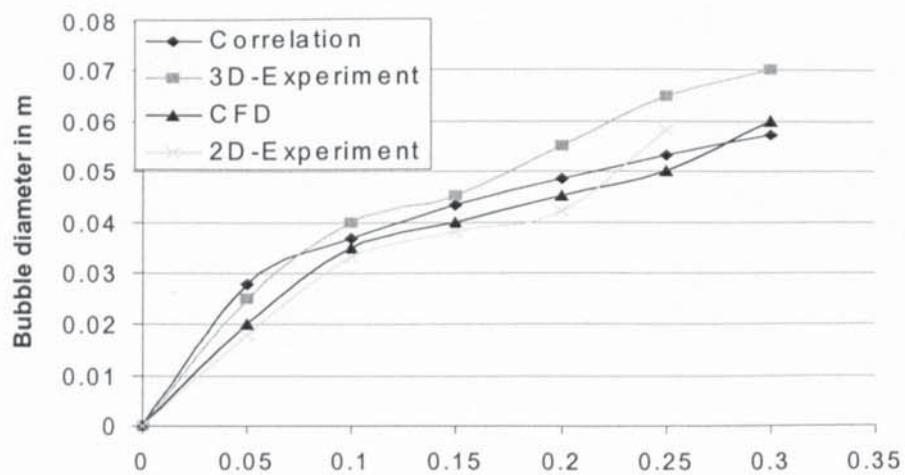
Figure 39 Bubble velocity (VII, VIII, IX)

There is quite a degree of variation between different bubbles. Even for exactly the same conditions they may vary considerably in terms of velocity, size and shape. This dynamic and irregular behaviour is very well captured in the CFD analysis and cannot possibly be obtained by a simple correlation that is only capable of giving an average.

It is also noteworthy that bubble velocity is only a well defined and easily measured variable for small reactor scales. At larger scales, the movement of bubbles is no longer a simple upward motion, but is of a rather more complex nature. This is illustrated in Figure 40, which should be compared with the ease, with which a bubble velocity can be deduced from the pictures shown in Figure 41.
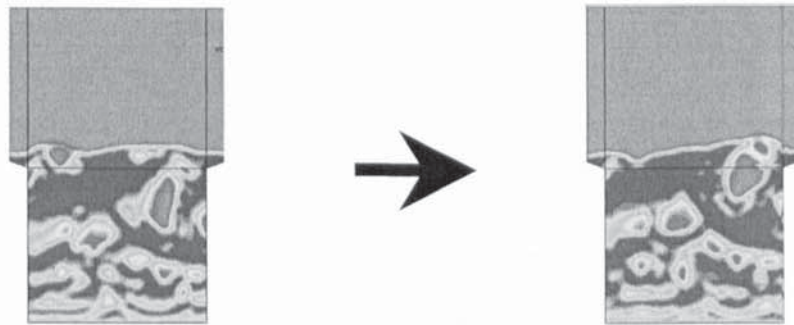
Figure 40 Illustration of bubble movement (V) for larger bed diameters (0.1 seconds between the two pictures, diameter 0.5 m)
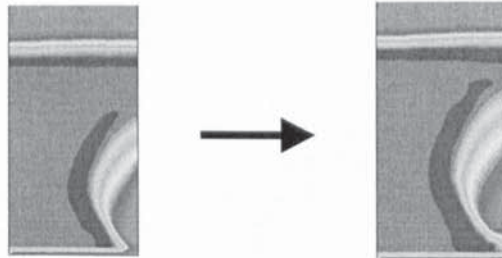
Figure 41 Illustration of measurement of bubble velocity with a well defined single bubble (X) at smaller scales (0.04 seconds between the two pictures)

BUBBLE DIAMETER

In comparison to the bubble velocity the diameter shows an even greater range of variation. Correlations therefore usually only give the maximum diameter rather than an

average that would be difficult to apply. A correlation by Mori and Wen[137] has been chosen for purposes of comparison (see Figure 42) with experimental and CFD results:

$$d_B = (u-u_{mf})^{0.4}*[1.49D^2-(1.49D^2-1.38g^{-0.2}A_B{}^{0.4})e^{-0.3h/D}]$$

The bubble diameter was taken as that of a circle with an equivalent area. The limiting volume fraction was taken as 75%. This choice was made for purposes of definitional clarity. The exact cut-off point should not have an impact on the comparison between CFD and experimental results. One could equally well have chosen 70% or 80%.
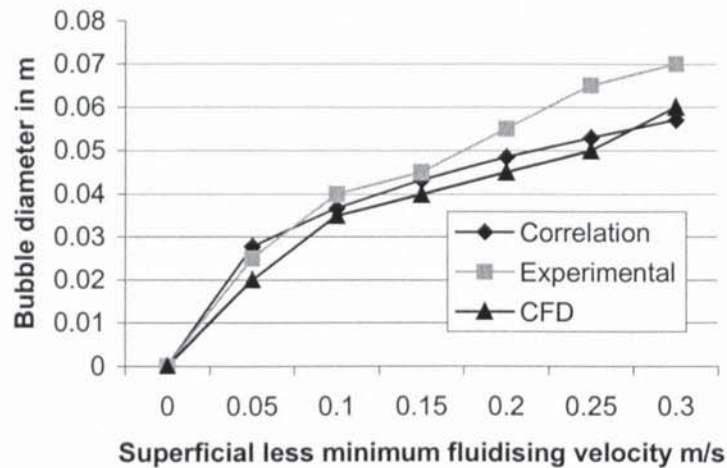
Figure 42 Maximum bubble diameter (VII, VIII)

The correlation by Mori and Wen predicts the actual maximum bubble diameter fairly well, though it underpredicts for higher minimum fluidising velocities. The CFD calculations give lower values for the maximum at all velocities in this particular comparison. One reason was the small number of bubbles that could be modelled within the available computing time in comparison to the number available for experimental study, a problem that has been much ameliorated by faster computing equipment for comparisons performed at a later stage. Furthermore, at higher velocities convergence problems were encountered again reducing the number of bubbles available for comparison. Convergence issues, however, have continued to be a major problem, as is detailed in chapter 9 and elsewhere in this thesis.

A comparison between 2-D and 3-D results has also been performed and is illustrated in Figure 43. It shows that the bubble diameters in 2-D and 3-D correlate well. In this particular instance, 3-D gives slightly higher bubble diameters.
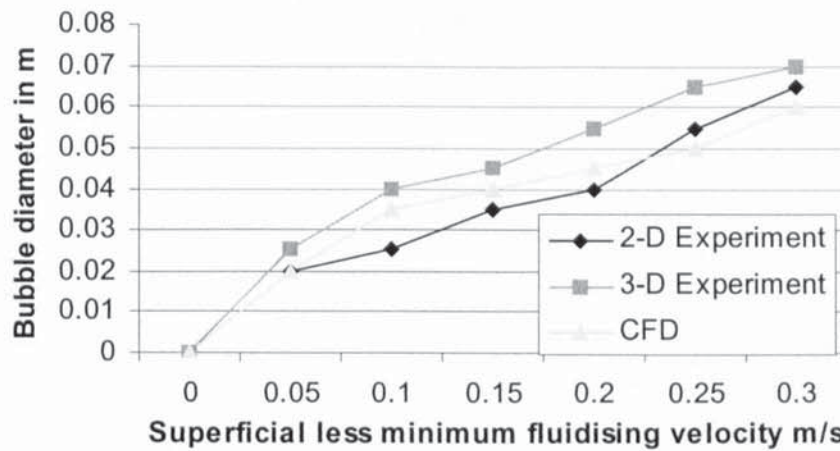
Figure 43 Bubble diameter obtained by 2-D, 3-D and CFD (IX, VII, VIII)

CFD predictions for the bubble diameter are also very good at larger scales, which could only be experimentally validated in the 2-D configuration. This is illustrated in Figure 44.
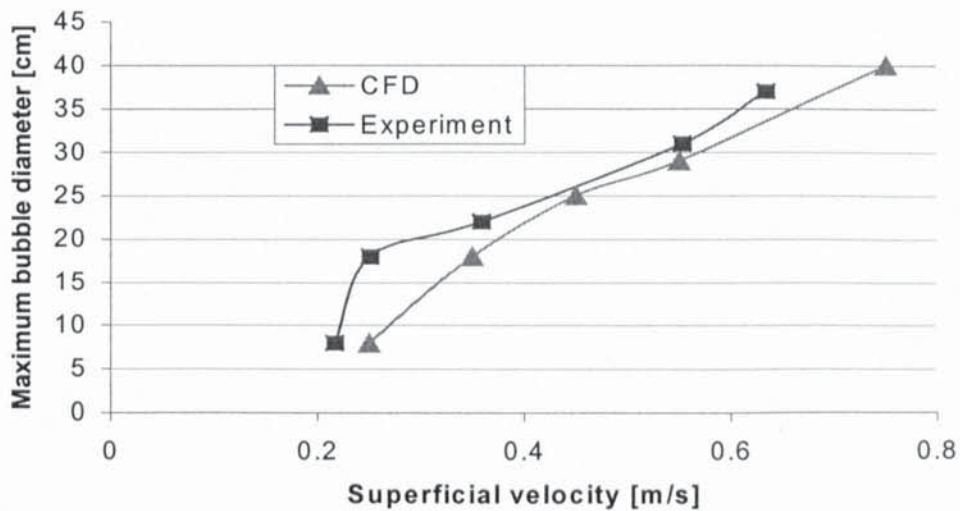
Figure 44 Bubble diameter for a larger reactor scale (XI, XII)

BED EXPANSION

The surface of the fluidised bed is not static, but rather subject to dynamic movement. For validation of the model the maximum height reached by the surface is therefore plotted in Figure 45.
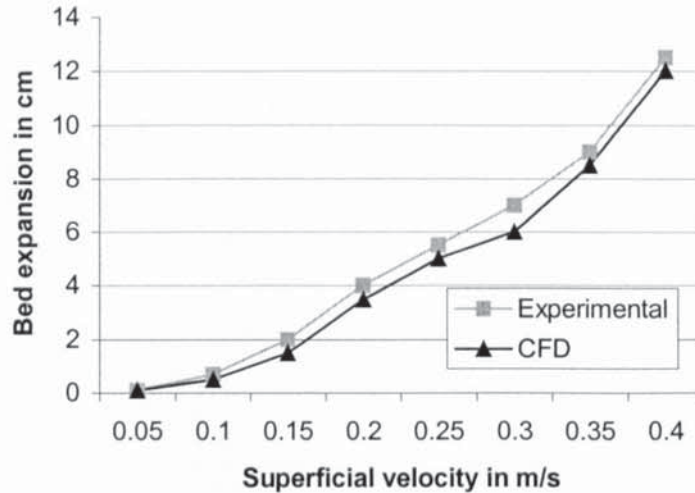
Figure 45 Bed expansion, experimental values from small 3-D rig (VII, VIII)

Values for bed expansion were measured by analysing videos taken of the fluidised bed in operation. For each configuration a number of bed heights were studied. CFD simulations of up to 40 seconds in length were then compared with experimental values using a standardised methodology:

The average height was taken over a number of frames that appeared typical. To judge what constituted typical behaviour visual observations of experimental bed behaviour were used, as this yielded considerably longer periods of observation than were available for CFD. Furthermore, construction of mpegs was only performed in a few cases, in general a series of snapshots available from the post-processing software included with CFX was deemed sufficient. The maximum height was the maximum height reached by the surface of the bed while still connected to the rest of the bed and just before spray formation became apparent. A typical 40 second recording was used for better comparability with the CFD results.

Results for maximum bed expansion applicable to a larger scale are illustrated in Figure 46 and show good agreement.
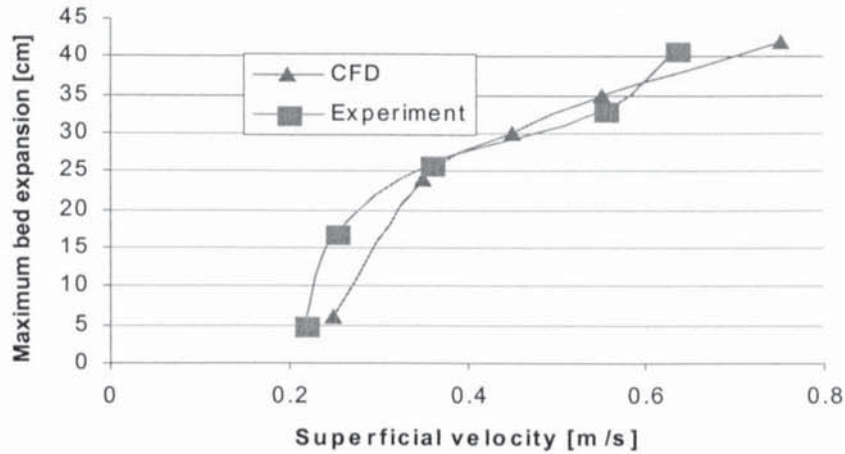
Figure 46 Maximum bed expansion (XI, XII)

Average bed expansion is much lower than maximum bed expansion, but shows very similar trends, as is illustrated in Figure 47. They are both important for the operating performance of the fluidised bed reactor.

Average bed expansion gives an indication of the heat transfer area available that is on average exposed to the body of the fluidised bed. As is pointed out in chapter 9, heat transfer is much greater between the body of the fluidised bed and walls than it is for heat transfer without the fluidised sand.
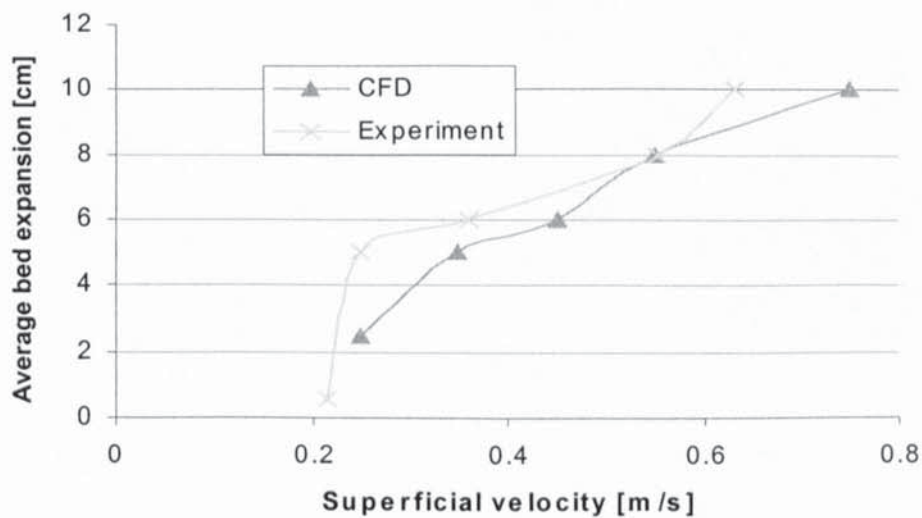
Figure 47 Average bed expansion (XI, XII)

The maximum height reached by the body of the bed, on the other hand, is of interest for determining entrainment, and the greater it is, the more easily sand and char will be entrained.

THE EFFECT OF PARTICLE DIAMETER

The particle diameter was found to have a considerable impact on fluidisation behaviour. Generally, lowering the particle diameter by 10-15% had a similar effect on bed hydrodynamics as raising the velocity by 5 to 10 cm/s. Three particle diameters were investigated specifically, namely 0.44 mm, 0.503 mm and 0.64 mm. It should be noted that these diameters are averages; sample size distributions are given in chapter 5. A very abbreviated selection of the CFD runs is given in Table 12.

Table 12 Sample list of CFD calculations performed for large scale 2-D rig

Config- uration	Velocity	u/u_{mf}	Particle Diameter	Density	Quality of Results	Time	Initial Sand Height
	m/s		m	kg/m^3		s	m
Standard	0.25	1.3	0.503	2440	good	5.2	0.33
Widening	0.55	2.9	0.44	2440	good	30	0.33
Widening	0.75	4.0	0.44	2640	good	5.2	0.33
Widening	0.35	1.9	0.503	2440	good	5.2	0.5
Standard	0.75	4.0	0.503	2440	bad	0.4	0.33
Standard	0.35	1.9	0.64	2440	good	2.5	0.33
Narrowing	0.35	1.9	0.44	2640	good	8	0.5
Narrowing	0.55	2.9	0.44	2640	good	8	0.5

A more detailed list can be found as an appendix. All the CFD calculations that varied the particle diameter were performed for comparison with experiments carried out on the large scale 2-D configurations.

An illustration of the impact of particle size on bed hydrodynamics is given in Figure 48. Apart from particle size all other variables are identical for the two figures.
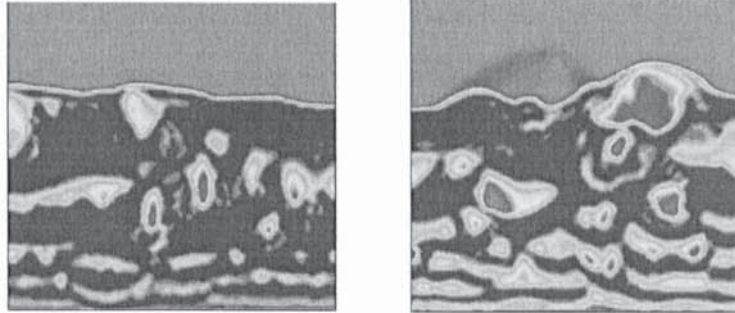
Figure 48 Comparison between fluid bed hydrodynamics for sand sized 0.64 mm (left, XIV) and 0.503 mm (right, XIII)

In the initial experiment where a particle diameter of 0.64 mm was examined it was noted that the visual comparison between CFD and experiment appeared to be unusually poor. It turned out that the reason was a sieving error – the sieves were too full, as mentioned in chapter 5 - and that after resieving the comparison between CFD and experiment was excellent. It has been suggested during the course of the work leading to this thesis that the comparison between CFD and experiment often appears to look too good to be true. One should stress in this regard that while the motion of individual bubbles is indeed quite random, there is a surprising amount of recurrent structures apparent in the overall picture presented by the movement of the bubbles. Furthermore, this overall picture appears quite different when fluidising conditions, such as the particle diameter, scale or fluidising velocity, are changed.

A quantitative comparison between experimental data and CFD calculations showing the effect of particle diameter is given in Figure 49. It should be said again that the qualitative comparison is in some respects even more meaningful than a quantitative comparison as performed in Figure 49. The measurement of the maximum bubble diameter, even with the best of efforts, is inherently rather difficult and at any rate does not capture the dynamic aspects very well. In other words, looking at pictures actually appears to be a much faster and reliable method of assessing the quality of the fit between experiment and CFD. As has been mentioned above, it was a visual assessment of the bubble behaviour that led to the discovery of an experimental error, rather than an assessment of such quantitative measures as for example maximum bubble diameter.

The accuracy of the quantitative measures is not of prime importance in the validation, that is there is no need to attempt to achieve a margin of error smaller than 10%.
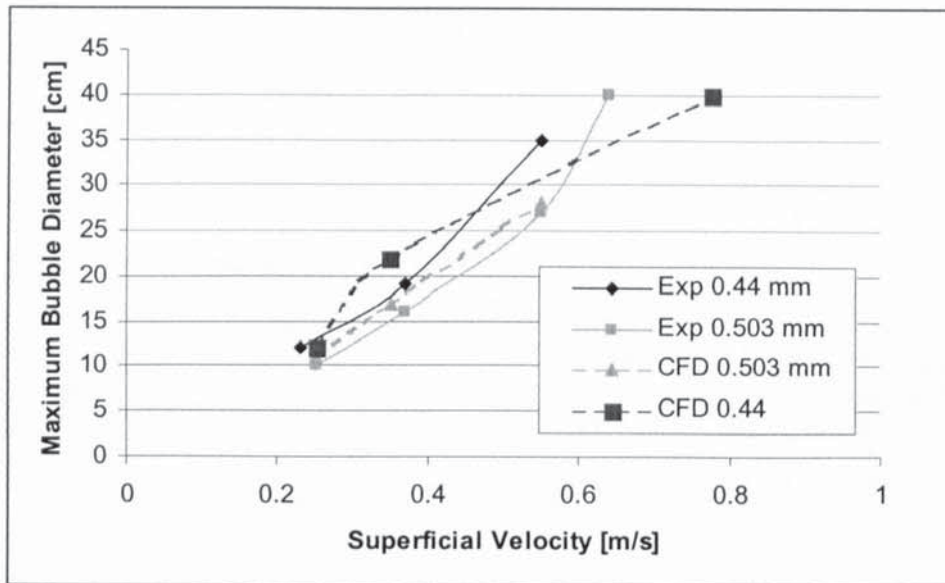
Figure 49 Effect of particle diameter on maximum bubble diameter (XI, XII, XV, XVI)

THE EFFECT OF PARTICLE DENSITY

As can be seen in Table 12 the particle density was also varied. The reason this was deemed necessary was that the particle density is not known accurately. Values from the literature and measurements undertaken with three different methods[10] varied by around 10%. It was therefore decided to check how great the impact of a small change in density would be and calculations were performed with values of 2440 and 2640 kg/m^3. A comparison is illustrated in Figure 50. The differences are minor in terms of the overall flow structure and largely random. This kind of difference would be expected from starting a run with minutely different start-up conditions. What is once again illustrated is that while details, such as for example the location of the large bubble at the side in Figure 50, change, the overall picture presented by a given combination of geometry, fluidising velocity and other variables is remarkably consistent. In other words, while there is randomness with the exact location of bubbles changing all the time, the combinations of size, shape and position are much less random and clear markers of a given combination of fluidising velocity, bed material and other variables.

106
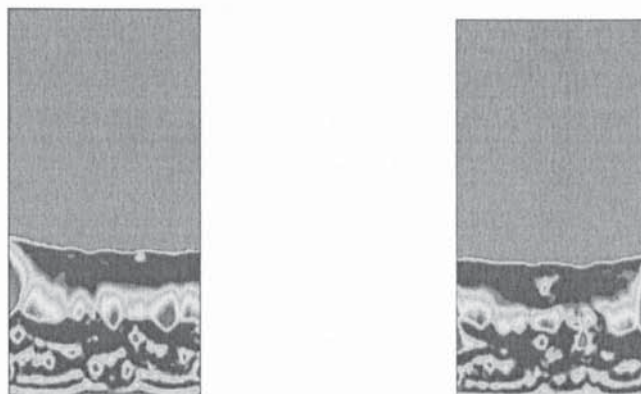
Figure 50 Impact of density, 2440 kg/m³ (left, XVII) and 2640 kg/m³ (right, XVIII)

THE IMPACT OF REACTOR GEOMETRY AND SCALE

A number of geometries and scales were examined, both experimentally and via CFD simulations. The experimental configurations examined in cold flow rigs are described in chapter 5. On top of those configurations, simulations were performed for Wellman's pilot plant and the 5 kg/h pyrolysis rig available at Aston University. Furthermore, to investigate the impact of scale-up beyond the size of the Wellman pilot plant, simulations were also performed up to a diameter of 5 m.

The small 3-D cold flow rig

The geometries employed in the simulations undertaken to compare with the small scale 3-D cold flow rig are illustrated in Figure 51 and Figure 52. Simulations were performed both with and without an annulus, which is described in chapter 5. A comparison between the two designs used experimentally showing maximum and minimum bed expansions is given in Figure 53. The main difference between the two designs lies in the position of the widening, which is related to the plateaus seen in the graph. In the original design, the minimum value of the bed expansion reaches a plateau at about 7 cm. Because the widening in the modified design is positioned higher up no plateau for the minimum value of the bed expansion is reached, while the plateau for the maximum value of the bed expansion is at a height of about 16 cm compared to 13 cm in the original design.

107

Vapour/gas phase speed, m/s
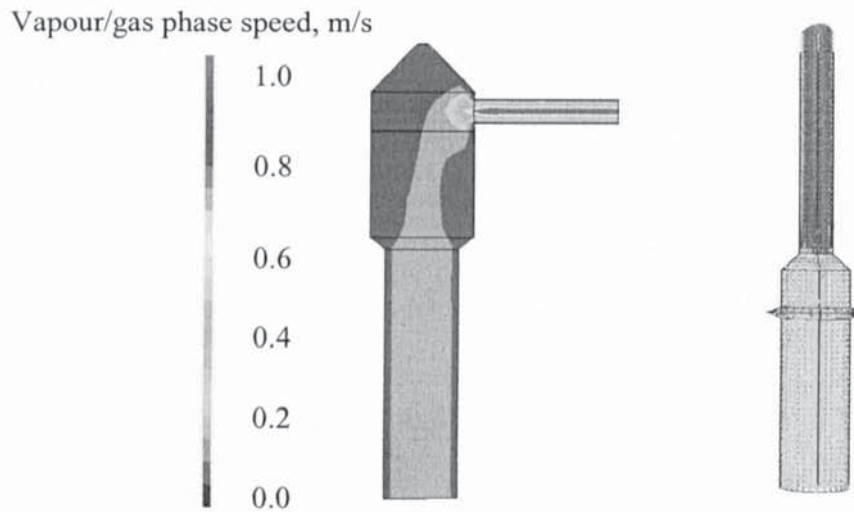
Figure 51 Simulation of original 1 kg/h cold flow rig showing a contour plot of vapour speed (left, XIX), simulation of modified cold flow rig with extended freeboard and disentrainment annulus showing a vector plot of vapour phase velocity (right, XX)
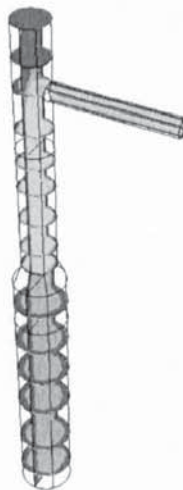
Figure 52 Modified cold flow rig showing contour plots of speed along cross sections of the reactor (XXI)
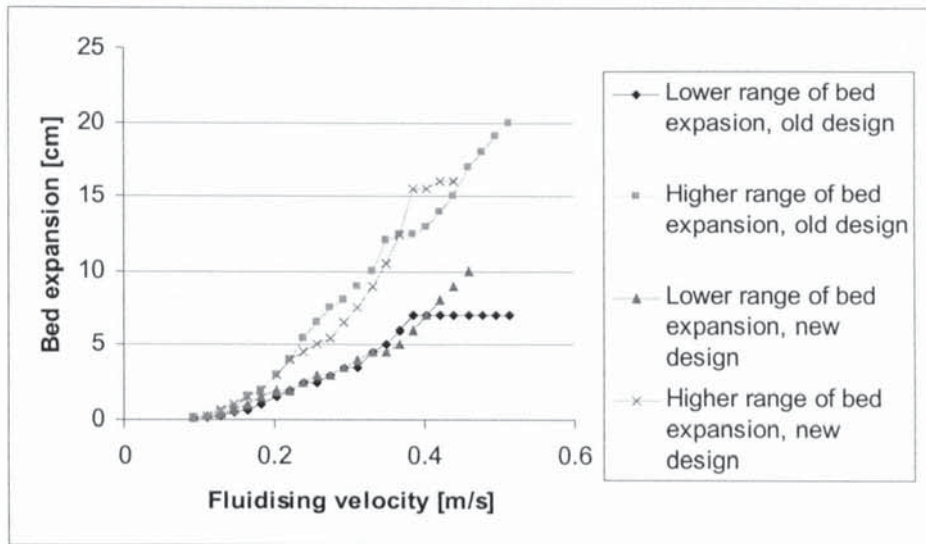
Figure 53 Experimental values for minimum and maximum bed expansion obtained for original and modified cold flow rig designs (VII, XXII)

A graph showing the fit between CFD and experiment has already been given in Figure 45. It should be noted that this earlier graph does not cover the full range of experimentally obtained values, and in particular it does not resolve the plateau visible in Figure 53. The bed expansion is an important factor for determining entrainment and is further discussed in chapter 8, where the reader can also find a detailed discussion of the advantages of widening or narrowing the freeboard.

Simulation of 5 kg/h reactor and Wellman pilot plant

The geometries employed in the simulations of the 5 kg/h reactor at Aston University and of the Wellman pilot plant are illustrated in Figure 54 and Figure 55. The modified geometry considered for the 5 kg/h reactor is largely based on entrainment considerations and is further discussed in chapter 8. With regards to the hydrodynamics, the advantage of the modification is that it can cut the variability of the bed expansion, as has been illustrated for the small 3-D cold flow rig in Figure 53.

Excessive bed height variability can lead to the loss of sand in appreciable amounts, as is illustrated in Figure 55. The potential for this loss is related to the maximum bed expansion. As has been pointed out previously, the average bed expansion is more relevant

for determining the amount of heat transferred to the fluidised bed via its walls. A design modification that reduced the difference between average and maximum bed expansion can therefore be used to enhance this trade off. In other words, it would be desirable for design modifications to raise the average bed expansion (and thereby potentially increase the amount of heat transfer) while keeping the maximum bed expansion constant (and thereby prevent excessive sand losses).

It might be pointed out at this stage that the use of a widening close to the bed surface to reduce slugging was already a feature of the seminal Winkler coal gasifier[13] that entered operation in 1926. A widening has also found application in fluidised bed biomass gasification to provide a disengaging section in the freeboard[138].
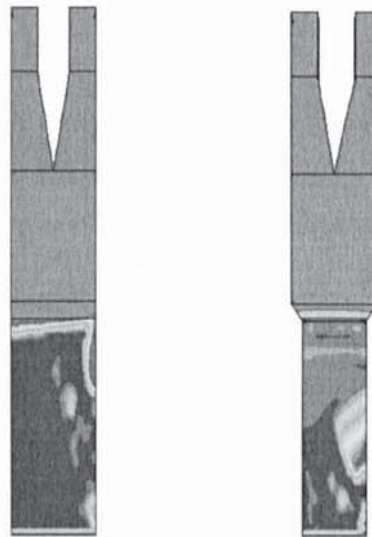
Figure 54 Simulation of the existing 5 kg/h pyrolysis reactor (left, XXIII) and of a future modification (right, XXIV)

Figure 55 Simulation of Wellman pilot plant showing the potential for large sand losses, plot of volume fraction of vapours (XXV)

A further aspect of the Wellman pilot plant modelled was the overall pressure drop, which is estimated as 13 kPa by Wellman. Figure 56 illustrates the results obtained graphically. Expressed quantitatively the pressure drop varied between 10 kPa and 16 kPa, which is in good agreement with the predictions made by Wellman.
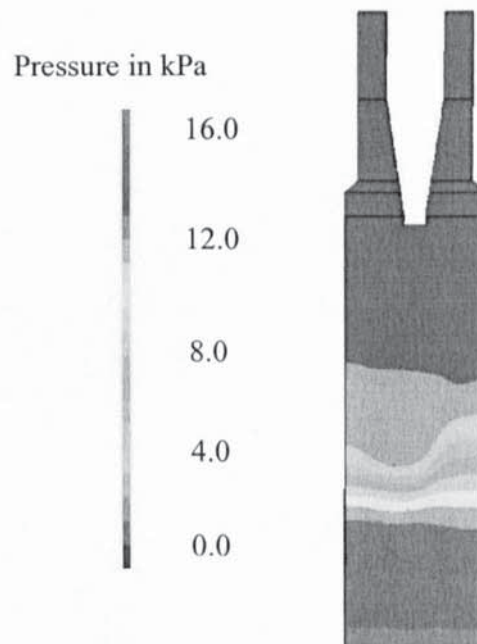
Figure 56 Contours of pressure modelled for Wellman pilot plant (XXV)

The pressure drop can also be estimated by using the following equation:

$$\Delta P = \rho_{bulk} \, g \, h_{bed}$$

$$= 2440 * (1-0.4) * 9.81 * 0.9$$

$$= 13 \text{ kPa}$$

What the CFD adds is a measure of the variation of the pressure drop with time. Also, one should say that obtaining the correct number for pressure drop partially validates the CFD, at least, it is a way to show potential errors.

THE EFFECT OF BED HEIGHT AND SCALE

Greater bed heights were found to lead to larger bubbles and greater absolute fluctuations in the bed height. This was examined experimentally in particular on the 2-D large scale configurations, where the bed height was systematically varied from 5 to 50 cm. The impact of initial bed height on average bed expansion is illustrated in Figure 57. Again the fit between CFD and experimental data is good. While the error is apparently substantial at one point (an initial height of 15 cm), this is likely largely, possibly even entirely, due to the relatively crude method used for obtaining an average bed height from the available data, that is measurement with a ruler on a screen considering five to ten frames (either from video recordings of the experiment or from post-processing of the CFD data). Processing the data available from CFD and experiment more accurately through writing or sourcing appropriate software would have required an effort that, after relatively detailed consideration of the matter, appeared unjustifiable and unwarranted.

For the range considered in Figure 57 there is a nearly linear relationship between initial bed height and average bed expansion.

The impact on bubble size is visually depicted in Figure 58. With otherwise identical conditions raising the initial bed height also gives a nearly linear increase in maximum bubble diameter for the conditions examined experimentally. The fact that average bed expansion considered in absolute rather than relative terms is also greater, is not as

112

immediately apparent. However, one can see that the bubble hold-up is at least as large for the large scale depicted as for the smaller sized one, which in turn is the basic reason why bed expansion scales nearly linearly between these two particular initial bed heights.
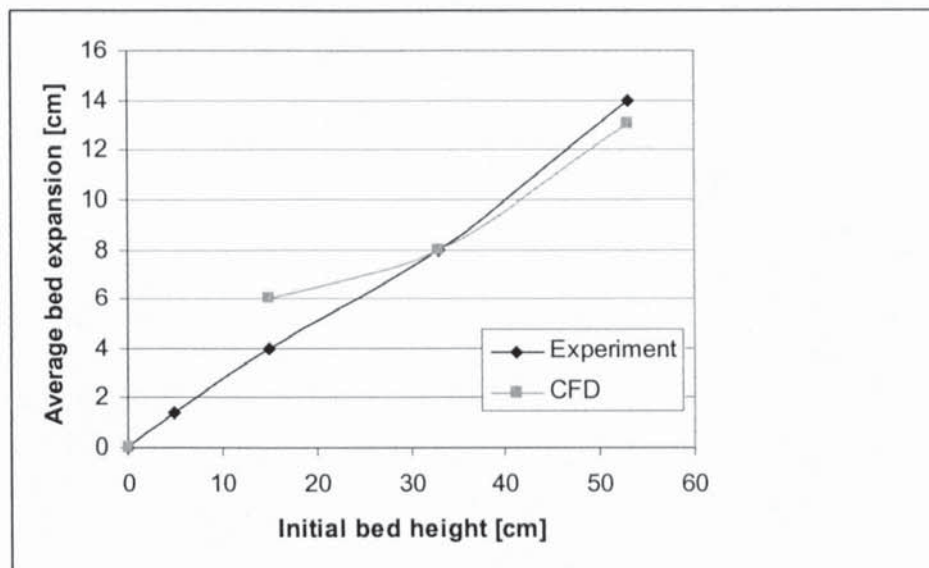
Figure 57 Impact of initial bed height on average bed expansion (XXVI, XXVII)
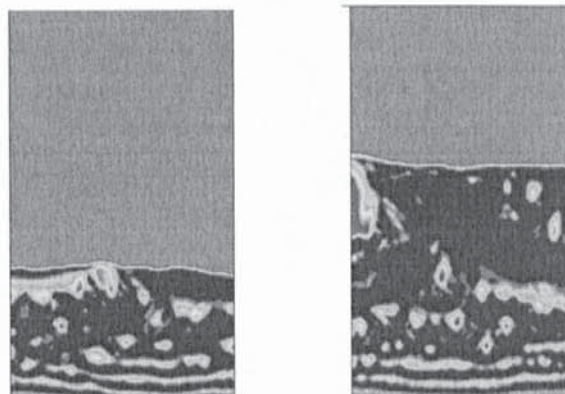
Figure 58 Illustration of impact of initial bed height (XXVIII)

In addition to CFD simulations reflecting the experimental 2-D configurations, a number of simulations were performed to study the effect of further scaling up to bed diameters of 5 m. Figure 59 shows a plot of bubble diameter against bed diameter derived from these simulations. It indicates that the bubble diameter increases with scale, but also that this increase flattens out beyond a bed diameter of roughly 1 m. The results are based on air at

113

room temperature as the fluidising gas and a fluidising velocity of 0.5 m/s. In visual terms this effect is illustrated in Figure 60, where it can be seen that the bed diameter to bubble diameter ratio is different for the two scales, 0.5 m diameter and 2.5 m diameter, shown. It should be noted again that the bubble diameter of irregularly shaped bubbles is calculated from the bubble cross-sectional area based on an equivalent circle with the same area, as has been pointed out earlier. Figure 60 also shows that the ratio of initial bed height to bed expansion is different for the two scales shown. Thus the bubble size and bed expansion do not scale proportionally when the bed diameter and other bed dimensions are raised by a factor of 5 (for bed diameter from 0.5 m to 2.5 m).
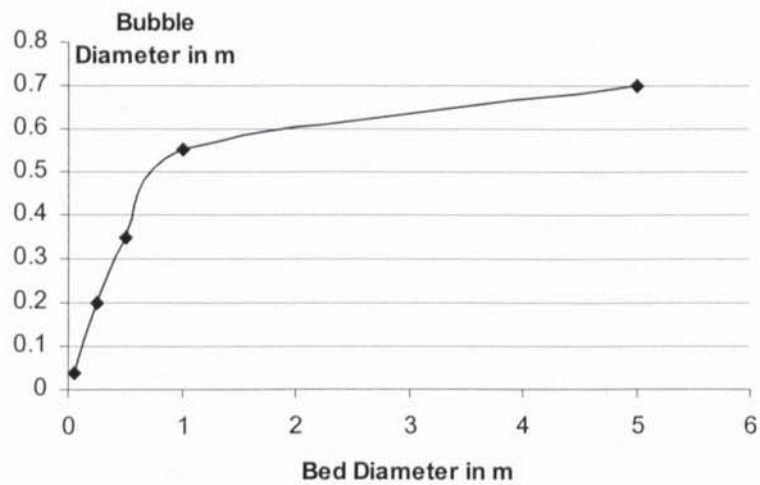
Figure 59 Plot of bed diameter against bubble diameter (XXIX)
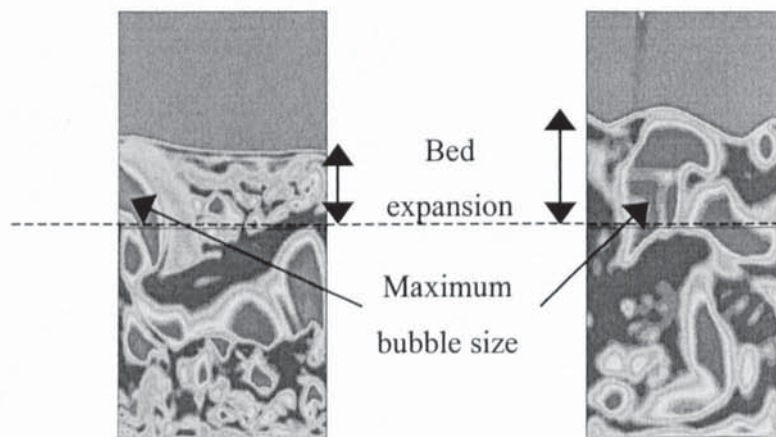
Figure 60 Same conditions (XXIX) except for scale

Left 2.5 m bed diameter, Right 0.5 m bed diameter

Relatively few simulations were performed for diameters beyond 1 m. There is therefore still some uncertainty attached to these novel simulation results. They are, however, in broad agreement with the results of simulations done for cracking catalyst particles by Krishna and van Baten[139], who find that the bubble hold-up declines with increased scale. Lower bubble hold-up in their simulations would imply a decrease in bed expansion, which is the variable considered in this work. The modelling strategy employed by Krishna and van Baten differs significantly from the one used in this thesis. While they do use Eulerian modelling, the two phases referred to are the dense or emulsion phase and the dilute or bubble phase. The bubble diameter was therefore an input that Krishna and van Baten had to obtain via the use of a correlation. It is well known that there is a maximum diameter beyond which bubbles in beds of cracking catalyst particles will not grow.

However, as Geldart points out[131]; *[when fluidisation] was applied to processes far removed from oil cracking, different solids had to be used, but there was a tendency to assume that published conclusions drawn from using cracking catalyst were also applicable to these other powders, which often had quite different particle sizes and densities.*

The experience from cracking catalyst is not necessarily a good guide to the behaviour of sand. Furthermore, different results may be obtained, when changing other variables, such as the fluidising velocity, the particle diameter or the fluidising medium.

Kunii and Levenspiel[13] give graphs for maximum bubble diameter against bed diameter that extend to Geldart class B and D particles, that is the Geldart classifications that apply to sand. Cracking catalyst particles may be classified as Geldart class A. A further explanation of the Geldart classification system may be found in chapter 3.

The results given by Kunii and Levenspiel are in broad agreement with Figure 59 in giving a nearly linear correlation between bed and bubble diameter for bed diameters below 1 m. They do not, however, cover values greater than 1 m, which is the novel aspect considered in this work.

Kunii and Levenspiel explain the maximum bubble diameter as a result of an equilibrium between bubble coalescense and break-up. They note that *overall, bubbles reach a small*

limiting size in fine particle systems, are larger in larger particle systems, and seem to grow without limit in very large particle systems.

For sand beds such as the one examined here, no simple theoretical explanation is available that would pinpoint the stage at which equilibrium between bubble coalescence and break-up might be reached. This is in opposition to beds of smaller particles such as cracking catalyst particles, where there is such a theoretical framework.

In the classical two-phase theory of fluidised beds it is assumed that all of the gas flow in excess of what is required for minimum fluidisation passes through the bed in the form of bubbles. This leads to the formation of two phases, the emulsion and the bubble phase, each of which has a constant density. When also assuming that the bubble nose and shape are stable, the velocity of a single rising bubble is then given solely as a function of its diameter. Davidson and Harrison[136] point out that bubbles with a greater velocity than the terminal velocity of the particles forming the fluidised bed would collapse, as particles in the wake of the bubble would be carried into the bubble. This observation, in conjunction with the relationship between bubble diameter and velocity, leads to a simple estimate of the maximum bubble size:

$$d_{B\,max} \approx 2\,U_T^2/g$$

For sand particles with a terminal velocity of 3.5 m/s this would imply a maximum diameter of approximately 2 m. However, the classical two-phase theory has significant weaknesses. In particular, Cranfield and Geldart[140] note that for larger particles, such as sand at 0.5 mm or above, the visible bubble flow may represent less than half of the excess gas flow. Hatzantonis et al[141] advise that the criterion for maximum diameter advanced by Davidson and Harrison should be used with caution as the maximum bubble diameter strongly depends both on particle characteristics and bed geometry.

For Geldart class B and D, that is larger sand particles, Kunii and Levenspiel note that large bubbles may rise more slowly than the gas in the emulsion phase, which is in agreement with both the CFD simulations and the experimental runs undertaken for the work here reported. It is therefore apparent that the rise velocity of bubbles need not be the decisive criterion for maximum bubble size reached.

When bubble size determines bubble velocity, two bubbles that coalesce into a bigger one will speed up to reach smaller bubbles above them, and upon reaching those will grow bigger and speed up even more. In a sand bed, such as the one studied, this is not necessarily the main mechanism and sideways movement of bubbles is just as or even more important for coalescence. With the equilibrium between bubble break-up and coalescence dependent on complex flow and recirculation patterns within the bed, determining the maximum bubble diameter for beds of large sand particles is therefore far from straightforward.

In summary it may be said that neither theoretical considerations, nor experimental evidence are available in the literature surveyed that could either disprove or confirm the estimate provided by CFD in this thesis. There may not be a maximum bubble diameter for the kind of sand bed investigated, or it may differ significantly from the value here obtained.

THE IMPACT OF GEOMETRY ON THE LARGER 2-D CONFIGURATIONS

A number of geometries were investigated in addition to a simple rectangular configuration, notably a widening, a narrowing and a dummy cyclone (see Figure 61). For a selective list of simulations performed for these configurations the reader is referred back to Table 12.
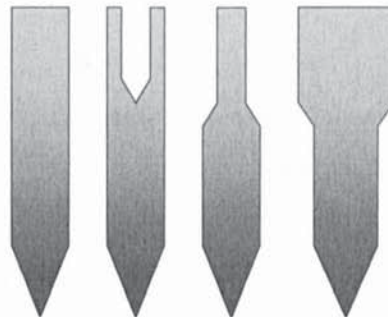
Figure 61 Generic illustration of a number of reactor geometries

The primary motivation for investigating these different configurations is the impact on entrainment (described in chapter 8) rather than on the hydrodynamics. The main effect with regards to the latter is related to bed expansion. In the straight configuration, the

increase in bed expansion depends nearly linearly on fluidising velocity. In the configuration with a widening, this increase is interrupted by a temporary plateau, as can be seen illustrated in Figure 47, which was given earlier to illustrate the dependence of average bed expansion on the fluidising velocity on the large scale 2-D rig, and in Figure 53, which was also given earlier and which shows the formation of an intermediate plateau in the small 3-D rig. By contrast a narrowing accelerated the degree of bed expansion in response to increasing fluidising velocity and could potentially lead to large sand losses, as was illustrated earlier for the Wellman pilot plant in Figure 55. In 2-D experimentation this was experienced as a quick shower of sand over the experimenters.

The difference in behaviour induced by a narrowing and a widening respectively is depicted in Figure 62. It is apparent that the widening smoothes the surface of the bed by comparison. The narrowing does not just result in more expansion, but also in much larger bubbles for otherwise identical conditions. There are two reasons for this, one quite certain, the other more speculative. As the narrowing leads to more bed expansion, the bubbles have more time to grow. This effect would be in line with the results obtained for the effect of initial bed height, which were illustrated earlier in Figure 57 and Figure 58. The second and slightly more speculative explanation is that bubbles are led to coalesce by the narrowing, while they are led apart by the widening. Without an explanation of this kind, the enormous increase in bubble size is not fully explained, as it is considerably in excess
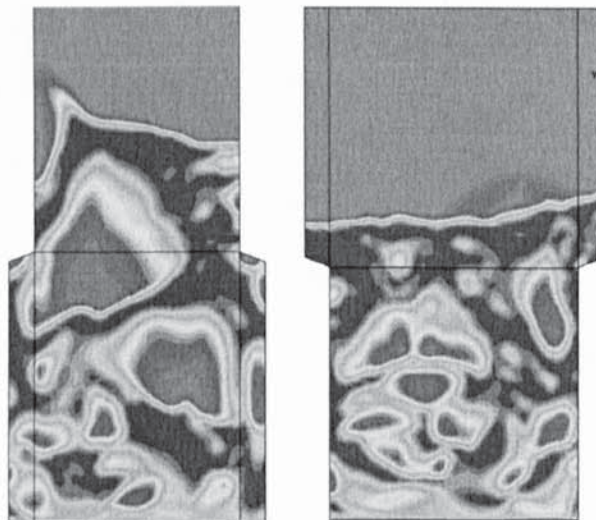
Figure 62 Hydrodynamics caused by narrowing and widening (XXX)

of the bubble size that would be obtained by just raising the initial bed height to the degree necessary to achieve the same bed expansion in either a configuration that is straight or experiences a widening.

The angle of the widening was also found to have an impact. The stabilising effect on the bed surface was enhanced by a greater angle of the widening. Figure 63 illustrates this aspect. Furthermore, it again shows that the geometry close to the bed surface is particularly important.
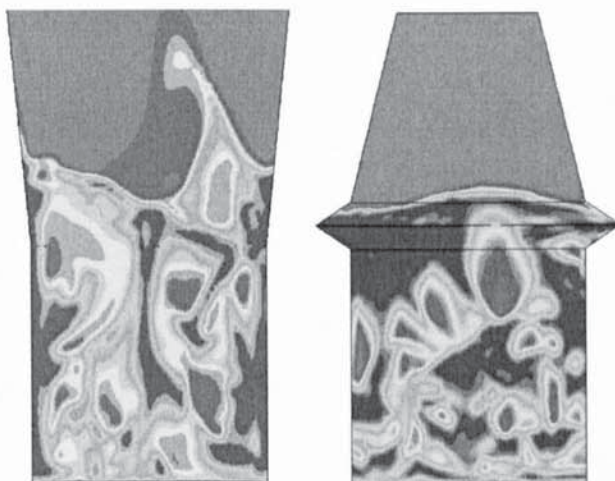
Figure 63 Further geometries investigated (XXXI, XXXII)

PRESSURE FLUCTUATIONS

Cold flow rigs have the advantage that bubble behaviour and therefore hydrodynamics are very visible. For industrial scale plants, another measure needs to be used instead. The rapid pressure fluctuations induced by the bubbles are easy to measure and may serve well for this purpose.

It should be noted that pressure measurements are commonly performed on industrial reactors to obtain information about bed expansion and to assist in the control of solids recirculation systems. However, the measurement of rapid pressure fluctuations is so far largely limited to laboratory cold flow models, though there are proposals for the application of the technique to industrial scale reactors[142].

The most interesting and the most important pressure fluctuations are those induced by bubbles. The frequency at which bubbles pass a point at the side of a fluidised bed tends to be of the order of 5 Hz according to Cranfield and Geldart[140], which is in agreement with the CFD simulations and experimental runs performed for the work here reported. Consequently, and also due to financial constraints, a choice was made to purchase pressure transmitters that should have been capable of providing 20 measurements per second. The actual performance turned out to be closer to 5 measurements per second, with the time between measurements varying between roughly 0.04 and 0.4 seconds and averaging 0.2 seconds.

Validation of CFD predictions

A CFD analysis was performed to predict local pressure fluctuations. The CFD gave equally spaced values every 0.00025 s (the command file used for producing the data is given in the appendices). To enable comparison with the experimentally obtained values, the sampling rate for the CFD results was adjusted to be 5 Hz. Plotting the CFD results without thinning out the data gave a similar curve that, however, included many considerably smaller fluctuations. An illustration of the data with the same sampling rate for both CFD and experiment can be found in Figure 64.

The impact of the sampling rate is illustrated in Figure 65. The fluctuations visible can be subdivided into three classes, only one of which can be recognised at a low sampling rate. The shortest fluctuations are responsible for the thickness of the line apparent in the graph given in Figure 65 for a high sampling rate (the individual points cannot be discerned in the graph, as there are so many of them, 4000 per second). Even a number of intermediate sized peaks and the exact location of peaks and troughs of the major fluctuations are lost, when the sampling rate is reduced. Nevertheless, the overall shape of the major fluctuations is still reasonably well represented.

While the CFD calculations provide a great number of equally and densely spaced values, getting forty seconds worth of data required over a week of computation. The number of samplings at 5 Hz over a time period of forty seconds is just 200. For two such periods a comparison of the standard deviation and absolute average deviation was performed.

120
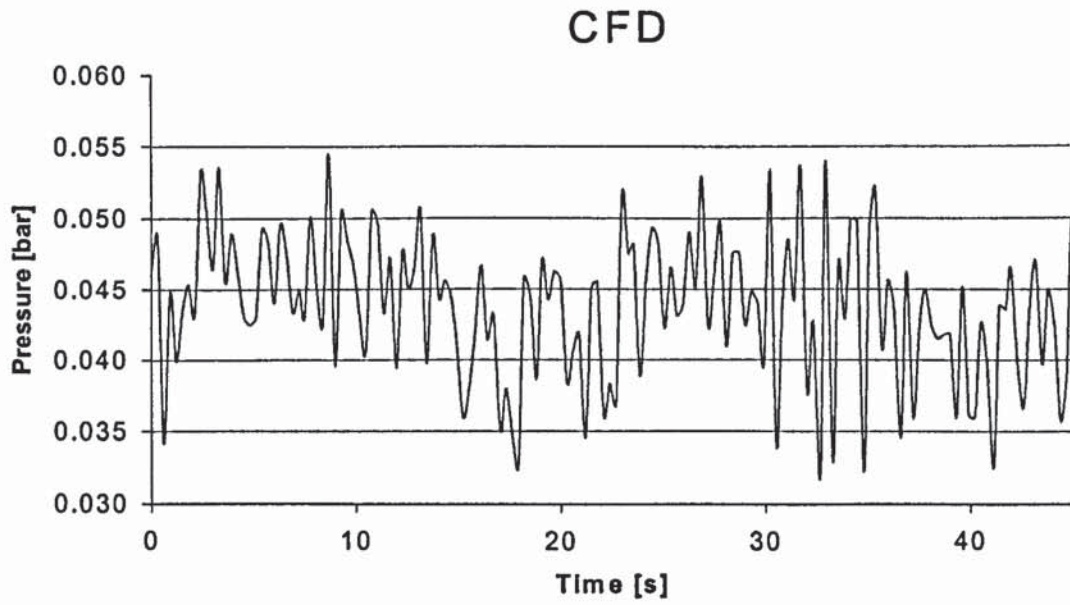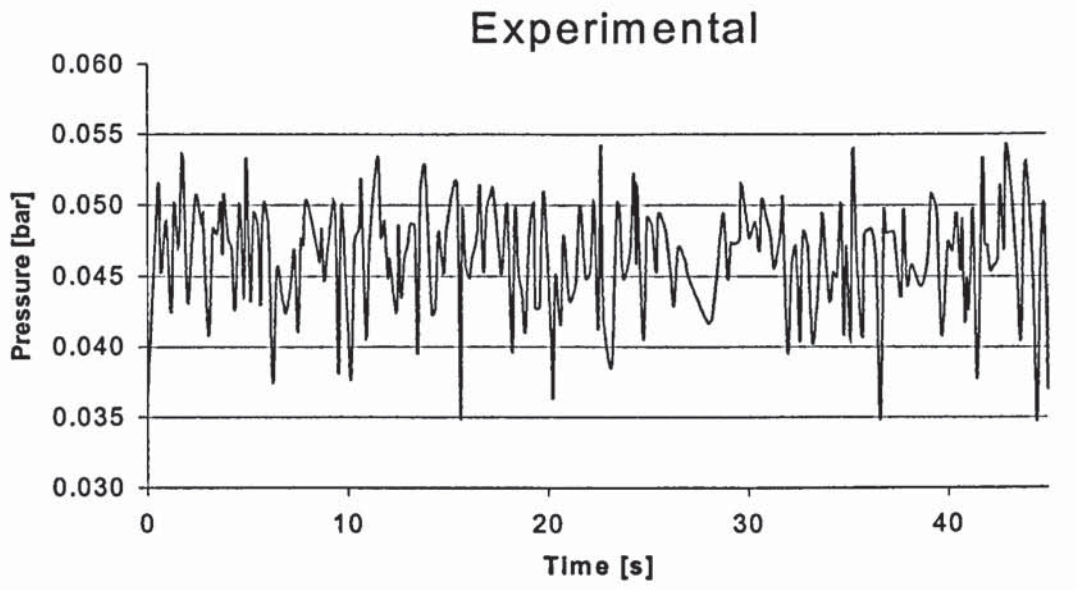
Figure 64 Comparison of pressure fluctuations with the same sampling rate for CFD and experiment (XXXIII, XXXIV)
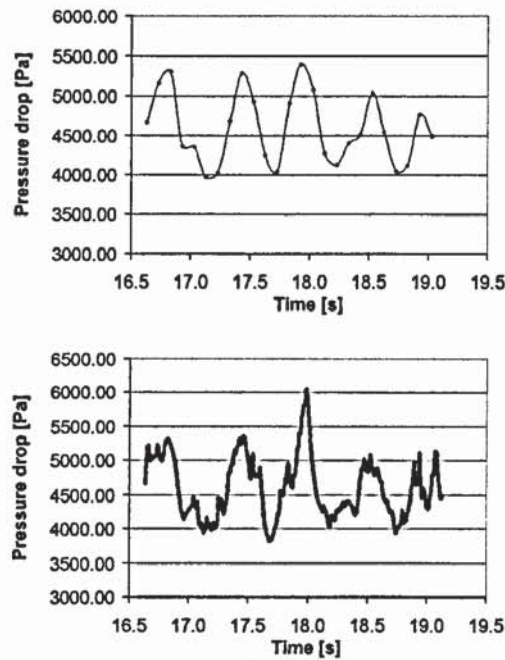
Figure 65 Comparison (XXXIII) of low sampling rate (top), and high sampling rate (bottom)

The experimental value for the standard deviation of 390 Pa compared to 378 Pa for one CFD calculated interval and to 511 Pa for another. The experimental mean absolute deviation of 308 Pa compared to values of 311 Pa and 405 Pa. Considering the length of the comparison interval and the uneven sampling of the experimental values, the differences are within the scope for sampling error.

A spectral analysis has been performed. As the common sampling interval of forty seconds at 5 Hz contains relatively few values, three separate analyses are presented, one for the common interval, one for periods in excess of forty seconds, which therefore can only rely on experimental data, and finally one for the very high sampling frequencies available from CFD. It should also be noted that spectral analysis requires evenly spaced data. There is no agreement on how best to interpolate unevenly sampled data[143]. As the experimental sampling intervals average out to 0.2 seconds over longer periods, this value was chosen as the most suitable and applied to the series of pressure data without adjusting those data for the actual sample interval, which varied between roughly 0.04 and 0.4 seconds. The programme used for the spectral analysis was the Singular Spectrum Analysis - MultiTaper

122

Method (SSA-MTM) Toolkit[144], which was run on a 900 MHz AMD Duron processor using Red Hat Linux 7.2.

The power spectral density of the experimental measurements for a period of ten minutes is shown in Figure 66. To obtain the values, the maximum entropy method (MEM) with an order of 40 and 256 sampling frequencies was employed. There was a small linear trend in the data, which with very high likelihood was due to experimental error, such as for example the rig slowly sliding into a slightly different angle, or some sand being lost through entrainment. The average pressure drop through fluidised beds is equal to the weight of the particles, and should therefore not change linearly with time. The spectral analysis picks the linear trend up as very low frequency but high amplitude pressure fluctuations. As those are believed to be spurious, only frequencies about 0.1 Hz are given in Figure 66.
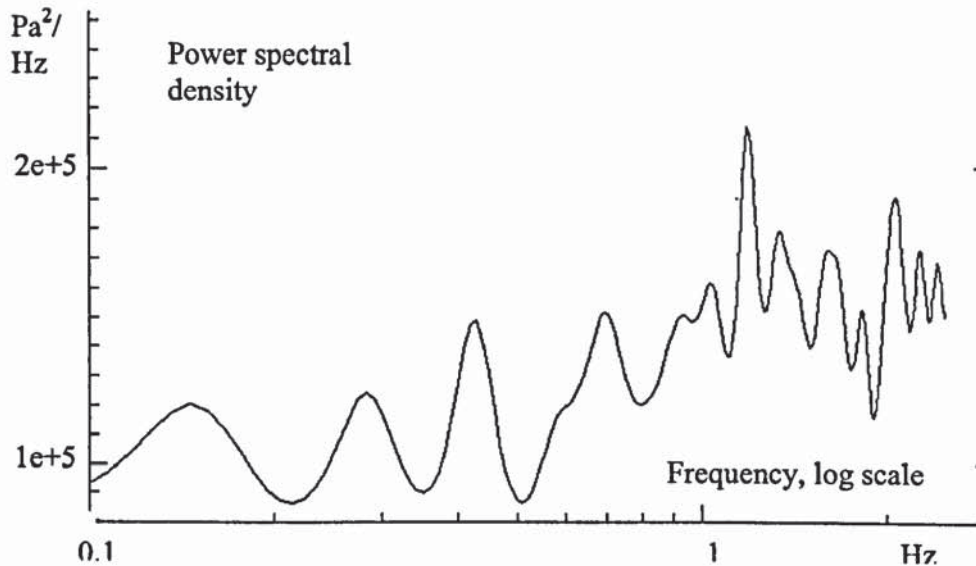
Figure 66 MEM spectrum of ten minutes of experimental sampling data (XXXIV)

A MEM analysis for the sample interval of forty seconds is shown in Figure 67. It employs the same order and number of sampling frequencies as the analysis shown in Figure 66. The results should be treated with caution due to the low number of samplings used. Nevertheless, as with Figure 66 the most important peaks are around 1 to 2 Hz.

In addition to the MEM analysis, a Blackman Tukey spectrum was produced using a Bartlett Window of size 69 and 256 sample frequencies. This analysis, which includes error bars, is shown in Figure 68.
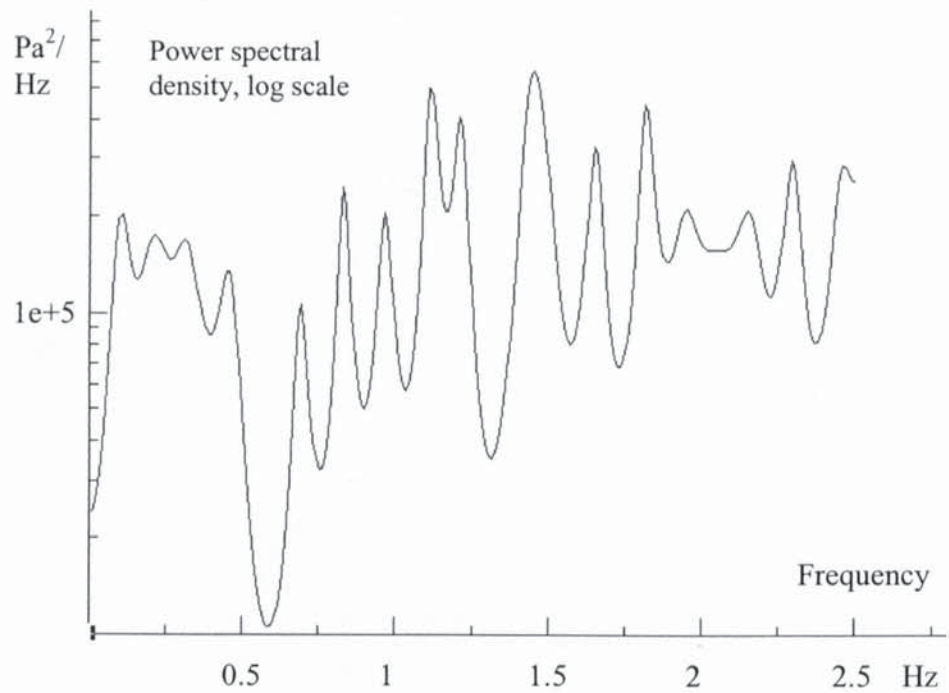
Figure 67 MEM spectrum of the experimental series given in Figure 64
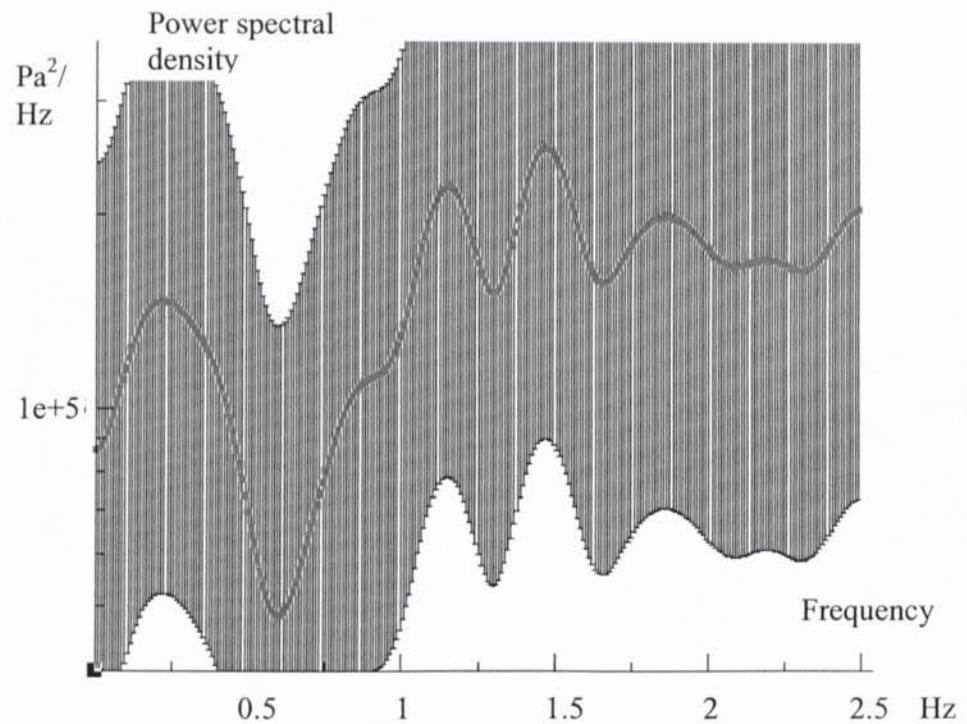
Figure 68 Blackman Tukey spectrum of the experimental series given in Figure 64

The respective spectra for the CFD pressure fluctuation predictions, sampled at 5 Hz, are shown in Figure 69 and Figure 70. They indicate peaks in the spectral density around 0.1 Hz and around 1 to 2 Hz, both of which are clearly visible from a visual inspection of the
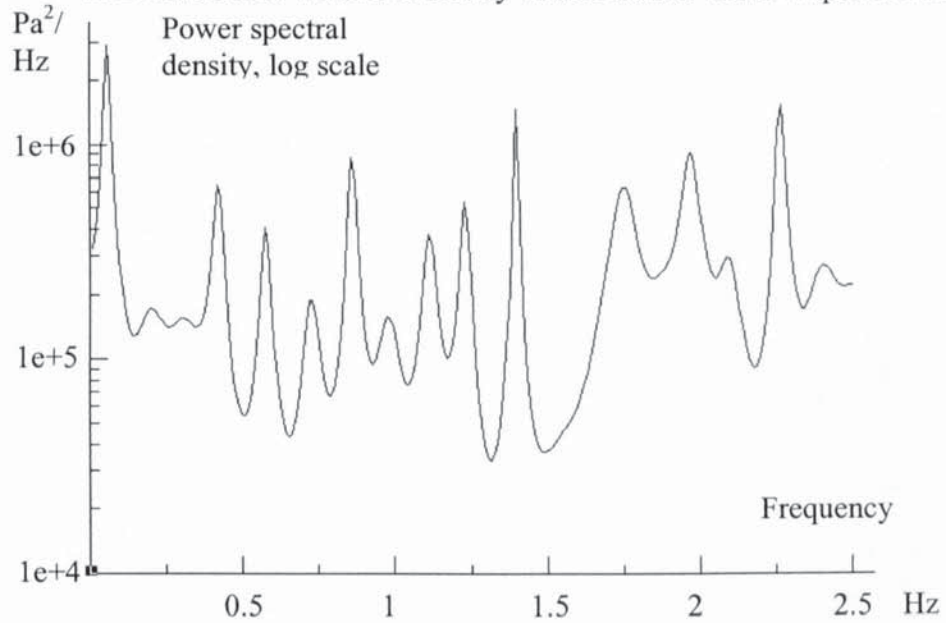
Figure 69 MEM spectrum of the data series from CFD given in Figure 64
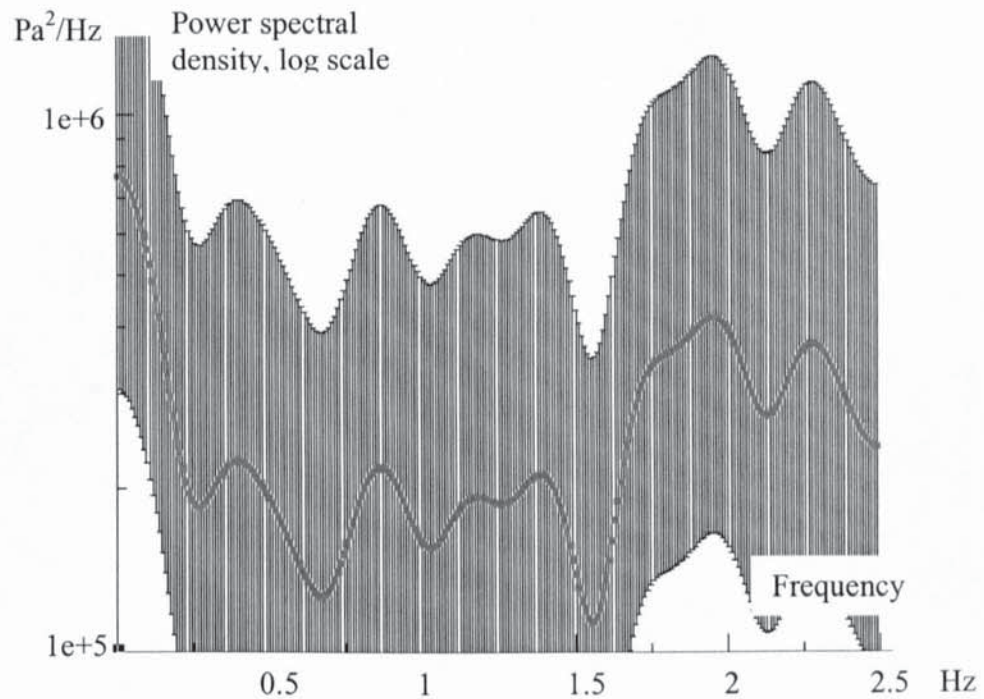
Figure 70 Blackman Tukey spectrum of the data series from CFD given in Figure 64

data shown in Figure 64. It is not readily apparent whether the fluctuations at around 0.1 Hz are due to sampling error, nor is it clear whether they would be found in a longer interval as well. The pressure data given by CFX are in the form of text files, and each of those files contains a maximum of 10000 time steps, that is 2.5 seconds with a time step of 0.00025 seconds. Each text file was transferred to Excel and then a filter was applied to reduce the number of samplings to a frequency of 5 Hz. After this step the data was pasted into a single file. Pasting the unfiltered data together to obtain a file with approximately two hundred thousand samplings over forty to fifty seconds would have required considerable effort. The spectral analysis of the unfiltered CFD data was therefore limited to a period of 2.5 seconds. A MEM spectrum using an order of 40 and 256 sampling frequencies is shown in Figure 71.
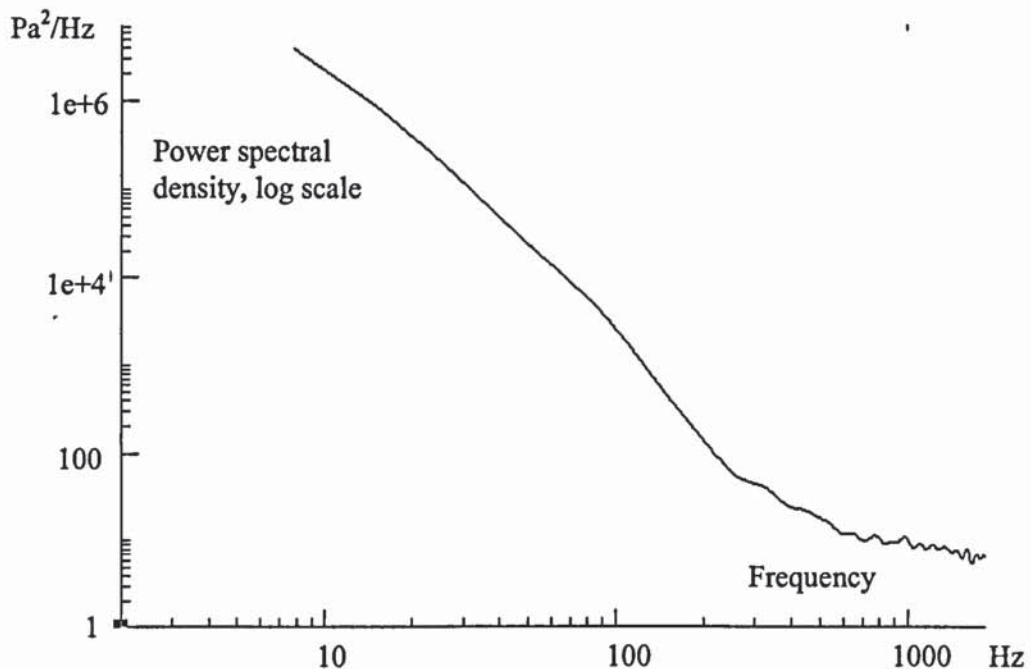
Figure 71 MEM spectrum of CFD data, sampling interval 2.5 seconds (XXXIII)

The highest spectral density in Figure 71 is found at 5 Hz. For higher frequencies a very rapid decline in the amplitude of the fluctuations is observed, as would be expected when supposing that the frequency of passage of bubbles is the primary cause for the observed pressure fluctuations. The spectral density at 5 Hz is greater than any of the peaks in the previous figures, which cover frequencies from 0.1 to 2.5 Hz.

126

Both the spectra obtained by CFD and by experiment compare well with values given by van Wachem et al[130], which are illustrated in Figure 72. They looked at three possible implementations of Eulerian-Lagrangian modelling for comparison with experiment. van Wachem et al used Eulerian modelling for the gas phase and Lagrangian modelling for the particle phase; the strategies referred to apply to the Lagrangian side of the modelling, which as has been pointed out earlier in chapter 5 is an approach that was not pursued further in this thesis. To keep the number of particles down to 3000-4000, they therefore had to look at a small fluidised bed (0.0898 m by 0.09 m) and very large particles (diameter of 1.545 mm). With gas properties similar to air and a solids density of 1150 kg/m^3, they used a superficial velocity of 0.9 m/s, which corresponds to u/u_{mf} of 1.2. The conditions are sufficiently similar to allow a qualitative comparison between their experimental values and the CFD results presented in this thesis. The spectral density shows a peak above 10^6 Pa^2/Hz at 2 Hz, a rapid decline for higher frequencies, and spectral densities declining to around 10^5 Pa^2/Hz at lower frequencies. This is in good agreement with the CFD calculations obtained in this thesis from 0.1 to 100 Hz, and also in good agreement with the experimental values presented earlier in Figure 66 for frequencies between 0.1 and 2.5 Hz.
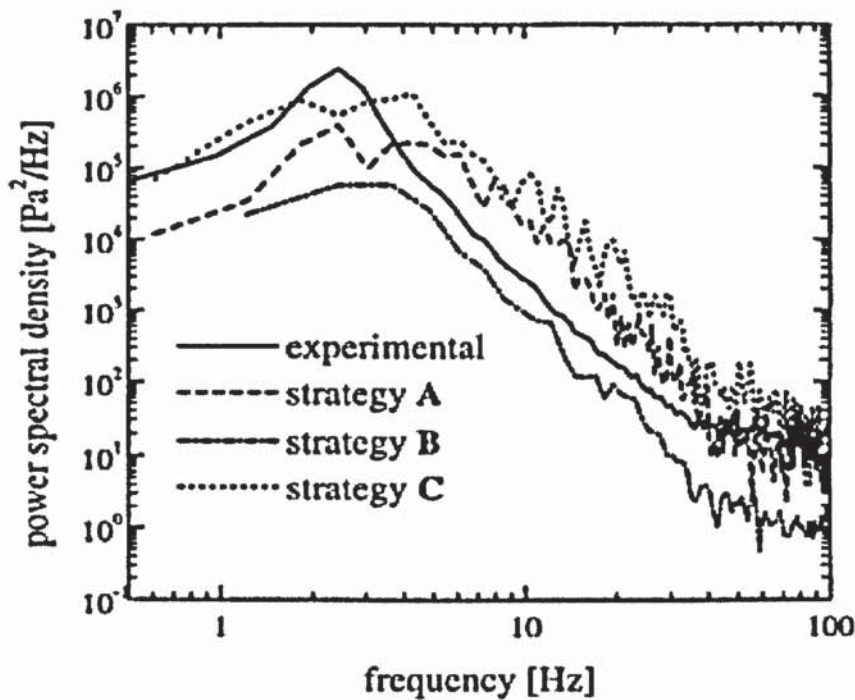
Figure 72 Spectra for experimental and predicted (three strategies) pressure fluctuations, taken from[130]

127

Figure 73 illustrates what happens when the superficial velocity is slowly raised. For the unfluidised bed the pressure drop is constant for a given velocity and a direct measure of that velocity. When the bed is fluidised the average pressure drop is nearly independent of the superficial velocity. However, the average scale of fluctuations induced by the bubbles rises.

Figure 73 is an interesting extension of a similar figure given in many chemical engineering textbooks, for example Coulson and Richardson[145], which, however, do not show the impact of fluidising velocity on the instantaneous pressure drop. Showing only the average may mislead the reader into thinking that the pressure drop is, if anything steadier, when fluidisation occurs compared to the situation in a fixed bed. In fact, as Figure 64 shows fluidisation results in a permanently changing pressure drop, where only the average stays constant.
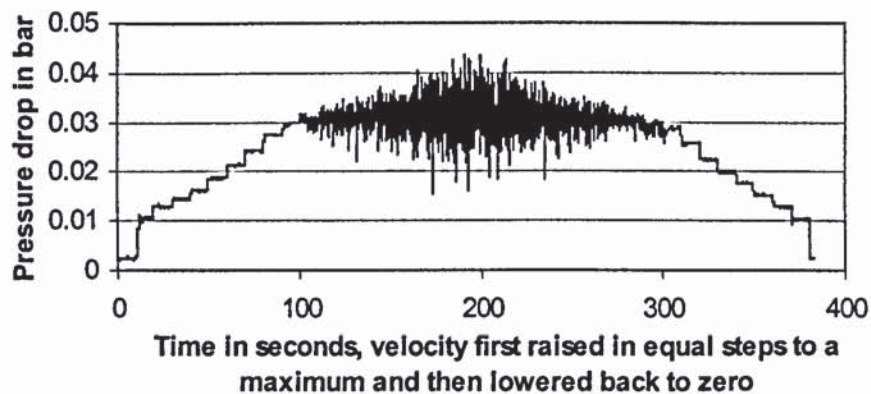
Figure 73 Pressure drop as a function of velocity (XXXV)

IMPACT OF GRID SPACING ON CFD RESULTS

Apart from physical influences on the modelled hydrodynamics, there may also be an impact from the kind of grid spacing employed. It is desirable to keep the amount of computing time required as low as possible without compromising the quality of the

128

simulations. Therefore, an investigation into the effect of grid spacing was undertaken to ascertain the impact of going towards a finer grid.

The effect of doubling the fineness of the gridding is illustrated in Figure 75 and the corresponding grids are depicted in Figure 74. Finer gridding only has fairly modest impact. The shape of the bubble is essentially the same, however it appears slightly smaller and more clearly defined, also a second bubble forming is more clearly visible in this particular case. All variables apart from grid spacing were identical for this comparison.
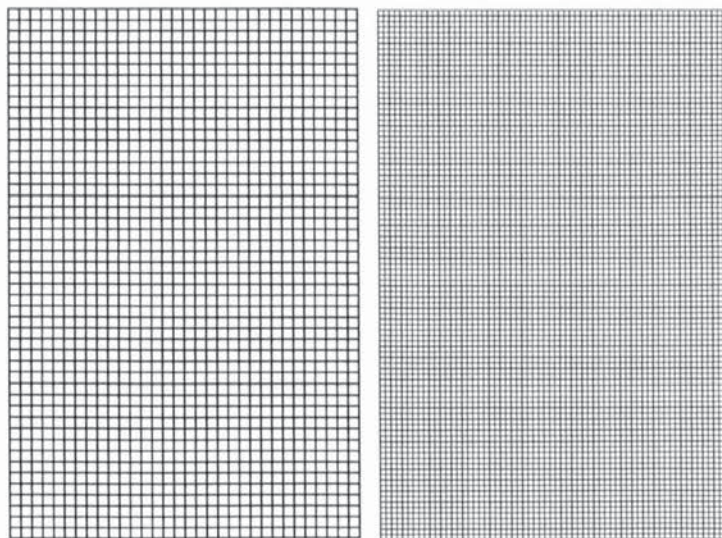
Figure 74 Illustration of possible grids, grid shown to the right twice as fine as grid shown to the left
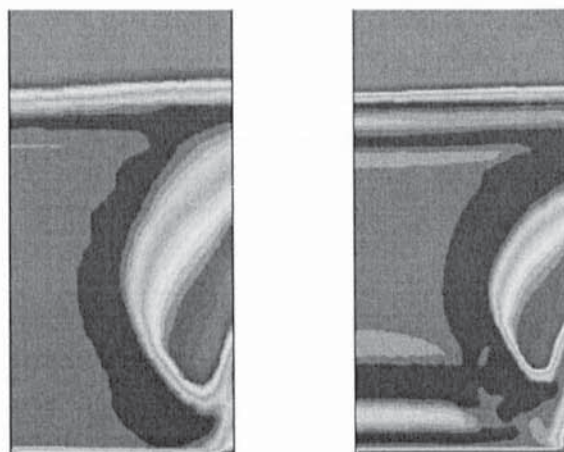
Figure 75 Illustration of impact of fineness of gridding, finer grid to the right (XXXVI)

It should be noted that the appropriate number of grid points is to a degree scale dependent. Larger scales generally require a greater number of points to resolve individual bubbles. Figure 76 illustrates this for a simulation performed with a coarse grid (similar to the one used in Figure 75), but at a much larger scale, namely for a bed diameter of 5 m. While the bubbles are not resolved individually, the coarse grid nevertheless still gives an estimate of bubble hold-up and bed expansion.

Figure 76 Simulation at large scale (5 m diameter) with coarse grid (XXXVII)

CFD QUASI 2-D AND BREAKING OF THE SYMMETRY

To investigate the differences between 2-D and 3-D, an intermediate kind of simulation was performed that was genuinely 3-D, but where the third dimension was still significantly smaller than the other two. In other words, rather than not modelling the third dimension at all by only allowing one grid cell, as was the case for most simulations performed in the course of this work, the third dimension was modelled with just a few grid points (typically 4 or 5, which compares to on the order of 100 cells in the x and y directions). This kind of gridding is shown in Figure 77.

Having four grid cells in the z direction, rather than just one, roughly quadruples the computing time. This clearly favours the use of only one grid cell in the z direction, that is to employ a genuine 2-D simulation. The experimental 2-D configuration, of course, does have a third dimension, even though that dimension is much smaller than the other two. It

was therefore deemed worthwhile to investigate, whether resolving that third dimension for simulations of the experimental 2-D rig would have a noticeable impact.
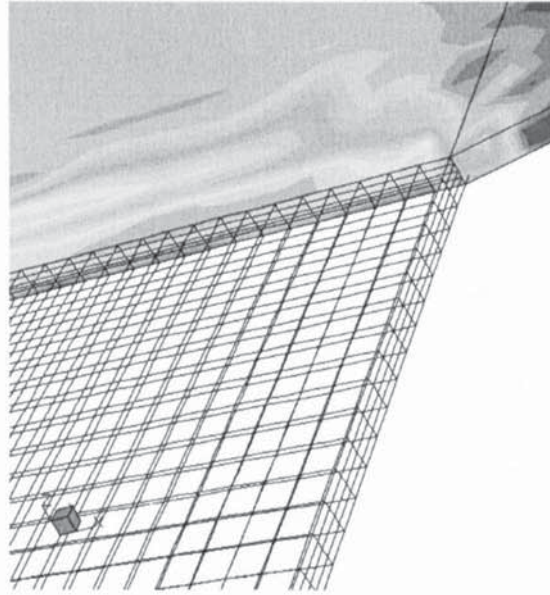
Figure 77 Illustration of gridding for semi 2-D calculations, colours shown are for contrast only

Convergence behaviour was found to be more difficult with the quasi 2-D simulations, which seriously limited their usefulness and comparability. A comparison at an early stage is illustrated in Figure 78. While the behaviour is not identical, it is fairly similar.

Figure 78 is also an indication of how the perfect symmetry imposed by the start-up conditions affects the initial development of the simulation. Namely, instead of bubbles bands are formed. For simulations undertaken during the early stages of this work, this initial symmetry was broken by the introduction of a jet for a very short period of time, often 0.05 seconds.

The effect of such a short jet is depicted in Figure 79, where the bubble induced by the jet can be seen together with a band. A few seconds of simulation time later, no bands are visible any longer.

It was found at a later stage that small numerical errors would accumulate and break the symmetry on their own. Later simulations therefore omitted the step of introducing a short jet to break the symmetry.
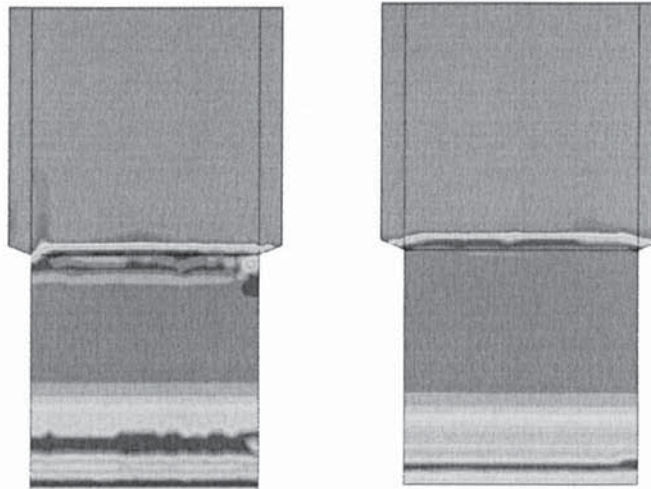
Figure 78 Comparison between semi 2-D (left, XXXVIII) and true 2-D (right, XXXIX)
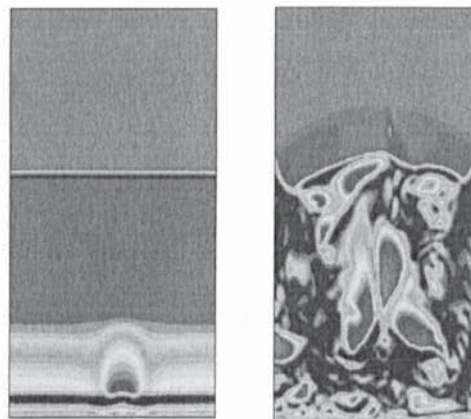
Figure 79 Illustration of breaking of symmetry (XL)

3-D SIMULATIONS

Modeling all three dimensions in full is even more computing resource intensive than performing the quasi 2-D simulations. To obtain a similar resolution with on the order of 100 grid points in each direction then multiplies the computing requirements by roughly a

factor 100. It is therefore desirable to avoid the need to have to simulate all three dimensions. To assess this requirement a comparison between 2-D and 3-D behavior was performed, both in terms of simulations and experiment. The latter has already been described earlier and is well illustrated in Figure 31 and Figure 39.

In addition, the literature was consulted and found to be ambiguous about the applicability of 2-D simulations to 3-D reactors, as it was felt that there would be a number of situations where the 2-D simulation might behave differently in a significant fashion[139].

As with the quasi 2-D calculations convergence was found to be a great problem for the 3-D simulations, which presented a further obstacle. Nevertheless a few good simulations were obtained, which showed behaviour similar to the 2-D simulations. A small number of those are illustrated in Figure 80 and Figure 81.
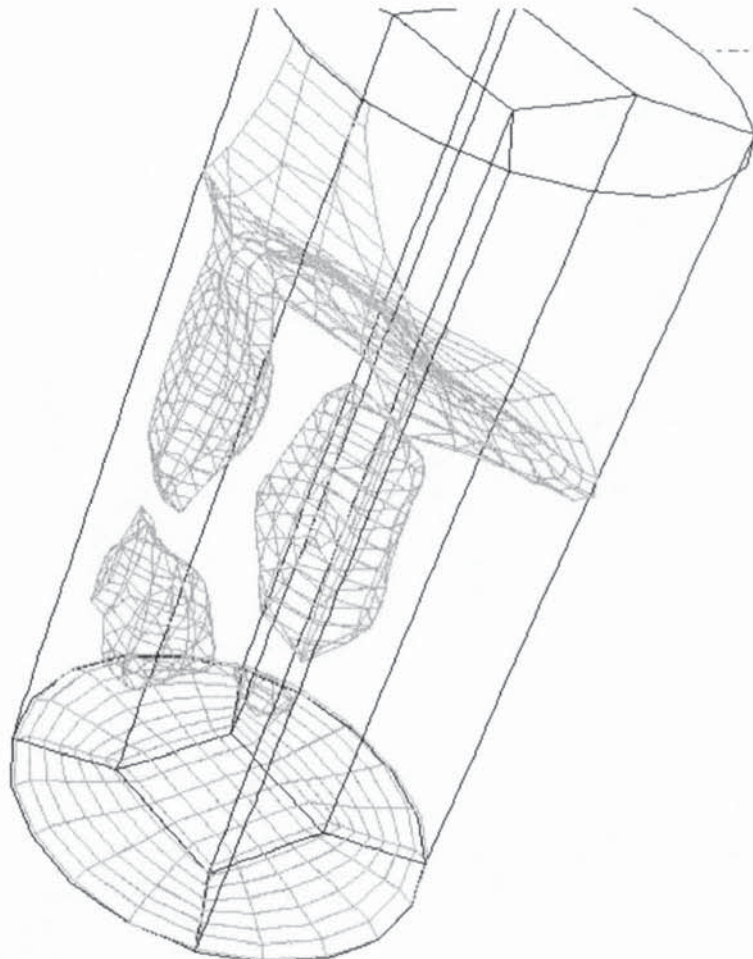
Figure 80 Isotimic of volume fraction of gas phase (0.8), illustrating bubbles in 3-D (XLI)
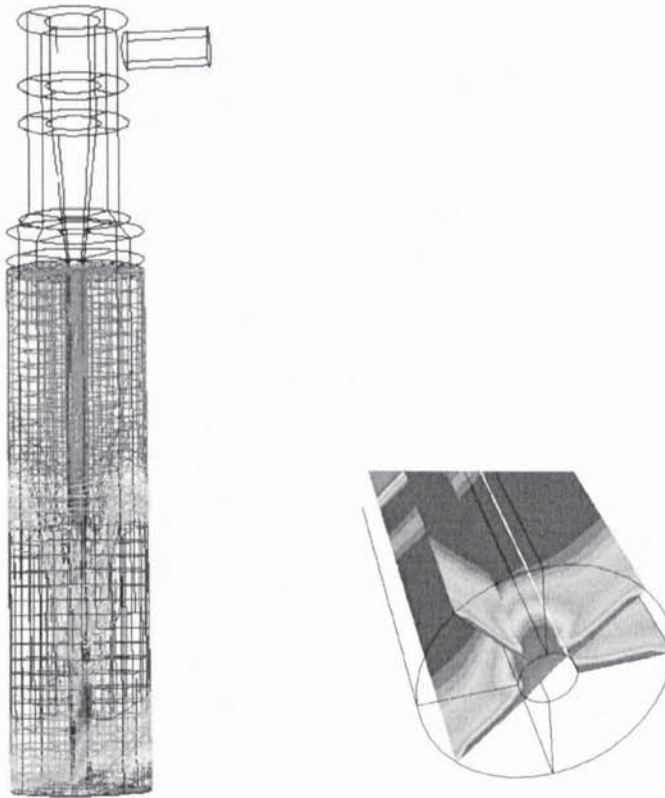
Figure 81 Plots of volume fraction (XLII)

While there are no three dimensional simulations of fluidised bed reactors for fast pyrolysis in the literature, some work has been done for other processes, such as coal combustion, e.g by Witt et al[146]. As with the work reported in this thesis, the large computational requirements seriously limited the amount of time that could be simulated, in the case of the above reference to two runs of 2 seconds each.

IMPACT OF TEMPERATURE

The temperature is an important variable that influences fluid viscosity and density in particular. Simulations were performed for both hot (500 degrees Celsius) and cold conditions (room temperature). The fluid viscosity increased from 0.000018 kg m^{-1} s^{-1} to 0.00004 kg m^{-1} s^{-1}, when the temperature was raised, while the density fell from 1.2 kg m^{-3} to 0.46 kg m^{-3}. For otherwise identical conditions, the temperature change had minor impact, as is illustrated in Figure 82, and resulted in a very small increase in bed expansion.
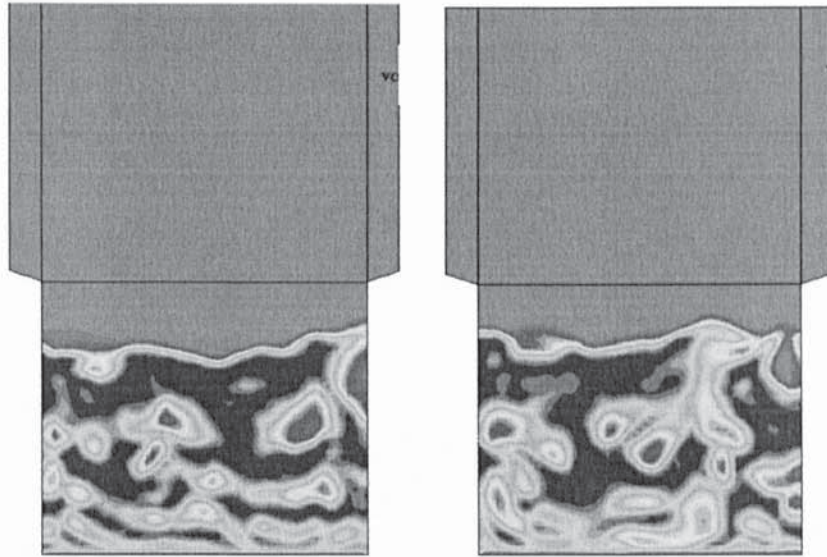
Figure 82 Fluidised bed (XLIII) at room temperature (left) and at 500 degrees Celsius (right)

7. Reaction Kinetics

This chapter explores the interaction between reaction kinetics and hydrodynamics, which is particularly relevant for scale-up. The modelling procedure used for incorporating the reaction kinetics is explained. Results from the calculations performed are presented and conclusions with regards to the consequences for reactor performance are drawn. Finally, the results are discussed and compared with the work of other authors.

INTRODUCTION

For the design of fluidised bed reactors a knowledge of the kinetics is vital and may, as is detailed in this chapter, be of significance in determining the hydro-dynamic behaviour of the reactor. A number of possible models for the reaction kinetics were discussed earlier in chapter 2. The extended Broido-Shafizadeh scheme was chosen as a basis for implementation of the reaction kinetics in Fortran subroutines, as it is simple and also the most widely used and accepted[147,16,148,149] (see chapter 2 also). A further discussion of this choice is presented at the end of this chapter. Sample versions of the Fortran subroutines that were developed are included as an appendix.

MODEL IMPLEMENTATION

A schematic of the reaction kinetics scheme applied in this work can be found in Figure 83.

Biomass

$K_1 \downarrow$

Primary pyrolysis products

K_2 K_3

x Char + y Gas   Organic vapours and water

$K_4 \downarrow$

Gas
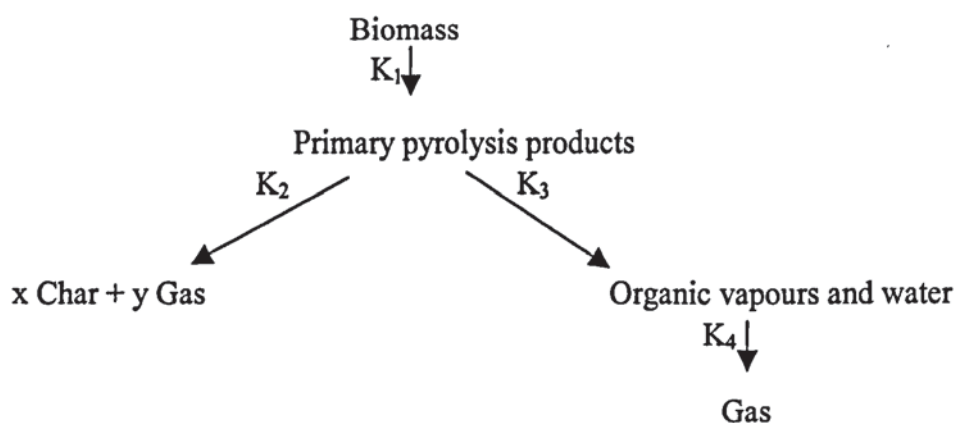
Figure 83 Illustration of reaction scheme used, based on Broido-Shafizadeh

The values of the kinetic parameters used in the code are based on work by Bradbury[150] (for the first three reactions) and Liden[151] (for the fourth reaction) and are summarised in Table 13.

Table 13 Kinetic parameters

Parameter	Value adopted
E_1	$242.8*10^6$ J kmol^{-1}
E_2	$150.7*10^6$ J kmol^{-1}
E_3	$196.8*10^6$ J kmol^{-1}
E_4	$108.0*10^6$ J kmol^{-1}
A_1	$2.8*10^{19}$ s^{-1}
A_2	$1.3*10^{10}$ s^{-1}
A_3	$3.2*10^{14}$ s^{-1}
A_4	$2.6*10^6$ s^{-1}
x	0.35
y	0.65

Biomass, primary pyrolysis products and char were implemented as scalars within the solid phase, while vapours and gas were taken to be components of the gas/vapour phase. Scalars are equivalent to concentrations or mass fractions. They share the same temperature, velocity and pressure, but can diffuse along a concentration gradient. Sand was not implemented as a particular scalar. Instead it is the assumed background fluid for the solid phase, which is justified as sand does not take part in any chemical reactions as either a product or reactant and as sand makes up over 99% of that phase.

It should be noted that no account was taken of density differences between the organic vapours and the fluidising gases. They are treated, as if they had the same physical properties. The primary advantage of this approach of course is simplicity. Taking account of density differences between the pyrolysis vapours and gases and the fluidising gases would have required considerable extra programming effort in the form of Fortran subroutines and would have slowed down the calculations. There is also some justification

for assuming that the most important properties of the vapours and non-condensable gases originating from pyrolysis, and of the fluidising gases are similar.

Most of the volume of the vapours in fact consists of water, which typically makes up 15-30% of the vapours by mass[152]. The organic constituents of the vapours have high molecular weights and are very unstable[153]. A sample composition of the pyrolysis vapours and gases based on work by Hague[154] is shown in Table 14.

Table 14 IEA poplar, pyrolysis results, values based on experimental work by Hague

Product	Percentage Yield (basis, total vapour and gas produced)
Gases (total)	18.7%
carbon monoxide	8.3%
carbon dioxide	8.6%
Organics	54.8%
Water	26.5%

Based on this sample composition, one can calculate the volume taken up by a kg of pyrolysis vapours and gases and compare it with that taken up by a kg of typical fluidising gases, which may be assumed to consist of a mixture of approximately two thirds nitrogen and one third carbon dioxide in the case of the Wellman pilot plant[155]. Oja[153] obtains values for the molecular weight of the organics of around 200 kg/kmol. However, as the overall volume is dominated by the other pyrolysis products, the impact of varying the molecular weight of the organics is limited. Assuming 100 kg/kmol for the organics gives the pyrolysis products roughly 81% of the volume of the fluidising gases for the same mass, while assuming 400 kg/kmol will only reduce this to 69%.

To recap, the density of the pyrolysis vapours and gases is not the same, in fact it is slightly higher and variable, than that of the fluidising gases. While it may be desirable to incorporate these density differences into the modelling effort at some later stage, it was assumed that they could be neglected for the calculations presented in this work.

Within the solid phase, the changes in mass fractions resulting from reaction in a particular control volume during the course of a particular time step were calculated as shown in the following equations. Sand of course does not participate in any of the reactions, which, as mentioned earlier, is one of the reasons it need not be explicitly modelled as a mass fraction of the solid phase.

$$X_{t+\Delta t}^{biomass} = X_t^{biomass} - X_t^{biomass}\left(A_1 \exp\left(\frac{E_1}{RT}\right)\right)\Delta t$$

$$X_{t+\Delta t}^{primary} = X_t^{primary} + X_t^{biomass}\left(A_1 \exp\left(\frac{E_1}{RT}\right)\right)\Delta t -$$

$$X_t^{primary}\left(A_2 \exp\left(\frac{E_2}{RT}\right)\right)\Delta t - X_t^{primary}\left(A_3 \exp\left(\frac{E_3}{RT}\right)\right)\Delta t$$

$$X_{t+\Delta t}^{char} = X_t^{char} + xX_t^{primary}\left(A_2 \exp\left(\frac{E_2}{RT}\right)\right)\Delta t$$

The evolution of vapours and gas resulting from the decomposition/evaporation of the primary pyrolysis products is modelled with the help of a mass source term in the vapour phase. No sink was implemented in the solid phase (sinks and sources are terms used in CFD to describe additions or subtractions in the mass balance that are not due to standard hydro-dynamic considerations). This is permissible, as the amount of mass leaving the solid phase during the relatively short simulations that are feasible with the available computing hardware is a negligible fraction of the total mass of the solid phase. The mass source term for the vapour/gas phase on the other hand is highly significant. The difference is explained by the fact that the density of the solid phase is three orders of magnitude higher than for the vapour/gas phase.

The mass source term complicates the calculations of the mass fractions of the components of the vapour/gas phase and makes it necessary to first compute the absolute amounts of vapour and gas in each control volume, as well as the absolute amounts of vapour and gas added in each control volume over the course of a time step from the pyrolysis reaction:

$$m_t^{gas} = V\rho_\alpha r_\alpha X_t^{gas}$$

$$m_{\Delta t}^{gas} = V\rho_\beta r_\beta \; yX_t^{primary}\left(A_2 \exp\left(\frac{E_2}{RT}\right)\right)\Delta t$$

$$m_t^{vapours} = V\rho_\alpha r_\alpha X_t^{vapours}$$

$$m_{\Delta t}^{vapours} = V\rho_\beta r_\beta \; X_t^{primary}\left(A_3 \exp\left(\frac{E_3}{RT}\right)\right)\Delta t$$

$$X_{t+\Delta t}^{gas} = \frac{\left(m_t^{gas} + m_{\Delta t}^{gas}\right)}{\left(m_t^{gas} + m_{\Delta t}^{gas} + m_t^{vapours} + m_t^{vapours}\right)}$$

$$X_{t+\Delta t}^{gas} = \frac{\left(m_t^{vapours} + m_{\Delta t}^{vapours}\right)}{\left(m_t^{gas} + m_{\Delta t}^{gas} + m_t^{vapours} + m_t^{vapours}\right)}$$

Then the fourth reaction in the extended Broido-Shafizadeh scheme, which involves no volume change and is therefore easier to deal with, is applied in each control volume.

$$X_{t+\Delta t*}^{gas} = X_{t+\Delta t}^{gas} + X_{t+\Delta t}^{gas}\left(A_4 \exp\left(\frac{E_4}{RT}\right)\right)\Delta t$$

$$X_{t+\Delta t*}^{vapours} = X_{t+\Delta t}^{vapours} - X_{t+\Delta t}^{vapours}\left(A_4 \exp\left(\frac{E_4}{RT}\right)\right)\Delta t$$

Entrainment of the char is estimated in a separate procedure (see chapter 8), as accumulation of char in the reactor would take minutes to hours, while the CFD simulation runs currently feasible only model on the order of seconds of the hydro-dynamic behaviour of the bed. The pyrolysis reaction is assumed to be controlled by the kinetics, rather than by mass and heat transfer limitations to the biomass particles, which implies very small

particles. For larger particles a different approach would have to be adopted, as is discussed in more detail towards the end of this chapter and in chapter 12.

As discussed in chapter 4 biomass feedpoints are modelled as inlet boundaries with the only difference to the inlet boundaries at the distributor being the fact that the volume fraction of the solid phase and the scalar representing biomass are not equal to zero.

Yields were calculated once the simulation had approached a steady state. The yield of organic vapours was obtained by comparing the biomass feed rate with the flow rate of organic vapours through the outlet. The yield of gas was calculated by subtracting the flow rates of organic vapours through the outlet, of gas added with the biomass and of fluidising gases from the mass flow rate through the outlet. Finally, the yield of char was calculated by difference.

Furthermore, a number of mass balance checks were performed to check the accuracy of the implementation of the code. In particular, sums were calculated for the total enthalpy, mass and mass of specific components, such as organic vapours, held by the solid and gas/vapour phases. This was done by adding up the respective values for all the control volumes.

IMPACT OF FLOW PATTERNS AND SCALE ON YIELDS

The most important variable affecting yields is the average residence time of the vapours. This is so, as the temperature in the reactor is effectively constant and the same everywhere in the fluidised bed. The heat capacity of the sand is several orders of magnitude larger than that of the fluidising gases and organic vapours. This gives the fluidised bed reactor a significant thermal inertia and means that the reactor temperature will not change much during a simulation. In practical operation, this property of fluidised beds is actually very desirable giving good temperature control that allows operation close to the optimum temperature that maximises liquid yields. Heat transfer within the bed is also excellent, both in terms of heat transfer between the two phases and in terms of heat transfer, mostly through particle convection, between different parts of the bed.

Yields have been calculated for the Wellman pilot plant, again illustrated in Figure 84, with a diameter of 50 cm and a height from bottom to top of nearly 2.8 m. The yield as detailed above mainly depends on the residence time, which in turn depends on the superficial velocity. The conversion itself determines the amount of gas and organic vapours added and therefore influences the superficial velocity. With a superficial velocity of the fluidising gases of just over 0.2 m/s and a total superficial velocity (which includes the gas and organic vapours added via pyrolysis) fluctuating around 0.7 m/s, the yields shown in Table 15 were obtained. They represent an average over 10 seconds and are believed to be the result of a stable equilibrium that would be expected to persist over the longer term.

Table 15 Calculated product yields for the Wellman pilot plant

Product	Yield
Char	13%
Bio-oil	57%
Gas	30%
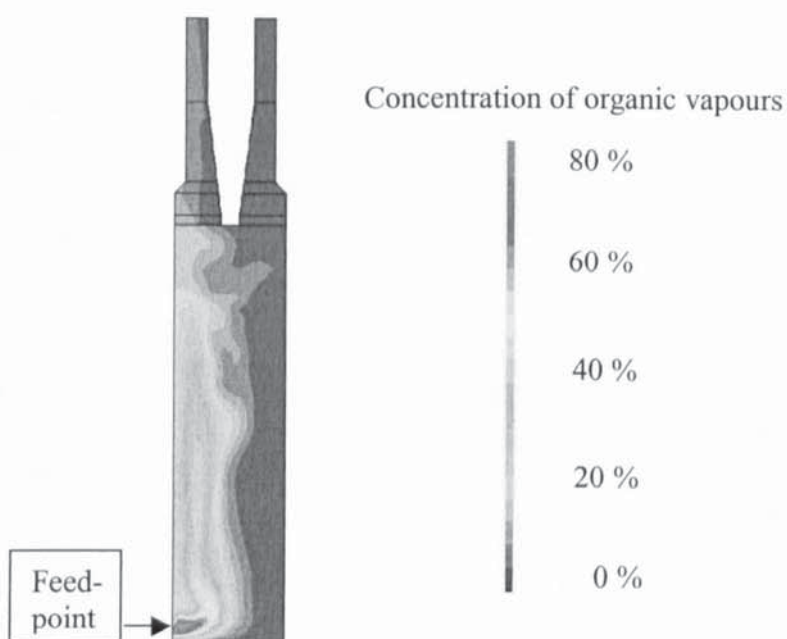
Figure 84 Illustration of modelled reactor, plot shows concentration of organic vapours
(XLIV)

These low yields can be explained by the long residence time experienced by the organic vapours, which allows significant secondary cracking; in smaller laboratory reactors, such as the 150 g/h rig available at Aston University, with residence times below 2 seconds yields in excess of 75% are commonly obtained. The residence time of the vapours is primarily determined by the path they take and the overall superficial velocity of both vapours and fluidising gases.
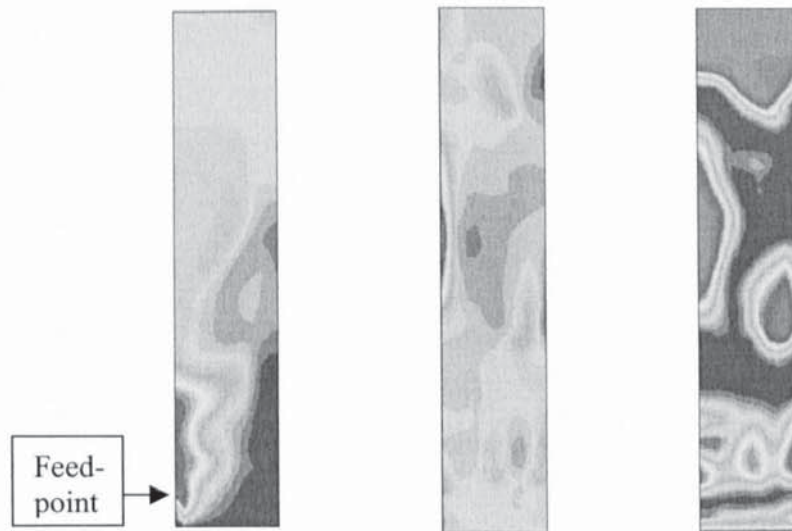
Figure 85 Illustration of calculations for the 5 kg/h rig, fluidising velocity for the fluidising gases alone 0.26 m/s (XLV)

Left - Concentration of organic vapours   Centre – v (upward component of) velocity

Right – Volume fraction of gas/vapours

(red is high, blue low in all plots, some information is lost without colour for the central picture in particular, note that the highest velocity is indicated towards the left on the wall)

Scale for v velocity

3 m/s

2 m/s

1 m/s

0 m/s

- 0.6 m/s
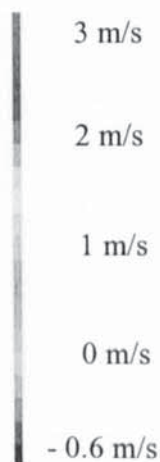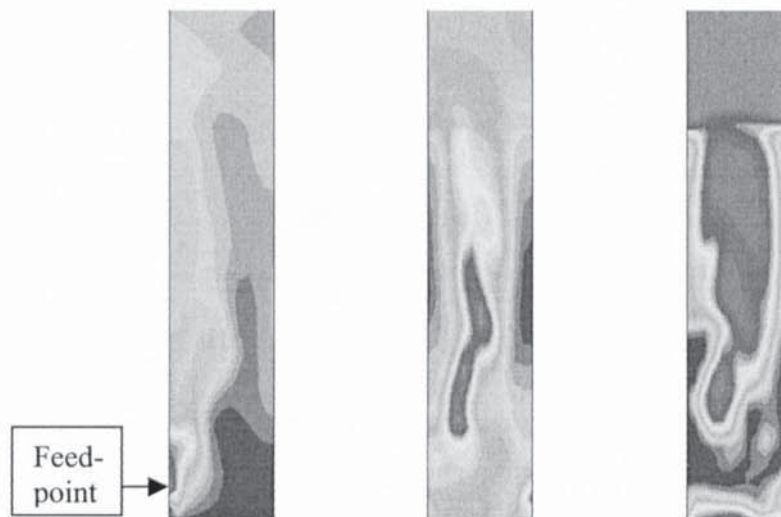
Figure 86 Illustration of calculations for the 5 kg/h rig, fluidising velocity for the fluidising gases alone 0.45 m/s (XLVI)

Left - Concentration of organic vapours   Centre – v (upward component of) velocity

Right – Volume fraction of gas/vapours

(red is high, blue low in all plots, some information is lost without colour for the central picture in particular, note that the highest velocity is indicated towards the centre and the lowest on the walls)

This fact may be further illustrated by calculations performed for the 5 kg/h unit illustrated in Figure 85 and Figure 86. They show, as expected, that the velocity is highest within large bubbles. In Figure 85 the largest bubble is located next to the wall towards the left of the reactor. This is also where the highest v velocity (the upward component of the velocity) occurs. The same observation can be made for Figure 86. The largest bubble is located towards the centre of the bed, where one can also observe the highest velocity.

The concentration of organic vapours is highest close to and above the feed point. They are therefore caught up in the upward movement of the bubble visible in Figure 85 to a much greater degree than is the case for the large central bubble apparent in Figure 86. Consequently and surprisingly, the yield of organic vapours is actually lower in this case for a superficial velocity of the fluidising gases of 0.45 m/s than it is for a velocity of 0.26 m/s. This is illustrated in Table 16 and can be said to be a powerful illustration for how important the hydro-dynamics of the bubbles are in determining the residence time of the organic vapours and therefore the yield of bio-oil. It may be surmised that the flow structures shown in Figure 85 and in Figure 86 may actually be fairly stable. At the lower

fluidising velocity the vapours evolved may be sufficient to force bubble formation just over the feedpoint, while a higher fluidising gas velocity may lead to preferential bubble formation towards the centre and thereby force the solids down towards the side preventing bubble formation above the feedpoint, which in turn significantly slows down the upward movement of the organic vapours.

The averaging period employed of 4-5 seconds is, however, too short to make a clear judgement on the reasonableness of this proposed mechanism. When attempting to continue the calculations to achieve a longer averaging period, no convergence could be achieved, as the residuals (which are a measure of the error in the numerical solution of the equations, which indicates how close the iterations are to providing a solution for each time step) would abruptly, and without prior warning or apparent reason, spike towards infinity causing an overflow error, which would terminate the run.

Table 16 Calculated product yields for the 5 kg/h rig

Product	Yield at 0.26 m/s	Yield at 0.45 m/s
Char	11%	11%
Bio-oil	83%	81%
Gas	6%	8%

A scale-up by a factor 10 in each dimension from the Wellman plant was performed as a test. This translates into a factor 1000 by volume giving 250 tonnes per hour or of the order of 20000 barrels per day of oil equivalent, which compares to fluid catalytic cracking of oil[156], but would be exceptionally high for any conceivable commercial bio-oil plant (due to constraints on feedstock availability[157]). To calculate yields, the run would have had to be continued to the point where the vapours reached the exit and steady operation was achieved. Considering the very low yields that could easily be estimated would result, this was not done, as it would have required excessive computing time.

However, the initial 12 seconds of simulation are quite instructive. The resulting flow patterns are illustrated in Figure 87. Rather than moving significantly upwards, the biomass vapours move towards the centre of the bed, as they are caught in a very large recirculation

145

pattern. One should say that this is exacerbated by the low superficial velocity of the fluidising gases of just 0.2 m/s in this particular run together with a low biomass feed rate.
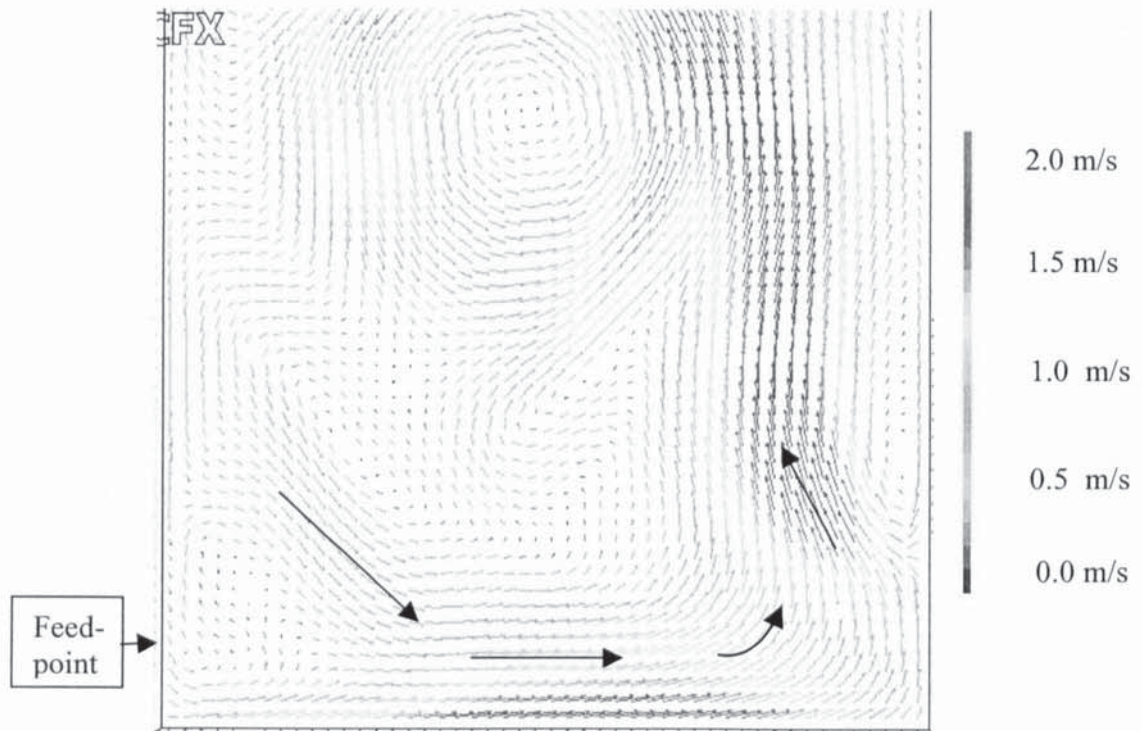
Figure 87 Flow patterns of the vapour/gas phase in the Wellman reactor scaled to a diameter of 5 m (XLVII)

As can be seen in the vector plot illustrated in Figure 87, the initial movement of the vapours is largely sideways, not up. It is quite noticeable that very high speeds are obtained on the side opposite to the feedpoint. Therefore the vapours have to travel an additional 5 metres in this simulation before they join the upward movement again illustrating the potential for flow patterns to lengthen the residence time of the vapours, which may deleteriously affect bio-oil yields.

For larger scales, it is frequently observed in the simulations performed during the course of this work that down movement at the walls is combined with upward movement towards the centre of the fluidised bed. As the biomass is commonly fed through an opening in the wall, it could therefore tend to be caught up in this downward movement. The flow patterns of the solid and vapour/gas phase do differ markedly, as there is no net upward

movement for the solid phase, while the movement of the vapour/gas phase must average out to be equivalent to the superficial velocity. It is therefore unsurprising that the downward movement at the walls is driven by the solid phase. The gas/vapour phase is either slowed down there, or even forced to move down together with the solid phase.
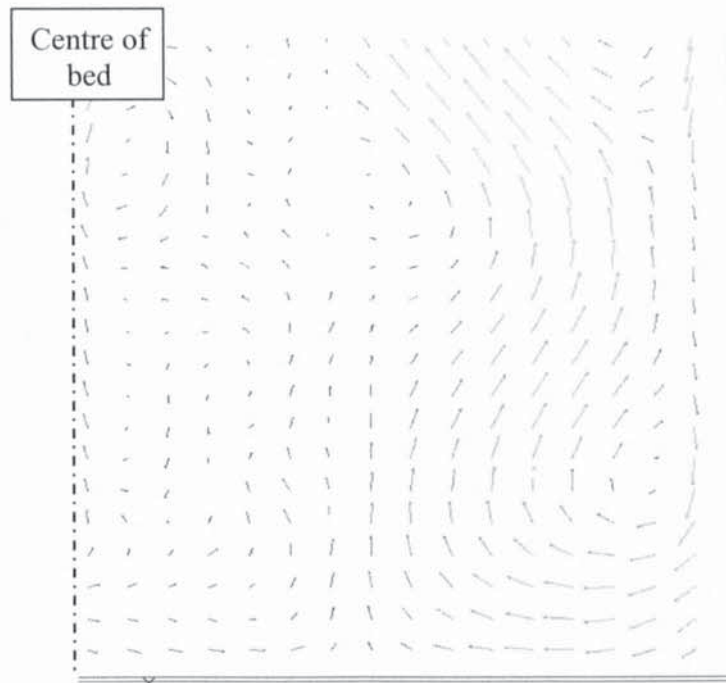
Figure 88 Illustration of common flow patterns of the solid phase observed in larger fluidised beds (section shown has dimensions of 0.25 by 0.25 m and is located within a reactor with a diameter of 0.5 m that is similar to the Wellman pilot plant, XLIV, same scale for vector plot as Figure 87)

POTENTIAL FOR MALDISTRIBUTION

There is a close interdependency between the hydro-dynamics and the reaction kinetics in that the path taken by the organic vapours influences the residence time and therefore the bio-oil yield, while the location where the pyrolysis reaction liberates organic vapours and gas impacts the flow in the fluidised bed. Because the speed of the solid phase tends to be low close to the feedpoint and as the pyrolysis reaction proceeds rather quickly, the bulk of the pyrolysis reaction takes place quite close to the feedpoint, generally within on the order of 10 cm. As the vapours and gas released by the pyrolysis reaction make up a sizeable proportion of the overall gas/vapour phase flow rate, this very localised evolution holds the potential for maldistribution, as is shown in Figure 89 for a bed with a diameter of roughly

147

50 cm and a height of approximately 2.7 m. Figure 89 also illustrates that maldistribution is less of an issue for thin and tall beds than it is for shallow beds with a very large diameter.

Figure 89 Illustration of potential for maldistribution – volume fraction of sand shown (red is high, blue is low) – dimensions are similar to those of the Wellman pilot plant (XLVIII)

A calculation in three dimensions has also been performed for a reactor of dimensions – height 2.4 m, depth 0.32 m and width 0.48 m - that are similar, in terms of order of magnitude, to the Wellman pilot plant. As can be seen in Figure 90, the evolution of organic vapours leads to the development of bubbles close to and above the feedpoint in quite a similar fashion as shown in Figure 89 for the two-dimensional case.

Whether maldistribution actually represents a problem depends on the individual case considered. Its effect on particular reactor geometries will differ. A few potential problems are: localised temperatures close to the feedpoint that are lower than the average in spite of the excellent heat transfer customarily afforded by fluidised bed reactors, lower heat transfer to the bed via the bed walls and higher char concentrations in the bed leading to more secondary cracking reactions.
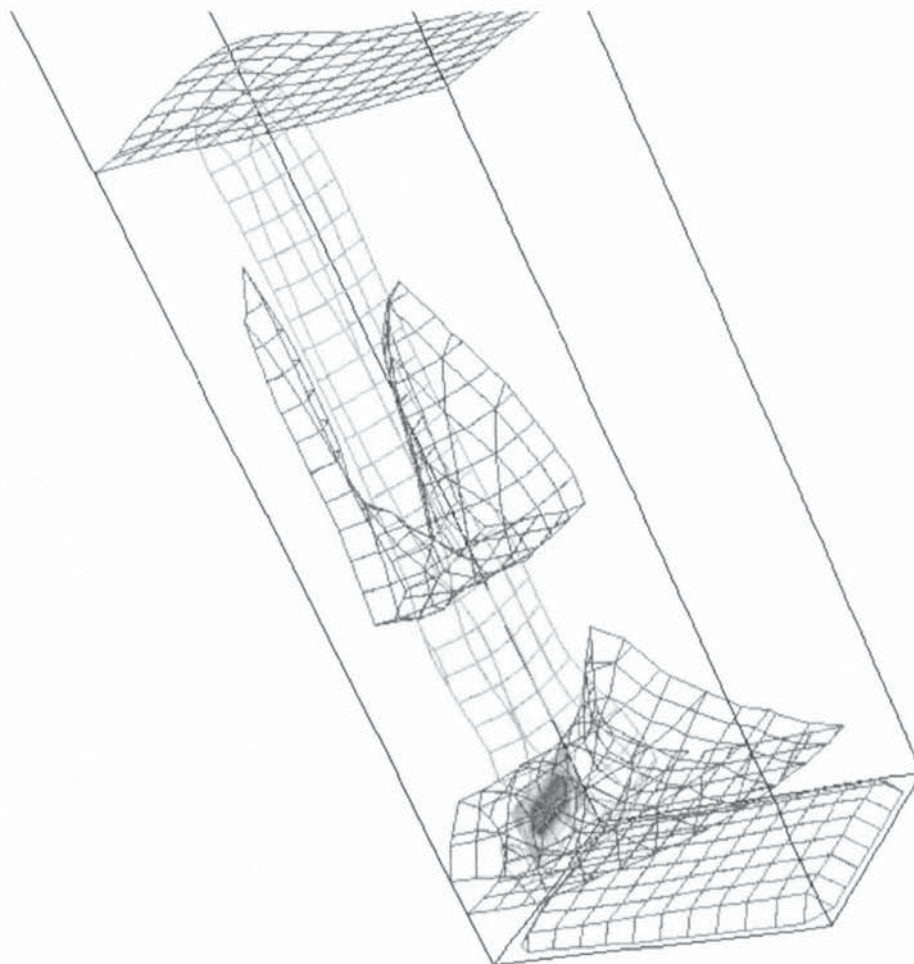
Figure 90 3-dimensional reactor modelling (XLIX), isotimic of volume fraction of the vapour/gas phase in red (surface illustrated is for a volume fraction of 0.85, in black and white it is the darker lattice) – isotimic of the concentration of vapours in green (surface illustrated is for a concentration of 0.2, in black and white it is the light grey lattice) – feedpoint in dark red (in black and white small, filled in oval towards the bottom of the reactor, note that the oval is an artefact of the interpolation procedure used by the post-processing package, the actual shape of the inlet is rectangular)

The velocity of the bubbles is in general higher than the superficial velocity as pointed out earlier. Consequently, maldistribution may have a positive impact, if it leads to a greater fraction of the organic vapours in the bubbles than in the rest of the fluidised bed. In the case of the simulations performed to obtain the yields given in Table 15 maldistribution was not significant and the average bubble actually contained a slightly lower fraction of organic vapours than the bed as a whole.

To avoid maldistribution it may be necessary to use several feedpoints. This option has been explored with two feedpoints in a simulation of a reactor with a diameter of 0.5 m and a height of 2.8 m (comparable to the Wellman pilot plant), which is illustrated in Figure 91. When comparing with Figure 84 it becomes clear that the objective of an even distribution of the organic vapours has been achieved in this case.

Figure 91 Pyrolysis reactor with two feed points, plot shows concentration of organic vapours (L)

DISCUSSION AND COMPARISON WITH OTHER MODELS

As has been pointed out already earlier, the main purpose of combining the CFD modelling of the hydro-dynamics of fluidised beds with pyrolysis reaction kinetics is to consider their interdependency and the resulting impact on the design of scaled up reactors. In particular, the location where vapours evolve impacts the hydro-dynamics significantly, while the residence time, and to a lesser extent the local temperature, of the organic vapours and biomass, and therefore product yields, are determined by the hydro-dynamics.

The reaction kinetics themselves are not scale dependent. The decomposition of a given biomass particle only directly depends on the local conditions, such as the temperature, of the medium in its immediate vicinity. The size of the fluidised bed has an indirect impact,

namely in the way it influences the local conditions experienced by individual biomass particles and by the organic vapours.

A number of models have been proposed for the reaction kinetics (see chapter 2). While those could be used to find optimum pyrolysis temperatures for a particular feedstock, laboratory experiments can be considered much more reliable[158] and may be performed at relatively moderate cost, certainly when compared to pilot plant work. It should therefore be stressed that design of commercial plant should primarily rely on experimental data for obtaining reaction kinetics data. The use of a Broido-Shafizadeh type reaction kinetics scheme in the work here reported is to be understood as concept proofing. While that particular scheme is widely accepted and gives as good and workable an approximation of the kinetic behaviour of general biomass as is available in the literature, it is still not as good as experimental data from the bench scale. The scheme should therefore be checked against such data from experimentation when applied to an actual design calculation for a particular feedstock, as has for example been done by Larfeldt et al[159] for a model of wood pyrolysis.

The most important points that need to be verified, be it against fresh experiments or against published data for similar feedstocks, are the composition of the primary pyrolyis products and the way in which secondary reactions are impacted by the local temperature and the residence time of the vapours. Another important consideration is the time taken by the primary gases and vapours to evolve, which could also be estimated from experimentation, for example by radiative flash pyrolysis of single particles[160]. Failing that there are models, for example the work by Chunjian et al cited earlier[148] or the modelling work of di Blasi[161,162,163,164], which consider the interaction of reaction kinetics, hydro-dynamics and heat transfer within a single, large particle, that could be used instead to obtain an estimate of the time taken by the primary pyrolysis vapours and gases to evolve.

Single particle models do take a similar approach as this thesis. However, they limit themselves to the conditions within a single particle, and the interdependency of mass/heat transfer and the reaction kinetics within it. In terms of computational effort this approach is much easier than considering the fluid dynamics of the fluidised bed itself. This is so, as a one-dimensional model that only considers the radial position within the particle will generally suffice. By contrast Eulerian CFD modelling of fluidised beds has to take

account of at least two dimensions and uses the full Navier-Stokes equations, while the single particle models can make do with using the Darcy equation, in which the velocity only depends on the pressure gradient multiplied by a constant. Single particle models can therefore be solved explicitly, using direct time stepping and a simple spreadsheet software package such as MS Excel, within fractions of a second of computing time, while CFD modelling of fluidised beds takes on the order of days of computing time.

For coupling the single particle model with the hydro-dynamics of the fluidised bed, di Blasi has used correlations to determine important hydro-dynamic variables[162,164]. A quote illustrates that kind of procedure:

"in this study extra-particle tar evolution is also described assuming an isothermal plug-flow behaviour [...]. More precisely, all the particles undergo the same thermal (and conversion) history and the total tar vapours produced undergo extra-particle cracking only along the expanded bed height, with residence times estimated on the basis of the bubble velocity"[162]

As has been shown in this chapter, estimating the residence time of the vapours based on the bubble velocity may not give satisfactory results. Furthermore, correlations for bubble velocity are unreliable for new geometries, where CFD can still be applied successfully, as has been shown in chapter 6.

The only model found in the literature that considers a combination of reaction kinetics with CFD modelling of the fluidised bed hydro-dynamics is by Lathouwers and Bellan[16]. Their model is very complex so that it can only cope with very simple geometries involving relatively few grid points. One reason for this complexity is that the model tries to predict optimum temperatures for different feedstocks, which could be obtained more reliably and accurately by bench scale laboratory experimentation.

Lathouwers and Bellan only look at a scale factor of 3, at an absolute bed height between 16.3 cm and 48.9 cm and at an absolute diameter between 10 and 30 cm. Furthermore, they only consider bio-oil yield and ignore limitations due to heat transfer or char entrainment and also the potential for greater char fines production, if the bed is fluidised more vigorously. Their conclusion is that the fluidising velocity should be proportionally raised

with reactor height to maintain low residence times. While it is certainly true that residence times will tend to increase in rough proportion with bed height, it is not necessary to use a CFD model to come to that conclusion.

The potential for maldistribution in a large fluidised bed reactor is also obvious without needing to resort to CFD, the degree of maldistribution in a particular reactor and the point at which it becomes a problem, on the other hand, are not. A similar consideration applies to the impact of large-scale flow patterns on organic vapour residence time and therefore bio-oil yield.

In comparison to the model by Lathouwers and Bellan the modelling work presented in this thesis takes account of more aspects of interest such as entrainment. The computational effort for the CFD modelling is kept within reasonable limits by keeping these aspects out of the main CFD runs. For example, the potential for char accumulation resulting from insufficient entrainment is estimated based on data from a relatively short CFD run (see chapter 8). The consequences of the char accumulation are then assessed in another CFD run that has an elevated level of the solid phase compared to the first run. Because char accumulation is a slow process, when compared to the hydro-dynamics of the bed modelled by CFD, that is it takes minutes to hours rather than seconds, this approach is entirely justified and little accuracy is lost.

Likewise, there is no need to implement a complex reaction kinetics model that tries to predict the behaviour of different types of feedstock within the CFD code. It is easier to determine the reaction kinetics based on experimental data on the bench scale, and to then modify the reaction kinetics scheme used to take account of those data.

Finally, it should be pointed out that validation of the results for yield was not feasible at this stage. Where hydrodynamics does not govern, the implemented model itself is empirical and therefore already validated, while where hydrodynamics does govern no suitable experimental cases exist.

8. Entrainment and Attrition

In this chapter entrainment and attrition are considered. An estimating procedure for entrainment is presented and compared with experimental data, both qualitatively and quantitatively. Furthermore, experimental results on terminal velocities are presented and employed to check the validity of the assumptions used in CFD particle tracking. The theoretical impact of attrition is discussed together with some data available from experiment.

INTRODUCTION

Entrainment and attrition are critical parameters for fluidised bed design, yet they are still ill understood. Often correlations will differ by several orders of magnitude. Furthermore, they tend to be obtained on small laboratory fluidised beds and scale quite poorly[13].

As Geldart[131] comments, *it is therefore not surprising that entrainment and carryover cannot be calculated from first principles, nor that empirical correlations give predictions which differ by factors of over 100.*

For a discussion of available correlations for entrainment the reader is referred back to chapter 3.

Fluidised bed fast pyrolysis of biomass requires selective entrainment of char particles that are less dense than the main bed material sand, but of roughly the same or even larger size[152]. This is a rare combination. In fluidised bed combustors the aim is to prevent loss of carbon before it has had time to react. Only the fly ash, which is of a much smaller average diameter is allowed to escape the reactor to be collected by cyclones and filters[165]. A lot of the work on entrainment has also been performed for cracking catalyst, which likewise has a rather small diameter[166]. In fast fluidised beds used for catalytic cracking of oil, it should be said that the limitations on entrainment are of a different nature than in fast pyrolysis. Because all the particles are small enough to be entrained, the rate of entrainment is determined by the capacity of the gas for pneumatic transport[91].

Large char concentrations in the bed are believed to degrade bio-oil yield and quality[152], as has already been pointed out in chapter 7. Consequently, efficient entrainment needs to be aimed at minimising the concentration of char in the fluidised bed. As operating and capital costs, and the thermal efficiency of the process are related to recycle gas throughput, it is also desirable to minimise the amount of recycle gas required for fluidisation and char removal. Smaller equipment sizes help to reduce capital and operating costs, and thermal efficiency is raised when less recycle gas needs to be cooled down from 500° to 25° Celsius and then heated back up to 500°. As long as sand is not recycled to the reactor, it is also necessary to aim at keeping it in the bed.

Entrainment should be supportive of downstream efforts to remove small char and sand particles from the bio-oil vapours and consequently the bio-oil itself, where they are believed to contribute to the instability of the oil and also to problems in engine applications[167]. Longer char residence times and more vigorous fluidisation lead to more char fines, which makes the task of removing them in the subsequent downstream equipment (such as cyclones) more difficult.

The Eulerian-Eulerian method introduced in chapter 4 is not capable of predicting the movements of single particles and also fails, when the particle concentration becomes too low (in a similar fashion as the Navier-Stokes equations fail for very low pressures combined with very small dimensions). On the other hand, an approach that is purely Lagrangian requires excessive computing resources, as has already been discussed in chapter 4. Consequently, it was decided to pursue the development of an estimating procedure for entrainment that uses both methods.

PARTICLE TRACKING

Particle tracking in the freeboard is performed with the help of Newton's second law taking account of the drag force exerted by the gas on the particles:

$$F_D = 0.125 \, \pi \, d^2 \, \rho \, C_D \, |v_R| \, v_R$$

The effect of the particle movement on the fluid phase, and interactions between particles are neglected. This is justified because the number of particles in the freeboard is low.

Particles are allowed to bounce off walls, where a coefficient of restitution of 0.8 is applied, which is based on the elasticity of sand and metal collisions but can be varied considerably (from 0.5 to 0.9) without affecting the entrainment results noticeably. A discussion of work in the literature that does consider collisions between particles was presented earlier in chapter 4.

ENTRAINMENT MECHANISM

When a fluid is allowed to rise through a loose bed of particles, there will be a pressure drop across the bed that acts as a lifting force on the particles. At the point of incipient fluidisation this pressure drop, as has already been discussed in chapter 3, has become large enough to balance the weight of the particles forming the bed. Further fluid flow then percolates through the bed in the form of bubbles.

The eruption of these bubbles at the bed surface is responsible for the ejection of particles of all size classes into the freeboard. Very fine particles may even be entrained without the assistance of a bubble, if their terminal falling velocity is below the superficial gas velocity in both the bed and the freeboard.

There is no agreement in the literature whether ejected particles originate at the nose or the wake of bubbles; experimental evidence supporting both mechanisms has been found[168,131]. The visual evidence from observation of recorded bubbles obtained in the work reported in this thesis indicates that virtually all ejected particles originate at the nose of bubbles. It can also be clearly seen, not just in the videos obtained from experiment but also in the CFD, that the surface layer of bubbles becomes smaller as the bubble bursts and then falls back towards the bed. The origin of ejected particles is therefore considered to lie at the nose of bursting bubbles.

Linking particle tracking and the two-phase fluidised bed model is not straightforward, because individual particle velocities are subsumed in the local averages and therefore not directly available from the fluidised bed model. Consequently, the initial particle velocities for particle tracking have to be obtained from what the fluidised bed model does give, namely the extent of bed expansion, the position and velocity of the bubble, gas velocities and local averages for particle velocities. It should be stressed that this step is by far the

156

most uncertain in the whole procedure for estimating entrainment. Particle tracking in the freeboard and the determination of two-phase flow in the fluidised bed itself have a very solid and well validated basis by comparison.

Several models in the literature[169,170] use the bubble velocity to estimate the initial particle velocity without distinguishing between different particle sizes and densities, that is heavier and bigger particles are given the same starting velocity as lighter and smaller ones. This wrong assumption (in actual fact large particles have much lower starting velocities than smaller particles) implemented in particle tracking would indicate that large particles reach a greater height than small ones, completely contrary to experimental observation.

The particle tracking is therefore divided into two phases. In the first the acceleration within the fast gas jets that are found in and just above the erupting bubbles is simulated and in the second the accelerated particles are followed through the freeboard.

A further question that needs to be answered is the number of particles drawn into the gas jets during bubble eruptions. Based on the literature[171,172] and experimental observations undertaken during the course of this study, it is assumed that a layer with a thickness equal to the mean particle diameter in the bed is involved in the ejection process. From the surface exposed to a particular gas jet the total mass of involved particles is then calculated. Size classes for char and sand particles are allocated the same percentage of the ejected particle mass as in the bed as a whole.

SUMMARY OF ESTIMATING PROCEDURE FOR OBTAINING ENTRAINMENT

This section deals with the practical details of how the estimating procedure works, rather than the theoretical basis for it, which has largely been covered in the previous paragraph. A flow chart diagram illustrating the procedure is shown in Figure 92.

Obtain 2-D, or if time constraints allow 3-D, Eulerian/Eulerian simulations of the fluidised bed of a sufficient length to capture a representative number of bubble eruptions.

Divide the upper surfaces of the erupting bubbles into a number of area classifications based on the speeds of jets experienced in these areas.

Divide the particles into a number of size classifications

For each combination of classifications (bubble eruption, jet classification, particle size) obtain the position of the nose of the bubble and the velocity of the solids phase. Also estimate from the Eulerian/Eulerian simulations the magnitude of and time spent in the jets around bubble eruption.

Transfer the velocity of the particles to a particle tracking simulation in either 2-D or 3-D. Use a superficial velocity equal to that estimated from the Eulerian/Eulerian simulations and note the velocities and distances reached by the particles, after the estimated time spent in the jets has been achieved.

Take the position of the particles from the Eulerian/Eulerian simulations, add the distance spent being accelerated by jets, and fully specify the velocity by adding the direction, which has to be estimated from the initial direction of the particles and the velocity of the accelerating jet. Perform particle tracking in 2-D or 3-D with the same superficial velocity as found on average in the freeboard.

Count the particles reaching the exit and add up to get the proportion of ejected particles of a particular classification reaching the exit.

Calculate the mass flow rate for each classification by multiplying:
1. the proportion of particles of a particular classification reaching the exit
2. the frequency of the bubble eruption event
3. the mass equivalent to one layer of average particle diameter with the same surface area as that of the fraction of the nose of the particular bubble eruption event considered in the classification.
4. the mass fraction in the fluidised bed of the particle class considered
Finally, add all the mass flow rates together to get the rate of entrainment.

Figure 92 Flow chart diagram of estimating procedure for entrainment

158

The total entrainment is calculated by dividing it up into small classes (for example char between 180 and 300 microns, ejected from a bubble between 2 and 3 cm in diameter) and then summing the individual contributions. This addition was done on a spreadsheet and a sample calculation is included as an appendix.

The classifications used are to some degree arbitrary. They need to be sufficient in number to give a reasonably representative selection of bubble diameters and eruption locations, jet velocities and particle sizes.

The number of particles of a particular classification reaching the exit was counted with the help of a Fortran subroutine, a sample version of which is included as an appendix.

Finally, it should be clarified that most two-phase Eulerian calculations were performed in two dimensions, while most particle tracking operations were done in three dimensions. This was due to excessive computing times being required by the two-phase calculations.

EXPERIMENTAL VALIDATION ON THE 2-D MODEL

A small number of experiments were performed to obtain the equilibrium concentration of char established when it was fed to the 2-D model (for a description see chapter 5) and at the same time constantly removed from the bed via preferential entrainment. The estimation procedure just described was employed and compared. Figure 93 illustrates one set of data. The CFD estimate is clearly very conservative, but of the right order of magnitude and qualitatively accurate, which is a lot better than for any of the existing correlations. This was to be expected for several reasons. Apart from the assumptions of perfect mixing and the amount of char thrown into the freeboard, attrition was neglected at this stage. For a generic reactor design without knowledge of the feedstock, neglecting the effects of attrition is advisable, as this is an aspect that is very feedstock dependant.

159
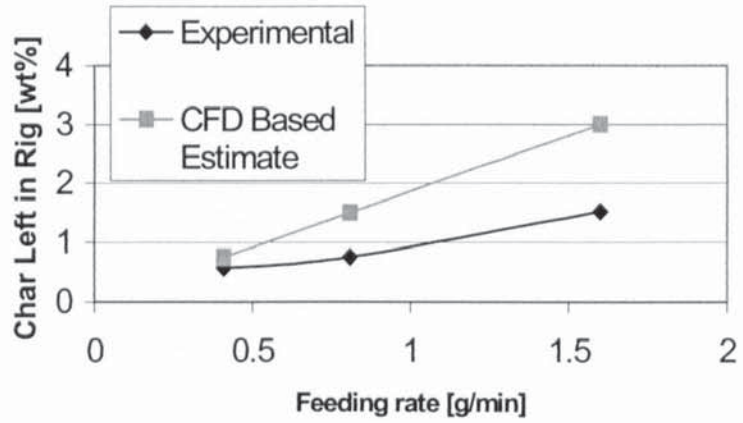
Figure 93 Comparison of experimental data (LI) and CFD based estimate (LII)

QUALITATIVE VALIDATION FROM EXPERIMENTS ON THE 5 KG/H RIG

An analysis of the material entrained from a number of the runs with the 5kg/h reactor (also described in chapter 5) showed very good qualitative agreement with predictions from CFD. It showed that very few sand particles were entrained and that their distribution was skewed with no sand particles greater than 500 microns. On a qualitative basis that is exactly what the CFD calculations predict (see Figure 94). The figure shows that the majority of large char particles and nearly all smaller char particles that are ejected are entrained, while sand particles with a diameter of 800 microns fall back.
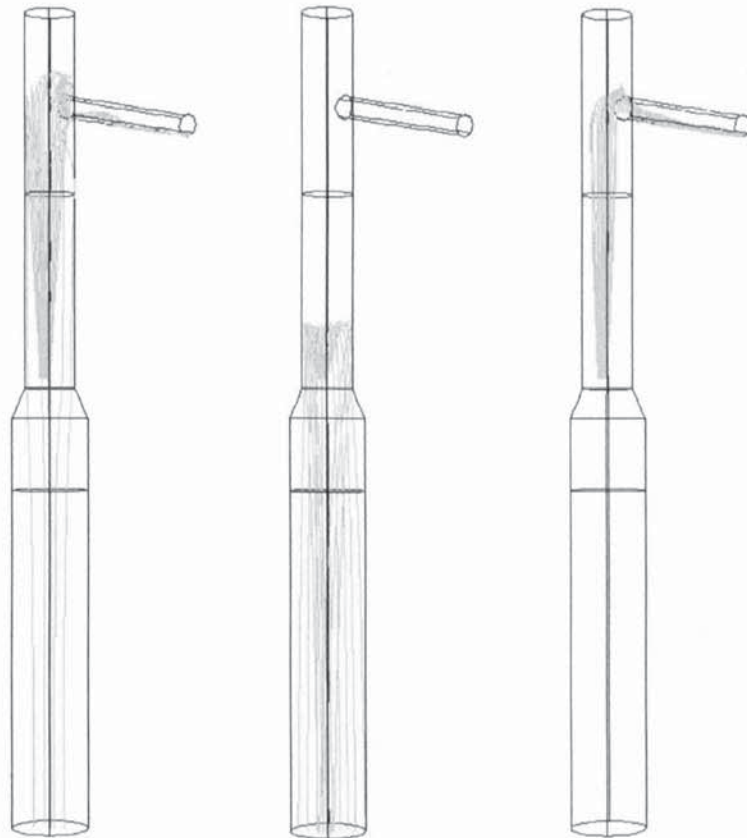
Figure 94 Particle tracks (LIII)

Left - large char particles (800 microns); Centre - sand (800 microns); Right – small char
particles (400 microns)

All particles close to maximum ejection height and velocity.

OPTIMISATION OF ENTRAINMENT

Three options for modification were investigated in detail with the change in geometry
confined to the freeboard, a narrowing, a dummy cyclone (which also serves to narrow the
cross-section available for flow) and a widening (see Figure 61 in chapter 6).

As discussed in the introduction to this section, efficient entrainment refers to a number of
desirable criteria, notably a low char concentration in the fluidised bed, low sand
entrainment and a low fraction of fines resulting from attrition should all be achieved at a
minimised recycle gas throughput. The effects of a change in geometry on its own are
illustrated in the following two graphs (Figure 95 and Figure 96) giving char concentration
and sand entrainment. The y axis is given without units, as the graphs apply to a range of

conditions of interest and are only of an illustrative nature. The rate of attrition is feedstock dependent, however, for all biomass feedstocks the rate of generation of fines by attrition will increase with greater char concentrations in the bed.
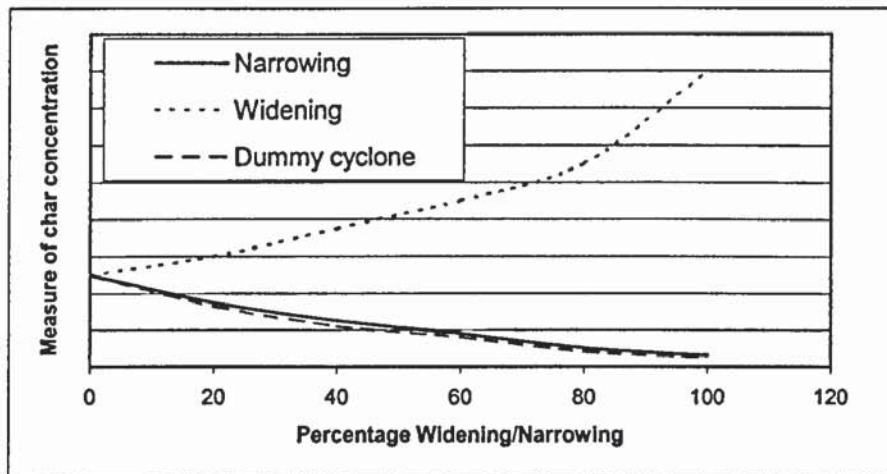
Figure 95 Effect of narrowing/widening on bed char concentration
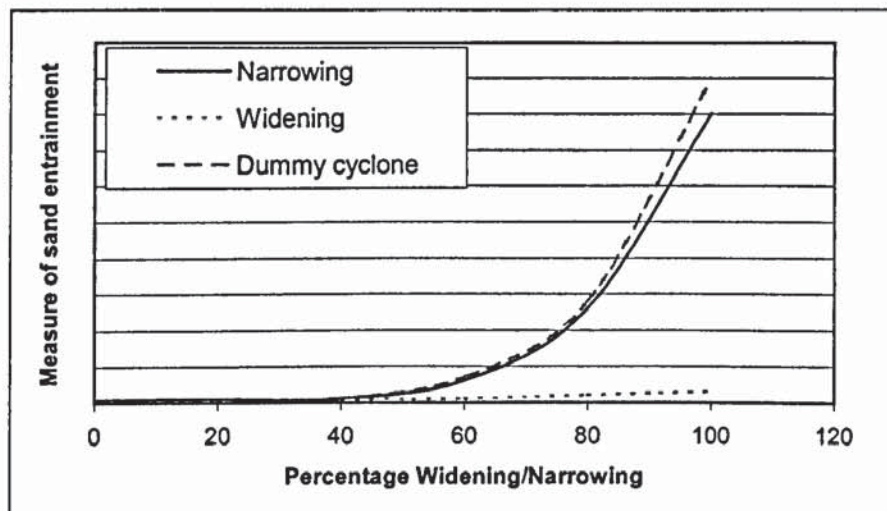
Figure 96 Effect of narrowing/widening on sand entrainment

The shape of these graphs and the conditions they pertain to deserve some further explanation. Size reduction of the biomass fed to the reactor is very costly. Consequently, it is economically desirable to work with relatively large biomass particle sizes that yield char of a similar range of diameters as the sand currently employed for fluidisation. This means that superficial velocities attainable for the fluidised bed itself are not sufficiently great to carry larger char particles higher after they have been thrown into the freeboard by

162

the eruption of bubbles. The only possibility to achieve those higher velocities is a freeboard narrowing. The mechanism of preferential entrainment for larger char particles is illustrated in Figure 97. The terminal velocities of the char particles are typically below 2m/s, while all but the tiniest sand particles are above that threshold.
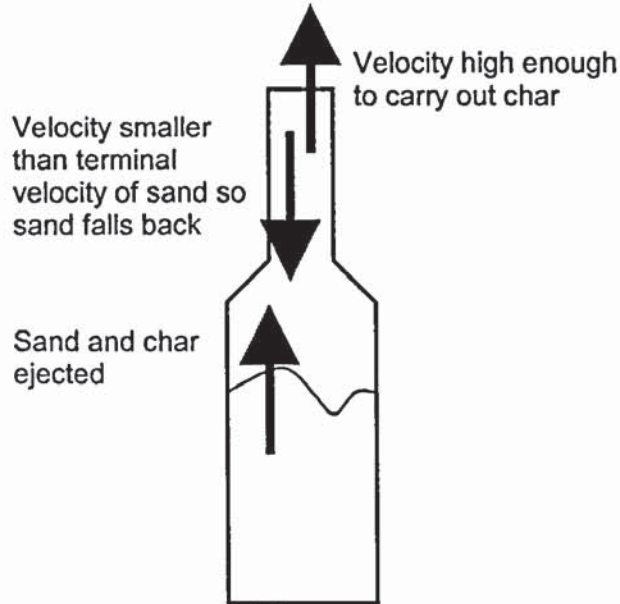
Figure 97 Illustration of preferential char entrainment mechanism.

In the graph illustrated in Figure 96, sand entrainment is only slightly increased for narrowings (with the dummy cyclone also resulting in a narrower cross section) up to around 50%. After that point it rises very rapidly.

In order to entrain larger char particles efficiently, a narrowing at the top of the freeboard is absolutely required. However, a widening also has advantages, notably bed height fluctuations are reduced substantially. Furthermore large beds will experience significant pressure drops leading to an expansion of the fluidising gas from the bottom to the top of the reactor. In addition, pyrolysis vapours are added increasing the velocity even more. To ensure that the bed is equally well fluidised across its whole height, a widening may therefore be necessary on the industrial scale.

The fluctuations in bed height become more important at large scales compared to the heights reached by particles thrown up by bubbles. When a narrowing is employed, as is

necessary to entrain larger char particles, large fluctuations in bed height may mean that the bed occasionally reaches up to the narrowing. Once this happens large amounts of material are lost from the bed all at once (illustrated in Figure 55 in chapter 6). This will reduce the height of the bed again. If char then accumulates faster than it is removed, the bed height can again reach up to the narrowing. In this fashion the bed loses more and more sand and is slowly transformed into a bed of char. The only way to prevent this by changing the operating variables and not the design may then be to reduce the biomass feed rate and therefore the capacity of the reactor.

The most troublesome variable to scale up is the height of the bed. Greater heights of the bed decrease the bed surface to volume ratio and therefore the ratio of surface available for entrainment to the amount of char that needs to be entrained. As pointed out above they also lead to large pressure drops and velocity changes from the bottom to the top of the bed and to more significant bed height fluctuations. The diameter of the bed is less important. However, the narrowing will have to be designed in such as fashion as to prevent large dead zones for entrainment, that is most of the bed surface should be close enough (i.e. less than a meter) to a narrowed exit for the gases/vapours that char particles thrown up by bubbles can make it to that exit.

The entrainment mechanism is affected by the bubble diameter, as larger bubbles lead to greater ejection velocities, which help efficient separation and removal of char from the fluidised bed. Consequently, a modelling study was undertaken to investigate the scale dependence of bubble diameter and velocity, which is illustrated in Figure 59 and explained in more detail in chapter 6. It was found that the increase in bubble size with scale levels off at a bed diameter of around one metre.

For scaling of the Wellman design beyond a diameter of 1 metre, char entrainment becomes such a serious capacity limitation that it would have to be addressed by a different reactor design or a reduction in the feedstock size employed. Some thought has been given to the question as to what geometric changes might represent the best solution for such scale-up. The subject is further discussed in chapter 10.

ATTRITION

Char and sand particles in the bed constantly collide with each other leading to abrasion and particle break-up. Experimental work performed by Hague and the author of this thesis indicates that the main variable affecting the attrition of char is the vigour of fluidisation[128]. This is illustrated in Figure 98.
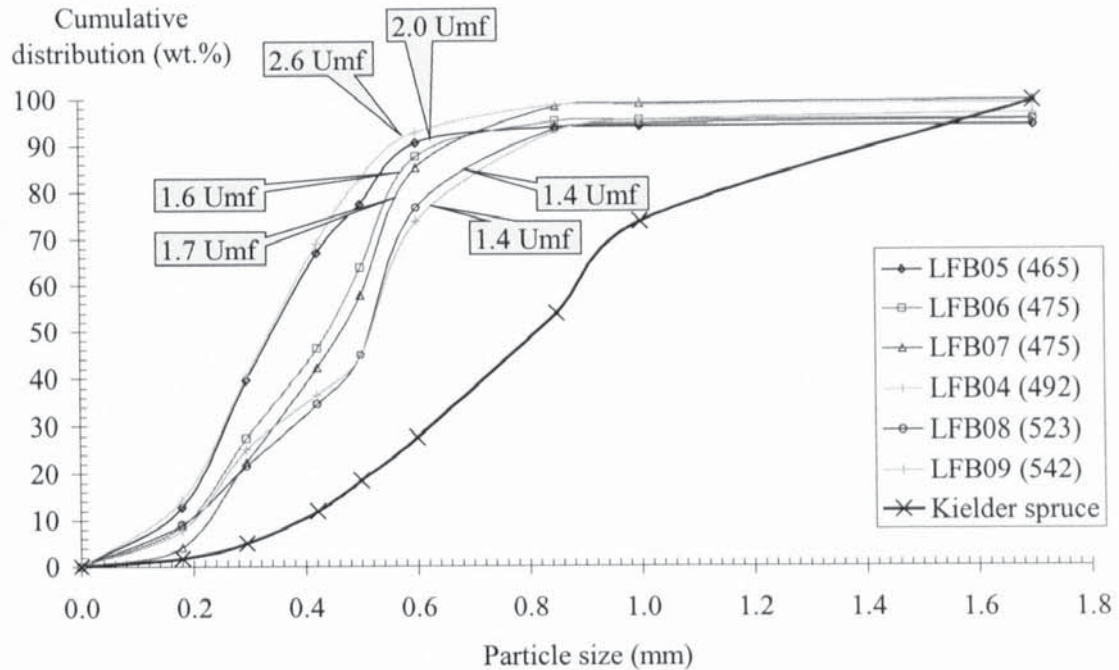
Figure 98 Experimental values for char size distribution obtained on the 5 kg/h rig (LIV)

In this fashion the average char particle diameter in the bed could be cut by 30% to 40% for spruce as the biomass feedstock making preferential entrainment of the char considerably easier, though at the expense of a more difficult separation task for the downstream equipment, notably the cyclones. Further experimental work for other biomass feedstocks is desirable and would be a very useful input for a more accurate prediction of entrainment. Merely applying attrition data already available from the study of other processes is unlikely to give accurate results, as the char produced by fast pyrolysis will have its own characteristics.

In the course of this work, a small number of experiments were carried out by the author to measure abrasion of sand on the 2-D rig. The rig was filled with sand fresh from the barrel.

Then air was supplied to the rig at a superficial velocity of 0.55 m/s and smaller sand particles were allowed to be entrained. Finally, a cyclone was fitted to the gas exit and the bed was run for several hours. The measured abrasion was less than 0.1% and within the scope of experimental error. This is quite promising, as it indicates that sand loss by abrasion is unlikely to be a serious problem.

TERMINAL FALLING VELOCITY

The terminal velocity that particles reach when in free fall is an important particle characteristic. It is also fairly straightforward to measure and was therefore used to check the accuracy and validity of the particle tracking model. The measurement technique is entrainment of a small sample of a particular size class in a narrow tube taking the average of the band within which 90% of the small sample are entrained. In the computational modelling of the particle tracks the upper end of the class size is used as the particle diameter and the particles are started from rest and from a falling velocity greater than their terminal velocity.

For sand the fit is very good (see Figure 99). The measured velocity is within the band indicated by particle tracking. For char (see Figure 100) the picture is slightly more complicated. For smaller diameters, the measured falling velocity is above and not within the range given by the particle tracking. The microscopic examination explains the reason.

The quantitative results of that examination are included in the appendices. For each size class 20 particles were chosen randomly for examination. The greatest length across each particle was recorded as its longest dimension. This is the column headed "long" in the spreadsheet. The entry in the column headed "short" in the spreadsheet was the greatest distance of the particle that could be obtained by drawing a line perpendicular to the one delineated by the longest dimension of the particle. The spreadsheet in the appendices also gives the ratio between the "long" and "short" dimensions and averages for the 20 particles.
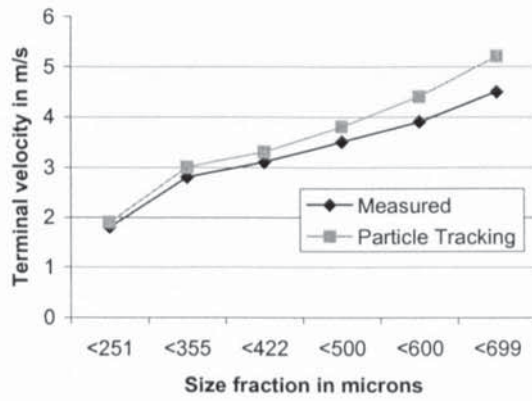
Figure 99 Terminal velocity of sand
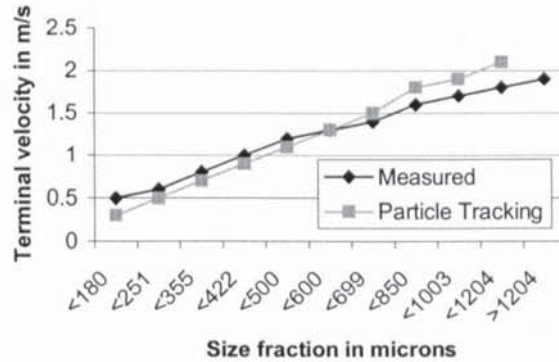
Figure 100 Terminal velocity of char.

While sand particles approximate spheres fairly closely, char particles are long and thin cylinders. Furthermore, the smaller the char particle the greater the aspect ratio. This may be explained by assuming that the char particles fall apart along the grain rather than across it. As sieving measures the diameter of the thin cylinders and not their length, the effective diameter is underestimated, particularly so for smaller char particles. Consequently, the diameters used in the particle tracking undertaken to estimate entrainment had to be adjusted. This was done by shifting the measured curve to the right until the measured and computed value for the size class corresponded.

A few pictures of char, wood and sand particles illustrating their shape were presented earlier as Figure 27 in chapter 5.

From Figure 99 and Figure 100, which illustrate the terminal falling velocities of the sand and char particles, it can be seen that virtually all char particles have a lower terminal velocity than the vast majority of sand particles. Based on this consideration, separation can therefore be effected within a gas stream that has a superficial velocity in between those of sand and char, that is about 1.5 to 2 m/s. Based on this consideration a number of modifications was implemented both in the CFD modelling work (described in chapter 6) and experimentally.

Figure 101 illustrates sand entrainment on the original cold flow rig. While the trend for sand entrainment estimated from the CFD calculations is correct, on a quantitative basis the under-prediction is significant, namely by a factor of up to three for the lower superficial velocities. The main source of error is probably the entrainment mechanism.

The next graph (Figure 102) shows the percentage of char entrained out of the original and modified designs. At the start of the experiment the bed consists of 95% sand and 5% char. The superficial velocity is 0.45 m/s.
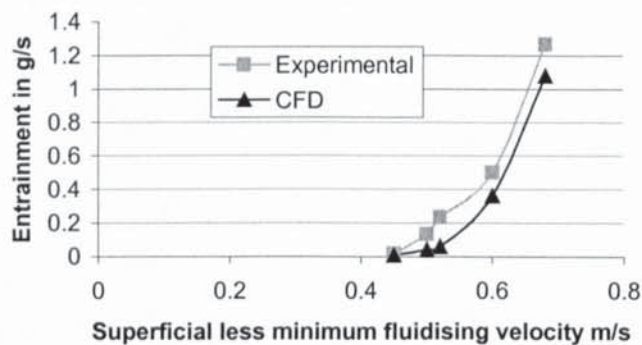
Fig.15

Figure 101 Sand entrainment on the original cold flow rig (LV)
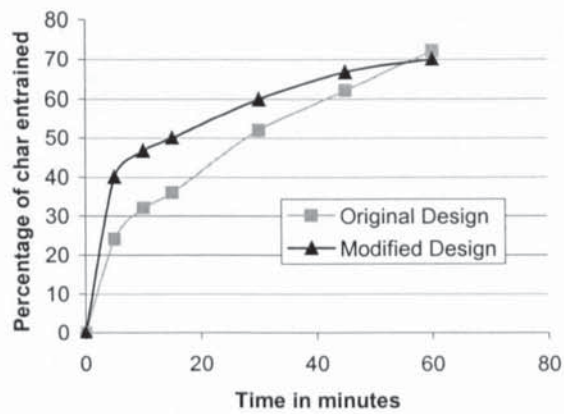
Figure 102 Comparison of mixed sand and char entrainment in original and modified cold flow rig design (LVII)

The graph indicates that the initial entrainment rate for the modified design is much greater than for the original design. The analysis of the entrained material also showed that in the improved design ten times fewer sand particles were entrained and that their distribution was skewed with no sand particles greater than 500 microns. On a qualitative basis that is exactly what the CFD calculations predict.

A modified hot reactor has been built, but no experimental work has been performed on it so far. It is expected that this will happen shortly after the submission of this thesis. An illustration of the CFD work performed for this modified design was shown earlier as Figure 54 in chapter 6, and a photographic illustration in Figure 20 in chapter 5.

9. Heat Transfer

In this chapter the results of direct Eulerian numerical modelling of heat transfer in a fluidised bed in two and three dimensions are presented and compared with correlations available from the literature and a similar attempt at modelling heat transfer in fluidised beds through a Eulerian approach that was performed ten years ago using two dimensions only. Furthermore, experimental heat transfer results obtained on the 2-D rig are presented. Finally, possible options and trade-offs for optimising plant performance with respect to heat transfer are discussed.

INTRODUCTION

The favourable heat transfer properties of fluidised beds are one of the most significant reasons, why they tend to be the preferred reactor choice for fast pyrolysis of biomass[173]. The area for inter phase heat transfer available in 1 cubic metre of particles with a diameter of 0.1 mm is equivalent to the surface area of one of the great pyramids in Egypt[131].

Fluidised beds also have great thermal inertia, as the heat capacity of the solid phase is very large compared to that of the fluidising gases. For example, a cubic metre of a fluidised bed of sand fluidised by air will contain roughly 1600 kg of sand and just 0.5 kg of air. As the heat capacity of sand is around 740 $Jkg^{-1}K^{-1}$ and that of air 1000 $Jkg^{-1}K^{-1}$, the respective amounts of heat held for each Kelvin of temperature difference by the sand and air in that cubic metre are over 1000 kJ and about 0.5 kJ respectively, that is the capacity of the solids to hold heat is around three orders of magnitude larger than that of the fluidising gases (property data taken from Atkins[174]).

Furthermore, heat transfer with surfaces, such as the vessel walls or immersed tubes, tends to be ten to twenty times greater with the solid phase present than with the gases alone[175].

The rate of heat transfer achievable by a given reactor design represents a capacity bottleneck limiting the amount of biomass that can be processed. Furthermore, it is desirable to supply heat to the pyrolysis reactor via heat transfer surfaces rather than to use

more or hotter recycle gas for fluidisation. Very high fluidising gas temperatures make it difficult to achieve pyrolysis under optimum temperature conditions and therefore reduce bio-oil yield and quality. Using large volumes of recycle gas on the other hand leads to larger equipment sizes and therefore costs, and is also deleterious for the thermal efficiency of the process.

HEAT TRANSFER MODELLING

Interphase heat transfer, that is heat transfer between the solid and gas/vapour phases, was accounted for using a correlation by Gunn[176]:

$$Nu = \left(7 - 10r_\alpha + 5r_\alpha{}^2\right)\left(1 + 0.7\,\mathrm{Re}^{0.2}\,\mathrm{Pr}^{1/3}\right) + \left(1.33 - 2.4r_\alpha + 1.2r_\alpha{}^2\right)\mathrm{Re}^{0.7}\,\mathrm{Pr}^{1/3}$$

The local thermal conductivity of the two phases was made dependent on the volume fraction using a correlation by Zehner and Schlunder[177]:

$$\lambda_\alpha{}^{\text{eff}} = \lambda_\alpha\left(\frac{1 - r_\alpha{}^{0.5}}{r_\alpha}\right)$$

$$\lambda_\beta{}^{\text{eff}} = \lambda_\alpha \frac{1}{(1 - r_\alpha)^{0.5}}\left(\omega\,A + (1 - \omega)\psi\right)$$

$$\psi = \frac{2}{\left(1 - \dfrac{B}{A}\right)}\left(\frac{B(A-1)}{A\left(1 - \dfrac{B}{A}\right)^2}\ln\left(\frac{A}{B}\right) - \frac{B-1}{1 - \dfrac{B}{A}} - \frac{1}{2}(B+1)\right)$$

$$B = 1.25\left(\frac{1 - r_\alpha}{r_\alpha}\right)^{\frac{10}{9}}$$

$$A = \frac{\lambda_\beta}{\lambda_\alpha}$$

No correlation was used for the wall heat transfer coefficient. Instead, the scope for modelling this heat transfer coefficient by using a progressively finer grid closing in on the wall was investigated. Figure 103 illustrates the kind of grid employed in this work. This

particular grid had 50 grid points in the x direction 100 in the y direction and 10 in the z direction. The spacing was a uniform 1 cm between grid points for the x and y directions. A one way bias was employed for the z direction to divide an overall distance of 1 cm into 10 smaller sections with the smallest one next to the wall and a third of the size of the largest section.
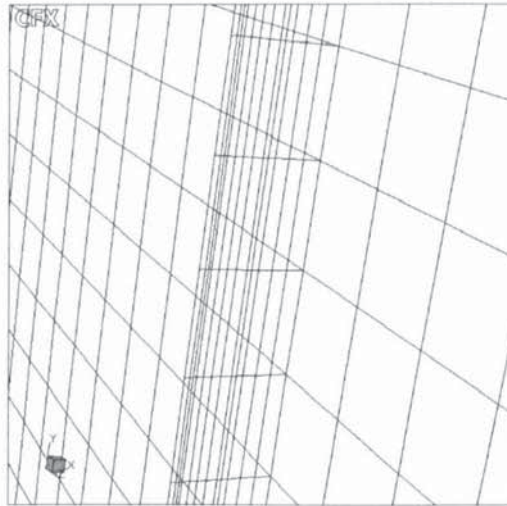
Figure 103 Illustration of gridding used in a typical CFD run

Two initial conditions for the thermal thickness of the pseudo boundary layer were used, zero and a thickness obtained by raising the thermal conductivity by a factor 1 million for about a thousandth of a second, that is three to four time steps of 0.00025 seconds each, before starting the main run. Using this approach the actual value of the heat transfer coefficient was approached from two sides and when they were sufficiently close a geometric average was taken as the result.

CALCULATION OF THE HEAT TRANSFER COEFFICIENT FROM THE EXPERIMENTAL RESULTS

For an explanation of the experimental set-up employed the reader is referred back to chapter 5. An illustration of the temperature readings obtained during a typical experiment is shown in Figure 104. On the hot summer day this particular experiment was performed on the inlet air temperature was around 28 degrees Celsius, while the temperature of the water went as high as 63 degrees Celsius.

172
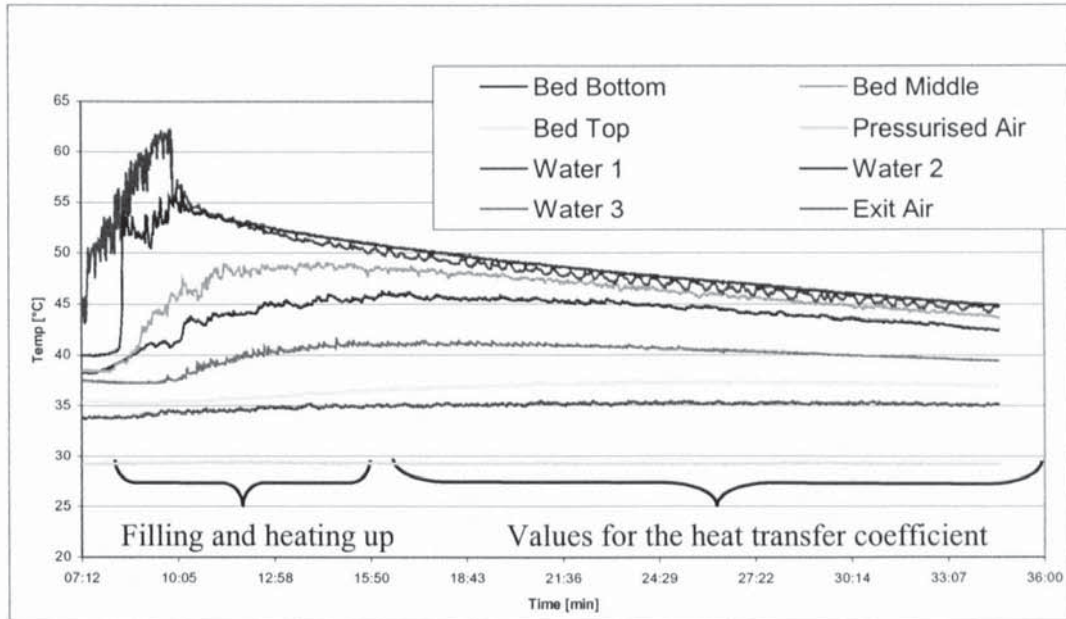
Figure 104 Illustration of temperature readings in a typical experiment

To calculate the heat transfer coefficient the heat given up by the water over a time span Δt was calculated. The mass of the water is calculated from the volume of water in the tank and its density. The heat losses to the surroundings were taken account of by assuming that the heat transfer coefficient to the environment was 8 W m^{-2} K^{-1}, which is in agreement with values from the literature for typical film coefficients[178,179] and an experiment run by the author and Gero Ferges without employing any sand. Furthermore, the heat gained by the air while passing through the fluidised bed was calculated as a check on the amount of heat lost.

$$Q_{Water} = m_{Water} c_{water} \Delta T_{Water}$$

$$Q_{Water} - Q_{losses} = Q_{transferred\_to\_bed}$$

$$Q_{Air} = m_{Air} c_{air} \Delta T_{air}$$

Knowing the heat transferred to the bed and the temperature difference between the bed and the water, that is the temperature driving force, the heat transfer coefficient could be calculated.

$$\alpha = \left(\frac{Q_1}{A \times t \times \Delta T} \right)$$

173

It should be noted that the thermocouples in the water tank were located on the wall itself. As the conductivity of the thin metal wall is very high, it could therefore be assumed that the heat transfer coefficient between the points at which thermocouples measured the temperature in the tank and in the fluidised bed was the same as the film coefficient on the fluidised bed side of the separating wall.

RESULTS

A side view showing the pseudo boundary layer – there is no real boundary layer in the hydro-dynamic sense for the solid phase - is given in Figure 105. The dimensions modelled were a height of 1 m, a width of 0.5 m and a depth of 0.01 m. The dimensions of the small section shown in Figure 105 are only around 2 mm by 2 mm.

330 K

320 K

310 K

298 K
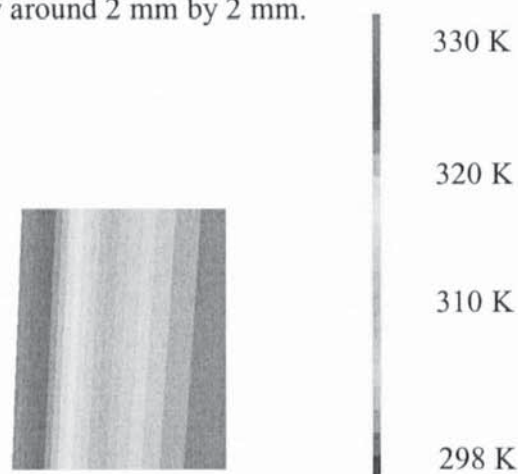
Figure 105 Small section of the pseudo boundary layer obtained via CFD calculations

(LVIII)

A boundary layer approach is more appropriate for the gas phase than the particle phase, notably as the size of the particles is quite close to the grid spacing employed. Unsieved sand employed in the experiments averaged 0.503 mm, with most of the particles sized between 0.35 and 0.7 mm. The smallest grid element used had a minimum dimension of 0.543 mm.

The fraction of the heat transfer attributable to the solid and gas phases is one indication of the caution that needs to be exercised, as the solid phase is responsible for on the order of 90% of the heat transfer, mostly via conduction[180]. Predicting this fraction within the right

order of magnitude is a first test for the model to be believable. A few of the values calculated are illustrated in Table 17.

Table 17 Sample values for the fraction of the heat transfer attributable to each phase calculated by the CFD model (LVIII)

Description of the run	Percentage due to the solid phase
Time step 115, time from start 0.024 s	94.6%
Time step 39, time from start 0.06 s, 3 time steps at the start were run using thermal conductivities raised by a factor of 1 million	96.7%
Time 111, continued from the above run	94.2%

A comparison of the results obtained for the heat transfer coefficient with the CFD model using just two dimensions rather than three with several correlations from the literature[145] was performed, which is illustrated in Figure 106. As can be seen in the figure, there is considerable disagreement between different correlations that is nearly as great as one order of magnitude. By comparison, direct Eulerian modelling gives quite accurate predictions.
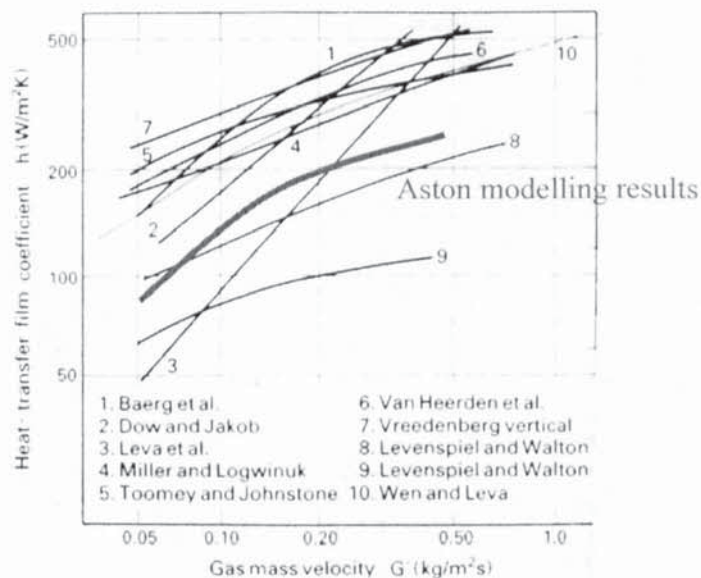
Figure 106 Comparison of CFD model in two dimensions (LIX) with values from the literature

A comparison with experimental values obtained on the 2-D rig was also done and is illustrated in Figure 107.
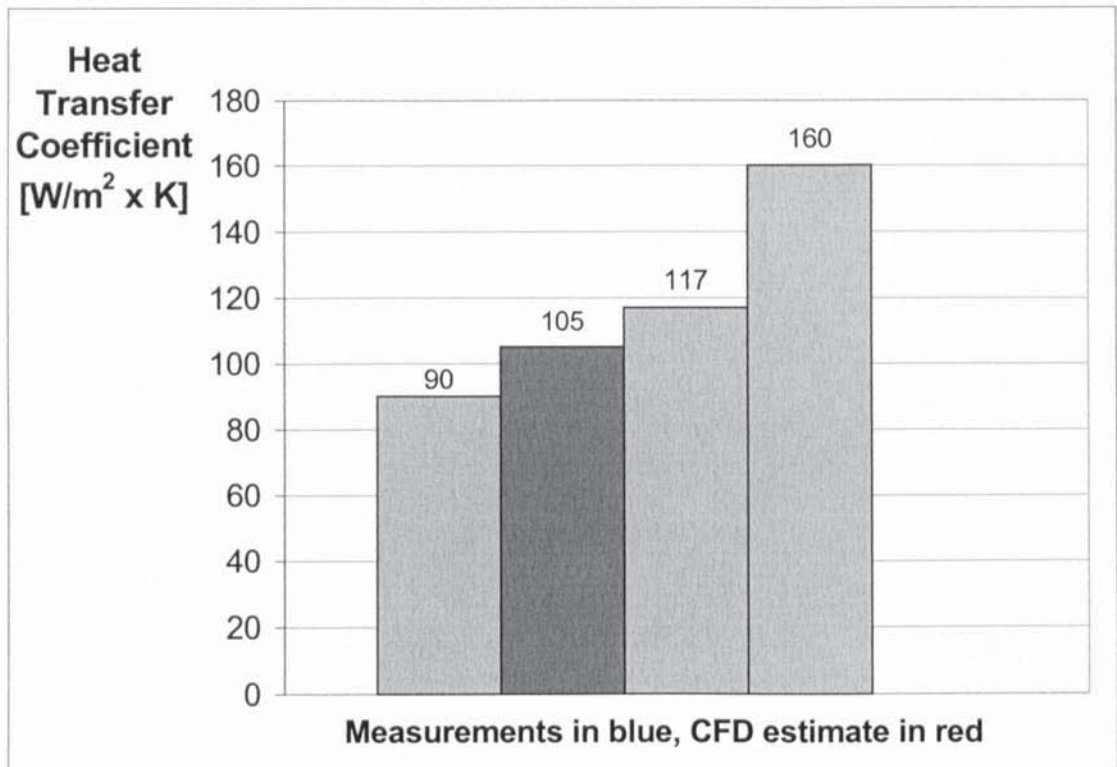
Figure 107 Comparison between CFD and measurement

Table 18 contains more detailed information about the specific conditions for the individual experiments and the CFD run.

Table 18 Experimental and CFD results for heat transfer coefficient

Conditions	Heat transfer coefficient W/m^{2}K
Bed height of 33 cm, particle diameter of 0.44 mm, fluidising velocity of 0.55 m/s	105
Bed height of 33 cm, particle diameter of 0.503 mm, fluidising velocity of 0.36 m/s	90
Bed height of 33 cm, particle diameter of 0.44 mm, fluidising velocity of 0.14 m/s	117
Bed height of 33 cm, particle diameter of 0.44 mm, fluidising velocity of 0.36 m/s	160

It should be noted that the CFD model employed when used for heat transfer and with tight gridding next to the wall, was very prone to numerical instability leading to divergence of the solution rather than convergence. This limited the number of conditions amenable to satisfactory solution with the model, a situation that could not be remedied by adaptive time stepping and other numerical measures, even those requiring significantly larger compute resources.

As can be seen in Table 18, the experimental conditions are not exactly the same as those of the CFD analysis. On the one hand, a velocity of 0.55 m/s led to such vibrations of the metal wall separating the water from the fluidised bed in the experiment, that the experimental run could not be finished. On the other hand, lower velocities confronted the CFD with insurmountable convergence difficulties. It is nevertheless apparent that the order of magnitude of the CFD prediction is excellent when comparing with the kind of accuracy available from correlations, as has already been pointed out above.

The impact of gas velocity and sand particle diameter was also investigated. It was found experimentally that within the range considered of 0.4-0.6 mm, the effect of particle diameter was very pronounced. Raising the particle diameter within that range nearly doubled the heat transfer coefficient. On the other hand, tripling the fluidising gas velocity from the minimum fluidising velocity was mildly beneficial and lead to an increase in the heat transfer coefficient of 35%.

COMPARISON WITH PREVIOUS CFD WORK

The only work found in the literature that employs a similar approach to predicting heat transfer from a fluidised bed to a surface is a PhD thesis by Kuipers[15] published in 1990.

As in the work reported in this chapter, Kuipers relied on a two phase Eulerian representation of the fluidised bed and modelled interphase transfer with the correlation by Gunn[176], the thermal conductivity of the fluidised bed with the correlation by Zehner and Schlunder[177], and heat transfer close to the wall by employing tighter gridding. A different approach was taken with regards to the initial conditions. Kuipers used an initial wall temperature that was the same as that of the bed and then slowly raised it, while the wall temperature was assumed to be constant in the work reported in this chapter.

As less computing power was available at that time the calculations were done in two dimensions and only employed seven grid cells to resolve the boundary layer. Furthermore, the number of simulations that could be performed was also very low; while no exact number is given it appears to have been around five simulation runs. No experimental validation was performed and comparison with experimental results from the literature only gave an order of magnitude confirmation of the CFD results.

Kuipers therefore pointed out that *it must be emphasised that the present model should be considered as a learning model and not as the most efficient way to predict, for example, average wall-to-bed heat transfer coefficients.*

Until such time as the convergence difficulties experienced in this work can be satisfactorily resolved, it must be said that the conclusion by Kuipers is still valid today.

TRADE-OFFS

The two most important limitations for scale-up of fluidised bed fast pyrolysis of biomass are represented by heat transfer and char removal via selective entrainment. Heat can be transferred to the fluidised bed reactor by pre-heating the fluidising gases, through the recirculation of sand heated externally, and through heat transfer surfaces. When the process is scaled, the available area for heat transfer, employing the same geometry for the reactor, will only rise with the second power, while the volume of the reactor will rise with the third power.

There are two principal options to provide the extra heat required via the fluidising gases without changing the geometry of the reactor, either the velocity of the fluidising gas used could be increased or its temperature. Both are undesirable options; raising the amount of fluidising gas leads to larger capital and operating costs for the equipment employed and is also detrimental to the overall thermal efficiency of the process, as the energy used for heating the fluidising gases to the operating temperature of the reactor of around 500 degrees Celsius is lost when the vapours are subsequently rapidly quenched to room temperature. If the carrier gas is too hot, the yield of pyrolysis oil may suffer as organic vapours are cracked to non-condensable gases[181].

178

Consequently, great reliance is placed on heat transfer through heat transfer surfaces in many fluidised bed fast pyrolysis plants. This work confirms that for the particle size range of interest the heat transfer coefficient is very sensitive to sand particle size and that raising it to the upper bound of the range significantly affects the quality of heat transfer and therefore may lower the effective capacity of the plant. On the other hand, work described in chapter 8 shows that the separation of sand and char by selective entrainment of the char becomes easier for larger sand particle sizes leading to the need to find an optimal trade-off that maximises plant output.

The particle size of char largely depends on the biomass feedstock size. Biomass comminution has an economic cost that grows quite large for sizes below two to three mm, which are equivalent to char sizes between 0.5 and 1 mm. This puts a lower limit on the sand particle size that can still effectively be separated from the char of around 0.4 mm. How closely this value should be approached depends on the exact reactor design and also on a trade-off between bio-oil yield and bio-oil production rate, a greater production rate being achievable at the expense of a slightly lower yield by allowing a greater equilibrium level of char in the bed. If the feedstock costs are high in comparison to the capital and fixed operating costs of the plant, this trade-off will likely involve a focus on yield rather than production rate.

10. Discussion of Design Options

There are a number of options for implementing fast pyrolysis reactors. This chapter discusses presently available and possible future designs in the light of the results obtained during the course of the work reported in this thesis.

COMPARISON OF PRESENTLY AVAILABLE DESIGNS

Many reactor configurations have been investigated and implemented for fast pyrolysis of biomass, as has been discussed in detail in chapter 2. While the earlier chapter presented the respective technologies, this chapter focuses on the strengths and weaknesses of the different options with particular emphasis on fluidised beds, as this is the technology investigated in the work reported in this thesis.

The bubbling fluidised bed has a number of advantages at laboratory scale that account for the fact that it is by far the most widely used system for bench-scale studies[21]. It is straightforward to operate and construct, there are no moving parts and it also easily provides accurate mass balance data. On a commercial scale, however, certain limitations become apparent that either do not matter much for laboratory purposes, such as the amount of inert fluidising gas required or the particle size the biomass has to be ground down to, or only constitute a significant limitation at larger scales, such as constraints imposed by heat transfer and entrainment, which were discussed in more detail in earlier chapters.

To keep residence times down, higher velocities need to be employed at larger scales, which in turn necessitates the use of larger sand particles to prevent excessive sand losses. This reduces heat transfer (see chapter 9), shifts bed behaviour towards Geldart class D instead of B (for an overview of this classification system see chapter 3) and limits the range of velocities giving satisfactory performance (see chapters 6 and 8).

Furthermore, it leads to more abrasion and therefore formation of char fines, which are difficult to remove in the downstream separation equipment and may end up in the bio-oil[182], where they are believed to contribute to the instability of the oil and also to problems

in engine applications[167,183]. As the inert fluidising gases have to be quenched together with the organic vapours and incondensable gases resulting from pyrolysis, they represent a drag on the overall thermal efficiency of the process. They also contribute to larger equipment sizes and thereby raise capital and operating costs for the process.

There are, however, also significant advantages of the bubbling fluidised bed when compared to the most important competing alternatives.

Vacuum pyrolysis entails significantly larger equipment sizes and therefore much higher capital and operating costs. The only company commercialising this technology, Pyrovac, has recently entered bankruptcy[184].

Ablative pyrolysis may involve moving parts (see chapter 2), produces large amounts of char fines[185] and scales based on heat transfer surfaces presented to the biomass. By comparison, fluidised beds present such large areas for heat transfer from the fluidised sand to the biomass that this factor is not limiting. Ablative pyrolysis has so far only been proven on the laboratory scale and there are currently no projects implementing scale-up to the pilot plant scale.

Excessive generation of char fines is also a potential problem for fast pyrolysis of biomass in circulating fluidised beds, which furthermore suffer from the fact that the volume fraction of sand is very low, which raises equipment sizes and therefore capital and operating costs.

An analogy can be made with reactors used for Fischer-Tropsch synthesis. While the circulating fluidised bed reactor was easier to design initially, as its hydro-dynamic behaviour is relatively straightforward to predict, it has much lower capacity for the same capital investment and on top of that higher operating costs than the dense fluidised bed technology developed by SASOL[186]. The initial development of the dense fluidised bed for Fischer-Tropsch by the Hydrocarbon Corporation, based at Carthage, Texas, had, however, failed, as the hydro-dynamic bed behaviour did not scale as expected[13].

While fast pyrolysis of biomass in circulating fluidised beds has been commercialised by Ensyn[187] for speciality food flavourings and more recently for speciality resins, there is no commercial use of this process for any other applications.

One way to deal with char fines is to filter them out of the hot gas[188]. One of the most serious problems experienced is that the filters tend to clog up very fast. The char layer formed may also degrade the bio-oil vapours reducing bio-oil yields. While the char can be removed from the filters by controlled oxidation, the ash remains in the filter cloth and may contribute to more rapid bio-oil cracking and even faster blinding of the interstices of the filter, which is experienced as an increase in the pressure drop across the filter[189].

THE OPTION OF SAND RECIRCULATION

Most of the problems faced when scaling up fluidised beds could be solved or ameliorated by adding sand recirculation between the fluidised bed pyrolyser and a char combustor, an option that is illustrated in Figure 108.
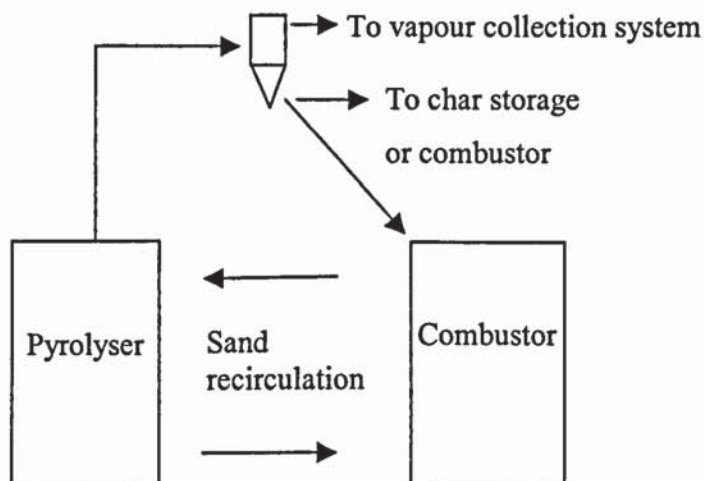
Figure 108 Illustration of sand recirculation as a design option

There are then two mechanisms for removing char from the reactor, one is entrainment with the vapours, and another is removal with the sand used for recirculation. This allows the removal of larger char particles without them being abraded down to sizes that are entrained more easily. It allows moderate velocities, that is steady and predictable operation and at the same time, velocities that are high enough to ensure good mixing in

the reactor, which is necessary to avoid the formation of a char layer on top of the bed, which could catalyse secondary reaction and thereby reduce bio-oil yields.

By suitable selection of feedpoints, which should be based on a combination of CFD and pilot plant studies, excessive maldistribution could be avoided, while supplying a minimum amount of inert fluidising gases. The main fluidising medium for the fluidised bed could then be constituted by the organic vapours and incondensable gases released by the pyrolysis reaction.

Recirculation entirely solves the problem of providing sufficient heat transfer. As this is often the major limitation for reactor capacity, eliminating the need for large heat transfer surfaces allows smaller reactor sizes.

Recirculation also lessens the load on the cyclones and the need for efficient entrainment. Because a sizeable fraction of the char is still collected in cyclones, one can control the temperature of the combustor well. In the current rotating cone design for fast pyrolysis developed by BTG, on the other hand, the char combustor or the sand bled from it have to be cooled down or extra heat has to be supplied to achieve the correct temperature at all times and for different feedstocks[190]. In a system where recirculation of sand is combined with char collection in cyclones, the heat produced in the combustor can be controlled by controlling the amount of char added from the cyclones, while the rest can go to bunker and be burnt later or sold.

Ash will be much smaller than the char particles and will be entrained easily from the char combustor. By suitable placement of the sand take off point from the char combustor, it should be possible to largely avoid recirculation of ash, which would be undesirable as ash is known to have catalytic properties[191] and therefore the potential to degrade bio-oil yields.

For the production of liquid fuels via fast pyrolysis not all secondary cracking is bad, some cracking of lignin may actually be necessary to improve fuel quality. This means that there will be an optimum residence time, which may change slightly depending on the concentration of char in the dense fluidised bed[192].

One way recirculation could be implemented would be a combination of two standpipes and pneumatic transport. The gases used for pneumatic transport could be separated from the transported mixture of sand and char in a cyclone and then reused.

For a 1 tonne per hour plant, possible design data might be, to give an illustrative example, 1 tonne of sand in the pyrolyser and a recirculation rate of 2 tonnes per hour. With a char concentration of 2% in the pyrolyser and a char yield of 12%, this would mean a third of the char produced would be moved from the pyrolyser to the char combustor together with the recirculating sand, while the other two thirds would be removed via cyclones.

A similar concept to sand recirculation between two fluidised beds has been developed by BTG[193,194,195]. Here sand recirculation occurs between a rotating cone reactor and a fluidised bed it is immerged in. In contrast to the concept proposed above, however, intermediate storage of the char is not included in the recirculation system advanced by BTG.

The circulating fluidised bed system commercialised by Ensyn also employs recirculation of hot sand. The disadvantages of this system have already been mentioned earlier.

COMBINING THE COMBUSTOR AND THE PYROLYSER

One solution to the heat transfer and char removal problems detailed in earlier chapters may be a combination of the char combustor and the pyrolysis reactor into one vessel with separate regions being assigned to the two functions, an option that is illustrated in Figure 109. A similar solution has been investigated for a circulating fluidised bed system by the Centre for Renewable Energy Resources in Greece[196] with some success, though the results are preliminary at this stage.

The advantages of employing just one vessel for both functions are similar to the option of recirculating the sand between the combustor and the pyrolyser. An additional benefit may be lower capital costs, as only one vessel would be required and the investment in the recirculation system could be done away with.

184

Pyrolysis vapours + ash to product collection system
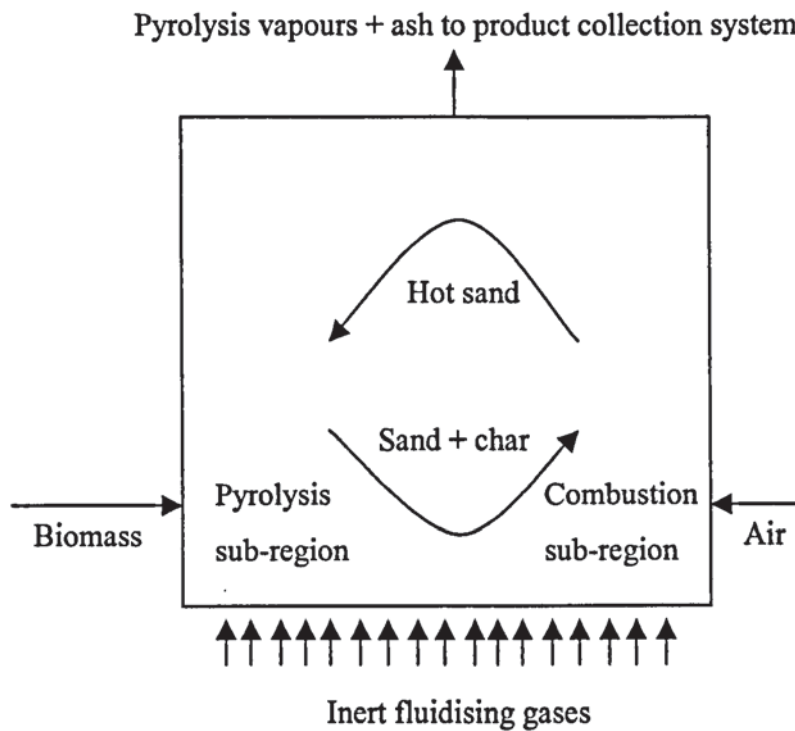
Figure 109 Combining the char combustor and pyrolyser in one vessel

The design proposed by the Centre for Renwable Energy Resources does still require collection of all of the char in cyclones and recirculation via a standpipe, as all of the char is removed from the fast fluidised bed used for fast pyrolysis together with the fluidising gases, and gases and vapours resulting from pyrolysis.

A disadvantage of recirculation within a single vessel may be that it presents particularly difficult scale-up problems, as flow structures within the bed become even more crucial in determining bio-oil yields.

The char would have to be separated from the vapours within the bed by differential movement. As has been shown in chapters 6 and 7, it is possible for the solid phase to be moving downwards consistently at one point of the bed, while the gas/vapour phase is still largely moving upwards. It does therefore appear that such a separation should be possible in principle.

The flow would have to be structured so that very little oxygen will reach the pyrolysis vapours and also so that the pyrolysis vapours do not experience residence times that are so great as to negatively affect the yield of bio-oil.

The concept presented in this section, that is circulating char and sand within a single vessel without the use of standpipes or other external recirculation methods, is completely novel. It is also high risk from a commercial point of view, as it is untried and likely to yield particularly difficult scale-up.

Before the concept can be taken any further, several possible geometries should be investigated by CFD and then the best option tested out in cold flow and pilot plant rigs. While the work reported in this thesis provides a considerable boost to confidence in the results of CFD modelling of fluidised beds, it is clear that the technique is not yet sufficiently advanced to do away with pilot plant work altogether.

SEVERAL SMALLER PYROLYSERS WITHIN A LARGER COMBUSTOR

Another possibility to deal with the difficulties of scale-up detailed in earlier chapters would be to employ several smaller pyrolysers within a single larger combustor, a design option that is illustrated in Figure 110.
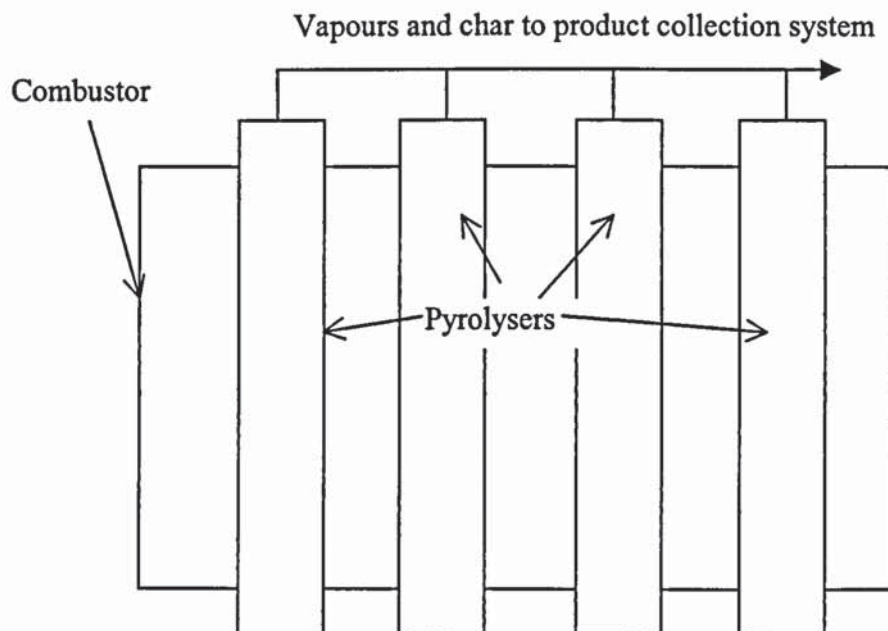
Figure 110 Multiple pyrolysers in single char combustor

186

As there would be no scale-up for the smaller pyrolysers, little would need to change in their design. The disadvantage of this, however, is that there would also be no significant economies of scale for the pyrolysers.

The design of the larger combustor would be complicated by the pyrolysers located within it. However, as fluidised bed coal combustion processes are already in wide commercial use for power generation[197], the scale-up of the combustor is not expected to present unsurmountable hurdles. A design procedure combing cold flow modelling, CFD and pilot plant work would again be recommendable for this step.

BED INTERNALS AND WALL GEOMETRY

Heat transfer could be improved by using fins or in-bed heating tubes filled with the gas exiting the combustor. This is, however, costly. Furthermore, it increases the complexity of the reactor, which in turn makes the system more difficult to model, both by CFD and experimentally, and makes it more likely that parts could fail. The in-bed heating tubes, for example, could suffer from corrosion. Even the design as a whole could fail, because flow patterns in the bed behave in unexpected ways and lead to longer residence times of the organic vapours or increased char concentrations, both of which could deleteriously affect bio-oil yields.

Entrainment could possibly be helped by suitably placed baffles. A combination of an initial widening and a later narrowing of the freeboard or a reduced height to diameter ratio could also be employed.

The disadvantages of employing baffles, or other bed internals, to aid with entrainment are similar to the case of improving heat transfer with fins, or other bed internals, just explained.

An initial widening followed by a later narrowing may be advantageous, as has been detailed with illustrations in chapters 6 and 8. It would likely cause a slight increase in capital costs for the reactor, which would be of little concern. More importantly, it would not deal with the need to keep residence times low, an aspect that was explored in detail in

chapter 7, and that would become a limiting factor at a similar stage of scale-up as char entrainment.

Lowering the height to diameter ratio would help with both entrainment and in keeping vapour residence times short, but could result in maldistribution, as has already been pointed out in chapter 7. Furthermore, the surface area available for heat transfer between the pyrolyser and combustor would be reduced.

The volume of the pyrolyser depends on the square of the diameter times its height, while the area available for heat transfer depends on the diameter times the height of the pyrolyser. Reducing the ratio of bed height to bed diameter by a factor ten will therefore lower the available heat transfer area by just over a factor 3. Therefore, lowering residence times through reducing the bed height to diameter ratio will make heat transfer to the fluidised bed a more difficult task.

COMPARISON BETWEEN THE POSSIBLE DESIGN CHOICES

The most promising choice appears to be sand recirculation between a pyrolyser and a combustor located in separate vessels. Combining the two functions into one vessel would be a risky approach that may not work.

The option of using several smaller pyrolysers in a larger combustor is likely to be commercially less attractive than employing sand recirculation. If this option were chosen nevertheless, the use of bed internals, of freeboard modifications and of a reduced bed height to diameter ratio could aid in maximising the achievable scale of the pyrolysers, though this would be at the expense of increased complexity.

Furthermore, the capital costs for the internals would partially off-set the economies of scale achieved and the lower bed height to diameter ratio would increase the potential for maldistribution to occur.

Relying only on the use of bed internals, variations in the bed height to diameter ratio and a widening of the freeboard followed by a narrowing, is unlikely to be sufficient for scale-up beyond around 100 tonnes per day, which would be in agreement with comments made by

the Chief Operating Officer of Dynamotive[198, 199], one of only a few companies currently commercialising biomass fast pyrolysis[200].

11. Conclusions

This chapter summarises the achievements of the work reported in this thesis.

HYDRO-DYNAMICS

The computational modelling of the bed hydro-dynamics via CFD has been successfully validated against experimental results on 2-D and 3-D rigs. The maximum, and also the most frequently considered, scale for the 2-D configuration was a diameter of 50 cm, which is significantly larger than other work available in the literature where validation has only been undertaken for scales of up to 20 cm in a similar manner as was done in the work reported in this thesis.

The geometry of the reactor and freeboard close to the surface of the fluidised bed has been found to be particularly important. A widening below the surface of the bed stabilises it and leads to smaller bubbles, while a narrowing increases bubble size and shifts overall bed behaviour towards Geldart class D. Under certain conditions a narrowing of the freeboard in the form of a dummy cyclone located close to the bed surface was found to hold the potential for sudden sand surges that would lead to the loss of a significant fraction of the bed sand inventory.

Other factors considered for validation included particle size and diameter, fluidising velocity, initial bed height and scale. For all of those good agreement between CFD predictions and experimental bed behaviour has been shown.

CFD results for the effect of temperature, and also for scaling beyond a diameter of 50 cm, could not be validated experimentally. The CFD calculations indicate that the effect of temperature is likely to be relatively minor. For scaling beyond approximately 1 m, it is found that the bubble size and bed expansion no longer expand linearly with bed diameter.

REACTION KINETICS

A model of the pyrolysis kinetics has been combined with the CFD calculations. The interaction of the kinetics and the hydro-dynamics is found to be vital for adequate prediction of both bed behaviour and product yields.

The residence time of the organic vapours largely determines the extent of secondary cracking and depends on the hydro-dynamics of the fluidised bed. It has been shown that under some circumstances, the impact of the interaction of bed hydro-dynamics and the location of vapour release is such that an increase in the fluidising velocity by a factor two may actually lead to a longer residence time for the organic vapours. This result is counter intuitive and unexpected.

It has also been shown that at least for small particles, the pyrolysis reaction is largely completed within on the order of 10 cm from the biomass feedpoint. Consequently, there is a significant potential for maldistribution within the fluidised bed, which may have negative impacts on heat transfer and entrainment, if it becomes excessive.

ENTRAINMENT

For the special situation of selective entrainment of char out of a bed of sand with a short freeboard, there are no adequate correlations available.

A CFD based estimating procedure has been developed and shown to give acceptable quantitative agreement with experimental results in cold-flow rigs. Good qualitative agreement has been shown on the 5 kg/h hot pyrolysis reactor. For design purposes the use of CFD for this problem represents major progress, particularly when considering the lack of suitable alternative methods.

HEAT TRANSFER

Direct modelling of heat transfer has been found to give results that are as accurate as the presently available correlations. However, numerical difficulties prevent the successful application of the technique in many cases.

CFD may still present a useful additional input into the prediction of heat transfer coefficients, as it can give estimates of bed expansion, and of bubble motion, as well as location. At the present time, however, it does not appear to be suitable as the primary tool for obtaining heat transfer coefficients in fluidised beds.

SCALED REACTORS

Heat transfer, vapour residence time and the selective entrainment of char are such significant hurdles to scale-up beyond 100 t/day that new reactor design concepts will likely be required.

The most promising options that have been identified are the use of sand recirculation between a pyrolyser and a combustor unit, and the placement of multiple pyrolysers within a single larger combustor.

12. Recommendations for Future Work

The modelling and experimental effort undertaken leads on to further work that would be desirable in the future. Priorities for such future work are outlined in this chapter.

Validation of the CFD work on the pilot plant scale should assist with gaining further confidence in the accuracy of the predictions. Particular emphasis will likely be placed on the measurement of pressure fluctuations, temperature, product yields and char entrainment.

It would be desirable to further enhance the reaction kinetics modelling by incorporating experimental data from the bench scale in a suitable fashion. If it proves impracticable to obtain primary product yields and vapour release times from experiments, it may also be worthwhile to again investigate the possibility of combining the CFD work with large particle models of pyrolysis.

Validation in 3-D configurations suffers from the fact that it is difficult to observe bed behaviour visually. One technique that could be employed to partially remedy this problem is Positron Emission Particle Tracking (PEPT)[201,202].

Tracking particles experimentally, which could be done using PEPT, would be particularly helpful in improving the estimation of entrainment. Based on a better understanding of the ejection behaviour of particles, it should be feasible to obtain a better estimate, which could be validated by determining entrainment from a bed of sand, where attrition is not a significant factor.

Ways to improve the numerical stability of the CFD solution should be investigated, as this issue was found to be a major obstacle to the successful deployment of CFD to the modelling of fluidised beds.

A number of reactor configurations have been identified that hold promise for scale-up. A closer investigation using CFD could be employed to confirm the potential of each concept in preparation for possible industrial use at a later stage.

Particular recommendations for the two most promising design choices can be made. The chemical engineering design of the sand recirculation system needs attention to determine what recirculation rate is optimal, and how best to implement the recirculation. CFD will likely be most suited to investigating the need for, and best location of, multiple feedpoints.

The design of a combustor holding several smaller pyrolysers is likely to benefit most from a combination of CFD, cold flow modelling and pilot plant work. There is no scale-up involved in the design of the pyrolysers, the work would therefore focus in particular on the combustor.

Nomenclature

LIST OF ABBREVIATIONS USED IN THE TEXT

avi	abbreviation for a standard for encoding videos
BTG	Biomass Technology Group
CFD	computational fluid dynamics
CFX	name of the commercial CFD code used in this thesis
daf	dry, ash free basis
EIA	Energy Information Administration of the United States of America
GC	gas chromatograph
IEA	International Energy Agency
IPCC	Intergovernmental Panel on Climate Change
IPSA	inter phase slip algorithm
jpeg	abbreviation for a standard for encoding pictures
MIPS	million instructions per second
mpeg	abbreviation for a standard for encoding videos
SIMPLE	semi implicit method for pressure linked equations
TDH	transport disengagement height

SYMBOLS AND UNITS

a	acceleration	m/s^2
A	dimensionless variable, measure of relative thermal conductivities	
A	frequency factor	$1/s$
A	surface area	m^2
A_B	distributor area over number of orifices	m^2
Ar	Archimedes number	
B	body forces	N/m^3
B	dimensionless variable, measure of volume fraction	
c	fines concentration	
c	heat capacity	J/kgK
c0	initial fines concentration	

195

$c_{\alpha\beta}$	interphase momentum transfer term	$kg/m^3 s$
$c_{\alpha\beta}^{(h)}$	interphase heat transfer term	$J\,m^{-3}s^{-1}\,K^{-1}$
C_d	orifice discharge coefficient	
C_D	drag coefficient	
d_B	bubble diameter	m
d	particle diameter	m
D	bed diameter	m
e	internal energy	m^2/s^2
E	activation energy	J/kmol
f_{or}	maximum fraction of the distributor area to be taken up by holes	
F	force	N
F	interphase non drag forces	N/m^3
F_D	drag force	N
g	gravitational acceleration	m/s^2
h	bed height	m
h_{bed}	bed height	m
H	enthalpy	J/kg
i	subscript indicating the number of cells in the x direction	
j	subscript indicating the number of cells in the y direction	
k	subscript indicating the number of cells in the z direction	
k	entrainment rate constant	
K	reaction rate	1/s
m	mass	kg
$\dot{m}$	mass flow between phases	$kg/m^3 s$
N_P	number of phases	
Nu	Nusselt Number	
Q	heat	J
Pr	Prandtl Number	
P	pressure	Pa
r	volume fraction	
R	universal gas constant	$J\,kmol^{-1}\,K^{-1}$
Re	Reynolds Number	
t	time	s
U	speed	m/s

U_T	terminal velocity	m/s
U	velocity	m/s
u	velocity in the x direction	m/s
u	superficial velocity	m/s
u_{mf}	minimum fluidising velocity	m/s
u_B	bubble velocity	m/s
u_W	superficial velocity in the distributor chamber	m/s
v	velocity in the y direction	m/s
v_R	fluid velocity relative to particle	m/s
V	volume of computational cell	m^3
w	velocity in the z direction	m/s
x	fraction of char produced in reaction 2 of the extended Broido-Shafizadeh scheme	
y	fraction of gas produced in reaction 2 of the extended Broido-Shafizadeh scheme	

α	heat transfer coefficient	W/m^{2}K
α, β	subscripts for the two phases	
ΔP	pressure drop across the bed	Pa
Δt	time step	s
ΔT	temperature difference	K
λ	thermal conductivity	W/mK
ρ	density	kg/m^3
ρ_{bulk}	bulk density	kg/m^3
ρ_{gw}	density of the gas in the distributor chamber	kg/m^3
μ	viscosity	kg/ms
ω	constant accounting for particle shape	
ψ	dimensionless variable	
X	mass fraction	

References

[1] EC Contract JOR3-CT97-0197, Development of advanced fast pyrolysis processes for power and heat

[2] Peacocke G.V.C. (1994) Ablative Pyrolysis of Biomass, PhD Thesis, University of Aston in Birmingham

[3] Werther J. (2000) Fluidization Technology development – the industry / academia collaboration issue, Powder Technology, Volume 113, p. 230-241

[4] Supply agreement G54XX between Aston University and Wellman Process Engineering Ltd.

[5] DTI offer of support B/T1/00748/00/00

[6] http://www.dynamotive.com/news/newsreleases/030526.html Press release announcing the construction of a 100 tpd bio-oil plant in Canada

[7] http://www.vtt.fi/pro/pro2/pro22/pyrolysis.htm Information on Fortum/Vapo 350 kg/h pilot plant

[8] Thong J. (1999) Modelling of Entrainment in a Fluidised Bed System, MEng Project Report, Aston University

[9] Williams M. (1999) Investigation into the Fluidising Behaviour of Multi-Solid Bubbling Beds for Application within a Fast Pyrolysis Reactor, MEng Project Report, Aston University

[10] Wunder B. (1999) Fluidisation characteristics and particle entrainment of multi-solid bubbling beds related to a fast pyrolysis reactor, MPhil Thesis, Technical University of Berlin

[11] Personal communication with representatives of Dynamotive

[12] http://www.state.nh.us/governor/energycomm/images/biooil-nrel.pdf Overview of Biomass Pyrolysis by Stefan Czernik mentioning Dynamotive and a requirement of small particle size for bubbling fluidised bed pyrolysis

[13] Kunii D., Levenspiel O. (1991) Fluidization Engineering, 2nd edn. Butterworth-Heinemann, Newton.

[14] van Wachem B.G.M. (1998) Eulerian Simulations of Bubbling Behaviour in Gas-Solid Fluidised Beds, Computers & Chemical Engineering, Volume 22, Supplement 1, p. S299-S306

[15] Kuipers J.A.M. (1990) A two-fluid micro balance model of fluidised beds, PhD Thesis, University of Twente

[16] Lathouwers D., Bellan J. (2001) Modelling of Biomass Pyrolysis for Hydrogen Production: The Fluidized Bed Reactor. In: Proceedings of the 2001 DOE Hydrogen Program Review, NREL/CP-570-30535

[17] Krams R. et al (1999) Effect of catheter placement on 3-D velocity profiles in curved tubes resembling the human coronary system, Volume 25, Issue 5, p. 803-810

[18] http://www.grida.no/climate/ipcc_tar/wg1/503.htm Climate Change 2001: The Scientific Basis, Intergovernmental panel on climate change

[19] Chunyan J. et al (2003) FCC unit modelling, identification and model predictive control, a simulation study, Chemical Engineering and Processing, Volume 42, Issue 4, p. 311-325

[20] Phylipsen G.J.M. and Alsema E.A. (1995) Environmental life-cycle assessment of multicrystalline silicon solar cell modules, Report No 95057, a study by commission of the Netherlands Agency for Energy and the Environment, NOVEM, available at: http://www.chem.uu.nl/nws/www/publica/95057.pdf

[21] Bridgwater A.V. et al (2002) A techno-economic comparison of power production by biomass fast pyrolysis with gasification and combustion, Renewable and Sustainable Energy Reviews, Volume 6, Issue 3, p. 181-246

[22] Wahlund B. et al (2002) A total energy system of fuel upgrading by drying biomass feedstock for cogeneration: a case study of Skellefteå bioenergy combine, Biomass and Bioenergy, Volume 23, Issue 4, p. 271-281

[23] http://www.ipcc.ch/ home page of the Intergovernmental Panel on Climate Change, the official body responsible for the science of climate change

[24] http://www.grida.no/climate/ipcc_tar/wg1/007.htm

[25] http://www.grida.no/climate/ipcc_tar/wg1/figspm-3.htm

[26] http://crgd.atmos.uiuc.edu/publications/ Mendelsohn R et al (1997) Country-Specific Market Impacts of Climate Change To appear in the proceedings of the IPCC Asia-Pacific Workshop on Integrated Assessment Models, 10-12 March 1997, United Nations University, Tokyo.

[27] http://www.econ.yale.edu/%7Enordhaus/homepage/web%20chap%207%20102599.pdf Nordhaus W. and Boyer J. (1999) Internet Edition of Warming the World: Economic Models of Global Warming

[28] http://www.eia.doe.gov/oiaf/kyoto3/execsummary.html Analysis of the Impacts of an Early Start for Compliance with the Kyoto Protocol, by the Energy Information Administration of the United States of America

[29] http://tonto.eia.doe.gov/FTPROOT/service/sroiaf(2002)03.pdf Impacts of a 10% Renewable Portfolio Standard, by the Energy Information Administration of the United States of America

[30] Meadows D.H. et al (1972) The Limits to Growth, a report for the Club of Rome's Project on the Predicament of Mankind, Earth Island Ltd, (London), (Distributed by Angus and Robertson), London

[31] http://www.oilcrisis.com/laherrere/usgs2000/johnwood.htm Comments made by Jean Laherrere

[32] http://www.oilcrisis.com/campbell/commons.htm Presentation by Colin Campbell to the House of Commons of the United Kingdom of Northern Ireland and Great Britain

[33] Cambell C. and Laherrere J. (1998) The End of Cheap Oil, Scientific American, March 1998 Issue

[34] http://sepwww.stanford.edu/sep/jon/world-oil.dir/lynch/worldoil.html Crying Wolf: Warnings about oil supply, by Michael Lynch, M.I.T.

[35] http://www.grida.no/climate/ipcc/emission/102.htm

[36] http://www.eia.doe.gov/cneaf/coal/reserves/front-1.html US coal reserves, 1997 update, by the Energy Information Administration of the United States of America

[37] http://www.bp.com/centres/energy2002/primary.asp# BP statistical review of world energy 2002

[38] http://www.grida.no/climate/ipcc_tar/wg1/figspm-5.htm

[39] Bruce N et al (2000) Indoor air pollution in developing countries: a major environmental and public health challenge, Bulletin of the World Health Organisation, 78 (9)

[40] Energy and Poverty, Chapter 13 in IEA's World Energy Outlook 2002

[41] Perttu K.L. (1998) Environmental justification for short-rotation forestry in Sweden, Biomass and Bioenergy, Volume 15, Issue 1, p. 1-6

[42] http://www.usda.gov/oce/oepnu/aer-814.pdf Shapouri H. et al (2002) The Energy Balance of Corn Ethanol: An Update, U.S. Department of Agriculture, Office of the Chief Economist, Office of Energy Policy and New Uses. Agricultural Economic Report No. 814.

[43] Forsberg G. (2000) Biomass energy transport Analysis of bioenergy transport chains using life cycle inventory method, Biomass and Bioenergy, Volume 19, Issue 1, p. 17-30

[44] http://www.businessweek.com/magazine/content/02_36/b3798055.htm Magnusson P. (2002) Commentary: Farm Subsidies: A Blight on the Economy, on-line edition of Business Week, 9 September 2002

[45] Kaltschmitt M. and Dinkelbach L. (1997) Biomass for Energy in Europe – Status and Prospects. In: Biomass Gasification & Pyrolysis State of the Art and Future Prospects (Ed. by M. Kaltschmitt and A.V. Bridgwater), CPL Press, Berkshire, for the European Commision

[46] Goor F. et al (2001) Assessment of the potential of willow SRC plants for energy production in areas contaminated by radionuclide deposits: methodology and perspectives, Biomass and Bioenergy, Volume 21, Issue 4, p. 225-235

[47] http://www.eia.doe.gov/oiaf/aeo/index.html Early release of the energy outlook 2003, published by the Energy Information Administration of the United States of America

[48] http://www.iea.org/leaflet.pdf Renewables in Global Energy Supply, an IEA fact sheet

[49] http://www.shell.com/home/media-en/downloads/scenarios.pdf Latest scenarios for 2050 from Shell

[50] http://gurusonline.tv/uk/conteudos/davis.asp A conversation with Ged Davis, VP Global Business Environment of Royal Dutch/Shell Group, explaining Shell Scenarios to 2020 and 2050

[51] http://europa.eu.int/comm/energy/library/execsum.pdf European Union Energy Outlook to 2020

[52] Commission of the European Communities Directorate General for Science Research and Development (1992) Biomass for energy and environment, agriculture and industry in Europe A Strategy for the Future, ed. by G. Grassi and A.V. Bridgwater, Publication Number EUR 14683 EN

[53] Beeharry R.P. (2001) Strategies for augmenting sugarcane biomass availability for power production in Mauritius, Biomass and Bioenergy, Volume 20, Issue 6, p. 421-429

[54] Boyle S. and Edwards R. (2002) Biomass project burns out, New Scientist, 30 November 2002

[55] Bridgwater A.V. et al (2002) A techno-economic comparison of power production by biomass fast pyrolysis with gasification and combustion, Renewable and Sustainable Energy Reviews, Volume 6, Issue 3, p. 181-246

[56] http://www.eia.doe.gov/cneaf/solar.renewables/page/rea_data/gl.html Glossary of the Renewable Energy Annual 2000

[57] http://www.iea.org/stats/defs/sources/coal.htm#top Definition of coal for IEA's Energy Balance Table

[58] http://www.managenergy.net/download/r1e.pdf Renewable Energy in Vaesternorrland

[59] http://www.iea.org/stats/files/renewables.htm Renewables Information 2002

[60] Price B. (1998) Electricity from biomass. Financial Times Energy, London

[61] Nordh N. and Weih M. (2002) Characterising willows for biomass and phytoremediation: growth, nitrogen and water use of 14 willow clones under different irrigation and fertilisation regimes. Biomass and Bioenergy, Volume 23, Issue 6, p. 397-413

[62] http://www.howstuffworks.com/question598.htm An explanation of soft and hardwoods by HowStuffWorks

[63] Lewandowski I. and Clifton-Brown J.C. (2002) Screening Miscanthus genotypes in field trials to optimise biomass yield and quality in Southern Germany, European Journal of Agronomy, Volume 16, Issue 2, p. 97-110

[64] Waldheim L. et al (2001) Biomass Power Generation: Sugar Cane Bagasse and Trash. In: Progress in Thermochemical Biomass Conversion (Ed. by A.V. Bridgwater), p. 509-523. Blackwell Science Ltd, Oxford

[65] ASTM standards D1102 Test Method for Ash in Wood, E871 Method for Moisture Analysis of Particulate Wood Fuels, E872 Test Method for Volatile Matter in the Analysis of Particulate Wood Fuels

[66] http://www.ecn.nl/phyllis Phyllis a database containing information on the composition of biomass and waste, maintained by ECN with the support of NOVEM

[67] Bridge S.A. (1990) Flash Pyrolysis of Biomass for Liquid Fuels, MPhil Thesis, Aston University

[68] Quaak P. et al (1999) Energy from Biomass A Review of Combustion and Gasification Technologies, World Bank Technical Paper Number 422, published by the World Bank, Washington, USA

[69] Diebold J.P. et al (1999) Proposed specifications for various grades of pyrolysis oils. In: Fast Pyrolysis of Biomass: A Handbook, p. 102-114, published by CPL Press, Berkshire, for Aston University, Bio Energy Research Group

[70] Leckner B. et al (1999) Kinetics of fluidised bed combustion of wood pellets. In: Proceedings of the 15th International Conference on Fluidized Bed Combustion, ASME, Paper Number FBC99-0047, Savannah, Georgia

[71] Bergander A. (2001) Local variability in chemical and physical properties of spruce wood fibres, PhD thesis, performed at the Swedish Pulp and Paper Research Institute, Royal Institute of Technology, Department of Pulp and Paper Chemistry and Technology, Division of Paper Technology

[72] http://www.swst.org/teach/set2/struct1.html Structure of Wood, Society of Wood Science and Technology Teaching Unit Number 1

[73] http://www.publiscan.fi/bl03e-1.htm Information on wood tar in Finland provided by Welcome to Finland

[74] Bridgwater A.V. (1999) An introduction to fast pyrolysis of biomass for fuels and chemicals. In: Fast Pyrolysis of Biomass: A Handbook, p. 1-13, published by CPL Press, Berkshire, for Aston University, Bio Energy Research Group

[75] Oasmaa A. (1999) Testing standard methods. In: Fast Pyrolysis of Biomass: A Handbook, p. 69-74, published by CPL Press, Berkshire, for Aston University, Bio Energy Research Group

[76] Bridgwater A.V. (2000) Fast pyrolysis processes for biomass. Renewable and Sustainable Energy Reviews, Volume 4, p. 1-73

[77] Lede J. et al (1988) Pyrolysis of biomass: Evidence for a fusionlike phenomenon. In: Pyroysis Oil from Biomass, Producing, Analyzing, and Upgrading (Ed. by E.J. Soltes and T.A. Milne), p. 66-78, ACS Symposium Series 376, American Chemical Society, Denver, Colorado

[78] Diebold J. and Scahill J. (1988) Production of primary pyrolysis oil in a vortex reactor. In: Pyroysis Oil from Biomass, Producing, Analyzing, and Upgrading (Ed. by E.J. Soltes and T.A. Milne), p. 31-40, ACS Symposium Series 376, American Chemical Society, Denver, Colorado

[79] Wagenaar B.M. (1994) The rotating cone reactor, PhD thesis, University of Twente, The Netherlands

[80] Janse A.M.C. (1998) A heat integrated rotating cone reactor system for flash pyrolysis of biomass, PhD thesis, University of Twente, The Netherlands

[81] http://www.btgworld.com/technologies/pyrolysis.html#technology Description of the rotating cone technology by BTG

[82] Roy C. et al (1988) Processing of wood chips in a semicontinuous multiple-hearth vacuum pyrolysis reactor. In: Pyroysis Oil from Biomass, Producing, Analyzing, and Upgrading (Ed. by E.J. Soltes and T.A. Milne), p. 16-30, ACS Symposium Series 376, American Chemical Society, Denver, Colorado

[83] Roy C. et al (1997) Development of a novel vacuum pyrolysis reactor with improved heat transfer potential. In: Developments in Thermochemical Biomass Conversion (Ed. by A.V. Bridgwater and D.G.B. Boocock), p. 351-367. Blackie Academic & Professional

[84] Antal M.J. et al (2001) New prospects for biocarbons. In: Progress in Thermochemical Biomass Conversion, (Ed. by A.V. Bridgwater), p. 1179-1185. Blackwell Science Ltd, Oxford

[85] Halling J.N. (1987) Modelling the liquid product distribution from the Waterloo fast pyrolysis process, PhD thesis, University of Waterloo, Canada

[86] Gronli M. (1996) A theoretical and experimental study of the thermal degradation of biomass, PhD thesis, The Norwegian University of Science and Technology

[87] Miller R.S. and Bellan J. (1997) A generalised biomass pyrolysis model based on superimposed cellulose, hemicellulose and lignin kinetics, Combustion Science and Technology, Volume 126, p. 97-137

[88] di Blasi C. (1998) Comparison of semi-global mechanisms for primary pyrolysis of lignocellulosic fuels, Journal of Analytical and Applied Pyrolysis, Volume 47, p. 43-64

[89] Miller R.S. and Bellan J. (1996) Analysis of reaction products and conversion time in the pyrolysis of cellulose and wood particles, Combustion Science and Technology, Volume 119, p. 331-373

[90] Yu C. and Zhang W. (2000) Process modelling of a cellulose particle during pyrolysis, Proceedings of the 1st World conference and Exhibition for Energy and Industry, held in Sevilla, June 5-9, Spain

[91] Zenz F.A. and Weil N.A. (1958) A Theoretical-Empirical Approach to the Mechanism of Particle Entrainment from Fluidized Beds. American Institute of Chemical Engineering Journal, Volume 4, p. 472-479

[92] Leva M. (1951) Elutriation of fines from fluidised systems, Chemical Engineering Progress, Volume 47, Number 1, p. 39-45

[93] Kunii D. and Levenspiel O. (1969) Entrainment and elutriation from fluidised beds, Journal of Chemical Engineering of Japan, Volume 2, p. 84-88

[94] Martin H. (1982) Heat and mass transfer in fluidised beds, International Chemical Engineering, Volume 22, Number 1, p. 30-43

[95] http://www.cham.co.uk/website/new/cfdintro.htm#target3 Short description of the history of the CFD industry by CHAM, an engineering-consultancy and software company, based in Wimbledon, England

[96] Anderson J.D. (1995) Computational Fluid Dynamics, McGraw Hill International Editions, Singapore

[97] http://www.cwi.nl/research/2001/Koren_Eng/ factsheet on "Understanding Flows by Means of a Computer" by Dr.ir. B. Koren of CWI, the National Research Institute for Mathematics and Computer Science in the Netherlands, date of publication given: September 2001

[98] Moravec H. (1998) Mere Machine to Transcendent Mind, Oxford University Press, Oxford, UK

[99] http://www.walmart.com Microtel SYSMAR402 800 MHz PC With Modem & Lycoris Desktop/LX, $248, as of end 2002

[100] http://www.dansdata.com/c3.htm Review of the C3 processor

[101] Wesseling P. (2000) Principles of Computational Fluid Dynamics, Springer-Verlag, Berlin, Heidelberg, New York

[102] Ferziger J.H. and Peric M. (1999) Computational Methods for Fluid Dynamics, Springer-Verlag, Berlin, Heidelberg, New York

[103] Shaw C.T. (1992) Using computational fluid dynamics, Prentice Hall, New York

[104] Abbot M.B. and Basco D.R. (1989) Computational fluid dynamics an introduction for engineers, Longman Group UK Ltd, Harlow, Essex

[105] Lomax H. et al (2001) Fundamentals of computational fluid dynamics, Springer, Berlin

[106] http://www.tru64unix.compaq.com/enterprisetoolkit/ent_edit.htm Product description by Compaq

[107] email from Lydia Guillorit, sales representative of Simulog, the company marketing Estet-Astrid

[108] http://www.simulog.fr/is/2estet1.htm product page of Estet-Astrid on the Simulog website, in French

[109] Thai Van D. et al (1994), Multidimensional two-fluid model computation of turbulent dispersed two-phase flows, Numerical Methods in Multiphase Flows, Proceedings of the

ASME Fluids Engineering Division Summer Meeting, Crowe, C.T., Johnson, R., Prospertti, A., Sommerfeld, M. & Tsuji, Y., June 19-23, Lake Tahoe, USA, FED-Vol.185, p. 277-291.

[110] http://www.cd-adapco.com/ product page of Star-CD

[111] http://www.fluent.com/ product page of Fluent

[112] http://h18009.www1.hp.com/fortran/ Fortran compiler product page of Compaq, now part of HP

[113] http://www.pgroup.com/ Portland Group Fortran product page

[114] http://www.software.aeat.com/cfx/products/cfx-5/media/supportedplatforms_linux.pdf supported platforms for CFX 5.5.1

[115] http://www.gcn.com/vol1_no1/daily-updates/3589-1.html Daukantas P. (2001) Cray enters Linux cluster market, Government Computer News published by PostNewsweek Tech Media, a division of Post Newsweek Media

[116] http://www.microsoft.com/windowsxp/64bit/overview.asp Windows XP product page

[117] http://www.windowsclusters.org/cpus.htm Windows Cluster Resource Centre, University of Southampton, UK

[118] http://www.cse.clrc.ac.uk/disco/ Computational Science and Engineering Department, Distributed Computing Support, Daresbury Laboratory, Council for the Central Laboratory of the Research Councils

[119] Wassen E (1998) Entwicklung paralleler Algorithmen zur numerischen Simulation von Gas-Partikel-Stroemungen unter Beruecksichtigung von Partikel-Partikel-Kollisionen, PhD Thesis, University of Chemnitz

[120] http://www.csar.cfs.ac.uk/ home page of CSAR

[121] Tsuji Y. et al (1993) Discrete particle simulation of two-dimensional fluidised bed, Powder Technology, Volume 77, p. 79-87

[122] Hoomans B.P.B et al (1996) Discrete particle simulation of bubble and slug formation in a two-dimensional gas-fluidised bed: A hard-sphere approach, Chemical Engineering Science, Volume 51, p. 99-118

[123] Gidaspow D. (1994) Multiphase Flow and Fluidization. Academic Press

[124] Ergun S. (1952) Fluid Flow through packed columns. Chem. Eng. Prog., Volume 48, p. 89-94

[125] Patankar S.V., Spalding D.B.(1972) A calculation procedure for heat, mass and momentum transfer in three-dimensional parabolic flows. International Journal of Heat and Mass Transfer, Volume 15, p. 1787-1806

[126] Spalding D.B. (1980) Numerical computation of multiphase flow and heat transfer. In: Recent Advances in Numerical Methods in Fluid Mechanics (Ed. by C. Taylor & K. Morgan), Pineridge, Swansea, p. 139-168

[127] Volume 3 "Solver" of the CFX-4 documentation, p. 3-26

[128] EC Contract JOR3-CT97-0197, Development of advanced fast pyrolysis processes for power and heat, Final Report

[129] Boemer A., Qi H. and Renz U. (1997) Verification of Eulerian simulation of spontaneous bubble formation in a fluidised bed. Chemical Engineering Science 53:1835-1846

[130] van Wachem et al (2001) Experimental validation of Lagrangian-Eulerian simulations of fluidised beds, Powder Technology, 116, p. 155-165

[131] Geldart D (1986) Gas Fluidization Technology, A Wiley-Interscience Publication

[132] Goldschmidt M.J.V. et al (2001) Hydrodynamic modelling of dense gas-fluidised beds using the kinetic theory of granular flow: effect of coefficient of restitution on bed dynamics, Chemical Engineering Science, Volume 56, p. 571-578

[133] Mathiesen V. et al (2000) Predictions of gas/particle flow with an Eulerian model including a realistic particle size distribution, Powder Technology, Volume 112, Issues 1-2, p. 34-45

[134] Benyahia S. et al (2000) Simulation of particles and gas flow behaviour in the riser section of a circulating fluidised bed using the kinetic theory approach for the particulate phase, Powder Technology, Volume 112, p. 24-33

[135] Samuelsberg A. and Hjertager B. H. (1996) An experimental and numerical study of flow patterns in a circulating fluidised bed reactor, International Journal of Multiphase flow, Volume 22, Issue 3, p. 575-591

[136] Davidson J.F., Harrison D. (1963) Fluidized Particles, Cambridge University Press, New York

[137] Mori S. and Wen C.Y. (1975) Estimation of Bubble Diameter in Gaseous Fluidized Beds, American Institute of Chemical Engineering Journal, Volume 21, p. 109-115

[138] Beck S.R. et al (1978) Variable velocity fluidized bed for pyrolysis of biomass. In: Solid wastes and residues, conversion by advanced thermal processes. A symposium

sponsored by the Division of Environmental Chemistryat the 175th Meeting of the American Chemical Society (Ed. by J.L. Jones and S.B. Radding), p. 307-322, ACS, Washington

[139] Krishna R., van Baten J.M. (2001) Using CFD for scaling up gas-solid fluidised bed reactors with Geldart A powders, Chemical Engineering Journal, Volume 82, p. 247-257

[140] Cranfield R.R. and Geldart D. (1974) Large particle fluidisation. Chemical Engineering Science, Volume 29, p. 935-947

[141] Hatzantonis H. (2000) Recent developments in modelling gas-phase catalysed olefin polymerisation Fluidised-bed reactors: The effect of bubble size variation on the reactor's performance, Chemical Engineering Science, Volume 55, p. 3237-3259

[142] Gallucci K. et al (2002) Cold model characterisation of a fluidised bed catalytic reactor by means of instantaneous pressure measurements. Chemical Engineering Journal, Volume 87, p. 61-71

[143] Hearn E.H. and Metcalfe A.V. (1995) Spectral analysis in engineering, Concepts and cases, Arnold, A member of the Hodder Headline Group, London

[144] http://www.atmos.ucla.edu/tcd/ssa/#ssa_availability Description of the Singular Spectrum Analysis - MultiTaper Method (SSA-MTM) Toolkit

[145] Coulson, J.M., Richardson, J.F. (1993) Chemical Engeneering, Volume 2, Pergamon

[146] Witt P.J. et al (1998) A numerical model for predicting bubble formation in a 3D fluidised bed. Applied Mathematical Modelling, Volume 22, p. 1071-1080

[147] Lede J. et al (1999) The nature and properties of intermediate and unvaporized biomass pyrolysis materials. In: Fast Pyrolysis of Biomass, A Handbook, published by CPL Press for the Bio Energy Research Group of the University of Aston in Birmingham

[148] Chunjiang Y. et al (2001) A modelling study on cellulose particle pyrolysis under fluidised bed conditions. In: Progress in Thermochemical Biomass Conversion, (Ed. by A.V. Bridgwater), p. 1091-1106. Blackwell Science Ltd, Oxford

[149] Boutin O. and Lede J (2001) Use of a concentrated radiation for the determination of cellulose thermal decomposition mechanisms. In: Progress in Thermochemical Biomass Conversion, (Ed. by A.V. Bridgwater), p. 1034-1045. Blackwell Science Ltd, Oxford

[150] Bradbury A.G.W. et al (1979) A Kinetic Model for Pyrolysis of Cellulose. Journal of Applied Polymer Science, Volume 23, p. 3271-3280

[151] Liden A.G. et al (1988) A kinetic model for the production of liquids from the flash pyrolysis of biomass. Chem. Eng. Comm., Volume 65, p. 207-221

[152] Bridgwater A.V. et al (2001) An Overview of Fast Pyrolysis. In: Progress in Thermochemical Biomass Conversion, (Ed. by A.V. Bridgwater), p. 977-997. Blackwell Science Ltd, Oxford

[153] Oja V. and Hajaligol M.R. (2000) The volatility of tars from pyrolysis of biomass materials. In: Progress in Thermochemical Biomass Conversion, (Ed. by A.V. Bridgwater), p. 1226-1233. Blackwell Science Ltd, Oxford

[154] Hague R A (1998) The Pre-Treatment and Pyrolysis of Biomass for the Production of Liquids for Fuels and Speciality Chemicals, PhD Thesis, University of Aston in Birmingham

[155] Personal communication from Richard Mclellan, manager gasification, Wellman Process Engineering Ltd.

[156] http://www.chevron.com/about/pascagoula/refiningprocess/proccrude.shtml

[157] Personal communication from Rodolfo Guido, Chief Operating Officer, Dynamotive

[158] Stenseng M. et al (2001) Thermal Analysis and Kinetic Modelling of Wheat Straw Pyrolysis. In: Progress in Thermochemical Biomass Conversion, (Ed. by A.V. Bridgwater), pp. 1061-1075. Blackwell Science Ltd, Oxford

[159] Larfeldt J. et al (2001) Modelling and measurements of drying and pyrolysis of large wood particles. In: Progress in Thermochemical Biomass Conversion, (Ed. by A.V. Bridgwater), p. 1046-1060. Blackwell Science Ltd, Oxford

[160] Boutin O. et al (1998) Radiant Flash Pyrolysis of Cellulose – Evidence for the formation of short life time intermediate liquid species, Journal of Analytical and Applied Pyrolysis, Volume 47, Issue 1, p. 13-31

[161] di Blasi C. (1996) Heat, momentum and mass transport through a shrinking biomass particle exposed to thermal radiation, Chemical Engineering Science, Volume 51, No. 7, p. 1121-1132

[162] di Blasi C. (2000) Modelling the fast pyrolysis of cellulosic particles in fluid-bed reactors. Chemical Engineering Science, Volume 55, p. 5999-6013.

[163] di Blasi C. (1998) Physico-chemical processes occurring inside a degrading two-dimensional anisotropic porous medium, International Journal of Heat and Mass Transfer, Volume 41, p. 4139-4150

[164] di Blasi C. (2002) Modelling Intra- and Extra-Particle Processes of Wood Fast Pyrolysis, AIChE Journal, Volume 48, Issue 10, p. 2386-2397

[165] Romeo L.M. and Cortes C. (1998) Simulation of a full-scale pressurized fluidised bed combustor by using semi-empirical pilot plant correlations, Revue Générale de Thermique, Volume 37, Issue 10, p. 862-873

[166] Santana D. et al (1999) Modelling fluidized bed elutriation of fine particles, Powder Technology, Volume 106, Issues 1-2, p. 110-118

[167] Oasmaa A., Peacocke C. (2001) A guide to physical property characterisation of biomass derived fast pyrolysis liquids, VTT Publications, Finland.

[168] Wen C.Y. and Chen L.H. (1982) Fluidised Bed Freeboard Phenomena: Entrainment and Elutriation, AIChE Journal, Volume 28, No. 1 p. 117-127

[169] Fung A.S., Hamdullahpur F. (1993) Effect of bubble coalescence on entrainment in gas fluidized beds. Powder Technology, Volume 77, p 251-265

[170] Do H.T. et al (1972) Particle Ejection and Entrainment from Fluidised Beds, Powder Technology, Volume 6, p. 195-200

[171] Pemberton S.T. and Davidson J.F. (1986) Elutriation from fluidised beds – I. Particle ejection from the dense phase into the freeboard, Chemical Engineering Science, Volume 41, No. 2, p. 243-251

[172] Pyle D.L. (1965) PhD Dissertation, University of Cambridge

[173] Scott D. et al (1999) A second look at fast pyrolysis of biomass—the RTI process, Journal of Analytical and Applied Pyrolysis, Volume 51, p. 23–37

[174] Atkins P.W. (1994) Physical chemistry, 5th Edition, Oxford University Press

[175] Howard J.R. (1989) Fluidised bed technology: principles and applications, IOP Publishing Ltd

[176] Gunn D.J. (1978) Transfer of heat or mass to particles in fixed and fluidised beds. Int. J. Heat and Mass Transfer, Volume 21, p. 467

[177] Zehner P., Schlunder E.U. (1970) Chemis Ing. Techn., Volume 42, p.933

[178] VDI Waermeatlas 6. Auflage (1991)

[179] Coulson J.M. et al. (1991) Coulson & Richardson's Chemical Engineering. Vol. 1, 4th Edition

[180] Bridgwater A.V., Meier D., Radlein D. (1999) An overview of fast pyrolysis of biomass. Organic Geochemistry, Volume 30, p. 1479-1493

[181] Bridgwater A.V., Diebold J.P. (1997) Overview of Fast Pyrolysis of Biomass for the Production of Liquid Fuels. In: Developments in Thermochemical Biomass Conversion (Ed. by A.V. Bridgwater and D.G.B. Boocock), p. 5-23. Blackie Academic & Professional

[182] Meier D. et al (1997) Properties of fast pyrolysis liquids: Status of test methods. In: Developments in Thermochemical Biomass Conversion, (Ed. by A.V. Bridgwater and D.G.B. Boocock), p. 391-407. Blackie Academic and Professional, London

[183] Chunjian Y. and Wennan Z. (1997) Modelling potassium release in biomass pyrolysis. In: Progress in Thermochemical Biomass Conversion, (Ed. by A.V. Bridgwater), p. 1107-1115. Blackwell Science Ltd, Oxford

[184] http://www.qc.hrdc-drhc.gc.ca/imt/quebec-metro/english/bul_eve/02july/even-3_e.html Labour Market Bulletin July 2002, Quebec City

[185] Peacocke C. et al (1997) Comparison of ablative and fluid bed fast pyrolysis products: yields and analyses. In: Developments in Thermochemical Biomass Conversion, (Ed. by A.V. Bridgwater and D.G.B. Boocock), p. 191-205. Blackie Academic and Professional, London

[186] Steynberg A.P. et al (1999) High temperature Fischer-Tropsch synthesis in commercial practice, Applied Catalysis A: General, Volume 186, p. 41-54

[187] http://www.ensyn.com/index.htm home page of Ensyn

[188] http://mango2.vtt.fi:84/ene/uet/sellueng/pyrolysis.htm Description of pyrolysis research undertaken by VTT of Finland

[189] Scahill et al (1997) Removal of residual char fines from pyrolysis vapours by hot gas filtration. In: Developments in Thermochemical Biomass Conversion, (Ed. by A.V. Bridgwater and D.G.B. Boocock), p. 253-266, Blackie Academic & Professional, London

[190] http://www.btgworld.com/technologies/pyrolysis.html Process Description for the Rotating Cone Technology by BTG

[191] Zanzi R. et al (2002) Rapid pyrolysis of agricultural residues at high temperature, Biomass and Bioenergy, Volume 23, p.357-366

[192] Scott D. et al (1999) A second look at fast pyrolysis of biomass—the RTI process, Journal of Analytical and Applied Pyrolysis, Volume 51, p. 23–37

[193] Janse A.M.C. et al (2000) A novel interconnected fluidised bed for the combined flash pyrolysis of biomass and combustion of char, Chemical Engineering Journal, Volume 76, p. 77-86

[194] Janse A.M.C. et al (2000) Granular flow in a rotating cone partly submerged in a fluidised bed, AIChE Journal, Volume 46, Issue 3, p. 499-508

[195] Janse A.M.C. et al (1997) Development of a small integrated pilot plant for flash pyrolysis of biomass. In: Developments in Thermochemical Biomass Conversion, (Ed. by

A.V. Bridgwater and D.G.B. Boocock), p. 368-377, Blackie Academic & Professional, London

[196] Boukis I. et al (2001) Biomass Fast Pyrolysis in an Air-blown Circulating Fluidised Bed Reactor. In: Progress in Thermochemical Biomass Conversion, (Ed. by A.V. Bridgwater), p. 1046-1060. Blackwell Science Ltd, Oxford

[197] McMullan et al (2001) Strategic considerations for clean coal R&R, Energy Policy, Volume 29, Issue 6, p. 441-452

[198] Personal Communication by Rodolfo Guido, Chief Operating Officer, Dynamotive Energy Systems Corporation

[199] http://www.dynamotive.com/flash.asp home page of Dynamotive Energy Systems Corporation

[200] Meier D. and Faix O. (1999) State of the art of applied fast pyrolysis of lingocellulosic materials – a review, Bioresource Technology, Volume 68, p. 71-77

[201] Stein M. et al (2002) Experimental verification of the scaling relationships for bubbling gas-fluidised beds using the PEPT technique, Chemical Engineering Science, Volume 57, p. 3649-3658

[202] Stein M. et al (1998) Attrition of porous glass particles in a fluidised bed, Powder Technology, Volume 100, p. 242-250

Appendices

List of Publications by the Author

Gerhauser H. et al (2001) CFD for the Modelling of Entrainment in Fluidised Bed Fast Pyrolysis of Biomass. In: Progress in Thermochemical Biomass Conversion, (Ed. by A.V. Bridgwater), p. 1281-1295. Blackwell Science Ltd, Oxford.

Gerhauser H., Bridgwater A. (2002) CFD Modelling of Heat Transfer in Fluidised Bed Reactors for the Fast Pyrolysis of Biomass. In: Proceedings of the 12th European Biomass Conference and Exhibition, 17-21 June 2002, Amsterdam, Netherlands

Gerhauser H., Bridgwater A. (2002) Scale Effects And Distribution Problems In Fluid Bed Fast Pyrolysis Using CFD Models Integrated With Reaction Kinetics. In: Proceedings of the Expert Meeting on Pyrolysis and Gasification of Biomass and Waste held in Strasbourg, France, 30 September – 1 October 2002

Gerhauser H. et al, The Influence of Reactor Geometry and Scale on the Hydrodynamics and Performance of Fluidised Bed Fast Pyrolysis Reactors, submitted to Powder Technology

List of runs from which data is presented in the text of the thesis

Explanations: When giving dimensions or gridding information, the x coordinates are always given first, followed by y and z. Boundaries are specified as groupings of grid points. Both the initial and the final point in the i, j, and, if applicable, the k directions are given to fully specify the location of each boundary.

I. Experimental run on the 2-D rig, 7.5 cm diameter, small geometry number 1 as described in chapter 5, sand particle diameter 0.503 mm, initial sand depth 0.15 m, minimum fluidising velocity 0.19 m/s, u/u_{mf} 1.6, video recording taken

II. Experimental run on the 3-D rig, 7.5 cm diameter, original geometry as described in chapter 5, sand particle diameter 0.503 mm, initial sand depth 0.15 m, minimum fluidising velocity 0.19 m/s, u/u_{mf} 1.6, video recording taken

III. CFD calculation, 2-D, 7.5 cm by 30 cm rectangular geometry, grid 31 by 48 cells, pressure boundary 1 31 48 48, initial inlet boundaries 1 30 1 1 at 0.2 m/s and 31 31 1 1 at 4 m/s, followed by 1 31 1 1 at 0.3 m/s, sand particle diameter 0.503 mm, initial sand depth 0.15 m, minimum fluidising velocity 0.19 m/s, u/u_{mf} 1.6, fixed time stepping for 1.25 s, followed by adaptive time stepping

IV. Experimental run on the 2-D rig, 50 cm diameter, widening as described in chapter 5, sand particle diameter 0.44 mm, initial sand depth 0.5 m, minimum fluidising velocity 0.15 m/s, u/u_{mf} 2.3, video recording taken

V. CFD calculation, 2-D, 50 cm diameter, widening as described in chapter 5, four blocks as per Figure 14, mesh size 1 cm, outlet pressure boundary at top of geometry, inlet boundary in block 1, location 1 50 1 1, velocity 0.35 m/s, u/u_{mf} 2.3, sand particle diameter 0.44 mm, initial sand depth 0.5 m, adaptive time stepping

VI. CFD calculation, 2-D, 50 cm diameter, widening as described in chapter 5, four blocks as per Figure 14, mesh size 1 cm, outlet pressure boundary at top of geometry, inlet boundary in block 1, location 1 50 1 1, velocity 0.75 m/s, u/u_{mf} 5.0, sand particle diameter 0.44 mm, initial sand depth 0.5 m, adaptive time stepping

VII. Experimental runs on the 3-D rig, 7.5 cm diameter, original geometry as described in chapter 5, sand particle diameter 0.503 mm, initial sand depth 0.15 m, minimum

fluidising velocity 0.19 m/s, u/u$_{mf}$ from incipient bubbling to slugging, video recordings taken

VIII. CFD calculations, 2-D, 7.5 cm by 30 cm rectangular geometry, grid 31 by 48 cells, pressure boundary 1 31 48 48, inlet boundary 1 31 1 1, sand particle diameter 0.503 mm, initial sand depth 0.15 m, minimum fluidising velocity 0.19 m/s, u/u$_{mf}$ from incipient bubbling to slugging

IX. Experimental runs on the 2-D rig, 7.5 cm diameter, small geometry number 1 as described in chapter 5, sand particle diameter 0.503 mm, initial sand depth 0.15 m, minimum fluidising velocity 0.19 m/s, u/u$_{mf}$ from incipient bubbling to slugging, video recordings taken

X. CFD calculation, 2-D, 20 cm by 59 cm rectangular geometry, grid 31 by 48 cells, pressure boundary 1 31 48 48, inlet boundaries 1 30 1 1 at 0.26 m/s and 31 31 1 1 at 5.78 m/s, sand particle diameter 0.503 mm, initial sand depth 0.3 m, minimum fluidising velocity 0.19 m/s, u/u$_{mf}$ 2.3, fixed time stepping

XI. CFD calculations, 2-D, 50 cm diameter, widening as described in chapter 5, four blocks as per Figure 14, mesh size 1 cm, outlet pressure boundary at top of geometry, inlet boundary in block 1, location 1 50 1 1, u/u$_{mf}$ from incipient bubbling to slugging, sand particle diameter 0.44 mm, initial sand depth 0.5 m, adaptive time stepping

XII. Experimental runs on the 2-D rig, 50 cm diameter, widening as described in chapter 5, sand particle diameter 0.44 mm, initial sand depth 0.5 m, minimum fluidising velocity 0.15 m/s, u/u$_{mf}$ from incipient bubbling to slugging, video recordings taken

XIII. CFD calculation, 2-D, 50 cm diameter, standard configuration as described in chapter 5, 50 cm by 100 cm rectangular geometry, grid 100 by 200 cells, outlet pressure boundary 1 100 200 200, inlet boundary 1 100 1 1, velocity 0.35 m/s, u/u$_{mf}$ 1.8, sand particle diameter 0.503 mm, initial sand depth 0.33 m, adaptive time stepping

XIV. CFD calculation, 2-D, 50 cm diameter, standard configuration as described in chapter 5, 50 cm by 100 cm rectangular geometry, grid 100 by 200 cells, outlet pressure boundary 1 100 200 200, inlet boundary 1 100 1 1, velocity 0.35 m/s, u/u$_{mf}$ 1.3, sand particle diameter 0.64 mm, initial sand depth 0.33 m, adaptive time stepping

XV. CFD calculations, 2-D, 50 cm diameter, widening as described in chapter 5, four blocks as per Figure 14, mesh size 1 cm, outlet pressure boundary at top of geometry, inlet boundary in block 1, location 1 50 1 1, u/u$_{mf}$ from incipient bubbling to

slugging, sand particle diameter 0.503 mm, initial sand depth 0.5 m, adaptive time stepping

XVI. Experimental runs on the 2-D rig, 50 cm diameter, widening as described in chapter 5, sand particle diameter 0.503 mm, initial sand depth 0.5 m, minimum fluidising velocity 0.19 m/s, u/u_{mf} from incipient bubbling to slugging, video recordings taken

XVII. CFD calculation, 2-D, 50 cm diameter, standard configuration as described in chapter 5, 50 cm by 100 cm rectangular geometry, grid 100 by 200 cells, outlet pressure boundary 1 100 200 200, inlet boundary 1 100 1 1, velocity 0.25 m/s, u/u_{mf} 1.8, sand particle diameter 0.44 mm, initial sand depth 0.33 m, sand density 2440 kg/m^3, adaptive time stepping

XVIII. CFD calculation, 2-D, 50 cm diameter, standard configuration as described in chapter 5, 50 cm by 100 cm rectangular geometry, grid 100 by 200 cells, outlet pressure boundary 1 100 200 200, inlet boundary 1 100 1 1, velocity 0.25 m/s, u/u_{mf} 1.8, sand particle diameter 0.44 mm, initial sand depth 0.33 m, sand density 2640 kg/m^3, adaptive time stepping

XIX. CFD calculation, 3-D, 7.5 cm diameter, original geometry of small 3-D rig as described in chapter 5, blocks as illustrated, mesh size roughly 1 cm, inlet velocity 0.1 m/s, modelled vapour/gas only, single phase

XX. CFD calculation, 3-D, 7.5 cm diameter, modified geometry of small 3-D rig as described in chapter 5, blocks as illustrated, mesh size roughly 1 cm, inlet velocity 0.2 m/s, modelled vapour/gas only, single phase

XXI. CFD calculation, 3-D, 7.5 cm diameter, modified geometry of small 3-D rig as described in chapter 5, blocks as illustrated, mesh size roughly 1 cm, inlet velocity 0.1 m/s, modelled vapour/gas only, single phase

XXII. Experimental runs on the 3-D rig, 7.5 cm diameter, modified geometry as described in chapter 5, sand particle diameter 0.503 mm, initial sand depth 0.15 m, minimum fluidising velocity 0.19 m/s, u/u_{mf} from incipient bubbling to slugging, video recordings taken

XXIII. CFD calculation, 2-D, 12 cm diameter, 5 kg/h reactor as described in chapter 5, blocks as illustrated, first block 31 by 31 grid cells, inlet boundaries 1 30 1 1 at 0.2 m/s and 31 31 1 1 at 1 m/s, sand particle diameter 0.503 mm, initial sand depth 0.31 m, u/u_{mf} 1.2, User Fortran for geometry and grid specification, fixed time stepping, step size 0.0005 s

XXIV. CFD calculation, 2-D, 12 cm freeboard diameter, 5 kg/h reactor, modified as described in chapter 5, blocks as illustrated, first block 30 by 30 grid cells, inlet boundaries 1 29 1 1 at 0.2 m/s and 30 30 1 1 at 3.6 m/s, sand particle diameter 0.503 mm, initial sand depth 0.3 m, u/u_{mf} 1.6, User Fortran for geometry and grid specification, fixed time stepping

XXV. CFD calculation, 2-D, 50 cm diameter, roughly 2.7 m height, exact dimensions cannot be revealed in this thesis, blocks as illustrated, grid spacing roughly 2.5 cm, inlet boundary 1 20 1 1 at 1 m/s, sand particle diameter 0.503 mm, initial sand depth 1.0 m, u/u_{mf} 5.3, gas/vapour phase viscosity 0.00004 kg/ms, gas/vapour phase density 0.46 kg/m^3, adaptive time stepping

XXVI. Experimental runs on the 2-D rig, 50 cm diameter, widening as described in chapter 5, sand particle diameter 0.44 mm, varying initial sand depth, minimum fluidising velocity 0.19 m/s, u/u_{mf} 2.8, video recordings taken

XXVII. CFD calculations, 2-D, 50 cm diameter, widening as described in chapter 5, four blocks as per Figure 14, mesh size 1 cm, outlet pressure boundary at top of geometry, inlet boundary in block 1, location 1 50 1 1, u/u_{mf} 2.8, sand particle diameter 0.44 mm, varying initial sand depth, adaptive time stepping

XXVIII. CFD calculations, 2-D, 50 cm diameter, standard configuration as described in chapter 5, 50 cm by 100 cm rectangular geometry, grid 100 by 200 cells, outlet pressure boundary 1 100 200 200, inlet boundary 1 100 1 1, velocity 0.25 m/s, u/u_{mf} 1.8, sand particle diameter 0.44 mm, initial sand depth 0.33 m and 0.5 m respectively, sand density 2440 kg/m^3, adaptive time stepping

XXIX. CFD calculations, 2-D, diameter varied from 7.5 cm to 5 m, one block, grid 100 by 200 for diameters above 0.5 m and 59 by 31 for smaller diameters, outlet pressure boundary at top, inlet boundary at bottom, velocity 0.5 m/s, u/u_{mf} 2.6, sand particle diameter 0.503 mm, initial sand depth equal to bed diameter, sand density 2440 kg/m^3, adaptive time stepping

XXX. CFD calculations, 2-D, diameter 50 cm, narrowing and widening configurations respectively as described in chapter 5, four blocks as shown, inlet at bottom, pressure boundary at top, velocity 0.55 m/s, u/u_{mf} 3.7, sand particle diameter 0.44 mm, initial sand depth 0.5 m, sand density 2640 kg/m^3, adaptive time stepping

XXXI. CFD calculation, 2-D, diameter 100 cm, widening to a diameter of 120 cm between heights of 100 and 200 cm, two blocks as shown, inlet at bottom, pressure boundary

at top, velocity 0.35 m/s, u/u_{mf} 1.9, sand particle diameter 0.44 mm, initial sand depth 0.5 m, sand density 2640 kg/m^3, adaptive time stepping

XXXII. CFD calculation, 2-D, diameter 100 cm, widening by 15 cm between heights of 100 and 120 cm, narrowing to 60 cm between heights of 120 and 200 cm, four blocks as shown, inlet at bottom, pressure boundary at top, velocity 0.35 m/s, u/u_{mf} 1.9, sand particle diameter 0.503 mm, initial sand depth 1 m, sand density 2440 kg/m^3, adaptive time stepping

XXXIII. CFD calculation, 2-D, 50 cm diameter, widening as described in chapter 5, four blocks as per Figure 14, mesh size 1 cm, outlet pressure boundary at top of geometry, inlet boundary in block 1, location 1 50 1 1, velocity 0.45 m/s, u/u_{mf} 2.4, sand particle diameter 0.44 mm, initial sand depth 0.33 m, adaptive time stepping

XXXIV. Experimental run on the 2-D rig, 50 cm diameter, widening as described in chapter 5, sand particle diameter 0.44 mm, initial sand depth 0.33 m, minimum fluidising velocity 0.19 m/s, u/u_{mf} 2.4, video recordings and pressure measurements (at 1.5 and 15 cm) taken

XXXV. Experimental run on the 2-D rig, 50 cm diameter, widening as described in chapter 5, sand particle diameter 0.44 mm, initial sand depth 0.33 m, minimum fluidising velocity 0.19 m/s, u/u_{mf} from incipient bubbling to slugging, video recordings and pressure measurements (at 1.5 and 15 cm) taken

XXXVI. CFD calculations, 2-D, 20 cm by 59 cm rectangular geometry, grids 31 by 48 cells and 32 by 96 cells respectively, pressure boundary at top, inlet boundaries at bottom, velocity 0.26 m/s and 5.78 m/s for a jet at the side, sand particle diameter 0.503 mm, initial sand depth 0.3 m, minimum fluidising velocity 0.19 m/s, u/u_{mf} 2.3, fixed time stepping

XXXVII. CFD calculations, 2-D, 5 m by 20 m, rectangular geometry, grid 10 by 40 cells, pressure boundary at top, inlet boundary at bottom, velocity 0.5 m/s, sand particle diameter 0.503 mm, initial sand depth 10 m, minimum fluidising velocity 0.19 m/s, u/u_{mf} 2.6, fixed time stepping

XXXVIII. CFD calculation, semi 2-D, 50 cm diameter, 4 cm deep, widening as described in chapter 5, four blocks as per Figure 14, mesh size 1 cm, outlet pressure boundary at top of geometry, inlet boundary in block 1, location 1 50 1 1, velocity 0.25 m/s, u/u_{mf} 1.7, sand particle diameter 0.44 mm, initial sand depth 0.5 m, adaptive time stepping

XXXIX. CFD calculation, 2-D, 50 cm diameter, widening as described in chapter 5, four blocks as per Figure 14, mesh size 1 cm, outlet pressure boundary at top of geometry,

219

inlet boundary in block 1, location 1 50 1 1, velocity 0.25 m/s, u/u_{mf} 1.7, sand particle diameter 0.44 mm, initial sand depth 0.5 m, adaptive time stepping

XL. CFD calculation, 2-D, 50 cm diameter, standard configuration as described in chapter 5, 50 cm by 100 cm rectangular geometry, grid 100 by 200 cells, outlet pressure boundary 1 100 200 200, inlet boundaries 1 50 1 1 and 61 100 1 1 at 0.55 m/s, 51 60 1 1 at 0.73 m/s followed by 1 100 1 1 at 0.55 m/s, u/u_{mf} 2.9, sand particle diameter 0.503 mm, initial sand depth 0.53 m, adaptive time stepping

XLI. CFD calculation, 3-D, 1 m diameter, height 2 m, gridding as illustrated, outlet pressure boundary at top, inlet boundaries at bottom, velocity at bottom of one of the four outer blocks at 1 m/s, remaining blocks at 0.4 m/s, u/u_{mf} 2.9, sand particle diameter 0.503 mm, initial sand depth 1 m, fixed time stepping

XLII. CFD calculation, 3-D, 50 cm diameter, dimensions are those of the Wellman pilot plant with a height of roughly 2.7 m, exact dimensions cannot be given in this thesis, average mesh size roughly 5 cm, block structure as illustrated, initial sand depth 1 m, velocity 1 m/s, u/u_{mf} 5.3, sand particle diameter 0.503 mm, under relaxation factors for u, v and w velocity 0.03, fixed time stepping

XLIII. CFD calculation, 2-D, 50 cm diameter, widening as described in chapter 5, four blocks as per Figure 14, mesh size 1 cm, outlet pressure boundary at top of geometry, inlet boundary in block 1, location 1 50 1 1, velocity 0.35 m/s, u/u_{mf} 1.9, sand particle diameter 0.503 mm, initial sand depth 0.33 m, adaptive time stepping, two temperatures as described in main text in chapter 6

XLIV. CFD calculation, 2-D, 50 cm diameter, dimensions are those of the Wellman pilot plant with a height of roughly 2.7 m, exact dimensions cannot be given in this thesis, average mesh size roughly 2.5 cm, block structure as illustrated, initial sand depth 1 m, sand particle diameter 0.503 mm, velocity 0.2 m/s, temperature 500 °C, biomass feedpoint between 7.5 cm and 12.5 cm, volume fraction of entrain gas 0.425, entrain gas and biomass fed at room temperature, velocity of entrain gas 0.3 m/s, velocity of biomass 0.0016 m/s, which is equivalent to adding 0.5 m/s of superficial velocity after conversion to gas and vapours, adaptive time stepping, bed initially at 500 °C and containing sand only, reaction kinetics modelled as described in chapter 7, u/u_{mf} not meaningful due to complex addition of gas, for User Fortran see appendix

XLV. CFD calculation, 2-D, 12 cm diameter, height 60 cm, distance between grid points 1 cm, single rectangular block, initial sand depth 0.3 m, sand particle diameter 0.44 mm, velocity 0.26 m/s, temperature 500 °C, biomass feedpoint between 2 cm and 3

cm, volume fraction of entrain gas 0.425, entrain gas and biomass fed at room temperature, velocity of entrain gas 0.1 m/s, mass flow rate of biomass through inlet 0.00002806 kg/s, adaptive time stepping, bed initially at 500 °C and containing sand only, reaction kinetics modelled as described in chapter 7, u/u_{mf} not meaningful due to complex addition of gas, for User Fortran see appendix

XLVI. CFD calculation, 2-D, 12 cm diameter, height 60 cm, distance between grid points 1 cm, single rectangular block, initial sand depth 0.3 m, sand particle diameter 0.44 mm, velocity 0.45 m/s, temperature 500 °C, biomass feedpoint between 2 cm and 3 cm, volume fraction of entrain gas 0.425, entrain gas and biomass fed at room temperature, velocity of entrain gas 0.1 m/s, mass flow rate of biomass through inlet 0.00002806 kg/s, adaptive time stepping, bed initially at 500 °C and containing sand only, reaction kinetics modelled as described in chapter 7, u/u_{mf} not meaningful due to complex addition of gas, for User Fortran see appendix

XLVII. CFD calculation, 2-D, 4.92 m diameter, height approximately 27 m, distance between grid points about 10 cm, block structure as for Wellman pilot plant, initial sand depth 10 m, sand particle diameter 0.44 mm, velocity 0.2 m/s, temperature 500 °C, biomass feedpoint between 40 cm and 60 cm, volume fraction of entrain gas 0.425, entrain gas and biomass fed at room temperature, velocity of entrain gas 0.1 m/s, velocity of biomass through inlet 0.0002 m/s, adaptive time stepping, bed initially at 500 °C and containing sand only, reaction kinetics modelled as described in chapter 7, u/u_{mf} not meaningful due to complex addition of gas, for User Fortran see appendix

XLVIII. CFD calculation, 2-D, 50 cm diameter, dimensions are those of the Wellman pilot plant with a height of roughly 2.7 m, exact dimensions cannot be given in this thesis, average mesh size roughly 2.5 cm, block structure as illustrated, initial sand depth 1 m, sand particle diameter 0.503 mm, velocity 0.2 m/s, temperature 500 °C, biomass feedpoint between 7.5 cm and 12.5 cm, volume fraction of entrain gas 0.425, entrain gas and biomass fed at room temperature, velocity of entrain gas 0.3 m/s, velocity of biomass 0.02 m/s, adaptive time stepping, bed initially at 500 °C and containing sand only, reaction kinetics modelled as described in chapter 7, u/u_{mf} not meaningful due to complex addition of gas, for User Fortran see appendix

XLIX. CFD calculation, 3-D, height 2.4 m, depth 0.32 m, width 0.48 m, average mesh size roughly 5 cm, single block, initial sand depth 1 m, sand particle diameter 0.44 mm, velocity 0.4 m/s, temperature 500 °C, biomass feedpoint between 2.5 cm and 7.5 cm and 20 cm wide, volume fraction of entrain gas 0.425, entrain gas and biomass fed at

room temperature, velocity of entrain gas 0.1 m/s, velocity of biomass 0.0001 m/s, adaptive time stepping, bed initially at 500 °C and containing sand only, reaction kinetics modelled as described in chapter 7, u/u_{mf} not meaningful due to complex addition of gas, for User Fortran see appendix

    L. As XLIV, but with two feedpoints, each of which having the same federate as the one feedpoint in XLIV

    LI. Experimental runs on the 2-D rig, 7.5 cm diameter, second small configuration as described in chapter 5, sand particle diameter 0.44 mm, initial sand depth 0.15 m, minimum fluidising velocity 0.15 m/s, u/u_{mf} 2.4, video recordings taken, measured the amount of char at equilibrium

    LII. CFD calculations, 2-D, 7.5 cm diameter, second small configuration as described in chapter 5, geometry and gridding as per III, sand particle diameter 0.44 mm, initial sand depth 0.15 m, minimum fluidising velocity 0.15 m/s, u/u_{mf} 2.4, procedure for estimating entrainment as explained in chapter 8

    LIII. CFD calculations, 3-D, 7.5 cm diameter, modified configuration, but without annulus, otherwise as described in chapter 5, grid spacing for 3-D particle tracking roughly 1 cm, particle diameter varying, nominal superficial velocity 0.3 m/s

    LIV. These data were obtained in runs on the 5 kg/h rig, where the contribution of the author was of a contributory rather than of a leading nature, LFB stands for large fluidised bed, the number after LFB is a run number, LFB05 for example is the fifth run that was done on the large fluidised bed, the number in brackets refers to the reactor temperature in degrees Celsius

    LV. Sand particle diameter 0.503 mm, initial sand depth 0.15 m

    LVI. CFD calculations, 2-D/3-D, 7.5 cm diameter, original configuration as described in chapter 5, geometry and gridding for two-phase calculation as per III, grid spacing for 3-D particle tracking roughly 1 cm, sand particle diameter 0.503 mm, initial sand depth 0.15 m, minimum fluidising velocity 0.15 m/s, u/u_{mf} varying, procedure for estimating entrainment as explained in chapter 8

    LVII. Sand particle diameter 0.503 mm, initial sand depth 0.15 m, char as received from runs on the 5 kg/h rig

    LVIII. CFD calculations, 3-D, grid as shown in Figure 103, bed height of 33 cm, particle diameter of 0.44 mm, fluidising velocity of 0.55 m/s, u/u_{mf} 3.7, adaptive time stepping

LIX. CFD calculations, 2-D, grid with closer spacing towards the wall, bed height of 15 cm, particle diameter of 0.503 mm, u/u$_{mf}$ varying, adaptive time stepping

Microscopic observations

12.10.1999

Char<355

	Long	Short	Ratio
1	1440	220	6.55
2	2100	240	8.75
3	1480	160	9.25
4	2040	200	10.20
5	880	320	2.75
6	1480	100	14.80
7	1220	200	6.10
8	1640	300	5.47
9	1440	240	6.00
10	1860	380	4.89
11	1160	380	3.05
12	2280	340	6.71
13	1400	600	2.33
14	1340	480	2.79
15	2420	380	6.37
16	1460	320	4.56
17	2000	320	6.25
18	1540	160	9.63
19	1480	240	6.17
20	500	80	6.25
Average	1486	272	6.44

Char 355-422

	Long	Short	Ratio
1	1200	440	2.73
2	1980	360	5.50
3	1440	340	4.24
4	1900	340	5.59
5	1760	460	3.83
6	2220	360	6.17
7	1420	360	3.94
8	1520	380	4.00
9	1440	480	3.00
10	2000	480	4.17
11	1280	360	3.56
12	1300	420	3.10
13	1380	480	2.88
14	1820	500	3.64
15	2660	280	9.50
16	1920	360	5.33
17	1880	420	4.48
18	1700	340	5.00
19	1520	400	3.80
20	1260	340	3.71
Average	1620	373	4.41

Char 422-500

	Long	Short	Ratio
1	2740	400	6.85
2	2400	420	5.71
3	1680	480	3.50
4	2200	420	5.24
5	1320	460	2.87
6	3020	320	9.44
7	740	540	1.37
8	2040	600	3.40
9	900	600	1.50
10	2160	560	3.86
11	1320	520	2.54
12	1680	680	2.47
13	1500	480	3.13
14	1940	560	3.46
15	2700	480	5.63
16	2080	340	6.12
17	1480	480	3.08
18	1800	560	3.21
19	2120	540	3.93
20	1600	520	3.08
Average	1734	478	4.02

Char 500-600

	Long	Short	Ratio
1	1100	680	1.62
2	2520	480	5.25
3	2120	580	3.66
4	1760	720	2.44
5	2240	660	3.39
6	2220	580	3.83
7	1780	600	2.97
8	2400	520	4.62
9	3120	500	6.24
10	1160	680	1.71
11	2340	620	3.77
12	2600	540	4.81
13	1220	760	1.61
14	2300	540	4.26
15	2340	520	4.50
16	1980	700	2.83
17	1200	680	1.76
18	2220	560	3.96
19	1600	680	2.35
20	1980	720	2.75
Average	1955	582	3.42

224

Char 600-699		18.10.1999			Char 699-850			
	Long	Short				Long	Short	Ratio
1	2040	700	2.91		1	2160	900	2.40
2	1760	900	1.96		2	1720	960	1.79
3	1900	600	3.17		3	2040	1080	1.89
4	1520	460	3.30		4	2240	980	2.29
5	1300	900	1.44		5	1960	1000	1.96
6	2220	680	3.26		6	2680	940	2.85
7	2640	680	3.88		7	1940	660	2.94
8	1020	400	2.55		8	1120	1100	1.02
9	1820	640	2.84		9	2000	1060	1.89
10	2640	700	3.77		10	2280	420	5.43
11	3000	720	4.17		11	3040	820	3.71
12	2340	620	3.77		12	2080	760	2.74
13	1560	820	1.90		13	2240	440	5.09
14	1500	820	1.83		14	1000	960	1.04
15	1280	780	1.64		15	1840	940	1.96
16	1420	720	1.97		16	2060	900	2.29
17	2080	640	3.25		17	1500	940	1.60
18	1940	500	3.88		18	1800	960	1.88
19	1740	700	2.49		19	1900	740	2.57
20	1680	700	2.40		20	2060	1000	2.06
Average	1768	649	2.82		Average	1875	833	2.47

Char 850-1003					Char >1003			
	Long	Short	Ratio			Long	Short	Ratio
1	2300	1020	2.25		1	1420	1220	1.16
2	3000	1140	2.63		2	2800	1300	2.15
3	1600	1340	1.19		3	1520	1340	1.13
4	2640	1160	2.28		4	1520	1380	1.10
5	3400	1020	3.33		5	2600	1400	1.86
6	1200	1120	1.07		6	2600	1340	1.94
7	2220	900	2.47		7	1760	1440	1.22
8	4500	1040	4.33		8	4600	1140	4.04
9	1900	960	1.98		9	1800	1280	1.41
10	2240	880	2.55		10	3600	1200	3.00
11	2620	1160	2.26		11	2260	1400	1.61
12	2460	1120	2.20		12	2380	1500	1.59
13	2200	1200	1.83		13	1700	1100	1.55
14	2100	1080	1.94		14	4000	800	5.00
15	1700	800	2.13		15	2600	1380	1.88
16	1440	1260	1.14		16	3500	1020	3.43
17	1780	1460	1.22		17	2260	1600	1.41
18	1880	1080	1.74		18	1500	1100	1.36
19	2040	780	2.62		19	3000	1100	2.73
20	1740	1000	1.74		20	2200	1500	1.47
Average	2133	1025	2.14		Average	2410	1216	2.05

Microscopic observations

18.10.1999

Sand<251

	Long	Short	Ratio
1	300	160	1.88
2	340	240	1.42
3	340	300	1.13
4	380	240	1.58
5	360	180	2.00
6	420	300	1.40
7	340	200	1.70
8	340	200	1.70
9	280	220	1.27
10	400	240	1.67
11	340	260	1.31
12	500	280	1.79
13	240	140	1.71
14	400	240	1.67
15	380	180	2.11
16	740	540	1.37
17	540	540	1.00
18	520	200	2.60
19	300	200	1.50
20	300	220	1.36
Average	373	246	1.61

Sand 251-353

	Long	Short	Ratio
1	540	360	1.50
2	440	200	2.20
3	400	320	1.25
4	600	360	1.67
5	340	320	1.06
6	400	320	1.25
7	360	300	1.20
8	440	320	1.38
9	500	360	1.39
10	500	340	1.47
11	420	300	1.40
12	420	300	1.40
13	420	380	1.11
14	400	300	1.33
15	440	340	1.29
16	400	360	1.11
17	360	320	1.13
18	460	420	1.10
19	400	360	1.11
20	600	400	1.50
Average	415	316	1.34

Sand 353-422

	Long	Short	Ratio
1	500	440	1.14
2	520	420	1.24
3	640	400	1.60
4	520	400	1.30
5	480	420	1.14
6	500	400	1.25
7	500	420	1.19
8	540	380	1.42
9	460	380	1.21
10	460	460	1.00
11	540	320	1.69
12	620	360	1.72
13	620	400	1.55
14	680	500	1.36
15	500	400	1.25
16	840	420	2.00
17	500	300	1.67
18	560	460	1.22
19	560	460	1.22
20	540	440	1.23
Average	529	387	1.37

Sand 422-500   12.10.1999

	Long	Short	Ratio
1	600	500	1.20
2	680	480	1.42
3	640	480	1.33
4	680	560	1.21
5	600	560	1.07
6	620	520	1.19
7	620	500	1.24
8	480	300	1.60
9	760	540	1.41
10	700	540	1.30
11	600	560	1.07
12	600	500	1.20
13	820	560	1.46
14	800	420	1.90
15	780	540	1.44
16	640	520	1.23
17	700	580	1.21
18	720	520	1.38
19	520	520	1.00
20	580	520	1.12
Average	627	486	1.30

Sand >500

	Long	Short	Ratio
1	580	360	1.61
2	700	520	1.35
3	980	860	1.14
4	960	700	1.37
5	920	600	1.53
6	940	520	1.81
7	1060	680	1.56
8	740	600	1.23
9	760	560	1.36
10	700	600	1.17
11	820	640	1.28
12	800	480	1.67
13	1000	640	1.56
14	820	740	1.11
15	920	640	1.44
16	600	400	1.50
17	880	540	1.63
18	800	740	1.08
19	800	600	1.33
20	780	520	1.50
Average	799	579	1.41

Estimating Procedure for Entrainment

sand			char			
size fraction		mass percentage	size fraction		mass percentage	
(microns)			(microns)			
<251		2	<180		2	
<355		8	<251		1	
<422		22	<355		3	
<500		33	<422		6	
<600		27	<500		15	
<699		8	<600		23	
			<699		19	
			<850		23	
			<1003		5	
			<1204		2	
			>1204		1	

Simplified classification

	microns	percentage		Representative diameter in microns		
1. Char particles		of char	of total	(taking shape into account)		
Small	<422	12	0.6	400		
Medium	<850	80	4	800		
Large	>850	8	0.4	1200		
2. Sand particles		of sand	of total			
Small	<355	10	9.5	300		
Medium	<500	55	52.25	400		
Large	>500	35	33.25	600		

Voidage of sand bed:	0.43	

It is assumed that particles are ejected from bubbles and that a layer with a thickness
equivalent to the average particle diameter in the bed is involved in the ejection

The cross-sectional area of the bubbles is subdivided into four groups to account for different
accelerations depending on the position of the particles being ejected.

Bubble size	Area in cm^2				
cm	5%	10%	20%	Remainder	
4	0.0314	0.0942	0.4082	24.7118	
5	0.049063	0.147188	0.637813	38.61219	
6	0.07065	0.21195	0.91845	55.60155	

Initial accelerations (from fluidised bed model, estimated based on the graphical output for volume
fraction and velocity)

Bubble size	Accelerations in m/s				
cm	5%	10%	20%	Remainder	
4	4	3.5	3	1	
5	4.5	5	5.5	1	
6	5	4.5	4	1	

From particle tracking:						
None of the particles ejected from the part of bubbles classified as "Remainder"						
can be entrained, as even 400 micron char particles at 1 m/s fall back down						
50% of ejected small char particles are entrained						
if ejected at top of range, likely velocity above 2 m/s and then capable of reaching exit						
20% of medium char particles entrained						
2.5% of large char particles entrained						
cannot be accelerated to much more than 2 m/s and then barely reaches outlet						
10% of small sand entrained						
1% of medium sand entrained						
0.25% of large sand entrained						

Bubble size						
cm	frequency					
4	0.2					
5	0.6					
6	0.2					

Bubble volume:			68.55667	ccm		
Volumetric flowrate through rest of bed:			0.000883	cubic metres per second		
Total flowrate:			0.001617	cubic metres per second		
Flowrate in bubbles:			0.000734	cubic metres per second		
Bubble frequency:			10.69979			
Surface area:			0.79756	sqcm		
Volume ejected:			0.183475	cubic cm per second		
Mass ejected:			484.374	mg/second	0.484374	g/s

Apply percentages estimated from particle tracking:

	percentage		g/s entrained		new size distribution	
1. Char particles	of total	entrained				
Small	0.6	50	0.001453		11.25	
Medium	4	20	0.003875		30.01	
Large	0.4	2.5	4.84E-05		0.38	
2. Sand particles						
Small	9.5	10	0.004602		35.64	
Medium	52.25	1	0.002531		19.60	
Large	33.25	0.25	0.000403		3.12	
Total	100		0.012912		100	

236

Pressure
readings

1025

505

630

450

300

150

15

50

500

620

237

Pressure
readings

MASSTAB	No Scale		CODE-NR.	
	DATUM	NAME	BENENNUNG	
GEZ.	09.08.01	Eerges.		20% narowing
GEPR.				
NORM.				
			ZEICHNUNGS-NR.	2-D_MODEL_
			DESIGN-FILE:	_ _ _ _ _ _ _ _ _

MF	INDEX	AENDERUNG	DATUM	NAME	URHEBERSCHUTZVERMERK SIEHE DIN 34	ZUSAMMENSTELLUNG SIEHE ZEICHNUNGS-NR.		
④								
③								
②								
①								
BESTIMMT FIER WERK			GEB.		BETR.	ANZAHL DER BILDER	A	B

238

Front View

Back view

239

	1		2		3		4

500

350

170 50

75

110

240

MASSTAB		No Scale	CODE-NR.	
	DATUM	NAME	BENENNUNG	
GEZ.	19.08.01	Eerges	7.5cm-Rig_with_Narrowing	
GEPR.				
VORM				
			ZEICHNUNGS-NR.	2-D_MODEL_
			DESIGN-FILE: _ _ _ _ _ _ _ _	
MF INDEX	AENDERUNG	DATUM NAME	URHEBERSCHUTZVERMERK SIEHE DIN 34	ZUSAMMENSTELLUNG SIEHE ZEICHNUNGS-NR.
BESTIMMT FUER WERK		GEB.	BETR.	ANZAHL DER BILDER / A/B

241

45

800

100

55

50

7

50

242

25

100

1000

107

50

7

50

MASSTAB	No Scale		CODE-NR.	
	DATUM	NAME	BENENNUNG	
GEZ.	09.08.01	Ferges.	Clamping_Left_Side_	
GEPR.				
NORM.				
			ZEICHNUNGS-NR. 2-D_MODEL_	
			DESIGN-FILE: _ _ _ _ _ _ _	

| MF INDEX | AENDERUNG | DATUM | NAME | URHEBERSCHUTZVERMERK SIEHE DIN 34 | ZUSAMMENSTELLUNG SIEHE ZEICHNUNGS-NR. | | |
| BESTIMMT FUER WERK | | GEB. | | BETR. | | ANZAHL DER BILDER | A B |

MASSTAB	No Scale		CODE-NR.		
	DATUM	NAME	BENENNUNG		
GEZ.	09.08.01	F.erges	Clamping_Right_Sidel		
GEPR.					
NORM.					
			ZEICHNUNGS-NR.	2-D_MODEL_	
			DESIGN FILE:		

MF INDEX	AENDERUNG	DATUM	NAME	URHEBERSCHUTZVERMERK SIEHE DIN 34	ZUSAMMENSTELLUNG SIEHE ZEICHNUNGS-NR.		
BESTIMMT FUER WERK		GEB.		BETR.		ANZAHL DER BILDER	A B

244

		DATUM	NAME	CODE-NR.
MASSTAR				
GEZ.		14.08.01	Ferges	BENENNUNG
GEPR.				Additional Clamping
NORM.				
				ZEICHNUNGS-NR. 2-D_MODEL_
				DESIGN-FILE:

MF INDEX ④ ③ ② ①

MF INDEX	AENDERUNG	DATUM	NAME	URHEBERSCHUTZVERMERK SIEHE DIN 34	ZUSAMMENSTELLUNG SIEHE ZEICHNUNGS-NR.

BESTIMMT FUER WERK GEB. BETR. ANZAHL DER BILDER A/R

dimensions: 5, 80, 32, 380, 150, 120, 32

2DRig modelling

Selective list of simulations performed

Standard configuration

Velocity m/s	Initial sand height m	Particle diameter microns	Density kg/m³	Quality of results	Time s	Location
0.25	0.33	503	2440	Good	5.2	CFDcomp1/2DRig1
0.35	0.33	503	2440	Good	1.1	CFDcomp2/2DRig1
0.55	0.33	503	2440	Good	0.88	CFDcomp3/2DRig1
0.75	0.33	503	2440	Acceptable	0.3	CFDcomp3/2DRig1
0.75	0.33	503	2440	Bad	0.4	CFDcomp4/2DRig1
0.25	0.53	503	2440	Good	1.4	CFDcomp1/2DRig1
0.35	0.53	503	2440	Good	1.45	CFDcomp2/2DRig1
0.55	0.53	503	2440	Acceptable	1.1	CFDcomp4/2DRig1
0.35	0.33	640	2440	Good	2.5	CFDcomp1/2DRig2
0.55	0.33	640	2440	Good	1.1	CFDcomp2/2DRig2
0.25	0.33	440	2440	Bad	0.05	CFDcomp1/2DRig2
0.25	0.33	440	2440	Good	1.05	CFDcomp1/2DRig3
0.25	0.33	440	2640	Good	1.2	CFDcomp3/2DRig3
0.385	0.33	440	2440	Good	1	CFDcomp2/2DRig4
0.56	0.33	440	2440	Good	0.5	CFDcomp2/2DRig4
0.775	0.5	440	2440	Good	0.6	CFDcomp1/2DRig5
0.348	0.5	440	2440	Good	0.7	CFDcomp4/2DRig5

Widening

Velocity m/s	Initial sand height m	Particle diameter microns	Density kg/m³	Quality of results	Time s	Location
0.75	0.5	440	2440	Good	5.2	CFDcomp1/20pcwidening
0.45	0.5	440	2440	Good	5.2	CFDcomp2/20pcwidening
0.35	0.5	503	2440	Good	5.2	CFDcomp3/20pcwidening
0.35	0.5	440	2440	Good	5.2	CFDcomp4/20pcwidening

0.55	0.5	440	2440	Good	5.2	CFDcomp3/20pcwidening
0.25	0.5	440	2440	Good	5.2	CFDcomp4/20pcwidening
0.25	0.33	440	2440	Good	5.2	CFDcomp2/20pcwidening1
0.75	0.33	440	2640	Good	5.2	CFDcomp2/20pcwidening1
0.45	0.33	440	2440	Good	5.2	CFDcomp3/20pcwidening1
0.55	0.33	440	2440	Good	30	CFDcomp3/20pcwidening1
0.35	0.33	440	2440	Good	5.2	CFDcomp4/20pcwidening1
0.45	0.33	440	2440	Good	30	CFDcomp4/20pcwidening1
Narrowing						
0.35	0.5	440	2640	Good	8	)comp1/CFDcomp2compiling
0.55	0.5	440	2640	Good	8	CFDcomp2/20pcnarrowing

```
>>CFX4
  >>SET LIMITS
    TOTAL REAL WORK SPACE 32000000
    TOTAL INTEGER WORK SPACE 8000000
  >>OPTIONS
    TWO DIMENSIONS
    NUMBER OF PHASES       2
    TRANSIENT FLOW
    BUOYANT FLOW
    END
>>MODEL TOPOLOGY
  >>CREATE PATCH
    PATCH TYPE 'INLET'
    PATCH NAME 'GAS INLET'
    BLOCK NAME 'Solid 1'
    PATCH LOCATION 1 1 1 25 1 1
    LOW I
    END
  >>CREATE PATCH
    PATCH TYPE 'INLET'
    PATCH NAME 'GAS JET'
    BLOCK NAME 'Solid 1'
    PATCH LOCATION 1 1 26 30 1 1
    LOW I
    END
  >>CREATE PATCH
    PATCH TYPE 'INLET'
    PATCH NAME 'GAS INLET'
    BLOCK NAME 'Solid 1'
    PATCH LOCATION 1 1 31 50 1 1
    LOW I
    END
  >>CREATE PATCH
    PATCH TYPE 'PRESSURE BOUNDARY'
    PATCH NAME 'OUTLET'
    BLOCK NAME 'Solid 2'
    HIGH I
    END
  >>CREATE PATCH
    PATCH TYPE 'PRESSURE BOUNDARY'
    PATCH NAME 'OUTLET'
    BLOCK NAME 'Solid 4'
    LOW J
    END
  >>CREATE PATCH
    PATCH TYPE 'PRESSURE BOUNDARY'
    PATCH NAME 'OUTLET'
    BLOCK NAME 'Solid 3'
    HIGH I
    END
>>MODEL DATA
  >>SET INITIAL GUESS
    >>INPUT FROM FILE
      READ DUMP FILE
      LAST DATA GROUP
      END
    >>SELECT VARIABLES FROM FILE
```

```
      ALL RELEVANT DATA
      END
>>TITLE
  PROBLEM TITLE 'REFERENCE EXAMPLE 28'
  END
>>WALL TREATMENTS
  SLIP
  END
>>RHIE CHOW SWITCH
  STANDARD
  END
>>PHYSICAL PROPERTIES
  >>BUOYANCY PARAMETERS
    GRAVITY VECTOR 0.0 -9.81 0.0
    BUOYANCY REFERENCE DENSITY 1.2
    END
  >>FLUID PARAMETERS
    PHASE NAME 'PHASE1'
    VISCOSITY       1.8E-5
    DENSITY         1.2
    END
  >>FLUID PARAMETERS
    PHASE NAME 'PHASE2'
    VISCOSITY       1.0E-12
    DENSITY         2640.0
    END
  >>TRANSIENT PARAMETERS
    >>ADAPTIVE TIME STEPPING
      NUMBER OF TIME STEPS 9999
      INITIAL TIME STEP 0.00025
      MINIMUM TIME STEP 0.0000000025
      MAXIMUM TIME STEP 0.00025
      MULTIPLY TIME STEP BY 5.0
      DIVIDE TIME STEP BY 5.0
      MINIMUM INTERVAL BETWEEN INCREMENTS 10
      MAXIMUM NUMBER OF CONTIGUOUS DECREMENTS 5
      END
  >>MULTIPHASE PARAMETERS
    >>INTER PHASE TRANSFER MODELS
      >>MOMENTUM
        >>PARTICLE DRAG MODEL
          FLOW REGIME 'AUTOMATIC'
          VISCOUS REGIME CORRELATION 'SCHILLER-NAUMANN'
          NEWTON COEFFICIENT 0.44
          DENSE PARTICLE EFFECTS 'GIDASPOW'
          END
    >>PHASE DESCRIPTION
      PHASE NAME  'PHASE1'
      GAS
      CONTINUOUS
      END
    >>PHASE DESCRIPTION
      PHASE NAME 'PHASE2'
      SOLID
      DISPERSE
      MEAN DIAMETER 0.44E-3
      KINETIC THEORY
```

```
              MODIFY EMPTY CELL VELOCITY 0.0001
              END
   >>SOLVER DATA
     >>PROGRAM CONTROL
       MINIMUM NUMBER OF ITERATIONS     2
       MAXIMUM NUMBER OF ITERATIONS     200
       END
     >>TRANSIENT CONTROL
       >>CONTROL PARAMETERS
         MINIMUM RESIDUAL VALUE 0.001
         MAXIMUM RESIDUAL VALUE 10.0
         REDUCTION FACTOR 1000.0
         DIVERGENCE RATIO 10000.0
       >>CONVERGENCE TESTING ON VARIABLE
         PRESSURE
   >>CREATE GRID
   >>MODEL BOUNDARY CONDITIONS
     >>PRESSURE BOUNDARIES
       PATCH NAME 'OUTLET'
       PHASE NAME 'PHASE1'
       VOLUME FRACTION 1.0
       PRESSURE  0.0
       END
     >>PRESSURE BOUNDARIES
       PATCH NAME 'OUTLET'
       PHASE NAME 'PHASE2'
       VOLUME FRACTION 0.0
       PRESSURE  0.0
       END
     >>INLET BOUNDARIES
       PATCH NAME 'GAS INLET'
       PHASE NAME 'PHASE1'
       VOLUME FRACTION 1.0
       V VELOCITY 0.35
       U VELOCITY 0.0
       END
     >>INLET BOUNDARIES
       PATCH NAME 'GAS INLET'
       PHASE NAME 'PHASE2'
       VOLUME FRACTION 0.0
       U VELOCITY 0.0
       V VELOCITY 0.0
       END
     >>INLET BOUNDARIES
       PATCH NAME 'GAS JET'
       PHASE NAME 'PHASE1'
       VOLUME FRACTION 1.0
       V VELOCITY 0.35
       U VELOCITY 0.0
       END
     >>INLET BOUNDARIES
       PATCH NAME 'GAS JET'
       PHASE NAME 'PHASE2'
       VOLUME FRACTION 0.0
       U VELOCITY 0.0
       V VELOCITY 0.0
       END
```

```
>>OUTPUT OPTIONS
  >>DUMP FILE OPTIONS
    TIME INTERVAL 0.04
    VOLUME FRACTION
    END
  >>LINE GRAPH DATA
    BLOCK NAME 'Solid 1'
    XYZ 0.01 0.055 0.0
    EACH TIME STEP
    FILE NAME 'TEST.TXT'
    PHASE NAME 'PHASE1'
    PRESSURE
    END
>>STOP
```

```
      SUBROUTINE USRINT(U,V,W,P,VFRAC,DEN,VIS,TE,ED,RS,T,H,RF,SCAL
     +                  ,CONV,XC,YC,ZC,XP,YP,ZP
     +                  ,VOL,AREA,VPOR,ARPOR,WFACT,DISWAL,IPT
     +                  ,IBLK,IPVERT,IPNODN,IPFACN,IPNODF,IPNODB,IPFACB
     +                  ,WORK,IWORK,CWORK)
C
C**********************************************************************
C
C    UTILITY SUBROUTINE FOR USER-SUPPLIED INITIAL FIELD.
C
C**********************************************************************
C
C    THIS SUBROUTINE IS CALLED BY THE FOLLOWING SUBROUTINE
C       CUSR   INIT
C
C**********************************************************************
C    CREATED
C        13/06/90 ADB
C    MODIFIED
C        07/08/91 IRH    NEW STRUCTURE
C        10/09/91 IRH    CORRECTION TO IUSED
C        26/09/91 IRH    ALTER ARGUMENT LIST
C        01/10/91 DSC    REDUCE COMMENT LINE GOING OVER COLUMN 72.
C        03/10/91 IRH    CORRECT COMMENTS
C        28/01/92 PHA    UPDATE CALLED BY COMMENT, ADD RF ARGUMENT,
C                        CHANGE LAST DIMENSION OF RS TO 6 AND IVERS TO 2
C        03/06/92 PHA    ADD PRECISION FLAG AND CHANGE IVERS TO 3
C        08/02/93 NSW    REMOVE REDUNDANT COMMENTS
C        23/11/93 CSH    EXPLICITLY DIMENSION IPVERT ETC.
C        03/02/94 PHA    CHANGE FLOW3D TO CFDS-FLOW3D, REMOVE COMMA
C                        FROM BEGINNING OF DIMENSION STATEMENT
C        03/03/94 FHW    CORRECTION OF SPELLING MISTAKE
C        09/08/94 NSW    CORRECT SPELLING
C                        MOVE 'IF(IUSED.EQ.0) RETURN' OUT OF USER AREA
C        19/12/94 NSW    CHANGE FOR CFX-F3D
C        30/01/95 NSW    INCLUDE NEW EXAMPLE
C        02/07/97 NSW    UPDATE FOR CFX-4
C
C**********************************************************************
C
C    SUBROUTINE ARGUMENTS
C
C       U      - U COMPONENT OF VELOCITY
C       V      - V COMPONENT OF VELOCITY
C       W      - W COMPONENT OF VELOCITY
C       P      - PRESSURE
C       VFRAC  - VOLUME FRACTION
C       DEN    - DENSITY OF FLUID
C       VIS    - VISCOSITY OF FLUID
C       TE     - TURBULENT KINETIC ENERGY
C       ED     - EPSILON
C       RS     - REYNOLD STRESSES
C       T      - TEMPERATURE
C       H      - ENTHALPY
C       RF     - REYNOLD FLUXES
C       SCAL   - SCALARS (THE FIRST 'NCONC' OF THESE ARE MASS FRACTIONS)
C       CONV   - CONVECTION COEFFICIENTS
```

```
C     XC    - X COORDINATES OF CELL CORNERS
C     YC    - Y COORDINATES OF CELL CORNERS
C     ZC    - Z COORDINATES OF CELL CORNERS
C     XP    - X COORDINATES OF CELL CENTRES
C     YP    - Y COORDINATES OF CELL CENTRES
C     ZP    - Z COORDINATES OF CELL CENTRES
C     VOL   - VOLUME OF CELLS
C     AREA  - AREA OF CELLS
C     VPOR  - POROUS VOLUME
C     ARPOR - POROUS AREA
C     WFACT - WEIGHT FACTORS
C     DISWAL - DISTANCE OF CELL CENTRE FROM WALL
C
C     IPT    - 1D POINTER ARRAY
C     IBLK   - BLOCK SIZE INFORMATION
C     IPVERT - POINTER FROM CELL CENTERS TO 8 NEIGHBOURING VERTICES
C     IPNODN - POINTER FROM CELL CENTERS TO 6 NEIGHBOURING CELLS
C     IPFACN - POINTER FROM CELL CENTERS TO 6 NEIGHBOURING FACES
C     IPNODF - POINTER FROM CELL FACES TO 2 NEIGHBOURING CELL CENTERS
C     IPNODB - POINTER FROM BOUNDARY CENTERS TO CELL CENTERS
C     IPFACB - POINTER FROM BOUNDARY CENTERS TO BOUNDARY FACES
C
C     WORK  - REAL WORKSPACE ARRAY
C     IWORK - INTEGER WORKSPACE ARRAY
C     CWORK - CHARACTER WORKSPACE ARRAY
C
C     SUBROUTINE ARGUMENTS PRECEDED WITH A '*' ARE ARGUMENTS THAT MUST
C     BE SET  BY THE USER IN THIS ROUTINE.
C
C     LOGICAL VARIABLE LRDISK IN COMMON BLOCK IOLOGC INDICATES WHETHER
C     THE RUN IS A RESTART AND CAN BE USED SO THAT INITIAL INFORMATION
C     IS ONLY SET WHEN STARTING A RUN FROM SCRATCH.
C
C     NOTE THAT OTHER DATA MAY BE OBTAINED FROM CFX-4 USING THE
C     ROUTINE GETADD, FOR FURTHER DETAILS SEE THE VERSION 4
C     USER MANUAL.
C
C*****************************************************************************
      LOGICAL LDEN,LVIS,LTURB,LTEMP,LBUOY,LSCAL,LCOMP
     +        ,LRECT,LCYN,LAXIS,LPOROS,LTRANS
      LOGICAL LRDISK,LWDISK
C
      CHARACTER*(*) CWORK
C
C+++++++++++++++ USER AREA 1 +++++++++++++++++++++++++++++++++++++++++++++++++
C---- AREA FOR USERS EXPLICITLY DECLARED VARIABLES
C
C+++++++++++++++ END OF USER AREA 1 +++++++++++++++++++++++++++++++++++++++++++
C
      COMMON
     + /ALL/    NBLOCK,NCELL,NBDRY,NNODE,NFACE,NVERT,NDIM
     + /ALLWRK/ NRWS,NIWS,NCWS,IWRFRE,IWIFRE,IWCFRE
     + /ADDIMS/ NPHASE,NSCAL,NVAR,NPROP
     +          ,NDVAR,NDPROP,NDXNN,NDGEOM,NDCOEF,NILIST,NRLIST,NTOPOL
     + /CHKUSR/ IVERS,IUCALL,IUSED
     + /DEVICE/ NREAD,NWRITE,NRDISK,NWDISK
     + /IDUM/   ILEN,JLEN
```

```
      + /IOLOGC/ LRDISK,LWDISK
      + /LOGIC/  LDEN,LVIS,LTURB,LTEMP,LBUOY,LSCAL,LCOMP
      +          ,LRECT,LCYN,LAXIS,LPOROS,LTRANS
      + /MLTGRD/ MLEVEL,NLEVEL,ILEVEL
      + /SGLDBL/ IFLGPR,ICHKPR
      + /TRANSI/ NSTEP,KSTEP,MF,INCORE
      + /TRANSR/ TIME,DT,DTINVF,TPARM


C
C++++++++++++++ USER AREA 2 +++++++++++++++++++++++++++++++++++++++++++++++
C---- AREA FOR USERS TO DECLARE THEIR OWN COMMON BLOCKS
C     THESE SHOULD START WITH THE CHARACTERS 'UC' TO ENSURE
C     NO CONFLICT WITH NON-USER COMMON BLOCKS
C
C++++++++++++++ END OF USER AREA 2 ++++++++++++++++++++++++++++++++++++++++++
C


      DIMENSION
      + U(NNODE,NPHASE),V(NNODE,NPHASE),W(NNODE,NPHASE)
      +,P(NNODE,NPHASE),VFRAC(NNODE,NPHASE)
      +,TE(NNODE,NPHASE),ED(NNODE,NPHASE),RS(NNODE,NPHASE,6)
      +,T(NNODE,NPHASE),H(NNODE,NPHASE),RF(NNODE,NPHASE,4)
      +,SCAL(NNODE,NPHASE,NSCAL)
      +,DEN(NNODE,NPHASE),VIS(NNODE,NPHASE),CONV(NFACE,NPHASE)
      DIMENSION
      + XC(NVERT),YC(NVERT),ZC(NVERT),XP(NNODE),YP(NNODE),ZP(NNODE)
      +,VOL(NCELL),AREA(NFACE,3),VPOR(NCELL),ARPOR(NFACE,3)
      +,WFACT(NFACE),DISWAL(NCELL)
      DIMENSION
      + IPT(*),IBLK(5,NBLOCK)
      +,IPVERT(NCELL,8),IPNODN(NCELL,6),IPFACN(NCELL,6),IPNODF(NFACE,4)
      +,IPNODB(NBDRY,4),IPFACB(NBDRY)
      DIMENSION
      + IWORK(NIWS),WORK(NRWS),CWORK(NCWS)
C
C++++++++++++++ USER AREA 3 +++++++++++++++++++++++++++++++++++++++++++++++
C---- AREA FOR USERS TO DIMENSION THEIR ARRAYS
C
C---- AREA FOR USERS TO DEFINE DATA STATEMENTS
C
C++++++++++++++ END OF USER AREA 3 ++++++++++++++++++++++++++++++++++++++++++
C
C---- STATEMENT FUNCTION FOR ADDRESSING
      IP(I,J,K)=IPT((K-1)*ILEN*JLEN+(J-1)*ILEN+I)
C
C----VERSION NUMBER OF USER ROUTINE AND PRECISION FLAG
C


      IVERS=3
      ICHKPR = 1
C
C++++++++++++++ USER AREA 4 +++++++++++++++++++++++++++++++++++++++++++++++
C---- TO USE THIS USER ROUTINE FIRST SET IUSED=1
C
```

254

```
      IUSED=1
C
C++++++++++++++ END OF USER AREA 4 ++++++++++++++++++++++++++++++++++++++
C
      IF (IUSED.EQ.0) RETURN
C
C---- FRONTEND CHECKING OF USER ROUTINE
      IF (IUCALL.EQ.0) RETURN
C
C++++++++++++++ USER AREA 5 ++++++++++++++++++++++++++++++++++++++++++++++
C
C---- AREA FOR INITIALISING VARIABLES U,V,W,P,VFRAC,TE,ED,RS,T,SCAL
C     ONLY.
C PHASE 1 = CONTINUOUS PHASE - GAS
C PHASE 2 = DISPERSED PHASE  - SOLID
      IC=1
      ID=2
C
C  GET SOLID PHASE DENSITY SET IN COMMAND FILE
C
      CALL GETADD('USRINT','RPHYS ','DENSIT',ILEVEL,JDENS)
C
      DENSOL=WORK(JDENS-1+ID)
C
C  SET INITIAL BED GAS VOLUME FRACTION
      VFINIT=0.425
C  SET INITIAL BED GAS VELOCITY TO MINIMUM FLUIDISATION VELOCITY
      VELP1=0.27
      VELP2=0.001
C
      EMPTY=1.0E-10
      FULL=1.0-EMPTY
C
C ONLY SET INITIAL CONDITIONS IF NOT DOING A RESTART
      IF(.NOT.LRDISK) THEN
C
C ----   GET OUTLET PATCH - PRESSURE BOUNDARY
C
         CALL IPREC('OUTLET','PATCH','CENTRES',IPT,ILEN,JLEN,
     +            KLEN,CWORK,IWORK)
C ----   FIND THE OUTLET PRESSURE
         INODE=IP(1,1,1)
         POUT=P(INODE,IC)
C ====   START SETTING VARIABLES ====================================
C
C ----   GET CELL NODES
C
      CALL IPALL('USER3D1','USER3D','PATCH','CENTRES',IPT,NPT,
     +            CWORK,IWORK)
C
C ----   FIRST SET ALL CELLS ASSUMING NO SOLIDS
C


      DO 111 I=1,NPT
         INODE=IPT(I)
         VFRAC(INODE,IC)=FULL
```

```fortran
                VFRAC(INODE,ID)=EMPTY
C ----   AIR VELOCITY SET TO MIN. FLUIDIZATION VEL.
                V(INODE,IC)=VELP1
                V(INODE,ID)=VELP2
C ----   SET PRESSURES TO OUTLET PRESSURE
                P(INODE,IC)=POUT
                P(INODE,ID)=POUT
  111  CONTINUE
       CALL IPALL('USER3D2','USER3D','PATCH','CENTRES',IPT,NPT,
      +          CWORK,IWORK)
C
C ----   FIRST SET ALL CELLS ASSUMING NO SOLIDS
C
       DO 121 I=1,NPT
          INODE=IPT(I)
          VFRAC(INODE,IC)=FULL
          VFRAC(INODE,ID)=EMPTY
C ----   AIR VELOCITY SET TO MIN. FLUIDIZATION VEL.
                V(INODE,IC)=VELP1
                V(INODE,ID)=VELP2
C ----   SET PRESSURES TO OUTLET PRESSURE
                P(INODE,IC)=POUT
                P(INODE,ID)=POUT
  121  CONTINUE
C ----   SET INITAL CONDITIONS IN LOWER SECTION OF BED
C
       CALL IPREC('Solid 1','BLOCK','CENTRES',IPT,ILEN,JLEN,KLEN,
      +          CWORK,IWORK)
          PCONST=DENSOL*(1-VFINIT)*9.81
C
          DO 203 K=1,KLEN
            DO 202 J=1,JLEN*36/73
              DO 201 I=1,ILEN
                INODE=IP(I,J,K)


C
                VFRAC(INODE,IC)=VFINIT
                VFRAC(INODE,ID)=1.0-VFRAC(INODE,IC)
C ----   SET VELOCITIES
                V(INODE,IC)= V(INODE,IC) / VFRAC(INODE,IC)
                V(INODE,ID)=VELP2
C ----   SET PRESSURE - ASSUMING CONSTANT DENSITY & VF IN BED
                P(INODE,IC)=PCONST*0.5+POUT
                P(INODE,ID)=P(INODE,IC)
C        SET INITIAL SOLIDS VELOCITY
                V(INODE,2)=0.0
C        SET INITIAL CONCENTRATION OF ACTIVATED BIOMASS
       CALL GETSCA('ACTIVATED',ISCAL,CWORK)
                SCAL(INODE,2,ISCAL)=0.0
       CALL GETSCA('BIOMASS',ISCAL,CWORK)
                SCAL(INODE,2,ISCAL)=0.0
                      CALL GETSCA('CHAR',ISCAL,CWORK)
                SCAL(INODE,2,ISCAL)=0.0
             T(INODE,1)=750.0
             T(INODE,2)=750.0
  201         CONTINUE
```

256

```
 202        CONTINUE
 203        CONTINUE


C ----    END OF INITIAL CONDITION SETUP
C
        ENDIF
C
C++++++++++++++++ END OF USER AREA 5 ++++++++++++++++++++++++++++++++++
C
        RETURN
        END
        SUBROUTINE USRSRC(IEQN,ICALL,CNAME,CALIAS,AM,SP,SU,CONV
       +                ,U,V,W,P,VFRAC,DEN,VIS,TE,ED,RS,T,H,RF,SCAL
       +                ,XP,YP,ZP,VOL,AREA,VPOR,ARPOR,WFACT,IPT
       +                , IBLK,IPVERT,IPNODN,IPFACN,IPNODF,IPNODB,IPFACB
       +                ,WORK,IWORK,CWORK)
C
C*********************************************************************************
C
C    UTILITY SUBROUTINE FOR USER-SUPPLIED SOURCES
C
C    >>> IMPORTANT                                              <<<
C    >>>                                                        <<<
C    >>> USERS MAY ONLY ADD OR ALTER PARTS OF THE SUBROUTINE WITHIN  <<<
C    >>> THE DESIGNATED USER AREAS                              <<<
C
C*********************************************************************************
C
C    THIS SUBROUTINE IS CALLED BY THE FOLLOWING SUBROUTINES
C       CUSR  SCDF  SCDS  SCED  SCENRG  SCHF  SCMOM  SCPCE  SCSCAL
C       SCTE  SCVF
C
C*********************************************************************************
C    CREATED
C       08/03/90  ADB
C    MODIFIED
C       04/03/91  ADB  ALTERED ARGUMENT LIST.
C       28/08/91  IRH  NEW STRUCTURE
C       28/09/91  IRH  CHANGE EXAMPLE + ADD COMMON BLOCKS
C       10/02/92  PHA  UPDATE CALLED BY COMMENT, ADD RF ARGUMENT,
C                      CHANGE LAST DIMENSION OF RS TO 6 AND IVERS TO 2
C       03/06/92  PHA  ADD PRECISION FLAG AND CHANGE IVERS TO 3
C       23/11/93  CSH  EXPLICITLY DIMENSION IPVERT ETC.
C       07/12/93  NSW  INCLUDE CONV IN ARGUMENT LIST AND CHANGE IVERS
C                      TO 4
C       03/02/94  PHA  CHANGE FLOW3D TO CFDS-FLOW3D
C       03/03/94  FHW  CORRECTION OF SPELLING MISTAKE
C       08/03/94  NSW  CORRECT SPELLING
C       09/08/94  NSW  CORRECT SPELLING.
C                      MOVE 'IF(IUSED.EQ.0) RETURN' OUT OF USER AREA.
C                      INCLUDE COMMENT ON MASS SOURCES.
C       19/12/94  NSW  CHANGE FOR CFX-F3D
C       02/07/97  NSW  UPDATE FOR CFX-4
C
C*********************************************************************************
```

```
C
C     SUBROUTINE ARGUMENTS
C
C        IEQN   - EQUATION NUMBER
C        ICALL  - SUBROUTINE CALL
C        CNAME  - EQUATION NAME
C        CALIAS - ALIAS OF EQUATION NAME
C        AM     - OFF DIAGONAL MATRIX COEFFICIENTS
C        SU     - SU IN LINEARISATION OF SOURCE TERM
C        SP     - SP IN LINEARISATION OF SOURCE TERM
C        CONV   - CONVECTION COEFFICIENTS
C        U      - U COMPONENT OF VELOCITY
C        V      - V COMPONENT OF VELOCITY
C        W      - W COMPONENT OF VELOCITY
C        P      - PRESSURE
C        VFRAC  - VOLUME FRACTION
C        DEN    - DENSITY OF FLUID
C        VIS    - VISCOSITY OF FLUID
C        TE     - TURBULENT KINETIC ENERGY
C        ED     - EPSILON
C        RS     - REYNOLD STRESSES
C        T      - TEMPERATURE
C        H      - ENTHALPY
C        RF     - REYNOLD FLUXES
C        SCAL   - SCALARS (THE FIRST 'NCONC' OF THESE ARE MASS FRACTIONS)
C        XP     - X COORDINATES OF CELL CENTRES
C        YP     - Y COORDINATES OF CELL CENTRES
C        ZP     - Z COORDINATES OF CELL CENTRES
C        VOL    - VOLUME OF CELLS
C        AREA   - AREA OF CELLS
C        VPOR   - POROUS VOLUME
C        ARPOR  - POROUS AREA
C        WFACT  - WEIGHT FACTORS
C
C        IPT    - 1D POINTER ARRAY
C        IBLK   - BLOCK SIZE INFORMATION
C        IPVERT - POINTER FROM CELL CENTERS TO 8 NEIGHBOURING VERTICES
C        IPNODN - POINTER FROM CELL CENTERS TO 6 NEIGHBOURING CELLS
C        IPFACN - POINTER FROM CELL CENTERS TO 6 NEIGHBOURING FACES
C        IPNODF - POINTER FROM CELL FACES TO 2 NEIGHBOURING CELL CENTERS
C        IPNODB - POINTER FROM BOUNDARY CENTERS TO CELL CENTERS
C        IPFACB - POINTER FROM BOUNDARY CENTERS TO BOUNDARY FACESS
C
C        WORK   - REAL WORKSPACE ARRAY
C        IWORK  - INTEGER WORKSPACE ARRAY
C        CWORK  - CHARACTER WORKSPACE ARRAY
C
C     SUBROUTINE ARGUMENTS PRECEDED WITH A '*' ARE ARGUMENTS THAT MUST
C     BE SET  BY THE USER IN THIS ROUTINE.
C
C     NOTE THAT WHEN USING MASS SOURCES, THE FLOWS THROUGH MASS FLOW
C     BOUNDARIES ARE UNCHANGED. THE USER SHOULD THEREFORE INCLUDE AT
C     LEAST ONE PRESSURE BOUNDARY FOR SUCH A CALCULATION.
C
C     NOTE THAT OTHER DATA MAY BE OBTAINED FROM CFX-4 USING THE
C     ROUTINE GETADD, FOR FURTHER DETAILS SEE THE VERSION 4
C     USER MANUAL.
```

```
C
C********************************************************************
C
      LOGICAL LDEN,LVIS,LTURB,LTEMP,LBUOY,LSCAL,LCOMP
     +       ,LRECT,LCYN,LAXIS,LPOROS,LTRANS
C
      CHARACTER*(*) CWORK
      CHARACTER    CNAME*6, CALIAS*24
C
C+++++++++++++++ USER AREA 1 +++++++++++++++++++++++++++++++++++++++++
C---- AREA FOR USERS EXPLICITLY DECLARED VARIABLES
C
C+++++++++++++++ END OF USER AREA 1 +++++++++++++++++++++++++++++++++++
C
      COMMON
     + /ALL/     NBLOCK,NCELL,NBDRY,NNODE,NFACE,NVERT,NDIM
     + /ALLWRK/ NRWS,NIWS,NCWS,IWRFRE,IWIFRE,IWCFRE
     + /ADDIMS/ NPHASE,NSCAL,NVAR,NPROP
     +          ,NDVAR,NDPROP,NDXNN,NDGEOM,NDCOEF,NILIST,NRLIST,NTOPOL
     + /CHKUSR/ IVERS,IUCALL,IUSED
     + /DEVICE/ NREAD,NWRITE,NRDISK,NWDISK
     + /IDUM/    ILEN,JLEN
     + /LOGIC/  LDEN,LVIS,LTURB,LTEMP,LBUOY,LSCAL,LCOMP
     +          ,LRECT,LCYN,LAXIS,LPOROS,LTRANS
     + /MLTGRD/ MLEVEL,NLEVEL,ILEVEL
     + /SGLDBL/ IFLGPR,ICHKPR
     + /SPARM/  SMALL,SORMAX,NITER,INDPRI,MAXIT,NODREF,NODMON
     + /TRANSI/ NSTEP,KSTEP,MF,INCORE
     + /TRANSR/ TIME,DT,DTINVF,TPARM
C
C+++++++++++++++ USER AREA 2 +++++++++++++++++++++++++++++++++++++++++
C---- AREA FOR USERS TO DECLARE THEIR OWN COMMON BLOCKS
C     THESE SHOULD START WITH THE CHARACTERS 'UC' TO ENSURE
C     NO CONFLICT WITH NON-USER COMMON BLOCKS
C
C+++++++++++++++ END OF USER AREA 2 +++++++++++++++++++++++++++++++++++
C
      DIMENSION AM(NCELL,6,NPHASE),SP(NCELL,NPHASE),SU(NCELL,NPHASE)
     +,CONV(NFACE,NPHASE)
C
      DIMENSION
     + U(NNODE,NPHASE),V(NNODE,NPHASE),W(NNODE,NPHASE),P(NNODE,NPHASE)
     +,VFRAC(NNODE,NPHASE),DEN(NNODE,NPHASE),VIS(NNODE,NPHASE)
     +,TE(NNODE,NPHASE),ED(NNODE,NPHASE),RS(NNODE,NPHASE,6)
     +,T(NNODE,NPHASE),H(NNODE,NPHASE),RF(NNODE,NPHASE,4)
     +,SCAL(NNODE,NPHASE,NSCAL)
C
      DIMENSION
     + XP(NNODE),YP(NNODE),ZP(NNODE)
     +,VOL(NCELL),AREA(NFACE,3),VPOR(NCELL),ARPOR(NFACE,3)
     +,WFACT(NFACE)
     +,IPT(*),IBLK(5,NBLOCK)
     +,IPVERT(NCELL,8),IPNODN(NCELL,6),IPFACN(NCELL,6),IPNODF(NFACE,4)
     +,IPNODB(NBDRY,4),IPFACB(NBDRY)
     +,IWORK(*),WORK(*),CWORK(*)
C
C+++++++++++++++ USER AREA 3 +++++++++++++++++++++++++++++++++++++++++
```

259

```fortran
C---- AREA FOR USERS TO DIMENSION THEIR ARRAYS
C
C---- AREA FOR USERS TO DEFINE DATA STATEMENTS
C
C+++++++++++++++++ END OF USER AREA 3 ++++++++++++++++++++++++++++++++++
C
C---- STATEMENT FUNCTION FOR ADDRESSING
      IP(I,J,K)=IPT((K-1)*ILEN*JLEN+(J-1)*ILEN+I)
C
C----VERSION NUMBER OF USER ROUTINE AND PRECISION FLAG
C
      IVERS=4
      ICHKPR = 1
C
C+++++++++++++++++ USER AREA 4 +++++++++++++++++++++++++++++++++++++++++
C---- TO USE THIS USER ROUTINE FIRST SET IUSED=1
C
      IUSED=1
C
C+++++++++++++++++ END OF USER AREA 4 +++++++++++++++++++++++++++++++++++
C
      IF (IUSED.EQ.0) RETURN
C
C---- FRONTEND CHECKING OF USER ROUTINE
      IF (IUCALL.EQ.0) RETURN
C
C---- ADD TO SOURCE TERMS
      IF (ICALL.EQ.1) THEN
C
C+++++++++++++++++ USER AREA 5 +++++++++++++++++++++++++++++++++++++++++
C
C---- EXAMPLE (HEAT SOURCE) ADD 100W PER UNIT VOLUME IN BLOCK
C     'BLOCK-NUMBER-2'
C
C   USE IPREC TO FIND ADDRESSES
C
      CALL IPALL('USER3D1','USER3D','PATCH','CENTRES',IPT,NPT,
     +          CWORK,IWORK)
C
C   Pressure type source
      CALL GETVAR('USRSRC','P       ',IVAR)
C
      IF (IVAR.EQ.IEQN) THEN
      DO 101 I=1,NPT
        INODE=IPT(I)
C
      CALL GETSCA('ACTIVATED',ISCAL,CWORK)
        T(INODE,1)=750.0
        T(INODE,2)=750.0
          SU(INODE,1)=SU(INODE,1)+VFRAC(INODE,2)*VOL(INODE)*
     +       SCAL(INODE,2,ISCAL)*(3.2E14*EXP(-196.8E6
     +       /T(INODE,2)/8314.51)+0.65*1.3E10*EXP(-150.7E6/T(INODE,2)
     +       /8314.51))*DEN(INODE,2)
      USRT1=USRT1+VFRAC(INODE,2)*VOL(INODE)*SCAL(INODE,2,ISCAL)
      USRHG1=USRHG1+H(INODE,1)*VOL(INODE)*VFRAC(INODE,1)*DEN(INODE,1)
      USRHS1=USRHS1+H(INODE,2)*VOL(INODE)*VFRAC(INODE,2)*DEN(INODE,2)
  101     CONTINUE
```

```
      ENDIF
      CALL IPALL('USER3D2','USER3D','PATCH','CENTRES',IPT,NPT,
     +          CWORK,IWORK)
C
C  Pressure type source
      CALL GETVAR('USRSRC','P      ',IVAR)
C
      IF (IVAR.EQ.IEQN) THEN

         DO 121 I=1,NPT
         INODE=IPT(I)
C
      CALL GETSCA('ACTIVATED',ISCAL,CWORK)
            T(INODE,1)=750.0
       T(INODE,2)=750.0
         SU(INODE,1)=SU(INODE,1)+VFRAC(INODE,2)*VOL(INODE)*
     +      SCAL(INODE,2,ISCAL)*(3.2E14*EXP(-196.8E6
     +      /T(INODE,2)/8314.51)+0.65*1.3E10*EXP(-150.7E6/T(INODE,2)
     +      /8314.51))*DEN(INODE,2)
      USRT2=USRT2+VFRAC(INODE,2)*VOL(INODE)*SCAL(INODE,2,ISCAL)
      USRHG2=USRHG2+H(INODE,1)*VOL(INODE)*VFRAC(INODE,1)*DEN(INODE,1)
      USRHS2=USRHS2+H(INODE,2)*VOL(INODE)*VFRAC(INODE,2)*DEN(INODE,2)
  121     CONTINUE

      USRT3=USRT1+USRT2
      USRHG=USRHG1+USRHG2
      USRHS=USRHS1+USRHS2
      USRHT=USRHG+USRHS
      WRITE (6,*) 'USR', USRT3
      WRITE (6,*) 'ENTHALPY GAS', USRHG
      WRITE (6,*) 'ENTHALPY SOLID', USRHS
      WRITE (6,*) 'TOTAL ENTHALPY', USRHT
      USRT1=0.0
      USRT2=0.0
      USRT3=0.0
      USRHG=0.0
      USRHG1=0.0
      USRHG2=0.0
      USRHS=0.0
      USRHS1=0.0
      USRHS2=0.0
      USRHT=0.0
      ENDIF
      CALL IPALL('USER3D3','USER3D','PATCH','CENTRES',IPT,NPT,
     +          CWORK,IWORK)
C     CALL GETVAR('USRSRC','H      ',IVAR)
C
C      IF (IVAR.EQ.IEQN) THEN
C      DO 201 I=1,NPT
C         INODE=IPT(I)
C         SU(INODE,1)=SU(INODE,1)+1000000.0*VOL(INODE)
C         SU(INODE,2)=SU(INODE,2)+1000000.0*VOL(INODE)
C      201    CONTINUE
C      ENDIF
C
C---- END OF EXAMPLE
C+++++++++++++++++ END OF USER AREA 5 +++++++++++++++++++++++++++++++++
```

```
      ENDIF
C
C---- OVERWRITE SOURCE TERMS
      IF (ICALL.EQ.2) THEN
C
C+++++++++++++++ USER AREA 6 ++++++++++++++++++++++++++++++++++++++++++
C
C---- EXAMPLE (HEAT SOURCE) OVERWRITE WITH 100W PER UNIT VOLUME IN
C                            ALL INTERIOR CELLS
C
C    CALL GETVAR('USRSRC','H      ',IVAR)
C
C    IF (IVAR.EQ.IEQN) THEN
C USE IPALL TO FIND 1D ADDRESSES OF ALL CELL CENTRES
C    CALL IPALL('*','*','BLOCK','CENTRES',IPT,NPT,CWORK,IWORK)
C LOOP OVER ALL INTERIOR CELLS
C    DO 200 I=1,NPT
C USE ARRAY IPT TO GET ADDRESS
C       INODE=IPT(I)
C OVERWRITE SOURCE TERMS
C       SU(INODE,1)=100.0*VOL(INODE)
C 200 CONTINUE
C    ENDIF
C
C---- END OF EXAMPLE
C+++++++++++++++ END OF USER AREA 6 ++++++++++++++++++++++++++++++++++++
C
      ENDIF
      RETURN
      END
      SUBROUTINE USRTRN(U,V,W,P,VFRAC,DEN,VIS,TE,ED,RS,T,H,RF,SCAL,
     +                  XP,YP,ZP,VOL,AREA,VPOR,ARPOR,WFACT,CONV,IPT,
     +                  IBLK,IPVERT,IPNODN,IPFACN,IPNODF,IPNODB,IPFACB,
     +                  WORK,IWORK,CWORK)
C
C*********************************************************************
C
C   USER SUBROUTINE TO ALLOW USERS TO MODIFY OR MONITOR THE SOLUTION AT
C   THE END OF EACH TIME STEP
C   THIS SUBROUTINE IS CALLED BEFORE THE START OF THE RUN AS WELL AS AT
C   THE END OF EACH TIME STEP
C
C   >>> IMPORTANT                                              <<<
C   >>>                                                        <<<
C   >>> USERS MAY ONLY ADD OR ALTER PARTS OF THE SUBROUTINE WITHIN  <<<
C   >>> THE DESIGNATED USER AREAS                              <<<
C
C*********************************************************************
C
C   THIS SUBROUTINE IS CALLED BY THE FOLLOWING SUBROUTINES
C      CUSR   TRNMOD
C
C*********************************************************************
C   CREATED
C      27/04/90  ADB
C   MODIFIED
C      05/08/91  IRH  NEW STRUCTURE
```

262

```
C       01/10/91  DSC  REDUCE COMMENT LINE GOING OVER COLUMN 72.
C       29/11/91  PHA  UPDATE CALLED BY COMMENT, ADD RF ARGUMENT,
C                      CHANGE LAST DIMENSION OF RS TO 6 AND IVERS TO 2
C       05/06/92  PHA  ADD PRECISION FLAG AND CHANGE IVERS TO 3
C       03/07/92  DSC  CORRECT COMMON MLTGRD.
C       23/11/93  CSH  EXPLICITLY DIMENSION IPVERT ETC.
C       03/02/94  PHA  CHANGE FLOW3D TO CFDS-FLOW3D
C       22/08/94  NSW  MOVE 'IF(IUSED.EQ.0) RETURN' OUT OF USER AREA
C       19/12/94  NSW  CHANGE FOR CFX-F3D
C       02/07/97  NSW  UPDATE FOR CFX-4
C       02/07/99  NSW  INCLUDE NEW EXAMPLE FOR CALCULATING FLUX OF A
C                      SCALAR AT A PRESSURE BOUNDARY
C
C*********************************************************************
C
C    SUBROUTINE ARGUMENTS
C
C       U      - U COMPONENT OF VELOCITY
C       V      - V COMPONENT OF VELOCITY
C       W      - W COMPONENT OF VELOCITY
C       P      - PRESSURE
C       VFRAC  - VOLUME FRACTION
C       DEN    - DENSITY OF FLUID
C       VIS    - VISCOSITY OF FLUID
C       TE     - TURBULENT KINETIC ENERGY
C       ED     - EPSILON
C       RS     - REYNOLD STRESSES
C       T      - TEMPERATURE
C       H      - ENTHALPY
C       RF     - REYNOLD FLUXES
C       SCAL   - SCALARS (THE FIRST 'NCONC' OF THESE ARE MASS FRACTIONS)
C       XP     - X COORDINATES OF CELL CENTRES
C       YP     - Y COORDINATES OF CELL CENTRES
C       ZP     - Z COORDINATES OF CELL CENTRES
C       VOL    - VOLUME OF CELLS
C       AREA   - AREA OF CELLS
C       VPOR   - POROUS VOLUME
C       ARPOR  - POROUS AREA
C       WFACT  - WEIGHT FACTORS
C       CONV   - CONVECTION COEFFICIENTS
C
C       IPT    - 1D POINTER ARRAY
C       IBLK   - BLOCK SIZE INFORMATION
C       IPVERT - POINTER FROM CELL CENTERS TO 8 NEIGHBOURING VERTICES
C       IPNODN - POINTER FROM CELL CENTERS TO 6 NEIGHBOURING CELLS
C       IPFACN - POINTER FROM CELL CENTERS TO 6 NEIGHBOURING FACES
C       IPNODF - POINTER FROM CELL FACES TO 2 NEIGHBOURING CELL CENTERS
C       IPNODB - POINTER FROM BOUNDARY CENTERS TO CELL CENTERS
C       IPFACB - POINTER FROM BOUNDARY CENTERS TO BOUNDARY FACESS
C
C       WORK   - REAL WORKSPACE ARRAY
C       IWORK  - INTEGER WORKSPACE ARRAY
C       CWORK  - CHARACTER WORKSPACE ARRAY
C
C    SUBROUTINE ARGUMENTS PRECEDED WITH A '*' ARE ARGUMENTS THAT MUST
C    BE SET  BY THE USER IN THIS ROUTINE.
C
```

263

```
C     NOTE THAT OTHER DATA MAY BE OBTAINED FROM CFX-4 USING THE
C     ROUTINE GETADD, FOR FURTHER DETAILS SEE THE VERSION 4
C     USER MANUAL.
C
C*********************************************************************
C
C
      LOGICAL LDEN,LVIS,LTURB,LTEMP,LBUOY,LSCAL,LCOMP
     +        ,LRECT,LCYN,LAXIS,LPOROS,LTRANS
C
      CHARACTER*(*) CWORK
C
C+++++++++++++++ USER AREA 1 +++++++++++++++++++++++++++++++++++++++++
C---- AREA FOR USERS EXPLICITLY DECLARED VARIABLES
C
C+++++++++++++++ END OF USER AREA 1 +++++++++++++++++++++++++++++++++++
C
      COMMON
     + /ALL/    NBLOCK,NCELL,NBDRY,NNODE,NFACE,NVERT,NDIM
     + /ALLWRK/ NRWS,NIWS,NCWS,IWRFRE,IWIFRE,IWCFRE
     + /ADDIMS/ NPHASE,NSCAL,NVAR,NPROP
     +          ,NDVAR,NDPROP,NDXNN,NDGEOM,NDCOEF,NILIST,NRLIST,NTOPOL
     + /CHKUSR/ IVERS,IUCALL,IUSED
     + /CONC/   NCONC
     + /DEVICE/ NREAD,NWRITE,NRDISK,NWDISK
     + /IDUM/   ILEN,JLEN
     + /LOGIC/  LDEN,LVIS,LTURB,LTEMP,LBUOY,LSCAL,LCOMP
     +          ,LRECT,LCYN,LAXIS,LPOROS,LTRANS
     + /MLTGRD/ MLEVEL,NLEVEL,ILEVEL
     + /SGLDBL/ IFLGPR,ICHKPR
     + /SPARM/  SMALL,SORMAX,NITER,INDPRI,MAXIT,NODREF,NODMON
     + /TIMUSR/ DTUSR
     + /TRANSI/ NSTEP,KSTEP,MF,INCORE
     + /TRANSR/ TIME,DT,DTINVF,TPARM
C
C+++++++++++++++ USER AREA 2 +++++++++++++++++++++++++++++++++++++++++
C---- AREA FOR USERS TO DECLARE THEIR OWN COMMON BLOCKS
C     THESE SHOULD START WITH THE CHARACTERS 'UC' TO ENSURE
C     NO CONFLICT WITH NON-USER COMMON BLOCKS
C
C+++++++++++++++ END OF USER AREA 2 +++++++++++++++++++++++++++++++++++
C
      DIMENSION
     + U(NNODE,NPHASE),V(NNODE,NPHASE),W(NNODE,NPHASE),P(NNODE,NPHASE)
     +,VFRAC(NNODE,NPHASE),DEN(NNODE,NPHASE),VIS(NNODE,NPHASE)
     +,TE(NNODE,NPHASE),ED(NNODE,NPHASE),RS(NNODE,NPHASE,6)
     +,T(NNODE,NPHASE),H(NNODE,NPHASE),RF(NNODE,NPHASE,4)
     +,SCAL(NNODE,NPHASE,NSCAL)
      DIMENSION
     + XP(NNODE),YP(NNODE),ZP(NNODE)
     +,VOL(NCELL),AREA(NFACE,3),VPOR(NCELL),ARPOR(NFACE,3)
     +,WFACT(NFACE),CONV(NFACE,NPHASE)
     +,IPT(*),IBLK(5,NBLOCK)
     +,IPVERT(NCELL,8),IPNODN(NCELL,6),IPFACN(NCELL,6),IPNODF(NFACE,4)
     +,IPNODB(NBDRY,4),IPFACB(NBDRY)
     +,IWORK(*),WORK(*),CWORK(*)
      DIMENSION SGNWL(6)
```

264

```
C
C++++++++++++++ USER AREA 3 +++++++++++++++++++++++++++++++++++++++++++++
C---- AREA FOR USERS TO DIMENSION THEIR ARRAYS
C
C---- AREA FOR USERS TO DEFINE DATA STATEMENTS
C
C++++++++++++++ END OF USER AREA 3 +++++++++++++++++++++++++++++++++++++++
C
      DATA SGNWL / 1.0, 1.0, 1.0, -1.0, -1.0, -1.0 /
C
C---- STATEMENT FUNCTION FOR ADDRESSING
      IP(I,J,K)=IPT((K-1)*ILEN*JLEN+(J-1)*ILEN+I)
C
C----VERSION NUMBER OF USER ROUTINE AND PRECISION FLAG
C
      IVERS=3
      ICHKPR = 1
C
C++++++++++++++ USER AREA 4 +++++++++++++++++++++++++++++++++++++++++++++
C---- TO USE THIS USER ROUTINE FIRST SET IUSED=1
C
       IUSED=1
C
C++++++++++++++ END OF USER AREA 4 +++++++++++++++++++++++++++++++++++++++
C
      IF (IUSED.EQ.0) RETURN
C
C---- FRONTEND CHECKING OF USER ROUTINE
      IF (IUCALL.EQ.0) RETURN
C
C++++++++++++++ USER AREA 5 +++++++++++++++++++++++++++++++++++++++++++++
C
      CALL IPALL('USER3D1','USER3D','PATCH','CENTRES',IPT,NPT,
     +            CWORK,IWORK)
      DO 101 I=1,NPT
        INODE=IPT(I)
C
       T(INODE,1)=750.0
       T(INODE,2)=750.0
      CALL GETSCA('BIOMASS',ISCAL,CWORK)
        SCAL(INODE,2,ISCAL)=SCAL(INODE,2,ISCAL)-SCAL(INODE,2,ISCAL)
     +     *2.8E19*EXP(-242.8E6/T(INODE,2)/8314.51)*DT
      CALL GETSCA('ACTIVATED',ISCAL1,CWORK)
        SCAL(INODE,2,ISCAL1)=SCAL(INODE,2,ISCAL1)+SCAL(INODE,2,ISCAL)
     +     *2.8E19*EXP(-242.8E6/T(INODE,2)/8314.51)*DT
        SCAL(INODE,2,ISCAL1)=SCAL(INODE,2,ISCAL1)-SCAL(INODE,2,ISCAL1)
     +     *(1.3E10*EXP(-150.7E6/T(INODE,2)/8314.51)
     +     +3.2E14*EXP(-196.8E6/T(INODE,2)/8314.51))*DT
      CALL GETSCA('CHAR',ISCAL2,CWORK)
        SCAL(INODE,2,ISCAL2)=SCAL(INODE,2,ISCAL2)+0.35*
     +       SCAL(INODE,2,ISCAL1)
     +     *1.3E10*EXP(-150.7E6/T(INODE,2)/8314.51)*DT
      CALL GETSCA('GAS',ISCAL3,CWORK)
      CALL GETSCA('TAR',ISCAL4,CWORK)
        SCAL(INODE,1,ISCAL4)=(SCAL(INODE,1,ISCAL4)*VFRAC(INODE,1)
     +     *VOL(INODE)*DEN(INODE,1)+
     +     SCAL(INODE,2,ISCAL1)*VFRAC(INODE,2)*VOL(INODE)*DEN(INODE,2)
```

```fortran
     +        *3.2E14*DT*EXP(-196.8E6/T(INODE,2)/8314.51))/
     +        (SCAL(INODE,1,ISCAL4)*VFRAC(INODE,1)
     +        *VOL(INODE)*DEN(INODE,1)+
     +        SCAL(INODE,2,ISCAL1)*VFRAC(INODE,2)*VOL(INODE)*DEN(INODE,2)
     +        *3.2E14*DT*EXP(-196.8E6/T(INODE,2)/8314.51)+
     +        SCAL(INODE,1,ISCAL3)*VFRAC(INODE,1)
     +        *VOL(INODE)*DEN(INODE,1)+0.65*
     +        SCAL(INODE,2,ISCAL1)*VFRAC(INODE,2)*VOL(INODE)*DEN(INODE,2)
     +        *1.3E10*DT*EXP(-150.7E6/T(INODE,2)/8314.51))
              SCAL(INODE,1,ISCAL3)=(SCAL(INODE,1,ISCAL3)*VFRAC(INODE,1)
     +        *VOL(INODE)*DEN(INODE,1)+0.65*
     +        SCAL(INODE,2,ISCAL1)*VFRAC(INODE,2)*VOL(INODE)*DEN(INODE,2)
     +        *1.3E10*DT*EXP(-150.7E6/T(INODE,2)/8314.51))/
     +        (SCAL(INODE,1,ISCAL4)*VFRAC(INODE,1)
     +        *VOL(INODE)*DEN(INODE,1)+
     +        SCAL(INODE,2,ISCAL1)*VFRAC(INODE,2)*VOL(INODE)*DEN(INODE,2)
     +        *3.2E14*DT*EXP(-196.8E6/T(INODE,2)/8314.51)+
     +        SCAL(INODE,1,ISCAL3)*VFRAC(INODE,1)
     +        *VOL(INODE)*DEN(INODE,1)+0.65*
     +        SCAL(INODE,2,ISCAL1)*VFRAC(INODE,2)*VOL(INODE)*DEN(INODE,2)
     +        *1.3E10*DT*EXP(-150.7E6/T(INODE,2)/8314.51))
           VFRACT=VFRAC(INODE,2)
           USRP1=XP(INODE)
           USRP2=YP(INODE)
           USRT1=SCAL(INODE,2,ISCAL)
           USRT2=SCAL(INODE,2,ISCAL1)
           USRT3=SCAL(INODE,2,ISCAL2)
           USRT4=SCAL(INODE,1,ISCAL3)
           USRT5=SCAL(INODE,1,ISCAL4)
           USRR1=3.2E14*DT*EXP(-196.8E6/T(INODE,2)/8314.51)
           USRR2=1.3E10*DT*EXP(-150.7E6/T(INODE,2)/8314.51)
           USRR3=2.8E19*EXP(-242.8E6/T(INODE,2)/8314.51)*DT
           USRT6=T(INODE,2)
           USRM=USRM+DEN(INODE,2)*VOL(INODE)*VFRAC(INODE,2)
           IF (USRT6.LT.749.0) THEN
           WRITE (6,*) 'Position', USRP1, USRP2
           WRITE (6,*) 'BIOMASS ETC', USRT1, USRT2, USRT3, USRT4, USRT5
           WRITE (6,*) 'Reaction rates', USRR1, USRR2, USRR3
           WRITE (6,*) 'Temperature', USRT6
        ENDIF
           IF (VFRACT.LT.0.05) THEN
           SCAL(INODE,2,ISCAL)=0.0
           SCAL(INODE,2,ISCAL1)=0.0
           SCAL(INODE,2,ISCAL2)=0.0
        ENDIF
     ENDIF
101     CONTINUE
        WRITE(6,*) 'Mass is', USRM
        USRM=0.0
     CALL IPALL('USER3D2','USER3D','PATCH','CENTRES',IPT,NPT,
     +           CWORK,IWORK)
        DO 121 I=1,NPT
        INODE=IPT(I)
C


     CALL GETSCA('BIOMASS',ISCAL,CWORK)
        SCAL(INODE,2,ISCAL)=SCAL(INODE,2,ISCAL)-SCAL(INODE,2,ISCAL)
```

266

```fortran
     +      *2.8E19*EXP(-242.8E6/T(INODE,2)/8314.51)*DT
     CALL GETSCA('ACTIVATED',ISCAL1,CWORK)
            SCAL(INODE,2,ISCAL1)=SCAL(INODE,2,ISCAL1)+SCAL(INODE,2,ISCAL)
     +      *2.8E19*EXP(-242.8E6/T(INODE,2)/8314.51)*DT
            SCAL(INODE,2,ISCAL1)=SCAL(INODE,2,ISCAL1)-SCAL(INODE,2,ISCAL1)
     +      *(1.3E10*EXP(-150.7E6/T(INODE,2)/8314.51)
     +      +3.2E14*EXP(-196.8E6/T(INODE,2)/8314.51))*DT
     CALL GETSCA('CHAR',ISCAL2,CWORK)
            SCAL(INODE,2,ISCAL2)=SCAL(INODE,2,ISCAL2)+0.35*
     +        SCAL(INODE,2,ISCAL1)
     +      *1.3E10*EXP(-150.7E6/T(INODE,2)/8314.51)*DT
     CALL GETSCA('GAS',ISCAL3,CWORK)
     CALL GETSCA('TAR',ISCAL4,CWORK)
            SCAL(INODE,1,ISCAL4)=(SCAL(INODE,1,ISCAL4)*VFRAC(INODE,1)
     +      *VOL(INODE)*DEN(INODE,1)+
     +      SCAL(INODE,2,ISCAL1)*VFRAC(INODE,2)*VOL(INODE)*DEN(INODE,2)
     +      *3.2E14*DT*EXP(-196.8E6/T(INODE,2)/8314.51))/
     +      (SCAL(INODE,1,ISCAL4)*VFRAC(INODE,1)
     +      *VOL(INODE)*DEN(INODE,1)+
     +      SCAL(INODE,2,ISCAL1)*VFRAC(INODE,2)*VOL(INODE)*DEN(INODE,2)
     +      *3.2E14*DT*EXP(-196.8E6/T(INODE,2)/8314.51)+
     +      SCAL(INODE,1,ISCAL3)*VFRAC(INODE,1)
     +      *VOL(INODE)*DEN(INODE,1)+0.65*
     +      SCAL(INODE,2,ISCAL1)*VFRAC(INODE,2)*VOL(INODE)*DEN(INODE,2)
     +      *1.3E10*DT*EXP(-150.7E6/T(INODE,2)/8314.51))
            SCAL(INODE,1,ISCAL3)=(SCAL(INODE,1,ISCAL3)*VFRAC(INODE,1)
     +      *VOL(INODE)*DEN(INODE,1)+0.65*
     +      SCAL(INODE,2,ISCAL1)*VFRAC(INODE,2)*VOL(INODE)*DEN(INODE,2)
     +      *1.3E10*DT*EXP(-150.7E6/T(INODE,2)/8314.51))/
     +      (SCAL(INODE,1,ISCAL4)*VFRAC(INODE,1)
     +      *VOL(INODE)*DEN(INODE,1)+
     +      SCAL(INODE,2,ISCAL1)*VFRAC(INODE,2)*VOL(INODE)*DEN(INODE,2)
     +      *3.2E14*DT*EXP(-196.8E6/T(INODE,2)/8314.51)+
     +      SCAL(INODE,1,ISCAL3)*VFRAC(INODE,1)
     +      *VOL(INODE)*DEN(INODE,1)+0.65*
     +      SCAL(INODE,2,ISCAL1)*VFRAC(INODE,2)*VOL(INODE)*DEN(INODE,2)
     +      *1.3E10*DT*EXP(-150.7E6/T(INODE,2)/8314.51))
          VFRACT=VFRAC(INODE,2)
          IF (VFRACT.LT.0.05) THEN
          SCAL(INODE,2,ISCAL)=0.0
          SCAL(INODE,2,ISCAL1)=0.0
          SCAL(INODE,2,ISCAL2)=0.0
        ENDIF
  121     CONTINUE
C
C+++++++++++++++ END OF USER AREA 5 +++++++++++++++++++++++++++++++++++
C
      RETURN
      END
      SUBROUTINE USRCVG(U,V,W,P,VFRAC,DEN,VIS,TE,ED,RS,T,H,RF,SCAL
     +                  ,XP,YP,ZP,VOL,AREA,VPOR,ARPOR,WFACT,CONV,IPT
     +                  ,IBLK,IPVERT,IPNODN,IPFACN,IPNODF,IPNODB,IPFACB
     +                  ,CMETH,MNSL,MXSL,RDFC,RESOR,URFVAR,LCONVG
     +                  ,WORK,IWORK,CWORK)
C
C*********************************************************************
C
```

267

```
C    THIS SUBROUTINE ALLOWS USERS TO MONITOR CONVERGENCE, ALTER
C    UNDER RELAXATION FACTORS, REDUCTION FACTORS ETC
C    AND WRITE SOLUTION DATA AS A FUNCTION OF ITERATION
C
C    >>> IMPORTANT                                              <<<
C    >>>                                                        <<<
C    >>> USERS MAY ONLY ADD OR ALTER PARTS OF THE SUBROUTINE WITHIN <<<
C    >>> THE DESIGNATED USER AREAS                              <<<
C
C*********************************************************************
C
C    THIS SUBROUTINE IS CALLED BY THE FOLLOWING SUBROUTINE
C         CUSR  CVGTST
C
C*********************************************************************
C    CREATED
C        09/12/88  ADB
C    MODIFIED
C        08/08/91  IRH  NEW STRUCTURE
C        03/09/91  IRH  ADD CONV TO ARGUMENT LIST
C        23/09/91  IRH  ADD USEFUL COMMON BLOCKS
C        29/11/91  PHA  UPDATE CALLED BY COMMENT, ADD RF ARGUMENT,
C                       CHANGE LAST DIMENSION OF RS TO 6 AND IVERS TO 2
C        03/06/92  PHA  ADD PRECISION FLAG AND CHANGE IVERS TO 3
C        07/07/92  IRH  CORRECT EXAMPLE
C        23/11/93  CSH  EXPLICITLY DIMENSION IPVERT ETC.
C        03/02/94  PHA  CHANGE FLOW3D TO CFDS-FLOW3D
C        03/03/94  FHW  CORRECTION OF SPELLING MISTAKE
C        22/08/94  NSW  MOVE 'IF(IUSED.EQ.0) RETURN' OUT OF USER AREA
C        19/12/94  NSW  CHANGE FOR CFX-F3D
C        25/03/96  NSW  CORRECT MAXIMUM VELOCITY EXAMPLE
C        02/07/97  NSW  UPDATE FOR CFX-4
C
C*********************************************************************
C
C    SUBROUTINE ARGUMENTS
C
C      U      - U COMPONENT OF VELOCITY
C      V      - V COMPONENT OF VELOCITY
C      W      - W COMPONENT OF VELOCITY
C      P      - PRESSURE
C      VFRAC  - VOLUME FRACTION
C      DEN    - DENSITY OF FLUID
C      VIS    - VISCOSITY OF FLUID
C      TE     - TURBULENT KINETIC ENERGY
C      ED     - EPSILON
C      RS     - REYNOLD STRESSES
C      T      - TEMPERATURE
C      H      - ENTHALPY
C      RF     - REYNOLD FLUXES
C      SCAL   - SCALARS (THE FIRST 'NCONC' OF THESE ARE MASS FRACTIONS)
C      XP     - X COORDINATES OF CELL CENTRES
C      YP     - Y COORDINATES OF CELL CENTRES
C      ZP     - Z COORDINATES OF CELL CENTRES
C      VOL    - VOLUME OF CELLS
C      AREA   - AREA OF CELLS
C      VPOR   - POROUS VOLUME
```

```
C       ARPOR   - POROUS AREA
C       WFACT   - WEIGHT FACTORS
C
C       IPT     - 1D POINTER ARRAY
C       IBLK    - BLOCK SIZE INFORMATION
C       IPVERT  - POINTER FROM CELL CENTERS TO 8 NEIGHBOURING VERTICES
C       IPNODN  - POINTER FROM CELL CENTERS TO 6 NEIGHBOURING CELLS
C       IPFACN  - POINTER FROM CELL CENTERS TO 6 NEIGHBOURING FACES
C       IPNODF  - POINTER FROM CELL FACES TO 2 NEIGHBOURING CELL CENTERS
C       IPNODB  - POINTER FROM BOUNDARY CENTERS TO CELL CENTERS
C       IPFACB  - POINTER FROM BOUNDARY CENTERS TO BOUNDARY FACES
C
C       CMETH   - SOLUTION METHOD
C       MNSL    - MINIMUM NUMBER OF SWEEPS
C       MXSL    - MAXIMUM NUMBER OF SWEEPS
C       RDFC    - REDUCTION FACTORS REQUIRED
C       RESOR   - NON LINEAR RESIDUALS
C       URFVAR  - UNDER RELAXATION FACTORS
C     * LCONVG  - LOGICAL CONVERGENCE FLAG
C
C       WORK    - REAL WORKSPACE ARRAY
C       IWORK   - INTEGER WORKSPACE ARRAY
C       CWORK   - CHARACTER WORKSPACE ARRAY
C
C     SUBROUTINE ARGUMENTS PRECEDED WITH A '*' ARE ARGUMENTS THAT MUST
C     BE SET  BY THE USER IN THIS ROUTINE.
C
C     NOTE THAT OTHER DATA MAY BE OBTAINED FROM CFX-4 USING THE
C     ROUTINE GETADD, FOR FURTHER DETAILS SEE THE VERSION 4
C     USER MANUAL.
C
C*********************************************************************************
C
      LOGICAL LDEN,LVIS,LTURB,LTEMP,LBUOY,LSCAL,LCOMP
     +        ,LRECT,LCYN,LAXIS,LPOROS,LTRANS
      LOGICAL LCONVG
C
      CHARACTER*(*) CMETH,CWORK
C
C+++++++++++++++++ USER AREA 1 ++++++++++++++++++++++++++++++++++++++++++++++
C---- AREA FOR USERS EXPLICITLY DECLARED VARIABLES
C
C+++++++++++++++++ END OF USER AREA 1 ++++++++++++++++++++++++++++++++++++++++
C
      COMMON
     + /ALL/     NBLOCK,NCELL,NBDRY,NNODE,NFACE,NVERT,NDIM
     + /ALLWRK/  NRWS,NIWS,NCWS,IWRFRE,IWIFRE,IWCFRE
     + /ADDIMS/  NPHASE,NSCAL,NVAR,NPROP
     +           ,NDVAR,NDPROP,NDXNN,NDGEOM,NDCOEF,NILIST,NRLIST,NTOPOL
     + /CHKUSR/  IVERS,IUCALL,IUSED
     + /DEVICE/  NREAD,NWRITE,NRDISK,NWDISK
     + /IDUM/    ILEN,JLEN
     + /LOGIC/   LDEN,LVIS,LTURB,LTEMP,LBUOY,LSCAL,LCOMP
     +           ,LRECT,LCYN,LAXIS,LPOROS,LTRANS
     + /MLTGRD/  MLEVEL,NLEVEL,ILEVEL
     + /RESID/   IRESID,NRESID
     + /SGLDBL/  IFLGPR,ICHKPR
```

269

```
      + /SPARM/   SMALL,SORMAX,NITER,INDPRI,MAXIT,NODREF,NODMON
      + /TRANSI/ NSTEP,KSTEP,MF,INCORE
      + /TRANSR/ TIME,DT,DTINVF,TPARM
C
C+++++++++++++++ USER AREA 2 ++++++++++++++++++++++++++++++++++++++++++++
C---- AREA FOR USERS TO DECLARE THEIR OWN COMMON BLOCKS
C      THESE SHOULD START WITH THE CHARACTERS 'UC' TO ENSURE
C      NO CONFLICT WITH NON-USER COMMON BLOCKS
C
C---- COMMON BLOCK FOR EXAMPLE IN USER AREA 6
C      COMMON /UC1/ VELOLD
C
C+++++++++++++++ END OF USER AREA 2 +++++++++++++++++++++++++++++++++++++
C
      DIMENSION
      + CMETH(NVAR,NPHASE),MNSL(NVAR,NPHASE),MXSL(NVAR,NPHASE)
      +,RDFC(NVAR,NPHASE),RESOR(NVAR,NPHASE),URFVAR(NVAR,NPHASE)
      DIMENSION
      + U(NNODE,NPHASE),V(NNODE,NPHASE),W(NNODE,NPHASE),P(NNODE,NPHASE)
      +,VFRAC(NNODE,NPHASE),DEN(NNODE,NPHASE),VIS(NNODE,NPHASE)
      +,TE(NNODE,NPHASE),ED(NNODE,NPHASE),RS(NNODE,NPHASE,6)
      +,T(NNODE,NPHASE),H(NNODE,NPHASE),RF(NNODE,NPHASE,4)
      +,SCAL(NNODE,NPHASE,NSCAL)
      DIMENSION
      + XP(NNODE),YP(NNODE),ZP(NNODE)
      +,VOL(NCELL),AREA(NFACE,3),VPOR(NCELL),ARPOR(NFACE,3)
      +,WFACT(NFACE),CONV(NFACE,NPHASE)
      +,IPT(*),IBLK(5,NBLOCK)
      +,IPVERT(NCELL,8),IPNODN(NCELL,6),IPFACN(NCELL,6),IPNODF(NFACE,4)
      +,IPNODB(NBDRY,4),IPFACB(NBDRY)
      +,IWORK(*),WORK(*),CWORK(*)
C
C+++++++++++++++ USER AREA 3 ++++++++++++++++++++++++++++++++++++++++++++
C---- AREA FOR USERS TO DIMENSION THEIR ARRAYS
C
C---- AREA FOR USERS TO DEFINE DATA STATEMENTS
C
C+++++++++++++++ END OF USER AREA 3 +++++++++++++++++++++++++++++++++++++
C
C---- STATEMENT FUNCTION FOR ADDRESSING
      IP(I,J,K)=IPT((K-1)*ILEN*JLEN+(J-1)*ILEN+I)
C
C----VERSION NUMBER OF USER ROUTINE AND PRECISION FLAG
C
      IVERS=3
      ICHKPR = 1
C
C+++++++++++++++ USER AREA 4 ++++++++++++++++++++++++++++++++++++++++++++
C---- TO USE THIS USER ROUTINE FIRST SET IUSED=1
C
      IUSED=1
C
C+++++++++++++++ END OF USER AREA 4 +++++++++++++++++++++++++++++++++++++
C
      IF (IUSED.EQ.0) RETURN
C
C---- FRONTEND CHECKING OF USER ROUTINE
```

```
      IF (IUCALL.EQ.0) RETURN
C
C+++++++++++++++ USER AREA 5 +++++++++++++++++++++++++++++++++++++++++++
C
C---- EXAMPLE: (TEST ON MAX OF MASS RESIDUAL AND ENTHALPY RESIDUAL)
C
C
C----END OF EXAMPLE
C
C+++++++++++++++ END OF USER AREA 5 +++++++++++++++++++++++++++++++++++++
C
C
C+++++++++++++++ USER AREA 6 +++++++++++++++++++++++++++++++++++++++++++
C
C---- EXAMPLE: MONITOR CHANGE IN MAXIMUM VELOCITY
C               ADJUST UNDER RELAXATION ACCORDINGLY
C
      VELMAX=0.0
      DO 20 IPHASE=1,NPHASE
C USE IPALL TO FIND 1D ADDRESSES OF ALL CELL CENTRES
      CALL IPALL('*','*','BLOCK','CENTRES',IPT,NPT,CWORK,IWORK)
C LOOP OVER ALL CELL CENTRE LOCATIONS IN FLOW DOMAIN
         DO 30 I=1,NPT
C USE ARRAY IPT TO GET ADDRESS
         INODE=IPT(I)
         VELMAX=MAX(VELMAX,ABS(U(INODE,IPHASE)),ABS(V(INODE,IPHASE)),
     +                ABS(W(INODE,IPHASE)))
 30      CONTINUE
 20      CONTINUE
C


      IF (NITER.GT.1) THEN
        DVEL=(VELMAX-VELOLD)/VELMAX
        URFMIN=0.01
        URFMAX=0.8
        URF=(1.0-DVEL)*URFMAX+DVEL*URFMIN
        CALL GETVAR('USRCVG','U      ',IU)
        CALL GETVAR('USRCVG','V      ',IV)
        CALL GETVAR('USRCVG','W      ',IW)
        DO 40 IPHASE=1,NPHASE
        URFVAR(IU,IPHASE)=URF
        URFVAR(IV,IPHASE)=URF
        URFVAR(IW,IPHASE)=URF
 40      CONTINUE


      ENDIF
C
      VELOLD=VELMAX
C
C----END OF EXAMPLE
C
C+++++++++++++++ END OF USER AREA 6 +++++++++++++++++++++++++++++++++++++
C
      RETURN
      END
```

```
            SUBROUTINE USRBCS(VARBCS,VARAMB,A,B,C,ACND,BCND,CCND
     +                       ,IWGVEL,NDVWAL
     +                       ,FLOUT,NLABEL,NSTART,NEND,NCST,NCEN
     +                       ,U,V,W,P,VFRAC,DEN,VIS,TE,ED,RS,T,H,RF,SCAL
     +                       ,XP,YP,ZP,VOL,AREA,VPOR,ARPOR,WFACT,IPT
     +                       ,IBLK,IPVERT,IPNODN,IPFACN,IPNODF,IPNODB,IPFACB
     +                       ,WORK,IWORK,CWORK)
C
C*********************************************************************
C
C   USER ROUTINE TO SET REALS AT BOUNDARIES.
C
C    >>> IMPORTANT                                                  <<<
C    >>>                                                            <<<
C    >>> USERS MAY ONLY ADD OR ALTER PARTS OF THE SUBROUTINE WITHIN <<<
C    >>> THE DESIGNATED USER AREAS                                  <<<
C
C*********************************************************************
C
C   THIS SUBROUTINE IS CALLED BY THE FOLLOWING SUBROUTINE
C     CUSR   SRLIST
C
C*********************************************************************
C    CREATED
C        30/11/88 ADB
C    MODIFIED
C        08/09/90 ADB  RESTRUCTURED FOR USER-FRIENDLINESS.
C        10/08/91 IRH  FURTHER RESTRUCTURING ADD ACND BCND CCND
C        22/09/91 IRH  CHANGE ICALL TO IUCALL + ADD /SPARM/
C        10/03/92 PHA  UPDATE CALLED BY COMMENT, ADD RF ARGUMENT,
C                      CHANGE LAST DIMENSION OF RS TO 6 AND IVERS TO 2
C        03/06/92 PHA  ADD PRECISION FLAG AND CHANGE IVERS TO 3
C        30/06/92 NSW  INCLUDE FLAG FOR CALLING BY ITERATION
C                      INSERT EXTRA COMMENTS
C        03/08/92 NSW  MODIFY DIMENSION STATEMENTS FOR VAX
C        21/12/92 CSH  INCREASE IVERS TO 4
C        02/08/93 NSW  INCORRECT AND MISLEADING COMMENT REMOVED
C        05/11/93 NSW  INDICATE USE OF FLOUT IN MULTIPHASE FLOWS
C        23/11/93 CSH  EXPLICITLY DIMENSION IPVERT ETC.
C        01/02/94 NSW  SET VARIABLE POINTERS IN WALL EXAMPLE.
C                      CHANGE FLOW3D TO CFDS-FLOW3D.
C                      MODIFY MULTIPHASE MASS FLOW BOUNDARY TREATMENT.
C        03/03/94 FHW  CORRECTION OF SPELLING MISTAKE
C        02/07/94 BAS  SLIDING GRIDS - ADD NEW ARGUMENT IWGVEL
C                      TO ALLOW VARIANTS OF TRANSIENT-GRID WALL BC
C                      CHANGE VERSION NUMBER TO 5
C        09/08/94 NSW  CORRECT SPELLING
C                      MOVE 'IF(IUSED.EQ.0) RETURN' OUT OF USER AREA
C        19/12/94 NSW  CHANGE FOR CFX-F3D
C        02/02/95 NSW  CHANGE COMMON /IMFBMP/
C        02/06/97 NSW  MAKE EXAMPLE MORE LOGICAL
C        02/07/97 NSW  UPDATE FOR CFX-4
C        08/09/98 NSW  CORRECT SIZE OF WALL ARRAY IN COMMENT
C        22/05/00 NSW  INITIALISE IUBCSF
C
C*********************************************************************
C
```

```
C    SUBROUTINE ARGUMENTS
C
C       VARBCS - REAL BOUNDARY CONDITIONS
C       VARAMB - AMBIENT VALUE OF VARIABLES
C       A      - COEFFICIENT IN WALL BOUNDARY CONDITION
C       B      - COEFFICIENT IN WALL BOUNDARY CONDITION
C       C      - COEFFICIENT IN WALL BOUNDARY CONDITION
C       ACND   - COEFFICIENT IN CONDUCTING WALL BOUNDARY CONDITION
C       BCND   - COEFFICIENT IN CONDUCTING WALL BOUNDARY CONDITION
C       CCND   - COEFFICIENT IN CONDUCTING WALL BOUNDARY CONDITION
C       IWGVEL - USAGE OF INPUT VELOCITIES (0 = AS IS,1 = ADD GRID MOTION)
C       NDVWAL - FIRST DIMENSION OF ARRAY IWGVEL
C       FLOUT  - MASS FLOW/FRACTIONAL MASS FLOW
C       NLABEL - NUMBER OF DISTINCT OUTLETS
C       NSTART - ARRAY POINTER
C       NEND   - ARRAY POINTER
C       NCST   - ARRAY POINTER
C       NCEN   - ARRAY POINTER
C       U      - U COMPONENT OF VELOCITY
C       V      - V COMPONENT OF VELOCITY
C       W      - W COMPONENT OF VELOCITY
C       P      - PRESSURE
C       VFRAC  - VOLUME FRACTION
C       DEN    - DENSITY OF FLUID
C       VIS    - VISCOSITY OF FLUID
C       TE     -. TURBULENT KINETIC ENERGY
C       ED     - EPSILON
C       RS     - REYNOLD STRESSES
C       T      - TEMPERATURE
C       H      - ENTHALPY
C       RF     - REYNOLD FLUXES
C       SCAL   - SCALARS (THE FIRST 'NCONC' OF THESE ARE MASS FRACTIONS)
C       XP     - X COORDINATES OF CELL CENTRES
C       YP     - Y COORDINATES OF CELL CENTRES
C       ZP     - Z COORDINATES OF CELL CENTRES
C       VOL    - VOLUME OF CELLS
C       AREA   - AREA OF CELLS
C       VPOR   - POROUS VOLUME
C       ARPOR  - POROUS AREA
C       WFACT  - WEIGHT FACTORS
C
C       IPT    - 1D POINTER ARRAY
C       IBLK   - BLOCK SIZE INFORMATION
C       IPVERT - POINTER FROM CELL CENTERS TO 8 NEIGHBOURING VERTICES
C       IPNODN - POINTER FROM CELL CENTERS TO 6 NEIGHBOURING CELLS
C       IPFACN - POINTER FROM CELL CENTERS TO 6 NEIGHBOURING FACES
C       IPNODF - POINTER FROM CELL FACES TO 2 NEIGHBOURING CELL CENTERS
C       IPNODB - POINTER FROM BOUNDARY CENTERS TO CELL CENTERS
C       IPFACB - POINTER TO NODES FROM BOUNDARY FACES
C
C       WORK   - REAL WORKSPACE ARRAY
C       IWORK  - INTEGER WORKSPACE ARRAY
C       CWORK  - CHARACTER WORKSPACE ARRAY
C
C    SUBROUTINE ARGUMENTS PRECEDED WITH A '*' ARE ARGUMENTS THAT MUST
C    BE SET  BY THE USER IN THIS ROUTINE.
C
```

273

```
C    NOTE THAT OTHER DATA MAY BE OBTAINED FROM CFX-4 USING THE
C    ROUTINE GETADD, FOR FURTHER DETAILS SEE THE VERSION 4
C    USER MANUAL.
C
C*********************************************************************
      LOGICAL LDEN,LVIS,LTURB,LTEMP,LBUOY,LSCAL,LCOMP
     +         ,LRECT,LCYN,LAXIS,LPOROS,LTRANS
C
      CHARACTER*(*) CWORK
C
C+++++++++++++++ USER AREA 1 +++++++++++++++++++++++++++++++++++++++++
C---- AREA FOR USERS EXPLICITLY DECLARED VARIABLES
C
C+++++++++++++++ END OF USER AREA 1 ++++++++++++++++++++++++++++++++++
C
      COMMON
     + /ALL/    NBLOCK,NCELL,NBDRY,NNODE,NFACE,NVERT,NDIM
     + /ALLWRK/ NRWS,NIWS,NCWS,IWRFRE,IWIFRE,IWCFRE
     + /ADDIMS/ NPHASE,NSCAL,NVAR,NPROP
     +          ,NDVAR,NDPROP,NDXNN,NDGEOM,NDCOEF,NILIST,NRLIST,NTOPOL
     + /BCSOUT/ IFLOUT
     + /CHKUSR/ IVERS,IUCALL,IUSED
     + /DEVICE/ NREAD,NWRITE,NRDISK,NWDISK
     + /IDUM/   ILEN,JLEN
     + /IMFBMP/ IMFBMP,JMFBMP
     + /LOGIC/  LDEN,LVIS,LTURB,LTEMP,LBUOY,LSCAL,LCOMP
     +          ,LRECT,LCYN,LAXIS,LPOROS,LTRANS
     + /MLTGRD/ MLEVEL,NLEVEL,ILEVEL
     + /SGLDBL/ IFLGPR,ICHKPR
     + /SPARM/  SMALL,SORMAX,NITER,INDPRI,MAXIT,NODREF,NODMON
     + /TRANSI/ NSTEP,KSTEP,MF,INCORE
     + /TRANSR/ TIME,DT,DTINVF,TPARM
     + /UBCSFL/ IUBCSF
C
C+++++++++++++++ USER AREA 2 +++++++++++++++++++++++++++++++++++++++++
C---- AREA FOR USERS TO DECLARE THEIR OWN COMMON BLOCKS
C     THESE SHOULD START WITH THE CHARACTERS 'UC' TO ENSURE
C     NO CONFLICT WITH NON-USER COMMON BLOCKS
C
C+++++++++++++++ END OF USER AREA 2 ++++++++++++++++++++++++++++++++++
C


      DIMENSION
     + VARBCS(NVAR,NPHASE,NCELL+1:NNODE),VARAMB(NVAR,NPHASE)
     +,A(4+NSCAL,NPHASE,NSTART:*)
     +,B(4+NSCAL,NPHASE,NSTART:*),C(4+NSCAL,NPHASE,NSTART:*)
     +,FLOUT(*),ACND(NCST:*),BCND(NCST:*),CCND(NCST:*)
     +,IWGVEL(NDVWAL,NPHASE)
C


      DIMENSION
     + U(NNODE,NPHASE),V(NNODE,NPHASE),W(NNODE,NPHASE),P(NNODE,NPHASE)
     +,VFRAC(NNODE,NPHASE),DEN(NNODE,NPHASE),VIS(NNODE,NPHASE)
     +,TE(NNODE,NPHASE),ED(NNODE,NPHASE),RS(NNODE,NPHASE,6)
     +,T(NNODE,NPHASE),H(NNODE,NPHASE),RF(NNODE,NPHASE,4)
```

274

```
      +,SCAL(NNODE,NPHASE,NSCAL)
C
      DIMENSION
     + XP(NNODE),YP(NNODE),ZP(NNODE)
     +,VOL(NCELL),AREA(NFACE,3),VPOR(NCELL),ARPOR(NFACE,3),WFACT(NFACE)
     +,IPT(*),IBLK(5,NBLOCK)
     +,IPVERT(NCELL,8),IPNODN(NCELL,6),IPFACN(NCELL,6),IPNODF(NFACE,4)
     +,IPNODB(NBDRY,4),IPFACB(NBDRY)
     +,IWORK(*),WORK(*),CWORK(*)
C
C+++++++++++++++ USER AREA 3 ++++++++++++++++++++++++++++++++++++++++++++
C---- AREA FOR USERS TO DIMENSION THEIR ARRAYS
C
C---- AREA FOR USERS TO DEFINE DATA STATEMENTS
C
C+++++++++++++++ END OF USER AREA 3 +++++++++++++++++++++++++++++++++++++
C
C---- STATEMENT FUNCTION FOR ADDRESSING
      IP(I,J,K)=IPT((K-1)*ILEN*JLEN+(J-1)*ILEN+I)
C
C----VERSION NUMBER OF USER ROUTINE AND PRECISION FLAG
C
      IVERS=5
      ICHKPR = 1
C
C+++++++++++++++ USER AREA 4 ++++++++++++++++++++++++++++++++++++++++++++
C---- TO USE THIS USER ROUTINE FIRST SET IUSED=1
C     AND SET IUBCSF FLAG:
C     BOUNDARY CONDITIONS NOT CHANGING                     IUBCSF=0
C     BOUNDARY CONDITIONS CHANGING WITH ITERATION          IUBCSF=1
C     BOUNDARY CONDITIONS CHANGING WITH TIME               IUBCSF=2
C     BOUNDARY CONDITIONS CHANGING WITH TIME AND ITERATION IUBCSF=3
C
      IUSED=1
      IUBCSF=0
C
C+++++++++++++++ END OF USER AREA 4 +++++++++++++++++++++++++++++++++++++
C
      IF (IUSED.EQ.0) RETURN
C
C---- FRONTEND CHECKING OF USER ROUTINE
      IF (IUCALL.EQ.0) RETURN
C
C+++++++++++++++ USER AREA 5 ++++++++++++++++++++++++++++++++++++++++++++
C
C---- AREA FOR SETTING VALUES AT INLETS, PRESSURE BOUNDARIES
C     AND OUTLETS. (NOTE THAT THE MASS FLOW AT OUTLETS IS
C     SPECIFIED IN USER AREA 7)
C
C     IF USING A REYNOLDS STRESS OR FLUX MODEL, NOTE THAT AT INLETS
C     IT IS IMPORTANT THAT THE USER SETS ALL COMPONENTS OF THE
C     REYNOLDS STRESS AND FLUX AND THE TURBULENT KINETIC ENERGY
C     AS WELL AS THE ENERGY DISSIPATION RATE.
C
C     SET THE VALUES IN VARBCS(NVAR,NPHASE,ILEN,JLEN,KLEN)
C
C---- EXAMPLE: SETTING A LINEAR T PROFILE ON INLET PATCH 'ENTRANCE'
```

```
C                     LEAVE OTHER VARIABLES AS SET IN COMMAND LANGUAGE
C
C--    INTERROGATE GETVAR FOR VARIABLE NUMBERS.
C
C         CALL GETVAR('USRBCS','T        ',IT)
C
C   SET IPHS = 1 FOR SINGLE PHASE FLOW.
C
C         IPHS = 1
C
C   USE IPREC TO FIND ADDRESSES
C
C         CALL IPREC('ENTRANCE','PATCH','CENTRES',IPT,ILEN,JLEN,KLEN,
C      +               CWORK,IWORK)
C
C      XMAX=2.0
C      XMIN=1.0
C      TMAX=300.0
C      TMIN=250.0
C   LOOP OVER PATCH
C      DO 103 K = 1, KLEN
C          DO 102 J = 1, JLEN
C              DO 101 I = 1, ILEN
C   USE STATEMENT FUNCTION IP TO GET ADDRESSES
C              INODE = IP(I,J,K)
C   SET VARBCS
C              F=(XP(INODE)-XMIN)/(XMAX-XMIN)
C              VARBCS(IT,IPHS,INODE) = F*TMAX + (1.0-F)*TMIN
C 101          CONTINUE
C 102      CONTINUE
C 103   CONTINUE
C
C----END OF EXAMPLE
C
C++++++++++++++++ END OF USER AREA 5 +++++++++++++++++++++++++++++++++++++
C
C++++++++++++++++ USER AREA 6 ++++++++++++++++++++++++++++++++++++++++++++
C
C---- AREA FOR SETTING VALUES AT WALLS
C
C      USE A(4+NSCAL,NPHASE,NNODE)
C      WHERE NSCAL = NO. OF SCALARS, AND NPHASE = NO. OF PHASES.
C
C      THE CONVENTION FOR VARIABLE NUMBERS IS DIFFERENT IN THIS ROUTINE
C      FROM THAT IN THE REST OF THE PROGRAM. IT IS:
C
C      IU = 1, IV = 2 , IW = 3, IT = 4, IS = 5
C
C---- EXAMPLE: SETTING FREE SLIP BOUNDARY CONDITIONS AT ALL WALLS
C              AND SETTING T=300.0 AND SCALAR1 AND SCALAR2 =0.0
C              ON WALL1. SET T=400.0 ON CONDUCTING SOLID BOUNDARY WALL2
C
C-- SET POINTERS
C
C      IU = 1
C      IV = 2
C      IW = 3
```

```
      IT = 4
C     IS = 5
C
C-- SET IPHS = 1 FOR SINGLE PHASE FLOW.
C
C     IPHS = 1
C
C  USE IPALL TO FIND 1D ADDRESSES OF A GROUP OF PATCH CENTRES
C
C     CALL IPALL('*','WALL','PATCH','CENTRES',IPT,NPT,CWORK,IWORK)
C
C  LOOP OVER GROUP OF PATCHES
C     DO 200 I=1,NPT
C  USE ARRAY IPT TO GET ADDRESS
C        INODE=IPT(I)
C        A(IU,IPHS,INODE) = 0.0
C        B(IU,IPHS,INODE) = 1.0
C        C(IU,IPHS,INODE) = 0.0
C
C        A(IV,IPHS,INODE) = 0.0
C        B(IV,IPHS,INODE) = 1.0
C        C(IV,IPHS,INODE) = 0.0
C
C        A(IW,IPHS,INODE) = 0.0
C        B(IW,IPHS,INODE) = 1.0
C        C(IW,IPHS,INODE) = 0.0
C 200    CONTINUE
C
C  USE IPREC TO FIND ADDRESSES OF SINGLE PATCH
C
      CALL IPALL('BOTTOM WALL','WALL','PATCH','CENTRES',IPT,NPT,CWORK,
     +     IWORK)
C  LOOP OVER PATCH
          DO 200 I=1,NPT
C  USE STATEMENT FUNCTION IP TO GET ADDRESSES
              INODE = IPT(I)
C


              A(IT,1,INODE) = 1.0
              B(IT,1,INODE) = 0.0
              C(IT,1,INODE) = 900.0
              A(IT,2,INODE) = 1.0
              B(IT,2,INODE) = 0.0
              C(IT,2,INODE) = 900.0




C
C              A(IS,IPHS,INODE) = 1.0
C              B(IS,IPHS,INODE) = 0.0
C              C(IS,IPHS,INODE) = 0.0
C
C              A(IS+1,IPHS,INODE) = 1.0
C              B(IS+1,IPHS,INODE) = 0.0
```

277

```
C                    C(IS+1,IPHS,INODE) = 0.0
C
  200            CONTINUE
C
C  USE IPALL TO FIND 1D ADDRESSES OF A GROUP OF PATCH CENTRES
C
C      CALL IPALL('WALL2','*','PATCH','CENTRES',IPT,NPT,CWORK,IWORK)
C
C  LOOP OVER GROUP OF PATCHES
C      DO 300 I=1,NPT
.C  USE ARRAY IPT TO GET ADDRESS
C          INODE=IPT(I)
C          ACND(INODE) = 1.0
C          BCND(INODE) = 0.0
C          CCND(INODE) = 400.0
C 300    CONTINUE
C
```

```
C----END OF EXAMPLE
C
C+++++++++++++++++ END OF USER AREA 6 ++++++++++++++++++++++++++++++++++++++
C
C
C+++++++++++++++++ USER AREA 7 ++++++++++++++++++++++++++++++++++++++++++++++
C
C----- DEFINE FLOW AT OUTLETS (MASS FLOW BOUNDARIES)
C        (TO TEMPERATURES AND SCALARS AT MASS FLOW BOUNDARIES USE
C         USER AREA 5)
C
C      SET PARAMETER IFLOUT:
C      IFLOUT = 1  ==> MASS FLOW SPECIFIED AT LABELLED OUTLETS.
C      IFLOUT = 2  ==> FRACTIONAL MASS FLOW SPECIFIED AT LABELLED OUTLETS
C      IFLOUT = 2
C
C      SET OUTLET FLOW RATES:
C      FLOUT(LABEL) = MASS FLOW OUT OF OUTLETS LABELLED LABEL (IFLOUT=1).
C      FLOUT(LABEL) = FRACTIONAL MASS FLOW OUT OF OUTLETS LABELLED LABEL
C                     (IFLOUT=2).
C      FOR MULTIPHASE FLOWS IT IS NECESSARY TO SET
C      EITHER
C                     FLOUT(LABEL) = TOTAL MASS FLOW
C                     IFLOUT = 1
C                     IMFBMP = 0
C      OR
C                     FLOUT(LABEL + (IPHASE-1)*NLABEL) FOR EACH PHASE
C                     IFLOUT = 1 OR 2
C                     IMFBMP = 1
C
C---- EXAMPLE: EQUIDISTRIBUTION OF FRACTIONAL MASS FLOW AMONGST OUTLETS
C
C      IFLOUT=2
C      FRAC = 1.0 / MAX( 1.0, FLOAT(NLABEL) )
```

```
C       DO 300 ILABEL = 1, NLABEL
C           FLOUT(ILABEL) = FRAC
C300   CONTINUE
C
C----END OF EXAMPLE
C
C+++++++++++++++++ END OF USER AREA 7 +++++++++++++++++++++++++++++++++++
C
        RETURN
        END
```

279

```
          SUBROUTINE USRPBM(CCALL,NN,E,CTYPE,CPATCH,CBLOCK,I,J,K
     +                      ,T,U,UPRIME,AMFG,XP,YP,ZP)
C
C*********************************************************************
C
C     THIS SUBROUTINE ALLOWS USERS TO MONITOR PARTICLES WHEN THEY LEAVE
C     THE DOMAIN THROUGH BOUNDARIES OR WHEN THEY HIT WALLS
C     THE USER CAN ALSO SET A VARYING COEFFICIENT OF RESTITUTION
C
C     >>> IMPORTANT                                                 <<<
C     >>>                                                           <<<
C     >>> USERS MAY ONLY ADD OR ALTER PARTS OF THE SUBROUTINE WITHIN <<<
C     >>> THE DESIGNATED USER AREAS                                 <<<
C
C*********************************************************************
C
C     THIS SUBROUTINE IS CALLED BY THE FOLLOWING SUBROUTINE
C          CUSR   TRACK
C
C*********************************************************************
C     CREATED
C        11/01/94  NSW
C     MODIFIED
C        22/08/94  NSW   MOVE 'IF(IUSED.EQ.0) RETURN' OUT OF USER AREA.
C                        INCLUDE CALL INFORMATION AND INCLUDE NEW EXAMPLE.
C                        VERSION NUMBER CHANGED TO 2.
C        10/09/98  NSW   INCLUDE PHYSICAL POSITION AND UPDATE VERSION
C                        NUMBER TO 3.
C        02/02/99  NSW   INCLUDE PARTICLE NUMBER.
C        05/07/99  NSW   INCLUDE CONTINUATION MARKER IN EXAMPLE
C
C*********************************************************************
C
C     SUBROUTINE ARGUMENTS
C
C        E       - COEFFICIENT OF RESTITUTION FOR PRESENT PARTICLE AT
C                  PRESENT POSITION
C                  E IS SET TO THE COMMAND LANGUAGE VALUE OF COEFFICIENT
C                  OF RESTITUTION ON ENTRY
C        NN      - PARTICLE NUMBER
C        CTYPE   - PATCH TYPE, EITHER INLET, OUTLET, PRESSURE OR WALL
C        CPATCH  - PATCH NAME
C        CBLOCK  - BLOCK NAME
C        I
C        J       - CONTROL VOLUME IN BLOCK
C        K
C        T       - PARTICLE INTEGRATION TIME
C        U       - PARTICLE INFORMATION
C                  U(1) - U(3) ARE VELOCITIES
C                  U(4) - U(6) ARE COMPUTATIONAL POSITION
C                  FOR COMBUSTION  U(7) IS TEMPERATURE
C                                  U(9) - U(11) ARE MASSES OF SPECIES
C                  FOR SPRAY MODEL U(7) IS MASS OF PARTICLE/DROPLET
C                                  U(8) IS TEMPERATURE
C                  OTHERWISE       U(7) - U(6+NMASS) ARE MASSES OF SPECIES
C                                  U(IPTT) IS TEMPERATURE
C        UPRIME  - RATE OF CHANGE OF ABOVE QUANTITIES WITH TIME
```

280

```
C      AMFG   - CONTINUOUS PHASE MASS FRACTIONS
C      XP
C      YP     - PHYSICAL POSITION OF PARTICLE
C      ZP
C
C   NMASS IS THE NUMBER OF PARTICLE MASS FRACTIONS
C   IN COMMON BLOCK /RPART/ RHO IS THE BASE PARTICLE DENSITY, AMDC
C   IS THE MASS OF BASE MATERIAL AND DIAM IS THE PARTICLE DIAMETER.
C
C   ITER IS THE PARTICLE ITERATION NUMBER
C   NTER IS THE NUMBER OF PARTICLE ITERATIONS
C
C   CCALL IS A CHARACTER VARIABLE SET EQUAL TO
C     'FIRST ' - AT THE START OF A PARTICLE TRANSPORT CALCULATION FOR
C                USERS TO INITIALISE THEIR VARIABLES.
C     'LAST  ' - AT THE END OF A PARTICLE TRANSPORT CALCULATION FOR
C                USERS TO WRITE OUT THEIR CALCULATED INFORMATION.
C     'NORMAL' - ALL CALLS DURING THE CALCULATION PROCEDURE.
C   ON FIRST AND LAST CALLS THE BLOCK AND PATCH NAMES ARE UNSET.
C
C*********************************************************************
C
      CHARACTER*6  CCALL
      CHARACTER*8  CTYPE
      CHARACTER*32 CPATCH,CBLOCK
C
C+++++++++++++++ USER AREA 1 +++++++++++++++++++++++++++++++++++++++++
C---- AREA FOR USERS EXPLICITLY DECLARED VARIABLES
C
C+++++++++++++++ END OF USER AREA 1 +++++++++++++++++++++++++++++++++++
C
      COMMON
     + /CHKUSR/ IVERS,IUCALL,IUSED
     + /DEVICE/ NREAD,NWRITE,NRDISK,NWDISK
     + /INTEGR/ NEQ,NTER,IPTT,IPTS,NSUP,NMASS,NVARV
     + /MLTGRD/ MLEVEL,NLEVEL,ILEVEL
     + /RPART/  DIAM,AMDC,RHO,CPBPAR,TVAP
     + /SGLDBL/ IFLGPR,ICHKPR
     + /SPRIT/  ITER
C
C+++++++++++++++ USER AREA 2 +++++++++++++++++++++++++++++++++++++++++
C---- AREA FOR USERS TO DECLARE THEIR OWN COMMON BLOCKS
C     THESE SHOULD START WITH THE CHARACTERS 'UC' TO ENSURE
C     NO CONFLICT WITH NON-USER COMMON BLOCKS
C
C+++++++++++++++ END OF USER AREA 2 +++++++++++++++++++++++++++++++++++
C
      DIMENSION
     + U(NEQ),UPRIME(NEQ),AMFG(*)
C
C+++++++++++++++ USER AREA 3 +++++++++++++++++++++++++++++++++++++++++
C---- AREA FOR USERS TO DIMENSION THEIR ARRAYS
C
C---- AREA FOR USERS TO DEFINE DATA STATEMENTS
C
C+++++++++++++++ END OF USER AREA 3 +++++++++++++++++++++++++++++++++++
C
```

281

```
C----VERSION NUMBER OF USER ROUTINE AND PRECISION FLAG
C
      IVERS=3
      ICHKPR = 1
C
C++++++++++++++++ USER AREA 4 +++++++++++++++++++++++++++++++++++++++++
C---- TO USE THIS USER ROUTINE FIRST SET IUSED=1
C
       IUSED=1
C
C++++++++++++++++ END OF USER AREA 4 ++++++++++++++++++++++++++++++++++
C
      IF (IUSED.EQ.0) RETURN
C
C---- FRONTEND CHECKING OF USER ROUTINE
      IF (IUCALL.EQ.0) RETURN
C
C++++++++++++++++ USER AREA 5 +++++++++++++++++++++++++++++++++++++++++
C
      IF (CCALL.EQ.'FIRST ') NPAREX = 0
      IF (CPATCH.EQ.'OUTLET' .AND. ITER.EQ.NTER) NPAREX = NPAREX + 1
      IF (CCALL.EQ.'LAST  ') THEN
          WRITE(NWRITE,*) 'NUMBER OF PARTICLES LEAVING THROUGH EXIT = ',
     +                   NPAREX
      END IF
C
C----END OF EXAMPLE
C
C++++++++++++++++ END OF USER AREA 5 ++++++++++++++++++++++++++++++++++
C
      RETURN
      END
```

```
            SUBROUTINE USRGRD(U,V,W,P,VFRAC,DEN,VIS,TE,ED,RS,T,H,RF,SCAL,
     +                         XP,YP,ZP,VOL,AREA,VPOR,ARPOR,WFACT,
     +                         XCOLD,YCOLD,ZCOLD,XC,YC,ZC,IPT,
     +                         IBLK,IPVERT,IPNODN,IPFACN,IPNODF,IPNODB,IPFACB,
     +                         WORK,IWORK,CWORK)
C
C*********************************************************************
C
C     USER SUBROUTINE TO ALLOW USERS TO GENERATE A GRID FOR CFX-4
C
C     >>> IMPORTANT                                              <<<
C     >>>                                                        <<<
C     >>> USERS MAY ONLY ADD OR ALTER PARTS OF THE SUBROUTINE WITHIN  <<<
C     >>> THE DESIGNATED USER AREAS                              <<<
C
C*********************************************************************
C
C     THIS SUBROUTINE IS CALLED BY THE FOLLOWING SUBROUTINES
C         CREATE  CUSR
C
C*********************************************************************
C     CREATED
C         27/04/90  ADB
C     MODIFIED
C         05/08/91  IRH  NEW STRUCTURE
C         09/09/91  IRH  CORRECT EXAMPLE
C         01/10/91  DSC  REDUCE COMMENT LINE GOING OVER 72 COLUMNS.
C         29/11/91  PHA  UPDATE CALLED BY COMMENT, ADD RF ARGUMENT,
C                        CHANGE LAST DIMENSION OF RS TO 6 AND IVERS TO 2
C         03/06/92  PHA  ADD PRECISION FLAG AND CHANGE IVERS TO 3
C         03/07/92  DSC  CORRECT COMMON MLTGRD.
C         23/11/93  CSH  EXPLICITLY DIMENSION IPVERT ETC.
C         03/02/94  PHA  CHANGE FLOW3D TO CFDS-FLOW3D
C         03/03/94  FHW  CORRECTION OF SPELLING MISTAKE
C         22/08/94  NSW  MOVE 'IF(IUSED.EQ.0) RETURN' OUT OF USER AREA
C         19/12/94  NSW  CHANGE FOR CFX-F3D
C         02/07/97  NSW  UPDATE FOR CFX-4
C
C*********************************************************************
C
C     SUBROUTINE ARGUMENTS
C
C     U       - U COMPONENT OF VELOCITY
C     V       - V COMPONENT OF VELOCITY
C     W       - W COMPONENT OF VELOCITY
C     P       - PRESSURE
C     VFRAC   - VOLUME FRACTION
C     DEN     - DENSITY OF FLUID
C     VIS     - VISCOSITY OF FLUID
C     TE      - TURBULENT KINETIC ENERGY
C     ED      - EPSILON
C     RS      - REYNOLD STRESSES
C     T       - TEMPERATURE
C     H       - ENTHALPY
C     RF      - REYNOLD FLUXES
C     SCAL    - SCALARS (THE FIRST 'NCONC' OF THESE ARE MASS FRACTIONS)
C     XP      - X COORDINATES OF CELL CENTRES
```

283

```
C       YP       - Y COORDINATES OF CELL CENTRES
C       ZP       - Z COORDINATES OF CELL CENTRES
C       VOL      - VOLUME OF CELLS
C       AREA     - AREA OF CELLS
C       VPOR     - POROUS VOLUME
C       ARPOR    - POROUS AREA
C       WFACT    - WEIGHT FACTORS
C  *    XC       - X COORDINATES OF CELL VERTICES
C  *    YC       - Y COORDINATES OF CELL VERTICES
C  *    ZC       - Z COORDINATES OF CELL VERTICES
C       XCOLD    - X COORDINATES OF CELL VERTICES AT START OF TIME STEP
C       YCOLD    - Y COORDINATES OF CELL VERTICES AT START OF TIME STEP
C       ZCOLD    - Z COORDINATES OF CELL VERTICES AT START OF TIME STEP
C
C       IPT      - 1D POINTER ARRAY
C       IBLK     - BLOCK SIZE INFORMATION
C       IPVERT - POINTER FROM CELL CENTERS TO 8 NEIGHBOURING VERTICES
C       IPNODN - POINTER FROM CELL CENTERS TO 6 NEIGHBOURING CELLS
C       IPFACN - POINTER FROM CELL CENTERS TO 6 NEIGHBOURING FACES
C       IPNODF - POINTER FROM CELL FACES TO 2 NEIGHBOURING CELL CENTERS
C       IPNODB - POINTER FROM BOUNDARY CENTERS TO CELL CENTERS
C       IPFACB - POINTER FROM BOUNDARY CENTERS TO BOUNDARY FACESS
C
C       WORK   - REAL WORKSPACE ARRAY
C       IWORK  - INTEGER WORKSPACE ARRAY
C       CWORK  - CHARACTER WORKSPACE ARRAY
C
C   SUBROUTINE ARGUMENTS PRECEDED WITH A '*' ARE ARGUMENTS THAT MUST
C   BE SET  BY THE USER IN THIS ROUTINE.
C
C   NOTE THAT OTHER DATA MAY BE OBTAINED FROM CFX-4 USING THE
C   ROUTINE GETADD, FOR FURTHER DETAILS SEE THE VERSION 4
C   USER MANUAL.
C
C*********************************************************************
C
      LOGICAL LDEN,LVIS,LTURB,LTEMP,LBUOY,LSCAL,LCOMP
     +       ,LRECT,LCYN,LAXIS,LPOROS,LTRANS
C
      CHARACTER*(*) CWORK
C
C+++++++++++++++ USER AREA 1 +++++++++++++++++++++++++++++++++++++++++
C---- AREA FOR USERS EXPLICITLY DECLARED VARIABLES
C
C+++++++++++++++ END OF USER AREA 1 +++++++++++++++++++++++++++++++++++
C
      COMMON
     + /ALL/     NBLOCK,NCELL,NBDRY,NNODE,NFACE,NVERT,NDIM
     + /ALLWRK/ NRWS,NIWS,NCWS,IWRFRE,IWIFRE,IWCFRE
     + /ADDIMS/ NPHASE,NSCAL,NVAR,NPROP
     +          ,NDVAR,NDPROP,NDXNN,NDGEOM,NDCOEF,NILIST,NRLIST,NTOPOL
     + /CHKUSR/ IVERS,IUCALL,IUSED
     + /CONC/    NCONC
     + /DEVICE/ NREAD,NWRITE,NRDISK,NWDISK
     + /IDUM/    ILEN,JLEN
     + /LOGIC/   LDEN,LVIS,LTURB,LTEMP,LBUOY,LSCAL,LCOMP
     +          ,LRECT,LCYN,LAXIS,LPOROS,LTRANS
```

```
      + /MLTGRD/ MLEVEL,NLEVEL,ILEVEL
      + /SGLDBL/ IFLGPR,ICHKPR
      + /SPARM/  SMALL,SORMAX,NITER,INDPRI,MAXIT,NODREF,NODMON
      + /TIMUSR/ DTUSR
      + /TRANSI/ NSTEP,KSTEP,MF,INCORE
      + /TRANSR/ TIME,DT,DTINVF,TPARM
C
C++++++++++++++++ USER AREA 2 ++++++++++++++++++++++++++++++++++++++++++++
C---- AREA FOR USERS TO DECLARE THEIR OWN COMMON BLOCKS
C     THESE SHOULD START WITH THE CHARACTERS 'UC' TO ENSURE
C     NO CONFLICT WITH NON-USER COMMON BLOCKS
C
C++++++++++++++++ END OF USER AREA 2 ++++++++++++++++++++++++++++++++++++++
C
      DIMENSION
      + U(NNODE,NPHASE),V(NNODE,NPHASE),W(NNODE,NPHASE),P(NNODE,NPHASE)
      +,VFRAC(NNODE,NPHASE),DEN(NNODE,NPHASE),VIS(NNODE,NPHASE)
      +,TE(NNODE,NPHASE),ED(NNODE,NPHASE),RS(NNODE,NPHASE,6)
      +,T(NNODE,NPHASE),H(NNODE,NPHASE),RF(NNODE,NPHASE,4)
      +,SCAL(NNODE,NPHASE,NSCAL)
      DIMENSION
      + XP(NNODE),YP(NNODE),ZP(NNODE),XC(NVERT),YC(NVERT),ZC(NVERT)
      +,XCOLD(NVERT),YCOLD(NVERT),ZCOLD(NVERT)
      +,VOL(NCELL),AREA(NFACE,3),VPOR(NCELL),ARPOR(NFACE,3)
      +,WFACT(NFACE)
      +,IPT(*),IBLK(5,NBLOCK)
      +,IPVERT(NCELL,8),IPNODN(NCELL,6),IPFACN(NCELL,6),IPNODF(NFACE,4)
      +,IPNODB(NBDRY,4),IPFACB(NBDRY)
      +,IWORK(*),WORK(*),CWORK(*)
C
C++++++++++++++++ USER AREA 3 ++++++++++++++++++++++++++++++++++++++++++++
C---- AREA FOR USERS TO DIMENSION THEIR ARRAYS
C
C---- AREA FOR USERS TO DEFINE DATA STATEMENTS
C
C++++++++++++++++ END OF USER AREA 3 ++++++++++++++++++++++++++++++++++++++
C
C---- STATEMENT FUNCTION FOR ADDRESSING
      IP(I,J,K)=IPT((K-1)*ILEN*JLEN+(J-1)*ILEN+I)
C
C---- VERSION NUMBER OF USER ROUTINE AND PRECISION FLAG
C
      IVERS=3
      ICHKPR = 1
C
C++++++++++++++++ USER AREA 4 ++++++++++++++++++++++++++++++++++++++++++++
C---- TO USE THIS USER ROUTINE FIRST SET IUSED=1
C
      IUSED=1
C
C++++++++++++++++ END OF USER AREA 4 ++++++++++++++++++++++++++++++++++++++
C
      IF (IUSED.EQ.0) RETURN
C
C---- FRONTEND CHECKING OF USER ROUTINE
      IF (IUCALL.EQ.0) RETURN
C
```

```
C++++++++++++++++ USER AREA 5 ++++++++++++++++++++++++++++++++++++++++++++
C
C---- EXAMPLE: DEFINE INITIAL GRID
C
C-- USE IPREC TO FIND ADDRESSES
      CALL IPREC('BLOCK-NUMBER-1','BLOCK','VERTICES',IPT,ILEN,JLEN,
     +           KLEN,CWORK,IWORK)

C-- LOOP OVER BLOCK
      DO 100 K=1,KLEN
        DO 120 J=1,JLEN
          DO 130 I=1,ILEN
C-- USE STATEMENT FUNCTION IP TO GET ADDRESSES
          INODE = IP(I,J,K)
C-- DEFINE LOCATION OF GRID VERTICES
          XC(INODE)=FLOAT(I-1)*0.003
          YC(INODE)=FLOAT(J-1)*0.01
          ZC(INODE)=FLOAT(K-1)*0.1
  130     CONTINUE
  120   CONTINUE
  100 CONTINUE
      CALL IPREC('BLOCK-NUMBER-2','BLOCK','VERTICES',IPT,ILEN,JLEN,
     +           KLEN,CWORK,IWORK)

C-- LOOP OVER BLOCK
      DO 200 K=1,KLEN
        DO 220 J=1,JLEN
          DO 230 I=1,ILEN
C-- USE STATEMENT FUNCTION IP TO GET ADDRESSES
          INODE = IP(I,J,K)
C-- DEFINE LOCATION OF GRID VERTICES
          XC(INODE)=FLOAT(I-1)*(0.003+FLOAT(J-1)*0.0002)-FLOAT(J-1)*
     +     0.003
          YC(INODE)=FLOAT(J-1)*0.005+0.3
          ZC(INODE)=FLOAT(K-1)*0.1
  230     CONTINUE
  220   CONTINUE
  200 CONTINUE
      CALL IPREC('BLOCK-NUMBER-3','BLOCK','VERTICES',IPT,ILEN,JLEN,
     +           KLEN,CWORK,IWORK)

C-- LOOP OVER BLOCK
      DO 300 K=1,KLEN
        DO 320 J=1,JLEN
          DO 330 I=1,ILEN
C-- USE STATEMENT FUNCTION IP TO GET ADDRESSES
          INODE = IP(I,J,K)
C-- DEFINE LOCATION OF GRID VERTICES
          XC(INODE)=FLOAT(I-1)*0.004-0.015
          YC(INODE)=FLOAT(J-1)*0.018+0.325
          ZC(INODE)=FLOAT(K-1)*0.1
  330     CONTINUE
  320   CONTINUE
  300 CONTINUE

      CALL IPREC('BLOCK-NUMBER-4','BLOCK','VERTICES',IPT,ILEN,JLEN,
     +           KLEN,CWORK,IWORK)
```

286

```
C-- LOOP OVER BLOCK
      DO 400 K=1,KLEN
        DO 420 J=1,JLEN
          DO 430 I=1,ILEN
C-- USE STATEMENT FUNCTION IP TO GET ADDRESSES
          INODE = IP(I,J,K)
C-- DEFINE LOCATION OF GRID VERTICES
          XC(INODE)=FLOAT(I-1)*(0.004-FLOAT(J-1)*0.0001)-0.015
          YC(INODE)=FLOAT(J-1)*0.009+0.505
          ZC(INODE)=FLOAT(K-1)*0.1
  430     CONTINUE
  420   CONTINUE
  400 CONTINUE
      CALL IPREC('BLOCK-NUMBER-5','BLOCK','VERTICES',IPT,ILEN,JLEN,
     +          KLEN,CWORK,IWORK)


C-- LOOP OVER BLOCK
      DO 500 K=1,KLEN
        DO 520 J=1,JLEN
          DO 530 I=1,ILEN
C-- USE STATEMENT FUNCTION IP TO GET ADDRESSES
          INODE = IP(I,J,K)
C-- DEFINE LOCATION OF GRID VERTICES
          XC(INODE)=FLOAT(I-1)*(0.004-FLOAT(J-1)*0.0001)+0.045
     +      +FLOAT(J-1)*0.002
          YC(INODE)=FLOAT(J-1)*0.009+0.505
          ZC(INODE)=FLOAT(K-1)*0.1
  530     CONTINUE
  520   CONTINUE
  500 CONTINUE
      CALL IPREC('BLOCK-NUMBER-6','BLOCK','VERTICES',IPT,ILEN,JLEN,
     +          KLEN,CWORK,IWORK)


C-- LOOP OVER BLOCK
      DO 600 K=1,KLEN
        DO 620 J=1,JLEN
          DO 630 I=1,ILEN
C-- USE STATEMENT FUNCTION IP TO GET ADDRESSES
          INODE = IP(I,J,K)
C-- DEFINE LOCATION OF GRID VERTICES
          XC(INODE)=FLOAT(I-1)*0.0025-0.015
          YC(INODE)=FLOAT(J-1)*0.009+0.64
          ZC(INODE)=FLOAT(K-1)*0.1
  630     CONTINUE
  620   CONTINUE
  600 CONTINUE
      CALL IPREC('BLOCK-NUMBER-7','BLOCK','VERTICES',IPT,ILEN,JLEN,
     +          KLEN,CWORK,IWORK)


C-- LOOP OVER BLOCK
      DO 700 K=1,KLEN
        DO 720 J=1,JLEN
          DO 730 I=1,ILEN
C-- USE STATEMENT FUNCTION IP TO GET ADDRESSES
          INODE = IP(I,J,K)
C-- DEFINE LOCATION OF GRID VERTICES
```

287

```
                XC(INODE)=FLOAT(I-1)*0.0025+0.075
                YC(INODE)=FLOAT(J-1)*0.009+0.64
                ZC(INODE)=FLOAT(K-1)*0.1
  730           CONTINUE
  720        CONTINUE
  700     CONTINUE
C---- END OF EXAMPLE
C
C++++++++++++++++ END OF USER AREA 5 ++++++++++++++++++++++++++++++++
C
      RETURN
      END
```